**DOT/FAA/TC-23/61**

Federal Aviation Administration
William J. Hughes Technical Center
Aviation Research Division
Atlantic City International Airport
New Jersey 08405

# Evaluation of Unmanned Aircraft Systems for Airport Obstacle Data Collection

September 2023

Final Report



U.S. Department of Transportation
**Federal Aviation Administration**

## NOTICE

**Technical Report Documentation Page**

| 1. Report No. | 2. Government Accession No. | 3. Recipient's Catalog No. |
|---|---|---|
| DOT/FAA/TC-23/61 | | |

| 4. Title and Subtitle | 5. Report Date |
|---|---|
| EVALUATION OF UNMANNED AIRCRAFT SYSTEMS FOR AIRPORT OBSTACLE DATA COLLECTION | September 2023 |
| | 6. Performing Organization Code: ANG-E261 |
| 7. Author(s): Jonathan Sheairs*, Garrison Canter, Sheldon Menezes**, David Hall**, Abby Castle**, Ethan Schreuder** | 8. Performing Organization Report No. |
| 9. Performing Organization Name and Address: GDIT*, 600 Aviation Research Boulevard, Egg Harbor Township, NJ 08234; Woolpert Inc.**, 4454 Idea Center Blvd, Beavercreek, OH 45430 | 10. Work Unit No. (TRAIS) |
| | 11. Contract or Grant No.: DTFACT-15-D-00007 |
| 12. Sponsoring Agency Name and Address: Department of Transportation, Federal Aviation Administration, Office of Airports Safety and Standards, 800 Independence Avenue S.W., Washington, DC 20591 | 13. Type of Report and Period Covered: Final Report |
| | 14. Sponsoring Agency Code: AAS-120 |

15. Supplementary Notes

The FAA Airport Technology Research and Development Branch Technical Monitor was Michael DiPilato. David Gothan, Mark Howard, and Greg Ziebarth from NOAA's NGS provided technical expertise and guidance for this research effort.

16. Abstract

The Federal Aviation Administration (FAA) Airport Technology Research and Development Branch initiated a research study in collaboration with the National Oceanic and Atmospheric Administration's (NOAA) National Geodetic Survey (NGS) to evaluate the use of small unmanned aircraft systems (UASs) for collecting obstacle data at airports. The objectives of this research effort were to evaluate the accuracy of UAS obstacle data, assess the benefits and limitations of this technology, develop technical and operational considerations for using UASs, and to identify practical use cases for the implementation of UASs for conducting obstacle data collection at airports.

UAS obstacle data collection was conducted at five airports using a variety of UAS platforms, camera payloads, and data collection parameters. These data sets were processed utilizing two types of aerial triangulation (AT) software and analyzed using three-dimensional (3D) stereoscopic analysis techniques. The UAS data sets were evaluated based on their image quality, completeness, and accuracy relative to current FAA standards. The accuracies of UAS-derived obstacle measurements were evaluated by comparing them with data sets collected using field survey techniques and aerial surveys utilizing manned aircraft.

The results of both FAA and NGS review of the data found that UAS aerial imagery, in conjunction with 3D stereo analysis, is capable of collecting obstacle measurement data that meets current FAA Advisory Circulars 150/5300-17 and 150/5300-18 accuracy standards. Furthermore, when compared to manned aircraft data, UAS imagery is significantly higher resolution, which could provide superior accuracy in measuring obstacle heights and can identify obstacles with smaller vertical cross-sections. The accuracy of obstacle data is dependent on a variety of factors, including camera sensor and lens quality, data collection parameters such as ground sample distance and overlap settings, choice of processing software, and site attributes such as dense vegetation or terrain. Due to technical and operational limitations, UASs are currently most practical for conducting small-scale surveys.

| 17. Key Words | 18. Distribution Statement |
|---|---|
| Unmanned Aircraft Systems, UAS, Obstruction Surveys, Obstacle, Obstacle Data Collection, Aerial Surveys, Remote Sensing | This document is available to the U.S. public through the National Technical Information Service (NTIS), Springfield, Virginia 22161. This document is also available from the Federal Aviation Administration William J. Hughes Technical Center at actlibrary.tc.faa.gov. |

| 19. Security Classif. (of this report) | 20. Security Classif. (of this page) | 21. No. of Pages | 22. Price |
|---|---|---|---|
| Unclassified | Unclassified | 170 | |

ACKNOWLEDGEMENTS

The Federal Aviation Administration (FAA) Airport Technology Research and Development Branch would like to thank the following organizations for their participation in this research effort:

- FAA Aeronautical Information Services Team (AJV-A)
- The National Oceanic and Atmospheric Administration National Geodetic Survey
- The South Carolina Aeronautics Commission
- The Delaware River and Bay Authority (DRBA)/Cape May County Airport, NJ
- Granbury Regional Airport, TX
- Perry-Foley Airport, FL
- Cincinnati-West Airport, OH
- Suffolk Executive Airport, VA

TABLE OF CONTENTS

LIST OF FIGURES

LIST OF TABLES

# LIST OF ACRONYMS

| | |
|---|---|
| 3D | Three-dimensional |
| AC | Advisory circular |
| AGL | Above ground level |
| APBN | Airport beacon |
| AT | Aerial triangulation |
| AWOS | Automated weather observing system |
| CFR | Code of Federal Regulations |
| DJI | Da-Jiang Innovations |
| EB | Engineering brief |
| FAA | Federal Aviation Administration |
| FPY | Perry-Foley Airport |
| GCP | Ground control point |
| GDJ | Granbury Regional Airport |
| GIS | Geographic information system |
| GNSS | Global navigation satellite system |
| GPS | Global positioning system |
| GSD | Ground sample distance |
| I67 | Cincinnati West Airport |
| ISO | International Organization for Standardization |
| LiDAR | Light detection and ranging |
| LSCS | Light signal clearance surface |
| MLT | Millinocket Municipal Airport |
| NAD83(2011) | 2011 adjustment of the North American Datum of 1983 |
| NAVD88 | North American Vertical Datum of 1988 |
| NGS | National Geodetic Survey |
| NOAA | National Oceanic and Atmospheric Administration |
| NRCAN | National Resources Canada |
| NSRS | National Spatial Reference System |
| OAS | Obstacle Authoritative Source |
| OIS | Obstruction identification surface |
| PACS | Primary airport control station |
| PAPI | Precision approach path indicator |
| PPK | Post-processed kinematic |
| QC | Quality control |
| RGB | red-green-blue |
| RMSE | Root-mean-square error |
| RPIC | Remote pilot in command |
| RTK | Real-time kinematic |
| SACS | Secondary airport control station |
| SFQ | Suffolk Executive Airport |
| UAS | Unmanned aircraft system |
| VO | Visual observer |
| VTOL | Vertical takeoff and landing |
| WWD | Cape May County Airport |
| XLL | Allentown Queen City Municipal Airport |

# EXECUTIVE SUMMARY

The Federal Aviation Administration (FAA) Airport Technology Research and Development Branch conducted a research effort in collaboration with the National Oceanic and Atmospheric Administration's National Geodetic Survey (NGS) to evaluate the use of small unmanned aircraft systems (sUASs) for collecting airport obstacle data. The objectives of this research effort were to evaluate the accuracy of UAS obstacle data, assess the benefits and limitations of this technology, develop technical and operational considerations for using UASs, and to identify practical use cases for the implementation of UASs for conducting obstacle data collection at airports.

UAS obstacle data collection was conducted at five airports using a variety of UAS platforms, camera payloads, and data collection parameters. These data sets were processed using two types of aerial triangulation (AT) software and analyzed using three-dimensional (3D) stereoscopic analysis techniques. The UAS data sets were evaluated based on their image quality, completeness, and accuracy relative to current FAA standards. The accuracies of UAS-derived obstacle measurements were evaluated by comparing them with data sets collected using field survey techniques and aerial surveys using manned aircraft.

The results of both FAA and NGS review of the data found that UAS aerial imagery, in conjunction with 3D stereo analysis, is capable of collecting obstacle measurement data that meets current accuracy standards in FAA Advisory Circular (AC) 150/5300-17, *Standards for Using Remote Sensing Technologies in Airport Surveys*, and, AC 150/5300-18, *General Guidance and Specifications for Submission of Aeronautical Surveys to NGS: Filed Data Collection and Geographic Information System (GIS) Standards*. Furthermore, when compared to manned aircraft data, UAS imagery is significantly higher resolution, which may provide superior accuracy in measuring obstacle heights and can identify obstacles with smaller vertical cross-sections.

The accuracy of obstacle data is dependent on a variety of factors, including camera sensor and lens quality, data collection parameters such as ground sample distance and overlap settings, choice of processing software, and site attributes such as dense vegetation or terrain. None of these individual considerations can be isolated, and many can be used to compensate for a challenging environment (e.g., highly vegetated) or for areas in which other considerations are lacking. Entities using UASs for obstacle data collection should conduct their own testing and quality control checks prior to data collection to ensure their specific combination of UAS hardware, camera payload, and processing software is able to achieve the required level of accuracy for a given project.

Due to technical and operational limitations, UASs are currently the most practical for conducting small-scale surveys. Suggested UAS obstacle data collection applications include, but are not limited to, FAA Engineering Brief (EB) #91 Vegetation Management Projects, augmenting FAA Order 5010.4 surveys, updating entries in the Obstacle Authoritative Source, and surveying Precision Approach Path Indicator and Visual Glide Slope Indicators Obstacle Clearance Surface and Light Signal Clearance Surfaces.

# 1. INTRODUCTION

The Federal Aviation Administration (FAA) Airport Technology Research and Development Branch conducted a research effort in collaboration with the National Oceanic and Atmospheric Administration's (NOAA) National Geodetic Survey (NGS) to evaluate the use of small unmanned aircraft systems (sUASs) for collecting obstacle data at airports. sUASs are defined in Title 14 Code of Federal Regulations (CFR) Part 107.3, *Definitions*, as an unmanned aircraft weighing less than 55 pounds on takeoff, including everything that is on board or otherwise attached to the aircraft. (Definitions, 2016). This research effort was the first systematic effort by the FAA to evaluate the accuracy of UAS obstacle data in the airport environment.

This report provides a summary of the testing and data analysis conducted during this research effort, and FAA and NGS findings regarding the accuracy of unmanned aircraft system (UAS) data and benefits and limitations of this technology. In addition, this report provides technical and operational considerations and suggested use cases for using UASs to conduct obstacle data collection at airports.

## 1.1 BACKGROUND

Natural or man-made obstacles penetrating an airport's imaginary surfaces can create potential safety risks for approaching and departing aircraft. Obstacles are defined in Advisory Circular (AC) 150/5300-18, *General Guidance and Specifications for Submission of Aeronautical Surveys to NGS: Filed Data Collection and Geographic Information System (GIS) Standards,* as, "Any object that has a vertical element to it and may or may not penetrate an obstruction identification surface" (FAA, 2014). Any obstacle that penetrates an obstruction identification surface is considered by the FAA to be an obstruction. Obstructions can have an adverse effect on flight procedures and potentially restrict safe and efficient use of an airport. Obstructions can also have economic consequences for communities, creating restrictions on the types of aircraft that can use an airport and the times of day that operations can take place.

Regulations regarding the identification and maintenance of airport obstructions can be found in Title 14 CFR Part 139, *Certification of Airports*, and Title 14 CFR Part 77 Subpart C, *Standards for Determining Obstructions to Air Navigation or Navigational Aids or Facilities*.

Title 14 CFR Part 77 Subpart C. provides criteria for determining if an obstacle on or around an airport is an obstruction, including the establishment of obstruction identification surfaces (OISs) on and around airports. If an obstacle penetrates an OIS, it is defined as an obstruction and therefore considered a hazard to air navigation (Standards for Determining Obstructions to Air Navigation or Navigational Aids or Facilities, 2010).

Title 14 CFR Part 139 governs the Certification of Airports in the United States. Title 14 CFR Part 139.331, *Obstructions*, requires that each airport certificated under Part 139 manage obstructions, stating:

> Ensure that each object in each area within its authority that has been determined by the FAA to be an obstruction is removed, marked, or lighted, unless determined to be unnecessary by an FAA aeronautical study. (Obstructions, 2004).

Additional OIS are defined in FAA AC 150/5300-13, *Airport Design*, and AC 150/5300-18.

Traditional methods for identifying obstacles include ground-based field surveys and aerial surveys using manned aircraft. Field surveys can provide a high level of accuracy but can be time-intensive; they are also generally limited to only collecting obstacles that are visible from the survey location, which could obscure other obstructions behind them. In contrast, aerial surveys using manned aircraft equipped with sophisticated remote sensing equipment, such as high-resolution cameras or light detection and ranging (LiDAR) sensors, can collect obstacles over a much wider area, such as an entire airport and surrounding properties. However, the higher fixed cost of these aerial surveys limits their utility on smaller projects, and the expense associated with this type of aerial surveying can make these financially unfeasible for some airports, particularly smaller general aviation airports. In addition, due to its relatively low resolution, traditional aerial surveys using manned aircraft can have difficulty accurately collecting smaller features, such as antennas, fences, and some types of vegetation.

## 1.2 PURPOSE

The purpose of this research effort was to evaluate the use of sUASs for collecting obstacle data at airports.

## 1.3 OBJECTIVES

The objectives of this research effort were to:

1. Assess the degree to which the positional accuracy of UAS obstacle data conforms to existing FAA accuracy standards for remote sensing surveys (AC 150/5300-17 and AC 150/5300-18) by conducting comparative analysis between the UAS data and control data sets (ground control survey and/or manned aircraft survey).

2. Assess the benefits and limitations of using current UAS technologies for airport obstacle data collection.

3. Develop and validate technical and operational considerations for the use of UAS to conduct airport obstacle data collection.

4. Identify possible use cases for the implementation of airport obstacle data collection by UAS.

## 1.4 RELATED DOCUMENTS

1. FAA AC 107-2, *Small Unmanned Aircraft System (Small UAS)*
2. FAA AC 150/5300-16, *General Guidance and Specifications for Aeronautical Surveys: Establishment of Geodetic Control and Submission to the National Geodetic Survey*
3. FAA AC 150/5300-17, *Standards for Using Remote Sensing Technologies in Airport Surveys*
4. FAA AC 150/5300-18, *General Guidance and Specifications for Submission of Aeronautical Surveys to NGS: Field Data Collection and Geographic Information System (GIS) Standards*
5. Title 14 CFR Part 139, *Certification of Airports*
6. Title 14 CFR Part 77, *Safe, Efficient Use, and Preservation of the Navigable Airspace*
7. FAA Order 8260.19, *Flight Procedures and Airspace*

## 1.5 RESEARCH APPROACH

For this research effort, UAS obstacle data collection was conducted with a variety of UAS platforms, camera payloads, and data collection parameters at the following five test airports:

1. Cape May County Airport (WWD), NJ
2. Granbury Regional Airport (GDJ), TX
3. Perry-Foley Airport (FPY), FL
4. Cincinnati West Airport (I67), OH
5. Suffolk Executive Airport (SFQ), VA

The initial four test airports were chosen due to their unique test environments, including a variety of man-made and natural obstacles, and both thick and sparse vegetation. The fifth test airport (SFQ) was selected by the NGS to validate findings from earlier airports. This airport also had variety of man-made and natural obstacles. All test airports were located in Class G (uncontrolled) airspace and therefore did not require an approved FAA airspace authorization to operate UASs. This helped to expedite testing at these airports, as the only approval required prior to testing was from the airport sponsor.

The research focused on collecting red-green-blue (RGB) aerial imagery with different types of commercially available UASs. Following each aerial survey, data sets were processed utilizing traditional photogrammetric techniques recommended in the guidance provided by AC 150/5300-17, including aerial triangulation (AT) and three-dimensional (3D) stereoscopic analysis (referred to herein as stereo analysis). The obstacle measurements taken from UAS surveys were compared to measurements taken from control data sets, including field surveys and manned aircraft aerial surveys, to determine their relative quality and accuracy.

The FAA research team also worked with NGS under an existing interagency agreement between FAA and NOAA for data review and validation. Throughout the execution of this research effort, FAA researchers held numerous technical interchange meetings and data exchange with the NGS to validate findings and provide an external (independent) review of collected data. During this process the NGS evaluated UAS obstacle data collected at FPY, I67, and SFQ. During their analysis the NGS assessed the relative accuracy of UAS data by comparing it to data collected using manned aircraft and field survey techniques.

## 2. METHODOLOGY

Sections 2.1 through 2.4 describe the specific methodologies for the collection and processing of geodetic and UAS aerial survey data.

### 2.1 SURVEY DATA COLLECTION

To accurately locate obstacles extracted from UAS imagery on the earth in reference to other surveyed features (e.g., runways, OISs), the imagery was tied to a known geodetic reference system. This is accomplished using geodetic control and photo control. Geodetic control consists of a network of stable, identifiable points with published values within the reference system, such as survey markers established by state or federal agencies. Photo control consists of well-defined features visible in the UAS imagery, such as ground control points (GCPs). GCPs are tied to the geodetic control through surveys, enabling the orientation of the UAS imagery to the geodetic control.

#### 2.1.1 Geodetic Data

Geodetic data collection was conducted in accordance with AC 150/5300-16B, *General Guidance and Specifications for Aeronautical Surveys: Establishment of Geodetic Control and Submission to the National Geodetic Survey*, which provides standards and guidance for establishing geodetic control on an airport. This guidance includes the selection of survey marks, establishment of global positioning system (GPS) on site, validation of data, and submission of data to the NGS (FAA, 2019).

In the airport environment, the FAA has delegated the task of standardizing geodetic control to the NGS which maintains the National Spatial Reference System (NSRS). The NSRS is a consistent coordinate system that defines latitude, longitude, height, scale, gravity, and orientation throughout the United States. The NSRS includes both static control marks, such as survey monuments established by the NGS, and dynamic marks like Continuously Operating Reference Stations. Survey monuments at each airport, known as the primary airport control station (PACS) and the secondary airport control station (SACS), were used as benchmarks to establish geodetic control.

All surveyed points were tied horizontally to the 2011 adjustment of the North American Datum of 1983 (2011) (NAD83(2011)), and vertically to the North American Vertical Datum of 1988 (NAVD88). The current national geoid model, GEOID18, was used for processing global navigation satellite system (GNSS) observational data, and the local State Plane Coordinate System was used to develop grid (Northing, Easting, Elevation) coordinates.

#### 2.1.2 Photo Control Data

Photo control is the process by which aerial imagery is tied to existing geodetic data and the NSRS through the use of surveyed GCPs. The accuracy standard for the establishment of GCPs can be found in AC 150/5300-17, which provides guidance for using remote sensing technologies for conducting aerial surveys at airports. This guidance identifies acceptable remote sensing technologies and provides requirements regarding the planning, execution, and submission of

aerial survey data to the FAA. With respect to GCPs, this AC states that GCPs must meet a minimum accuracy of 1 ft horizontally and 4 in. vertically, relative to the NSRS (FAA, 2017b).

At each test airport, a variety of GCPs were set and surveyed for imagery control and data validation purposes. The initial GCP layout was planned prior to data collection, using GIS software. Once on site, the final GCP layout at each airport was established under the supervision of a licensed professional surveyor who determined the appropriate processes to achieve the required accuracies. The photo control surveys performed at each airport to establish GCPs met or exceeded an accuracy of 0.10 ft vertical and 0.10 ft horizontal relative to the PACS. This ensured that each GCP was surveyed to an accuracy exceeding the minimum requirements of AC 150/5300-17, effectively ruling out GCPs as a source of significant error.

Varying construction methods for GCPs were used depending on the surface and availability of materials. GCPs were composed of a combination of existing photo identifiable points, aerial targets painted on existing hard surfaces, and field-set targets with a nail or rebar driven into the earth flush with the ground. Examples of these GCPs are shown in Figure 1.

In addition to following guidance in relevant ACs, the research team followed several best practices to ensure a high level of confidence in photo control data. The primary method of GCP establishment in this research effort was through real-time kinematic (RTK) GNSS surveying. RTK surveying was accomplished by having a GNSS base receiver set over the known position of the PACS or SACS and a rover GNSS receiver set over the unknown GCP. This allowed for the accurate determination of the GCP's position relative to the PACS, and therefore to the NSRS as well.

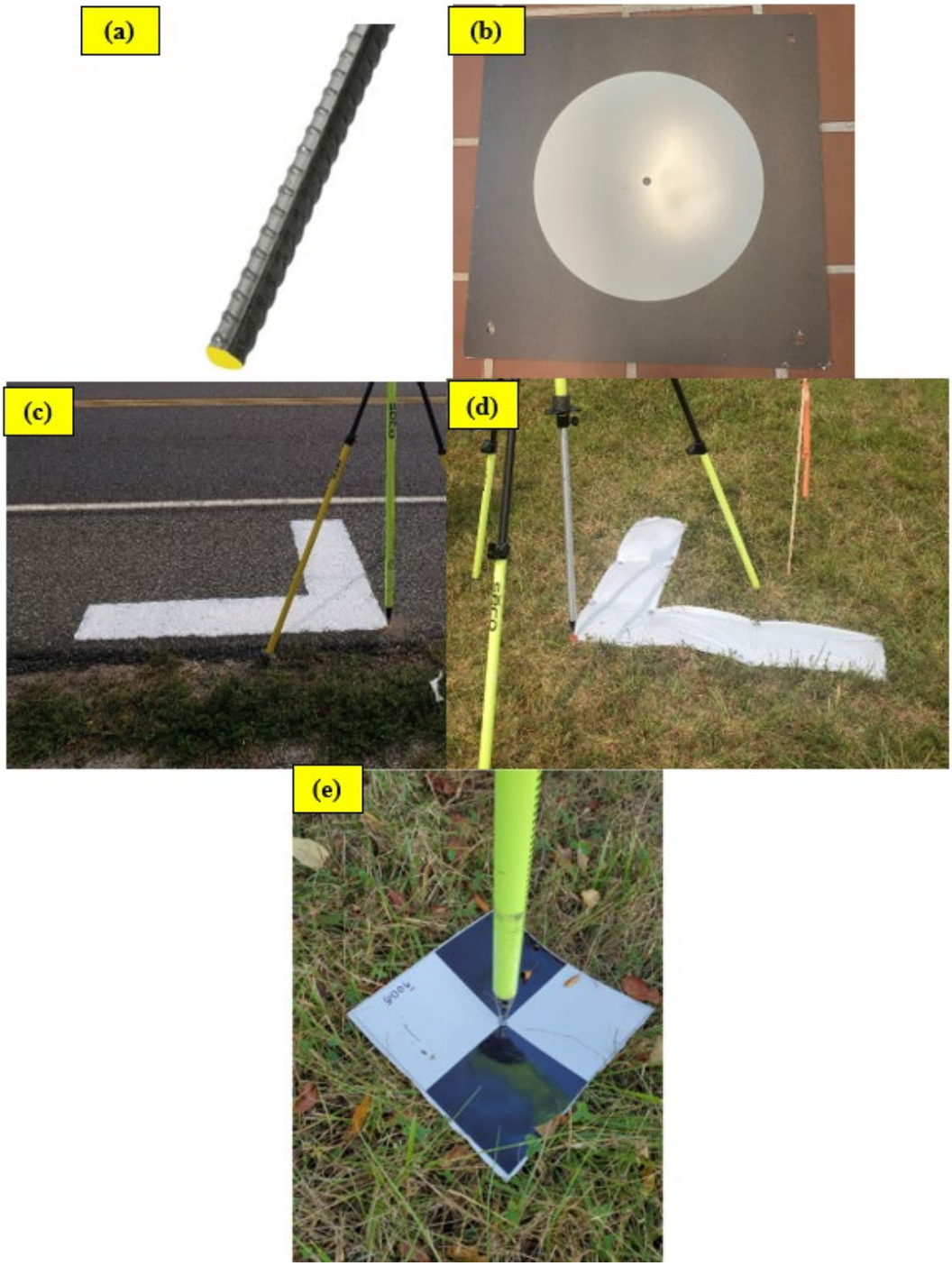


Figure 1. Ground Control Point Targets: (a) Rebar Spike, (b) Black and White Circle, (c) Chevron Painted on Pavement, (d) Vinyl Chevron Staked into Ground, and (e) Black and White Square

### 2.1.3 Survey Equipment

A variety of survey equipment was used to perform the necessary geodetic and photo control tasks at each airport.

Trimble® R8 Model 3™ Integrated GNSS receivers, pictured in Figure 2(a), were used for static and RTK GNSS observations. Pairs of GNSS receivers, one over a known position (such as a PACS or SACS) and one over an unknown position (such as a GCP while it is being established), allowed for the high-accuracy determination of positional data. A GNSS receiver established over a known position was referred to as a base station, and a receiver over the unknown point was referred to as a rover.

Trimble S6 Robotic Total Stations™ were used for establishing photo control in vegetated areas and for the collection of obstacle features. A total station is an angle and distance measuring device, which computes high-accuracy positions for remote objects when set up on known geodetic control. The Trimble S6 is equipped with Direct Reflex range measurement technology, which enables the measurement of distant features without the use of a prism. The Trimble S6 is pictured in Figure 2(b).

The Trimble DiNi™ digital auto level, shown in Figure 2(c) was used for establishing the vertical coordinates of photo control in areas where tree coverage made RTK less reliable. An auto level enables the transfer of elevation information from known points (geodetic control) to unknown points (photo control).

Seco® Graduated Collapsible GPS Tripods™ were used for all GNSS base observations. The most common form of operator error when performing GPS observations in the field is incorrect instrument height measurement. This Seco tripod has fixed height increments preventing this type of error.

Trimble Collapsible GPS Rover Rods™ with tripods, pictured in Figure 2(d), were used for all GNSS rover observations. The use of rods with fixed height increments prevents instrument height measurement errors while the locking bipods help ensure that the rover remains plumb for the duration of the observation.


Figure 2. Survey Equipment: (a) Trimble R8 Model 3 GNSS Receiver, (b) Trimble S6 Robotic Total Station, (c) Trimble DiNi Digital Auto Level, and (d) Trimble Collapsible GPS Rover Rod with Tripod

2.1.4 Quality Control Measures

Sections 2.1.4.1–2.1.4.2 describe the measures taken during survey data collection to ensure data quality and consistency at each test airport.

2.1.4.1 Equipment Calibration/Inspection

All total stations used on the project had current factory-authorized calibrations. In addition, all original equipment, manufacturer-recommended, daily field-calibration field routines were performed and documented.

Additionally, all GPS receivers, antennas, and equipment cables were inspected for defects or damage at the start of each day. If defects or damage had been discovered, corrective measures would have been taken to remove the faulty piece of equipment from the working equipment inventory.

#### 2.1.4.2 Tripod Check

Prior to GPS observations at the test airports, each fixed-height tripod was calibrated to eliminate potential blunders in centering error. Throughout GPS observations, the fixed-height tripod was checked for true vertical position (plumb). Many external factors can contribute to plumb drift during a survey, such as passing aircraft, moist loamy or sandy soil, or wind. If drifting had been detected, the instrument would be re-plumbed if the drift was minor. If a severe drift had been observed the session would have been aborted and restarted after corrections were made to the equipment. Severe drift is defined as when more than half of the plumb bubble moves outside of plumb circle embossed on the plumb bubble chamber.

## 2.2 UAS DATA COLLECTION

UAS aerial surveys were conducted by a contracted UAS flight service provider at each airport using various UAS platforms and RGB camera payloads. These aerial surveys collected nadir imagery (imagery captured with the camera facing straight down at the ground) over predefined study areas using system-specific, preprogrammed flight planning software. At each test airport, data sets were collected in localized areas to allow for relatively short survey flights. These shorter flights allowed for a larger number of individual tests of a variety of data collection parameters to determine technical and operational considerations. All data were collected with the trees in "leaf-on" condition in accordance with guidance specified in AC 150/5300-17 for manned aircraft obstacle data collection surveys (FAA, 2017b).

In addition to imagery, airborne GNSS on each UAS collected data specifying the aircraft's precise location and orientation when each picture was taken. On platforms that allowed for the use of GNSS base data, the platform's GNSS data were corrected through either RTK or post-processed kinematic (PPK) means, strengthening the tie to the NSRS geodetic control.

Sections 2.2.1 through 2.2.6 detail the equipment used to plan and conduct these surveys, and steps taken to coordinate and safely conduct each UAS operation.

### 2.2.1 UAS Platforms and Camera Payloads

#### 2.2.1.1 Selection Criteria

Prior to data collection, operational requirements and selection criteria were developed to select UAS platforms that could adequately perform obstacle data collection at airports. These selection criteria included camera payload imaging quality, safety features, deployment time, ease-of-use, environmental tolerance, and cost effectiveness.

- UAS Type

  A variety of UAS types were included in this research effort to provide a comprehensive assessment of UASs for performing aerial surveys at airports. These UAS types included multirotor, fixed-wing, and hybrid vertical takeoff and landing (VTOL) UASs.

- Camera Payload Specifications

  The specifications of the camera payloads used to collect aerial survey data have a critical effect on the quality and accuracy of the obstacle data. The camera payloads included in this research effort were selected to evaluate a variety of sensor sizes, focal lengths, resolutions, and shutter types.

- Safety

  Safety is the top priority for all activity in the airport environment. Therefore, UAS platforms selected for this research effort included safety features such as a lost link return-to-home failsafe mode and geo-fencing capability (restricting the ability of the UASs to leave the designated airspace limits) to minimize hazards with aircraft, people, and property.

- GPS Correction Technology

  UASs were included in the study that featured RTK and PPK GPS correction, and a single UAS that did not include this capability and relied solely on its onboard GPS.

- Cost Effectiveness

  Airport operators and companies vary significantly in the resources that can be utilized to purchase equipment. Therefore, UAS platforms ranging in price from $3,000 to $20,000 were included in testing to find solutions that could be effective for different organizational budgets.

#### 2.2.1.2 UAS Platforms

The UAS platforms that were used for obstacle data collection during this research effort included the Da-Jiang Innovations® (DJI) M210 RTK v2™, referred to herein as the M210; DJI Inspire 2™; SenseFly® eBee X RTK™, referred to herein as the eBee X; and the Wingtra® WingtraOne PPK™, referred to herein as the WingtraOne. These UASs are shown in Figure 3. A comparison of key specifications is presented in Table 1. Appendix A provides additional specifications for these UAS platforms.

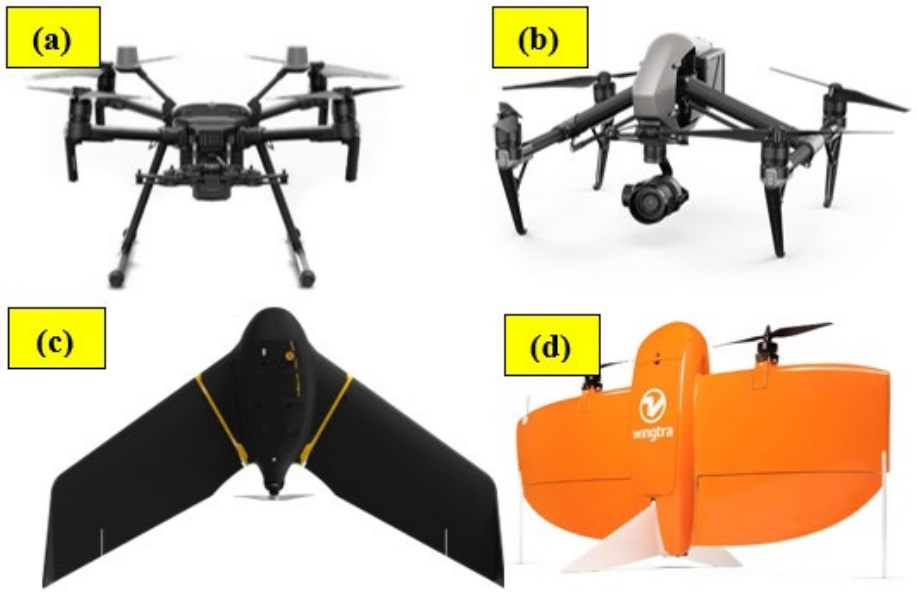


Figure 3. UAS Platforms: (a) M210, (b) Inspire 2, (c) eBee X, and (d) WingtraOne

Table 1. Comparison of UAS Specifications
(DJI, 2019; DJI, 2020; SenseFly, 2019; Wingtra, 2022)

| | **M210 RTK v2** | **Inspire 2** | **eBee X** | **WingtraOne** |
|---|---|---|---|---|
| **UAS Type** | Multirotor | Multirotor | Fixed-wing | Hybrid VTOL |
| **Maximum Take Off Weight** | 13.5lb | 9.37lb | 3.1 lb | 9.9 lb |
| **Airframe Dimensions** | 34.8″ x 34.9″ x 16.8″ | 16.8″ x 16.7″ x 12.5″ | 45.7″ wingspan | 49.2″ wingspan |
| **Endurance** | 24 min | 27 min | 90 min | 55 min |
| **Maximum Wind Resistance** | 26 mph | 22.37 mph | 29 mph | 28 mph |
| **3-Axis Gimbal** | Yes | Yes | No | No |
| **GPS Correction** | RTK | N/A | RTK | PPK |
| **Data Encryption** | AES 256-bit encryption | AES 256-bit encryption | AES 256-bit encryption | AES 128/256-bit encryption |
| **Estimated Cost** | $14,000 | $3,000 | $20,000 | $20,000 |

2.2.1.3 Camera Payloads

The UAS camera payloads used for obstacle data collection during this research effort included the: DJI Zenmuse X7, referred to herein as the X7; DJI Zenmuse X5S, referred to herein as the X5S; SenseFly® S.O.D.A. 3D; and Sony RX1R-II. Figure 4 shows pictures of these payloads and

Table 2 presents a comparison of key specifications. Appendix B provides additional specifications for each camera payload.


Figure 4. UAS Camera Payloads: (a) X7, (b) X5S, (c) S.O.D.A. 3D, and (d) RX1R-II

Table 2. Comparison of UAS Camera Payload Specifications
(DJI, 2018a; DJI, 2018b; SenseFly, 2020; Sony, 2015)

| | **X7** | **X5S** | **S.O.D.A. 3D** | **RX1R-II** |
|---|---|---|---|---|
| **Compatible UAS** | M210 & Inspire 2 | | eBee X | WingtraOne |
| **Sensor Size** | 23.5mm x 15.7mm | 17.3mm x 13mm | 12.8mm x 9.6mm | 36mm x 24mm |
| **Image Resolution** | 24 MP<br>6016 x 4008 | 20.8 MP<br>5280 x 3956 | 20 MP<br>5472 x 3648 | 42.18 MP<br>7952 x 5304 |
| **True Focal Length** | 16mm | 15mm | 10.6mm | 35mm |
| **35mm Equivalent** | 24mm | 30mm | 30mm | 35mm |
| **Shutter Type** | Electronic Rolling | Electronic Rolling | Mechanical Global | Mechanical Global |
| **Cost** | $4,050 | $2,000 | $4,000 | $3,300 |

2.2.2 Data Collection Parameters

The primary data collection parameters tested in this research effort were ground sample distance (GSD), and image overlap. Sections 2.2.2.1 through 2.2.2.2 discuss these further.

2.2.2.1 Ground Sample Distance

The resolution of UAS imagery is commonly expressed in GSD. GSD represents the area each pixel of an image equates to on the ground. For example, in an image with a 1 in. GSD, each pixel would represent 1 square inch of area on the ground. All other factors being equal, an image with a lower GSD value will have more detail than an image with a higher GSD.

As shown in Figure 5, the GSD is based on the specifications of the camera (i.e., focal plane, focal length, and lens), as well as the distance of the camera above ground level or the surface being mapped. This means that various cameras might have different GSD values when flying at the same altitude. This also means that images captured with the same camera at a higher or lower altitude will result in a higher or lower GSD value. It should be noted that actual GSD values can fluctuate from the planned GSD value due to changing terrain elevations and minor fluctuations in UAS altitude.

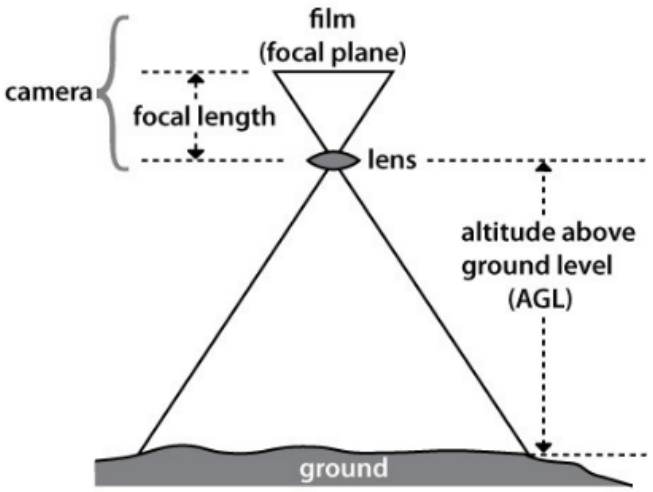


Figure 5. Illustration of GSD (NRCAN, 2016)

2.2.2.2 Image Overlap

The image overlap value describes the proportion of area covered by adjacent photos. Overlap values are expressed in percentages of forward and side overlap. Forward overlap is the overlap between images on the same flight line, while side overlap is the portion of images overlapping laterally across flight lines. Figure 6 shows examples of each of these types of overlap. All other factors being equal, higher overlap values will increase the likelihood of successful data processing but will result in longer flight and processing times due to the greater number of images captured and additional flight lines.

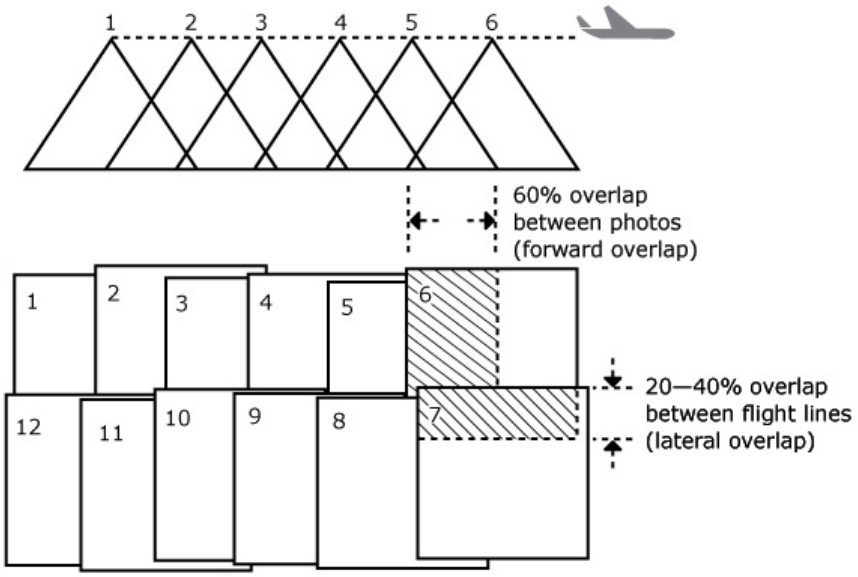


Figure 6. Image Overlap Illustration (NRCAN, 2016)

2.2.3 Mission Planning Software

All UAS operations took place using preprogrammed flight plans created using a flight management software application appropriate for each airframe. Flight planning limits stayed within the boundaries identified in each test's operational limits. Table 3 summarizes the flight planning applications used in this research effort for each platform. Figure 7 shows a screenshot of a multirotor flight plan taken from DJI GSPro™, and Figure 8 shows a screenshot of a fixed-wing flight plan from eMotion™.

Table 3. Mission Planning Software

| System(s) | Flight Planning Application |
|---|---|
| M210/Inspire 2 | DJI GSPro™ |
| eBee X | eMotion™ |
| WingtraOne | WingtraPilot™ |

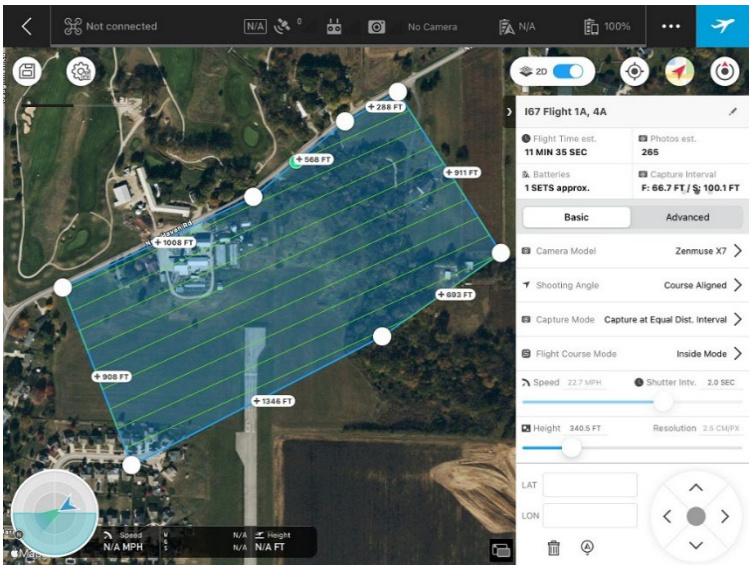


Figure 7. Example Multirotor Flight Plan

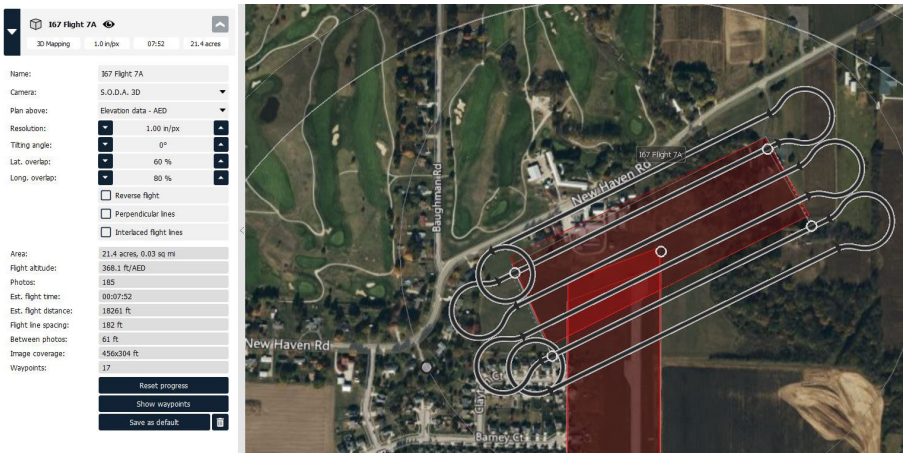


Figure 8. Example Fixed-Wing Flight Plan

## 2.2.4 Airport Coordination

Comprehensive coordination was conducted with the management at each airport included in this research effort. When requested, Field Survey Briefing Memos summarizing the mission objectives, flight profile parameters, and points of contact were submitted to the airport operator for approval prior to operating UASs on the premises.

## 2.2.5 Safety

The FAA contracted a UAS flight service provider that supported this research effort, which included developing and executing a comprehensive risk management plan to ensure safe UAS operations on each airfield. UAS operations complied with 14 CFR Part 107, including the requirement to remain within visual line-of-sight and fly below the maximum ceiling of 400 ft above ground level (AGL). When the planned UAS flight path included flying over public roads,

traffic control measures were used to ensure the UAS did not fly over any vehicles/nonparticipants (Small Unmanned Aircraft Systems, 2016).

Though not required by 14 CFR Part 107, designated visual observers (VOs) were used during all sUAS operations (Small Unmanned Aircraft Systems, 2016). Multiple VOs were used for flight plans that covered wide areas to ensure no nonparticipating persons or vehicles entered the flight operations area during data collection. All flight crew members wore high-visibility, reflective safety vests to aid in identifying members of the UAS team and enhancing visibility to other airport operations.

Where possible, UAS controllers equipped with Automatic Dependent Surveillance-Broadcast (ADS-B) In functionality were used for additional situational awareness and increased safety. The UAS flight crew also carried an air-band transceiver to increase situational awareness by monitoring the common traffic advisory frequency.

At a minimum, initial coordination and onsite safety briefing and interviews were conducted with airport management and operations teams to ensure all UAS operations would be executed safely and have no impact on airport operations.

## 2.3 UAS DATA PROCESSING AND ANALYSIS

During this research effort, UAS obstacle data were processed using commercially available AT software. AT is a method of determining the correct position and orientation of a series of overlapping aerial images to stitch them together to create an accurate 3D map. This map is then tied to an external coordinate system to allow for the measurement of features in the images relative to the earth.

Following the completion of AT, obstacle and GCP measurements were taken using 3D stereo analysis. Stereo analysis is the conventional technique used to measure obstacles in aerial imagery collected via manned aircraft and is the basis for the current FAA guidance and standards on using remote sensing technologies, AC 150/5300-17 (FAA, 2017b). This form of analysis involves two successively captured images presented simultaneously to a human analyst, one to each eye, which the brain interprets as a single 3D image. This technique, in conjunction with accurate geolocation associated with each of the images, allows for precise obstacle data collection and control verification.

Figure 9 presents a high-level overview of the UAS data processing workflow. Sections 2.3.1 through 2.3.5 describe the steps in the workflow and common issues that can arise during the process.

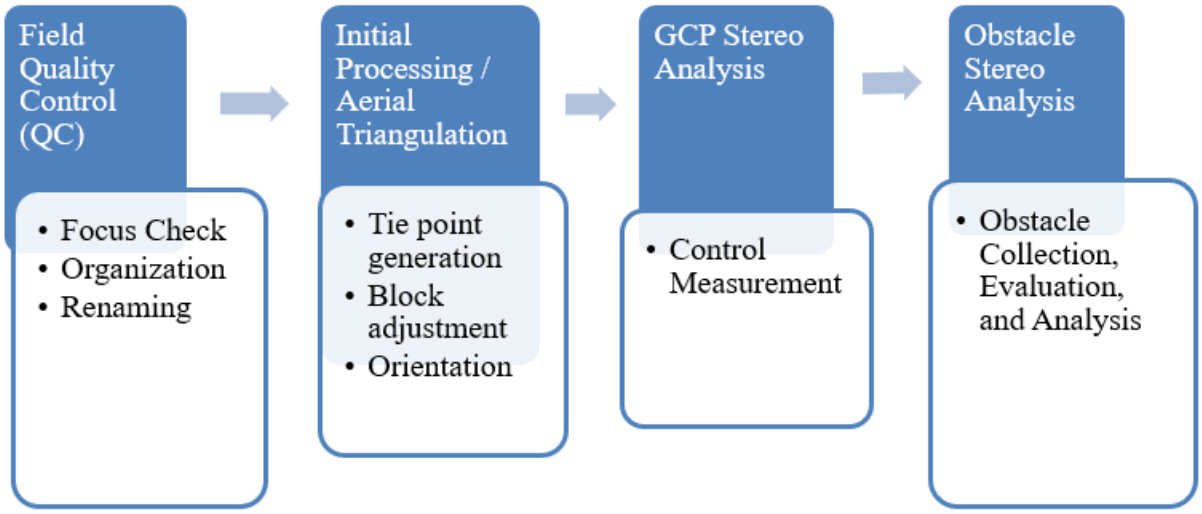


Figure 9. Unmanned Aircraft System Data Processing Workflow

A variety of software packages were used to collect and process aerial photography and survey data during this research effort. This software was evaluated and chosen based on its accessibility and performance. Both Pix4D® Mapper™ and UASMaster™ were used for AT solution production based on their ability to produce high-quality solutions. Table 4 lists each of the software packages used during this research program along with relevant details.

Table 4. Aerial Photography and Survey Software

| Software Type | Name | Developer | Version | Stage of Processing |
|---|---|---|---|---|
| Photogrammetry | Aeronautical Solutions™ | ESRI® | 10.2.2 | Flight Planning and Development |
| Photogrammetry | Summit Evolution™ | DAT/EM® | 5.5 | Stereo Analysis |
| Photogrammetry | Pix4D Mapper™ | Pix4D® | 4.5.6 | AT Solution |
| Photogrammetry | Airfield3D™ | DAT/EM | N/A | Stereo Analysis |
| Photogrammetry | Trimble UASMaster™ | Trimble | 11 | AT Solution |
| Survey | Trimble Business Center™ | Trimble | 5.32 (or newer) | Processing Surveyed GCPs |

### 2.3.1 Field QC/Initial Preparation

Immediately following the completion of UAS data collection, numerous quality control (QC) procedures were followed to ensure the imagery satisfied the minimum requirements of the

planned mission. First, raw imagery was reviewed in the field to identify flaws such as focus and exposure issues. In addition, the photos were inspected to ensure visibility of the GCPs, proper image orientation, and that planned camera settings were achieved. If imagery did not pass the initial QC, contingent on operational constraints, the flight was re-flown. After passing the initial QC, images were renamed and placed into directories designed to give a consistent organizational structure for the work to follow.

### 2.3.2 Image Processing/AT Solution Development

Following initial preparation, an AT software package was used to process the imagery and photo control data. First, the AT software package determined the corrected exterior orientation of each image and compiled them into an ordered and controlled set. The exterior orientation of an image refers to the position and orientation of the camera at the moment of image capture. The initial exterior orientation of the UAS-collected imagery was accurately tied to the geodetic control through the use of GCPs visible in the images.

AT software processing also consisted of image tie point extraction. Tie points are features, such as GCPs, that are visible in multiple images that can be used to stitch the images together. In addition, AT software processing included the measurement of photo control, which, in combination with tie point extraction, removed distortion in the imagery caused by the orientation of the camera and topography of the earth. This process of removing distortion in the imagery to accurately reflect the features of the earth is called orthorectification. Following orthorectification and the updating of imagery exterior orientation, the data sets were ready for stereo analysis.

A data set that has undergone processing by AT software is referred to as an AT solution. Data sets that are successfully processed are referred to as valid AT solutions, and data sets that are not able to be successfully processed are referred to as invalid AT solutions. It should be noted that an AT solution being considered valid does not necessarily mean that it can support the accurate measurement of features during stereo analysis. As a part of the processing workflow, each invalid AT solution was processed a minimum of two times to mitigate software or human error.

### 2.3.3 Ground Control Point Stereo Analysis

Once an AT solution was created, the images were viewed in stereo to measure the location of each GCP. These measurements were evaluated against the field-surveyed GCP locations collected as they were being established in the field to check for excessive residual error, or residuals. Excessive residuals are indicative of an AT solution that will fail to produce viable stereo imagery, however low residuals alone do not prove that the imagery set is without anomalies or distortions outside the immediate area of control measurement.

AC 150/5300-17 Section 8.1.1.2 states that the positions of well-defined points determined from stereo imagery must be within 3.28 ft (1 meter) relative to the NSRS for imagery to be accepted by the NGS (FAA, 2017b). While there is no specific standard for photo control GCP checks, this requirement was applied to determine whether each valid AT solution was viable for obstacle data collection in stereo analysis.

### 2.3.4 Obstacle Stereo Analysis

Next, stereo analysis of the imagery was performed using Airfield3D software from DAT/EM Systems to identify, measure, and inventory obstacles. When applicable, this step was also used for QC checks of field-surveyed obstacles.

Standards for the collection and submission of aeronautical survey data on or near an airport that can be used to identify obstacles are provided in AC 150/5300-18, *General Guidance and Specifications for Aeronautical Surveys to NGS: Field Data Collection and Geographic Information System (GIS) Standards*. Section 5.5.2 of AC 150/5300-18, *Obstacle*, establishes minimum accuracy requirements for the measurement of obstacles penetrating various types of imaginary surfaces at airports. The accuracy requirements for surveys of vertically guided primary and approach surfaces stated in this section are ±20 ft horizontal and ±3 ft vertical, which are equivalent to 1A accuracy specified in FAA Order 8260.19 (FAA, 2014). Table 5 presents the complete accuracy standards from FAA Order 8260.19 (FAA, 2020).

The accuracy requirements stated in AC 150/5300-18 originate in FAA Order 8260.19, *Flight Procedures and Airspace*. This order contains guidance pertaining to the management and maintenance of the FAA Flight Procedures and Airspace Program. Appendix C, *Obstacle Accuracy Standards, Codes, and Sources,* sets minimum accuracy tolerance standards for obstacle location data used in the development, review, or revision of instrument procedures (FAA, 2020).

Table 5. Federal Aviation Administration Order 8260.19 Accuracy Standards (FAA, 2020)

| **Horizontal Accuracy** | **Vertical Accuracy** |
|---|---|
| **Code Tolerance** | **Code Tolerance** |
| 1 +20 ft (6 m) | A +3 ft (1 m) |
| 2 +50 ft (15 m) | B +10 ft (3 m) |
| 3 +100 ft (30 m) | C +20 ft (6 m) |
| 4 +250 ft (75 m) | D +50 ft (15 m) |
| 5 +500 ft (150 m) | E +125 ft (38 m) |
| 6 +1,000 f. (300 m) | F +250 ft (75 m) |
| 7 +1/2 NM (900 m) | G +500 ft (150 m) |
| 8 +1 NM (1800 m) | H +1,000 ft (300 m) |

NM = Nautical mile

### 2.3.5 Common Processing Issues

Parallax is the apparent displacement in the location of an object in two images, resulting in an object's relative position appearing to be different in those images. This difference in the apparent location of an object is what creates the stereoscopic effect in the human brain, which is the ability to perceive three dimensions from imagery. However, while parallax is necessary for the perception/measurement of 3D features, excessive parallax inhibits stereoscopic vision.

Parallax increases as a function of base height ratio (the distance on the ground between the centers of overlapping photos, divided by aircraft altitude) and, as a result, is more prevalent in imagery

collected at low altitudes. This is a limitation of imagery collected by UASs operated under 14 CFR 107.51. Because of the 400-ft AGL altitude limit, UAS imagery is more susceptible to high parallax than manned imagery collected at 7,000 AGL (Operating Limitations for Small Unmanned Aircraft, 2016).

If there is significant parallax, geometric distortion, or control error noted that exceeds the standards specified in AC 150/5300-17, stereo analysis cannot be reliably performed, and the data set is considered unviable.

## 3. AIRPORT DATA COLLECTION AND RESULTS

Sections 3.1 through 3.5 details the collection, processing, and analysis of UAS obstacle data and control data at each test airport. These sections describe each test airport and the rationale behind their selection, depictions of the areas surveyed, and the layout of the GCPs. In addition, each section provides the data collection parameters for the UAS and manned aircraft aerial surveys, and additional types of control data sets, where applicable. Each section presents the initial AT solution processing results and comparisons of the measurements of GCP and obstacle locations taken from UAS and control data sets during stereo analysis. These sections conclude by presenting findings and lessons learned from each individual test effort.

### 3.1 CAPE MAY COUNTY AIRPORT

WWD is a dual-runway (1/19 and 10/28), non-towered airport located in Rio Grande, New Jersey. WWD is in uncontrolled (Class G) airspace from the surface to 700 ft AGL. WWD was selected as the initial test airport in the research effort due to its proximity to the FAA William J. Hughes Technical Center and an existing memorandum of agreement between the FAA and the Delaware River and Bay Authority, which owns and manages WWD. This allowed for the timely establishment of a robust calibration field of GCPs, which was intended to be used to evaluate varying levels of ground control.

UAS data collection at WWD included flights with varying overlap and GSD values to begin the development of technical and operational guidance regarding obstacle data collection. UAS obstacle data collected at WWD was compared to data collected using manned aircraft, a terrestrial scanner, and traditional field techniques.

Sections 3.1.1 through 3.1.6 describe the WWD study area, data collection parameters, procedures for obstacle data collection, results of data processing/analysis, and findings.

#### 3.1.1 Data Collection

The study area at WWD was located on the northwest quadrant of the airfield, as shown in the red-shaded area in Figure 10. The study area refers to the land area that is being surveyed for the presence of obstacles. This is distinct from the UAS operations area, which is slightly larger to accommodate aircraft turning radius, and additional flight lines to allow for the proper overlap along the edges of the survey area.

The survey area at WWD includes the decommissioned Runway 14/32, which is surrounded by dense and diverse vegetation. In addition, this area includes the FAA Research Taxiway, Taxiway C, which is adjacent to the decommissioned Runway 14/32. A diverse range of obstacles was present in this area, including natural obstacles, such as trees and terrain, and man-made structures, such as buildings, fencing, and airfield lights.

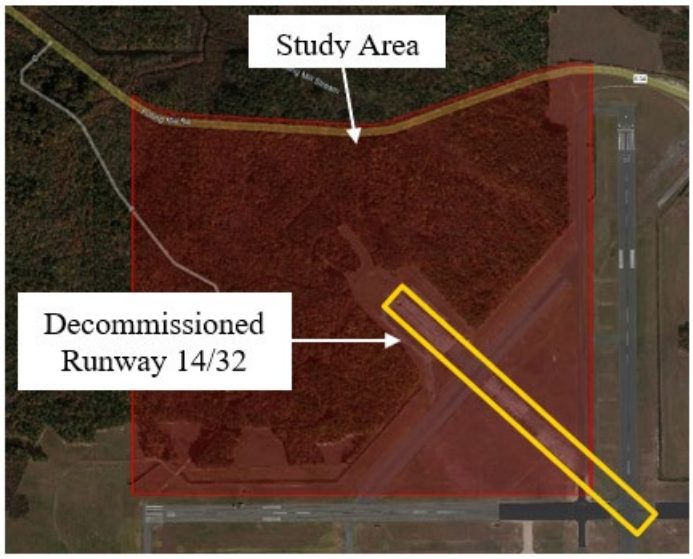


Figure 10. Cape May County Airport Study Limits and Decommissioned Runway 14/32

3.1.1.1 Onsite Preparation

To measure and validate the vertical and horizontal accuracy of the UAS obstacle data captured at WWD, a calibration field of GCPs was designed and established to provide photo control throughout the study area. During the initial test planning, it was believed that a spacing of 1,000 ft between GCPs would be sufficient to generate viable AT solutions. The final design spacing was 500 ft centered on the approximately 3,750-ft by 3,750-ft study limits. This denser grid allowed for up to half of the GCPs to be disabled in any given AT solution to allow the research team to iteratively remove points to test various control scenarios.

Once on site, the vegetation in the study limits was found to be significantly denser than originally estimated. Because of this, the full grid could not be set as originally designed. As a result of the unexpected field conditions, a control layout containing only 47 of the intended 64 GCPs was established. Figure 11 depicts the final layout and the approximate locations of the 47 GCPs that were used as part of the data post-processing workflow.


Figure 11. Cape May County Airport GCP Locations

For this initial testing at WWD, the level of vertical accuracy the UAS data would be able to achieve was unknown. Because of this, extra care was taken when establishing the GCPs so that the controlling variable would be the quality of the imagery itself. Static GPS surveying techniques were employed, and redundant observations were made on all points. In addition, a differential leveling survey was employed to ensure that the GCPs were as vertically accurate as possible. Differential leveling is a highly accurate surveying process by which vertical distances from a known elevation point are measured to determine the elevations of unknown points.

The calibration field failed to meet the team's goals of excessive ground control due to the dense vegetation covering much of the study area. The calibration field was not used for additional testing; however, some of these points were used as checkpoints when processing data sets.

3.1.1.2 UAS Data Collection Parameters

Initial data collection at WWD was performed using the M210 equipped with the X7 camera payload and the eBee X equipped with the S.O.D.A. 3D camera payload. A 1-in. GSD was selected as a starting point to collect the lowest possible resolution possible under the 400-ft AGL limitation of 14 CFR 107.51 (Operating Limitations for Small Unmanned Aircraft, 2016). Further tests included 0.75-in. and 0.5-in. GSD imagery to determine if higher resolutions have an impact on generating valid AT solutions for obstacle data collection.

To evaluate the effect of overlap on the data, two different sets of values were used, including 90%/75% forward and side overlap, and 80%/60% forward and side overlap. In total, seven UAS data sets were collected. Table 6 summarizes the collection parameters for each UAS aerial survey conducted at WWD.

Table 6. Cape May County Airport UAS Aerial Survey Parameters

| Date Collected | UAS | Sensor | Estimated GSD (in.) | Forward Overlap (%) | Side Overlap (%) | Altitude (ft AGL) | Sun Angle (degrees) | Flight Time (min) | Photo Count |
|---|---|---|---|---|---|---|---|---|---|
| 9/22/2020 | M210 | X7 | 0.75 | 90 | 75 | 257.4 | 47.1 | 250 | 5,263 |
| 9/23/2020 | eBee X | S.O.D.A. 3D | 0.75 | 90 | 75 | 276.9 | 38.4 | 79 | 2,410 |
| 9/23/2020 | eBee X | S.O.D.A. 3D | 1 | 90 | 75 | 369.2 | 48.1 | 54 | 1,782 |
| 9/23/2020 | M210 | X7 | 1 | 90 | 75 | 342.6 | 47.9 | 133 | 2,929 |
| 9/24/2020 | eBee X | S.O.D.A. 3D | 1 | 80 | 60 | 369.2 | 27.3 | 36 | 894 |
| 9/27/2020 | M210 | X7 | 1 | 80 | 60 | 342.6 | 36 | 48 | 934 |
| 4/13/2021 | WingtraOne | RXIR-II | 0.50 | 80 | 60 | 310.0 | 60.1 | 56 | 2,241 |

Due to challenges in generating acceptable AT solutions from the initial data sets collected with the M210 and eBee X, an additional data set was collected with the WingtraOne UAS. This UAS was selected due to its higher resolution camera, the Sony RXIR-II camera. The higher resolution of the camera payload produced a GSD of 0.5 in. when flying at a comparable altitude to other aerial surveys conducted at WWD. To further increase the likelihood of producing a valid and viable AT solution, the WingtraOne aerial surveys were conducted using a larger UAS operating area to help capture additional photos that included the GCPs along the road to the north and adjacent to Runway 10/28 to the south. Figure 12 compares the different UAS operating areas used during data collection at WWD.

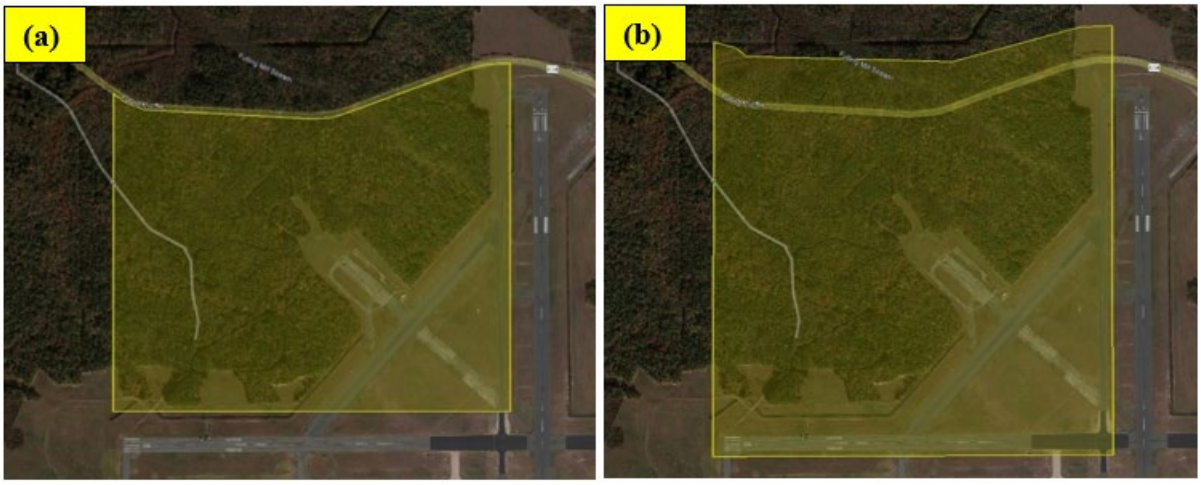


Figure 12. Cape May County Airport Operations Areas for (a) eBee and M210 and (b) WingtraOne

3.1.1.3 Manned Aircraft Data Collection Parameters

Approximately one month following the initial UAS data collection, a manned aircraft survey was completed at WWD in compliance with guidance stated in AC 150/5300-17. Due to the collection date (November) not all trees were in full leaf-on condition, but a large enough proportion of the

leaves remained that enough obstacles could be collected to provide comparison data to the UAS imagery. In addition, this area includes several pockets of evergreen trees in the study limits, which were used for comparing the UAS and manned data sets. Data were collected using an UltraCam Falcon P with a GSD of 3 in. and 60%/60% forward and side overlap values. Table 7 presents complete parameters for the manned aircraft aerial survey.

Table 7. Cape May County Airport Manned Aircraft Aerial Survey Parameters

| Date Collected | Sensor | Estimated GSD (in.) | Forward Overlap (%) | Side Overlap (%) | Altitude (ft AGL) | Flight Time (min) | Photo Count |
|---|---|---|---|---|---|---|---|
| 11/04/2020 | UltraCam Falcon P | 3 | 60 | 60 | 4,109.0 | 6 | 14 |

3.1.1.4 Terrestrial Scanner Data Collection Parameters

To compare the accuracy of the UAS obstacle data evaluation, a field point cloud data set of obstacles in the study area was collected at WWD using a Trimble SX10 LiDAR terrestrial scanner. The SX10 was placed on the approach end of the decommissioned Runway 14/32 to collect a data set looking from the runway end into the approach surface. The data set was composed of approximately 7 million 3D data points. The points collected by the Trimble SX10 have an accuracy of 2 mm +1.5 parts per million and an angular accuracy of 1 second relative to the station setup. When set over the geodetic control established at WWD, a total positional accuracy of 2 cm or greater was achieved relative to the PACS.

3.1.2 Data Processing Results

Table 8 lists the processing results for each UAS data set collected at WWD when processed using Pix4D. The table is color-coded to highlight the flights that did not produce a valid AT solution (red), a valid AT solution without viable stereo pairs (orange), and valid AT solutions with viable stereo pairs for analysis (green). Initial processing of each data set was performed using Pix4D software. This software was chosen because of its widespread use in the aerial mapping and surveying industry.

WWD data processing followed the technical approach defined in Section 2.3; however, there were unique considerations during processing. To test the effect of decreasing forward overlap in AT solutions and stereo analysis, a lower overlap data set was created from a higher overlap data set through the systematic removal of images. This allowed for the creation of three data sets with 70% forward overlap from a natively 90% forward overlap data set.

Table 8. Pix4D WWD Data Processing Results

| Test Number | Processing Software | UAS | Sensor | Estimated GSD (in.) | Forward and Side Overlap % | Processing Result |
|---|---|---|---|---|---|---|
| 1-1 | Pix4D | M210 | X7 | 0.75 | 90/75 | Valid AT solution, poor stereo analysis. Control residuals too high for obstacle data collection. |
| 2-1 | Pix4D | M210 | X7 | 0.75 | 70/75 | No valid AT solution. Only 51% of images calibrated, no tie point extraction, external orientation, or control measurement. |
| 3-1 | Pix4D | eBee X | S.O.D.A. 3D | 0.75 | 90/75 | Valid AT solution, poor stereo analysis. Control residuals too high for obstacle data collection. Parallax observed. |
| 4-1 | Pix4D | eBee X | S.O.D.A. 3D | 0.75 | 70/75 | No valid AT solution. Only 44% of images calibrated, no tie point extraction, external orientation, or control measurement. |
| 5-1 | Pix4D | eBee X | S.O.D.A. 3D | 1 | 90/75 | Valid AT solution, poor stereo analysis. Control residuals too high for obstacle data collection. Parallax observed. |
| 6-1 | Pix4D | eBee X | S.O.D.A. 3D | 1 | 70/75 | No valid AT solution. Only 55% of images calibrated, insufficient tie point extraction, external orientation, or control measurement. |
| 7-1 | Pix4D | M210 | X7 | 1 | 90/75 | Valid AT solution, poor stereo analysis. Control residuals too high for obstacle data collection. Parallax observed specifically in northeast corner. Significant gaps in tie point generation in vegetative areas. |
| 8-1 | Pix4D | M210 | X7 | 1 | 70/75 | No valid AT solution. Only 61% of images calibrated, insufficient tie point extraction, external orientation, or control measurement. |
| 9-1 | Pix4D | eBee X | S.O.D.A. 3D | 1 | 80/60 | No valid AT solution. Control residuals exceeding 100 ft. |
| 10-1 | Pix4D | M210 | X7 | 1 | 80/60 | No valid AT solution. Only 65% of images calibrated, insufficient tie point extraction, external orientation, or control measurement. |
| 11-1 | Pix4D | Wingtra One | RXIR-II | 0.5 | 80/60 | Valid AT solution, viable for stereo imagery. |

The analysis of processed data sets resulted in five valid AT solutions and six invalid AT solutions. The invalid solutions were attributed to sparse tie point generation and high control residuals. Data sets collected with the eBee X and M210 that resulted in valid AT solutions only did so because the forward and side overlap settings were extremely high (90%/70%) resulting in sufficient, however marginal, tie point generation. Four of the five valid AT solutions were taken into the stereo environment only to find that they were not viable for obstacle data collection.

The data set collected using the WingtraOne UAS and RX1R-II camera payload was the only data set that produced a valid AT solution and viable imagery suitable for stereo analysis. The success of the WingtraOne data set was attributed to multiple marginal improvements compared to the other data sets. “Traffic control” was used during the WingtraOne collection, which restricted cars during flight operations to allow for UAS imaging of GCPs along the road north of the survey area. The use of these GCPs, along with the RX1R-II’s higher resolution images and lower distortion lens, were believed to have increased both the quantity and quality of the tie point generation over the densely vegetated areas.

Figures 13, 14, and 15 show graphical depictions of lens distortion from the S.O.D.A. 3D, X7, and RXIR-II, respectively. The image area in each figure represents the field of view of each camera payload, and the severity of distortion introduced by the lens across each field of view is depicted by a series of two dots (one blue for origin and the other colored for severity) connected by a vector. Ideally both dots relating to each point would be directly on top of each other, indicating no distortion. As distortion increases the dots become farther apart, lengthening the vectors. The vectors are color-coded based on the level of distortion present at each point in the camera payload’s field of view. The green area in the middle section of the image depicts the area of lowest distortion, whereas the blue, yellow, and red areas depict escalating distortion values.

As shown in these figures, when compared to the X7 and S.O.D.A. camera payloads, the lens of the RX1R-II caused significantly less distortion, particularly along the edges of the images. Significant lens distortion along the edges of an image can result in a very small measurable area per image, which requires higher overlap values to compensate. In addition, lens distortion also compounds any error observed during control measurement.

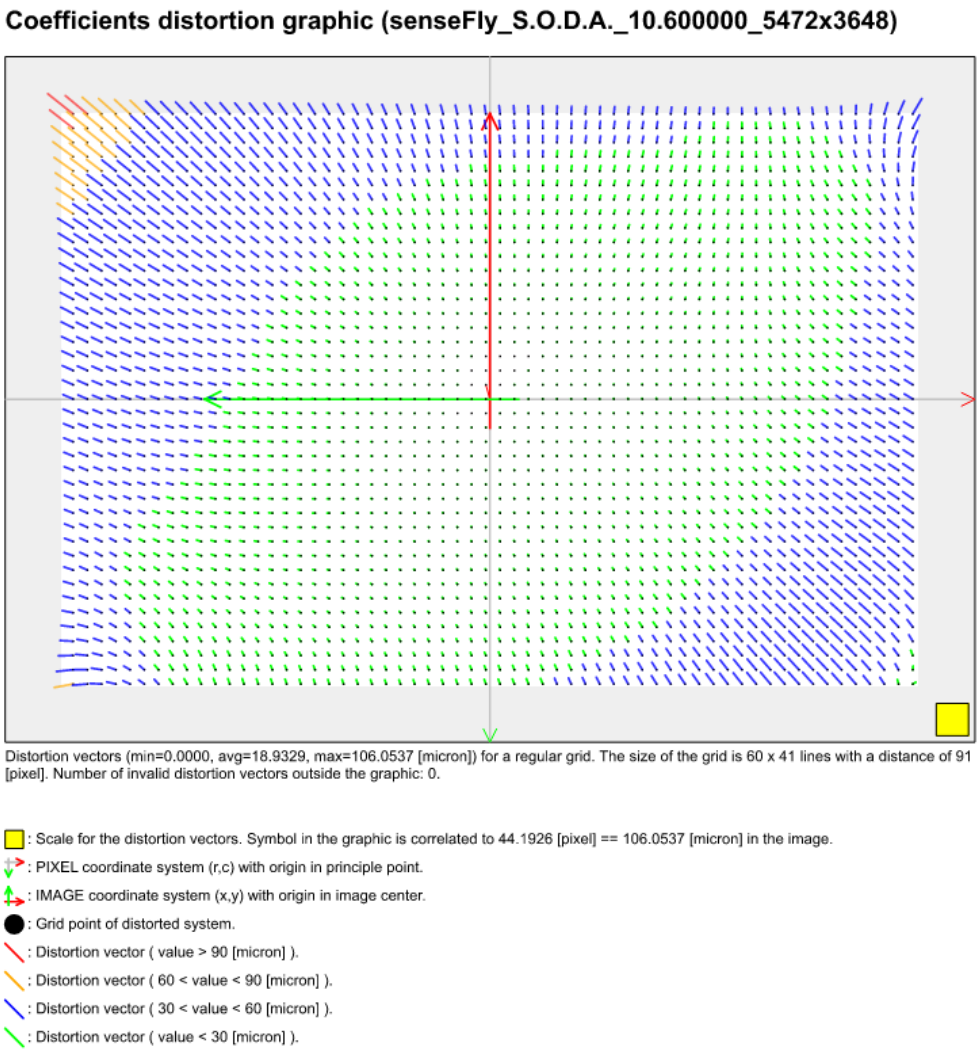


Figure 13. Visual Representation of Lens Distortion (S.O.D.A. 3D)

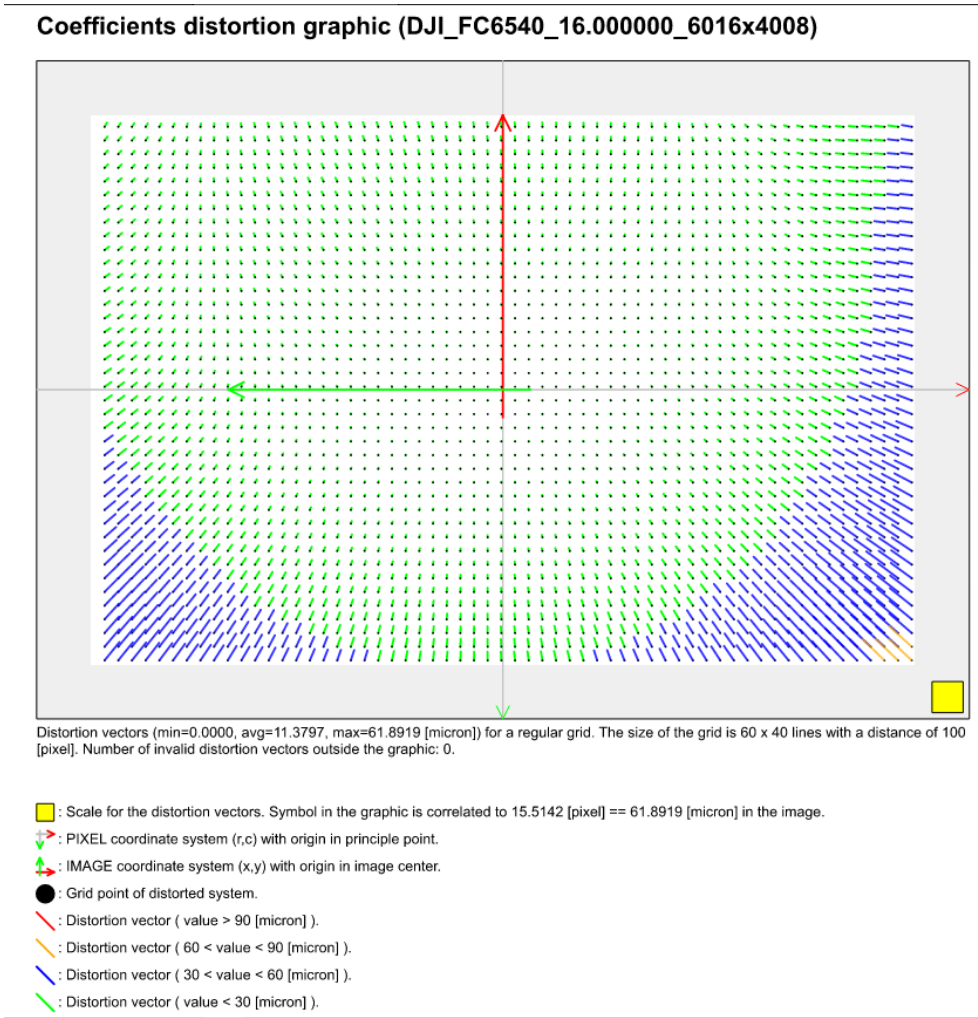


Figure 14. Visual Representation of Lens Distortion (X7)

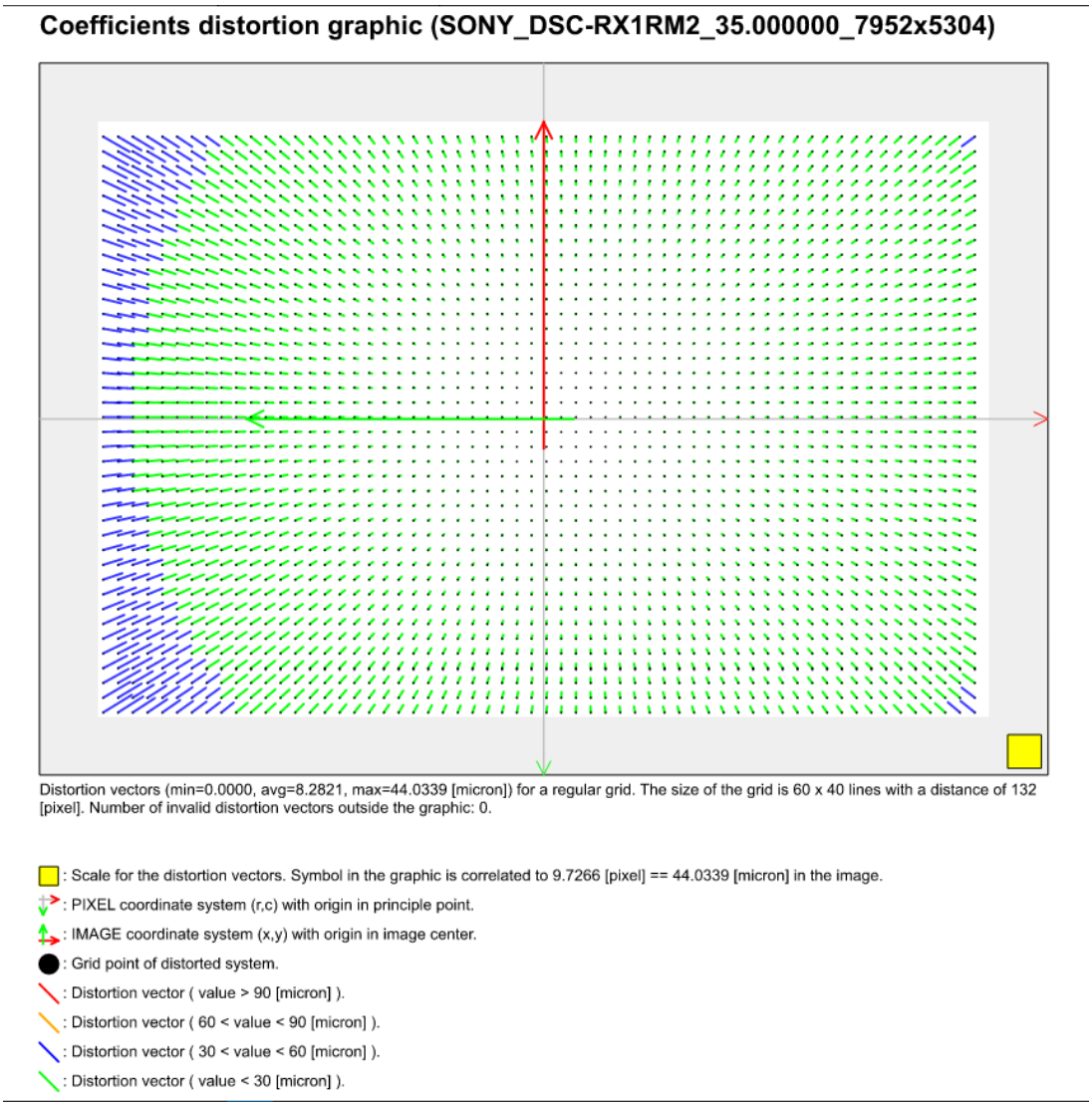


Figure 15. Visual Representation of Lens Distortion (RXIR-II)

Later in this research effort, representative data sets from WWD were reprocessed using Trimble UASMaster software in an attempt to produce more viable AT solutions. UASMaster was selected due to it having certain features, such as customizable calibrations for image pixel size, which were found to be necessary for processing data with certain camera payloads.

Table 9 lists each data set from WWD that was processed using UASMaster. None of these data sets produced a viable AT solution. It is unknown why WingtraOne data were able to achieve a valid AT solution viable for stereo imagery with Pix4D, but not with UASMaster.

Table 9. UASMaster WWD Data Processing Results

| Test Number | Processing Software | UAS | Sensor | Estimated GSD (in.) | Forward and Side Overlap (%) | Processing Result |
|---|---|---|---|---|---|---|
| 5-2 | UAS Master | eBee X | S.O.D.A. 3D | 1 | 90/75 | Insufficient calibrated images for a valid AT solution. |
| 7-2 | UAS Master | M210 | X7 | 1 | 90/75 | Insufficient calibrated images for a valid AT solution. |
| 11-2 | UAS Master | WingtraOne | RXIR-II | 0.5 | 80/60 | Insufficient calibrated images for a valid AT solution. |

### 3.1.3 Stereo Analysis—GCP Comparison Results

A stereo analysis effort was initiated to measure the GCP locations captured in the valid AT solution generated from UAS data collected during test 11-1 (WingtraOne). These locations were validated by comparing them to the field-surveyed GCP locations captured while they were being established. Table 10 illustrates the root-mean-square error (RMSE) between the GCP location measurements taken from the field survey and UAS imagery when viewed in stereo. These GCPs can be seen in Figure 11 in Section 3.1.1.1.

Table 10. Ground Control Point Location Variance between Field Survey and UAS Test 11-1 (WingtraOne)

| GCP | RMSE X (ft) | RMSE Y (ft) | RMSE Z (ft) | Maximum Horizontal Error (ft) | Highest Vertical Error (ft) |
|---|---|---|---|---|---|
| **A7** | 0.09 | 0.04 | 0.38 | 0.25 | 0.92 |
| **A8** | 0.03 | 0.08 | 0.11 | 0.15 | 0.29 |
| **B1** | 0.03 | 0.03 | 0.30 | 0.07 | 0.49 |
| **B2** | 0.07 | 0.05 | 0.26 | 0.14 | 0.50 |
| **B3** | 0.05 | 0.05 | 0.38 | 0.19 | 0.76 |
| **B4** | 0.04 | 0.07 | 0.19 | 0.13 | 0.37 |
| **B5** | 0.07 | 0.05 | 0.30 | 0.18 | 0.65 |
| **B6** | 0.06 | 0.04 | 0.29 | 0.29 | 0.78 |
| **B8** | 0.05 | 0.05 | 0.25 | 0.13 | 0.47 |
| **C4** | 0.06 | 0.04 | 0.29 | 0.15 | 0.49 |
| **C8** | 0.06 | 0.05 | 0.38 | 0.16 | 0.70 |
| **D1** | 0.04 | 0.05 | 0.33 | 0.14 | 0.68 |
| **D3** | 0.04 | 0.06 | 0.29 | 0.15 | 0.56 |
| **D4** | 0.04 | 0.04 | 0.26 | 0.17 | 0.68 |
| **D5** | 0.04 | 0.06 | 0.33 | 0.16 | 0.46 |
| **D7** | 0.06 | 0.06 | 0.38 | 0.22 | 0.64 |
| **D8** | 0.09 | 0.07 | 0.29 | 0.35 | 0.63 |
| **E2** | 0.02 | 0.04 | 0.18 | 0.10 | 0.36 |
| **E4** | 0.09 | 0.06 | 0.42 | 0.26 | 0.79 |
| **E5** | 0.03 | 0.05 | 0.32 | 0.09 | 0.57 |
| **E5B** | 0.07 | 0.09 | 0.40 | 0.31 | 0.85 |
| **E6** | 0.05 | 0.05 | 0.33 | 0.20 | 0.58 |
| **E7** | 0.06 | 0.03 | 0.28 | 0.13 | 0.45 |
| **E8** | 0.11 | 0.05 | 0.43 | 0.24 | 0.70 |
| **F2** | 0.08 | 0.07 | 0.32 | 0.46 | 1.07 |
| **F3** | 0.06 | 0.03 | 0.28 | 0.21 | 0.72 |
| **F4** | 0.03 | 0.06 | 0.20 | 0.18 | 0.55 |
| **F5** | 0.03 | 0.07 | 0.23 | 0.13 | 0.40 |
| **F6** | 0.08 | 0.04 | 0.34 | 0.19 | 0.59 |
| **F7** | 0.03 | 0.06 | 0.26 | 0.12 | 0.57 |
| **F8** | 0.10 | 0.03 | 0.31 | 0.21 | 0.67 |
| **G1** | 0.06 | 0.09 | 0.32 | 0.34 | 0.67 |
| **G2** | 0.06 | 0.08 | 0.37 | 0.21 | 0.62 |
| **G3** | 0.07 | 0.06 | 0.41 | 0.17 | 0.83 |
| **G4** | 0.07 | 0.05 | 0.37 | 0.31 | 1.14 |
| **G5** | 0.07 | 0.04 | 0.35 | 0.13 | 0.63 |
| **G6** | 0.05 | 0.06 | 0.26 | 0.21 | 0.62 |
| **G7** | 0.07 | 0.10 | 0.34 | 0.23 | 0.70 |
| **G8** | 0.03 | 0.03 | 0.22 | 0.07 | 0.26 |
| **H1** | 0.04 | 0.08 | 0.31 | 0.14 | 0.69 |
| **H2** | 0.07 | 0.04 | 0.32 | 0.13 | 0.54 |
| **H3** | 0.03 | 0.04 | 0.33 | 0.10 | 0.71 |
| **H4** | 0.27 | 0.10 | 0.46 | 1.05 | 1.05 |
| **H5** | 0.13 | 0.05 | 0.35 | 0.26 | 0.60 |
| **H6** | 0.13 | 0.09 | 0.43 | 0.27 | 0.95 |
| **H7** | 0.06 | 0.18 | 0.38 | 0.26 | 0.85 |
| **AVERAGE:** | **0.06** | **0.06** | **0.31** | | |

AC 150/5300-17 Section 8.1.1.2 states that the positions of well-defined points determined from stereo imagery must be within 3.28 ft (1 meter) relative to the NSRS for imagery to be accepted by the NGS (FAA, 2017b). While there is no specific standard for photo control GCP checks, the same accuracy standard was applied, and the green shading throughout Table 10 indicates that the average RMSEs are within this tolerance. This analysis confirmed that this UAS data set was viable for obstacle data collection.

### 3.1.4 Stereo Analysis—Manned Imagery Comparison Results

Nineteen obstacles were selected at WWD from the manned aircraft aerial survey conducted in November 2020 and used as the basis of comparison in evaluating the accuracy of the UAS-collected obstacle data. These obstacles, shown in Figure 16, were intentionally varied in both their geographic location and their type (e.g., wide tree canopy tops, a building, airfield light point features, narrow fence line features).


Figure 16. Obstacle Locations and Study Limit at WWD

Table 11 presents a comparison of the x, y, and z measurements for each of these obstacles as measured in stereo using both the UAS and manned aircraft imagery.

Table 11. Obstacle Location Variance between Manned Imagery and UAS Test 8-2 (WingtraOne)

| Obstacle | Manned Imagery (ft) | | | UAS Imagery (ft) | | | Delta (ft) | | |
|---|---|---|---|---|---|---|---|---|---|
| | x | y | z | x | y | z | x | y | z |
| **Airfield Light (AL-1)** | 376339.38 | 67296.75 | 22.16 | 376339.48 | 67297.40 | 23.39 | -0.10 | -0.65 | -1.23 |
| **Airfield Light (AL-2)** | 376334.02 | 65779.82 | 17.94 | 376334.04 | 65779.85 | 18.79 | -0.02 | -0.03 | -0.85 |
| **Airfield Light (AL-3)** | 375014.95 | 63996.41 | 19.39 | 375015.02 | 63996.42 | 19.51 | -0.06 | -0.01 | -0.12 |
| **Airfield Light (AL-4)** | 376224.07 | 64898.43 | 45.04 | 376224.41 | 64897.60 | 45.60 | -0.35 | 0.83 | -0.56 |
| **Building (BD-1)** | 375480.68 | 65013.63 | 28.86 | 375480.46 | 65013.54 | 29.13 | 0.23 | 0.09 | -0.27 |
| **Fence (F-1)** | 374560.96 | 66835.17 | 10.19 | 374560.45 | 66834.46 | 9.36 | 0.52 | 0.71 | 0.82 |
| **Fence (F-2)** | 373040.73 | 63984.2 | 25.48 | 373040.52 | 63984.10 | 24.83 | 0.21 | 0.10 | 0.65 |
| **Fence (F-3)** | 374557.74 | 65549.54 | 23.34 | 374557.62 | 65549.32 | 22.57 | 0.12 | 0.22 | 0.77 |
| **Ground (G-1)** | 376256.16 | 64243.93 | 16.44 | 376256.13 | 64243.95 | 16.20 | 0.03 | -0.01 | 0.24 |
| **Road (R-1)** | 372927.93 | 66920.85 | 6.77 | 372927.92 | 66920.85 | 6.28 | 0.00 | 0.00 | 0.49 |
| **Road (R-2)** | 372932.58 | 65741.73 | 8.48 | 372932.42 | 65741.80 | 8.40 | 0.16 | -0.07 | 0.07 |
| **Tree (T-1)** | 376158.15 | 67221.19 | 77.56 | 376157.52 | 67220.36 | 78.62 | 0.64 | 0.82 | -1.06 |
| **Tree (T-2)** | 374561.48 | 66898.74 | 62.27 | 374561.11 | 66899.27 | 63.08 | 0.37 | -0.53 | -0.81 |
| **Tree (T-3)** | 376055.63 | 65727.74 | 75.7 | 376056.48 | 65728.65 | 76.32 | -0.85 | -0.91 | -0.62 |
| **Tree (T-4)** | 372980.46 | 64134.4 | 78.21 | 372980.73 | 64133.42 | 81.15 | -0.27 | 0.98 | -2.94 |
| **Tree (T-5)** | 374542.47 | 64114.72 | 67.8 | 374540.89 | 64113.22 | 67.71 | 1.58 | 1.51 | 0.08 |
| **Tree (T-6)** | 374558.98 | 65679.9 | 38.97 | 374559.67 | 65681.90 | 39.35 | -0.69 | -2.01 | -0.37 |
| **Tree (T-7)** | 372877.43 | 67047.9 | 67.11 | 372874.50 | 67048.06 | 68.39 | 2.94 | -0.16 | -1.27 |
| **Tree (T-8)** | 373294.36 | 65610.49 | 83.33 | 373296.72 | 65609.22 | 83.44 | -2.36 | 1.27 | -0.10 |

As indicated by the green shading throughout Table 11, the deltas between obstacle measurements taken from UAS and manned imagery are within the most stringent (1A) accuracy requirement (20 ft horizontal, 3 ft vertical) for obstacles prescribed in AC 150/5300-18 (FAA, 2014). The data are also within the acceptable tolerance of 3.28 ft (1 meter) for well-defined points as prescribed in AC 150/5300-17 (FAA, 2017b).

In most cases, trees and airfield lights were observed to have a greater height when measured in the UAS imagery compared to the manned aircraft imagery. This difference was not seen in large flat features such as the ground, road, and building measurements, where the UAS and manned imagery performed very similarly. An equal and opposite effect was seen in the fence locations where the heights measured in the manned imagery were consistently higher than those measured in the UAS imagery.

### 3.1.5 Terrestrial Scanner Data Comparison Results

Terrestrial scanner LiDAR data were collected at WWD using a Trimble SX10 Scanning Total Station for the purpose of comparing with UAS data collected in the same timeframe and at the same location. Figure 17 presents a visual comparison of the point cloud derived from this terrestrial scanner compared to a point cloud derived from a UAS data set. This figure illustrates the inherent limitations of using a terrestrial scanner for the purposes of obstacle data collection. Similar to conventional field survey techniques, the scanner can only measure features that are within direct line of sight. As a result of this limitation, only the first layer of trees can be reliably collected using the terrestrial scanner. As seen in the UAS obstacle data shown in red, this limitation is overcome with UASs because it collects data from above, resulting in the ability to see beyond the first layer of obstacles.

Because the LiDAR data did not collect the vast majority of obstacles measured by the UAS and manned aircraft surveys, it was not used as a control data set to evaluate the accuracy of the UAS obstacle data.

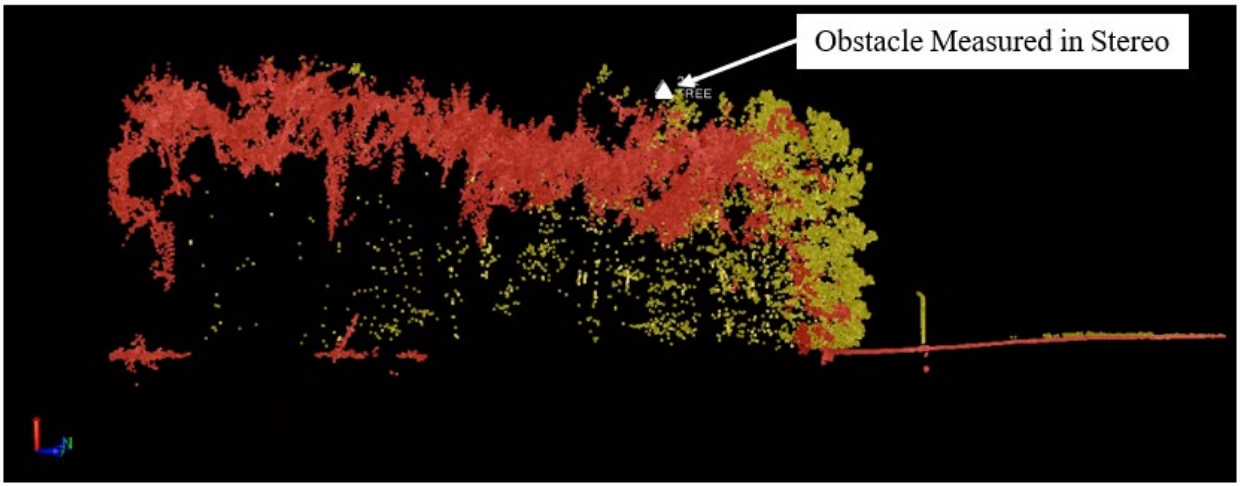


Figure 17. Visual Representation of a Terrestrial Scan Point Cloud (Yellow), UAS Point Cloud (Red), and Obstacle Measured in Stereo Imagery

### 3.1.6 Findings

Of the 14 obstacle data sets collected and processed, five were able to produce valid AT solutions, and one of these valid AT solutions was found to be viable for obstacle data collection and measurement. The viable AT solution was collected with the WingtraOne at 0.5 in. GSD using 80%/60% forward and side overlap values. When compared to measurements taken from data collected using manned aircraft, the UAS data set was within the accuracy tolerance (3.28 ft) for well-defined points stated in AC 150/5300-17 and within the most stringent accuracy requirements (20 ft horizontal, 3 ft vertical) for obstacles stated in AC 150/5300-18 (FAA, 2017b; FAA, 2014).

The choice of processing software had a significant effect on the viability of UAS data sets for obstacle data collection. The WingtraOne data set produced a valid and viable AT solution with Pix4D software, but the same data set failed to produce a valid AT solution with UASMaster. Due to the user's limited ability to adjust Pix4D's processing parameters, it was not possible to troubleshoot issues with tie point extraction and orthorectification with unsuccessful data sets.

The quality of AT solutions did not improve when generated using higher resolution 0.75 in. GSD imagery versus lower resolution 1 in. GSD imagery. While operating UASs under the 400 ft AGL limitation of 14 CFR Part 107, 1 in. was the highest practical GSD (lowest resolution) the sensors were capable of (Small Unmanned Aircraft Systems, 2016).

Increasing the forward and side overlap values from 80%/60% to 90%/75% did not significantly improve the quality of AT solutions but required nearly double the amount of time to complete data collection.

The GCP layout developed during this testing effort did not provide enough control in areas of dense vegetation and thus resulted in poor AT solutions that were not viable for obstacle data collection. Inability to place GCPs in the vegetated areas, as shown in Figure 11 in Section 3.1.1.1, resulted in inconsistent tie point generation and contributed to the issues experienced during the AT process.

Dense tree cover created significant challenges for generating viable data sets using UASs. This vegetation affected the ability of the processing software to properly compute tie points, which resulted in parallax. The parallax observed eroded the integrity of the solution and was aggravated by the movement of trees, the inconsistent resolution of the imagery, and high error in ground control. Due to the parallax, especially visible when measuring particularly tall obstacles, the research team was unable to produce solutions that were viable for obstacle data collection from all but one of the UAS/sensor combinations employed during testing at WWD.

Significant lens distortion along the edges of each UAS image resulted in a small measurable area per image. Lens distortion compounded the error observed during control measurement and was present in all UAS data collected during this effort.

## 3.2 GRANBURY REGIONAL AIRPORT

GDJ is a single runway (14/32), non-towered airport located in Granbury, Texas. GDJ is in Class G airspace from the surface to 700 ft AGL. GDJ was selected due to the availability of obstacle data in the study area collected using manned aircraft 1 month prior to UAS data collection.

UAS data collection at GDJ sought to replicate the successful data set collected at WWD in another environment, while also testing lower overlap settings and less capable cameras to further develop technical and operational considerations. UAS survey data collected at GDJ was compared to data collected using manned aircraft, and traditional field techniques.

Sections 3.2.1 through 3.2.5 describe the GDJ study area, data collection parameters, procedures for obstacle data collection, results of data processing/analysis, and findings.

### 3.2.1 Data Collection

The study area at GDJ was located southwest of the airfield, over the southern approach of a new runway, which was then under construction (Runway 1/19). This testing area coincided with where the research team had previously collected NGS-validated obstacle information with manned aircraft. A diverse range of obstacles were present in this area, including natural obstacles such as trees and bushes and man-made structures such a fuel tank, fencing, utility poles, and traffic lights. Figure 18 shows the study area and approximate location of Runway 01/19.

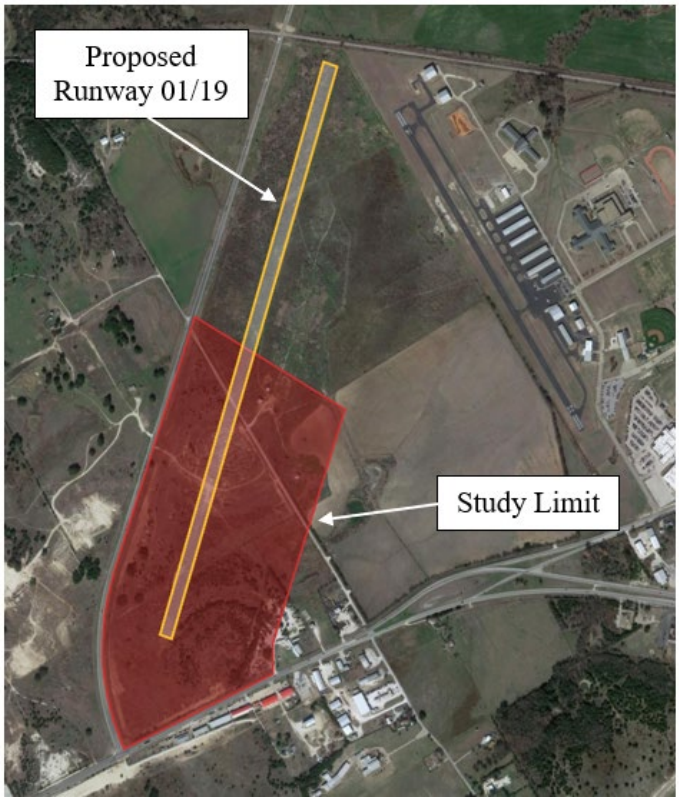


Figure 18. Granbury Regional Airport Study Limit and Proposed Runway 01/19

3.2.1.1 Onsite Preparation

Figure 19 depicts the approximate locations of the nine GCPs that were established at GDJ and used as part of the data post-processing workflow. No additional check points were set at GDJ due to unexpected construction occurring at the time of the survey, which limited ground access to a large central portion of the site. Inability to access the construction site limited the number of GCPs established, which resulted in all GCPs being used during processing, and none left over for use as check points. Flight operations were only conducted when the construction site was inactive and free from nonparticipants.

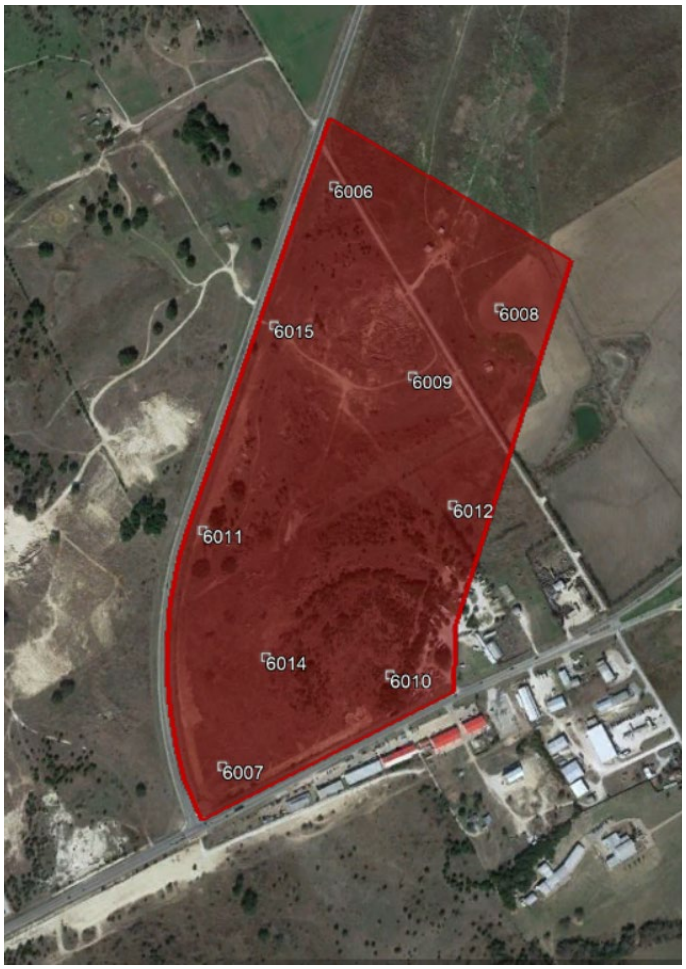


Figure 19. Granbury Regional Airport GCP Locations

The GCP layout at GDJ was designed qualitatively rather than utilizing a quantitative method like the one employed at WWD. Due to this methodology the spacing between GCPs varied from 500 ft to 1,000 ft. The test area at GDJ did not have areas of dense vegetation such as those present at WWD; however, onsite construction during the testing effort resulted in limited access to the center of the study area and required the GCP layout to be adjusted in the field. This resulted in the removal of planned GCPs in the center of the study area. Due to the ongoing construction, there were no obstacles in the construction area. Because no measurements were required in the

construction area it is unknown what possible impact the lack of control coverage had on the AT solution in this section of the study area.

3.2.1.2 UAS Data Collection Parameters

UAS data collection at GDJ sought to replicate and validate the successful data set from testing at WWD, while continuing to develop technical and operational considerations. A total of four data sets were collected using the M210. Due to constraints on site, such as active construction and roadways, fixed-wing systems like the eBee X and WingtraOne could not be tested at this location to ensure compliance with the 14 CFR Part 107 regulation restricting flight over nonparticipants. This was due to the increased turning radius of fixed-wing systems, which require a larger flight operations area, and their inability to pause flight and hover in place if nonparticipants enter the flight area. The X7 camera payload was used to replicate results from WWD, while the less capable X5S camera payload was also used to evaluate payload technical considerations.

Based on the finding from WWD showing that higher resolution imagery did not benefit the quality of data, a GSD of 1 in. was used for all flights. Regarding overlap, the 80%/60% forward and side settings used during the successful data set at WWD were replicated, as well as new minimum settings of 70%/60% forward and side overlap. Table 12 summarizes the collection parameters for each UAS aerial survey conducted at GDJ. Figure 20 depicts the UAS flight operations area.

Table 12. Granbury Regional Airport UAS Aerial Survey Data Collection Parameters

| Date Collected | UAS | Sensor | Estimated GSD (in.) | Forward Overlap (%) | Side Overlap (%) | Altitude (ft AGL) | Sun Angle (degrees) | Flight Time (min) | Photo Count |
|---|---|---|---|---|---|---|---|---|---|
| 10/28/2020 | M210 | X7 | 1 | 80 | 60 | 342 | 38.5 | 24 | 466 |
| 10/28/2020 | M210 | X7 | 1 | 70 | 60 | 342 | 22.2 | 20 | 316 |
| 10/28/2020 | M210 | X5S | 1 | 80 | 60 | 379 | 34.6 | 27 | 525 |
| 10/28/2020 | M210 | X5S | 1 | 70 | 60 | 379 | 29.5 | 30 | 362 |

Figure 20. Granbury Regional Airport UAS Operations Area

3.2.1.3 Manned Aircraft Data Collection

Approximately 1 month prior to UAS data collection, a manned aircraft survey was completed at GDJ in compliance with guidance stated in AC 150/5300-17. This survey was conducted as part of the planning process of proposed Runway 1/19. Data were collected using an UltraCam Eagle with a GSD of 6 in. and 60%/50% forward and side overlap values. Table 13 presents complete parameters for the manned aircraft aerial survey.

Table 13. Granbury Regional Airport Manned Aircraft Aerial Survey Parameters

| Date Collected | Sensor | Estimated GSD (in.) | Forward Overlap (%) | Side Overlap (%) | AGL (ft) | Flight Time (min) | Photo Count |
|---|---|---|---|---|---|---|---|
| 09/20/2020 | UltraCam Eagle | 6 | 60 | 50 | 6,650 | ~5 | 8 |

3.2.2 Data Processing Results

Each data set collected at GDJ was processed with both Pix4D and UASMaster. Table 14 presents the results of these processing efforts. The table is color-coded to highlight the flights that produced no valid AT solution (red), a valid AT solution without viable stereo pairs (orange), and valid AT solutions with viable stereo pairs for analysis (green).

Table 14. Granbury Regional Airport Data Processing Results

| Test Number | Processing Software | UAS | Sensor | Estimated GSD (in.) | Forward and Side Overlap % | Processing Result |
|---|---|---|---|---|---|---|
| **1-1** | UAS Master | M210 | X7 | 1 | 80/60 | Valid AT solution with viable stereo imagery. |
| **1-2** | Pix4D | M210 | X7 | 1 | 80/60 | Valid AT solution, poor stereo analysis. Control residuals too high for obstacle collection. Parallax observed. |
| **2-1** | UAS Master | M210 | X7 | 1 | 70/60 | Valid AT solution. Presence of parallax and geometric distortion in solution when analyzed in stereo, attributed due to low overlap and control. |
| **2-2** | Pix4D | M210 | X7 | 1 | 70/60 | Valid AT solution. Presence of parallax and geometric distortion in solution when analyzed in stereo, attributed due to low overlap and control. |
| **3-1** | UAS Master | M210 | X5S | 1 | 80/60 | Missing image metadata, unable to process. No AT solution generated. |
| **3-2** | Pix4D | M210 | X5S | 1 | 80/60 | Missing image metadata, unable to process. No AT solution generated. |
| **4-1** | UAS Master | M210 | X5S | 1 | 70/60 | Missing image metadata, unable to process. No AT solution generated. |
| **4-2** | Pix4D | M210 | X5S | 1 | 70/60 | Missing image metadata, unable to process. No AT solution generated. |

When comparing processing results from Test 1, both Pix4D and UASMaster resulted in valid AT solutions, but only the data set processed with UASMaster was deemed viable for stereo analysis. The Pix4D data set was deemed unusable for accurate obstacle measurement due to substantial parallax found while measuring ground control in stereo. During this analysis, the parallax resulted in a consistent error of ±1.0 ft at each GCP. During the analysis of the imagery processed via UASMaster, minimal parallax was observed, allowing for more accurate control comparison and obstacle measurement.

The discrepancy between processing results for this data set was attributed to the capability in UASMaster to use custom pixel calibrations allowing for irregular pixel sizes. Pix4D assumes all pixels are square while UASMaster has the capability to account for differing x and y pixel dimensions. Once this pixel dimension discrepancy was accounted for in UASMaster the parallax was greatly reduced, and a valid AT solution was produced for analysis.

Figures 21 and 22 illustrate the pixel sizes for data collected via the X7 when processed in Pix4D and UASMaster. As shown in Figure 21, UASMaster allows the AT solution to account for non-square pixel sizes by allowing for differing x and y values. Figure 22, however, shows that Pix4D

defines pixel size with a single value, and, therefore, requires pixels to be square. This resulted in a non-viable imagery set.

**Camera**

**Camera data (DJI_FC6540_16.000000_6016x4008)**

| | | |
|---|---|---|
| Manufacturer | DJI | |
| Model | FC6540 | |
| Serial number | | |
| Sensor (width / height) [pixel] | 6016 | 4008 |
| Pixel size (x / y) [micron] | 3.8997 | 3.9167 |
| Ground sampling distance (x / y) [ft (US)] | 0.0880 | 0.0884 |
| Camera calibration | SelfCalibrated | |
| Distortion type | Coefficients | |
| Additional parameters | 5 parameters (Physical) | |
| Focal length [mm / pixel] | 15.9724 | 4086.9127 |
| Standard deviation [mm / pixel] | 0.0679 | 17.3726 |
| Focal length (Fx / Fy) [pixel] | 4095.8420 | 4078.0222 |
| Principal point (x / y) [mm \| pixel] | 0.1213 \| 3026.6975 | -0.0752 \| 1972.3858 |
| Standard deviation (x / y) [mm \| pixel] | 0.0021 \| 0.5429 | 0.0030 \| 0.7718 |
| Distortion parameter: K0 / K1 | 0.000000E+00 | 2.029534E-05 |

Figure 21. DJI Zenmuse X7 Pixel Size Dimensions—UASMaster

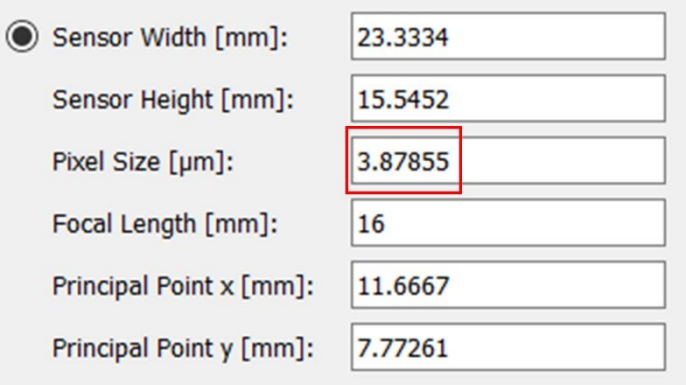


Figure 22. DJI Zenmuse X7 Pixel Size Dimensions—Pix4D

When comparing the data sets from Flight 2, both Pix4D and UASMaster produced valid AT solutions; however, the considerable presence of parallax, geometric distortion, and high control residuals resulted in impractical stereo analysis for both data sets. This was attributed to a low forward overlap setting (70%) given the GCP layout.

Tests 3 and 4 captured data with the Zenmuse X5S. During processing of these data sets, it was found that metadata were missing that is vital to the AT process. This metadata included the Omega, Phi, and Kappa values that describe the rotation of the camera at the moment of capture along the x, y, and z axes within a coordinate system. Without the Omega and Phi, the exterior orientation of an image cannot be determined. The X5S was found to be incompatible with either processing software, and while these values are present in the metadata of the raw imagery, they are unable to be exported to an external format and manually uploaded into the processing software. Without the ability to manually input these values and the failure of the software to interpret them, no viable AT solutions could be generated.

### 3.2.3 Stereo Analysis—GCP Comparison Results

A stereo analysis effort was initiated to measure the GCP locations captured in the valid AT solution generated from UAS data collected during Test 1-1. These locations were validated by comparing them to the field surveyed GCP locations captured while they were being established.

Table 15 illustrates the RMSEs between the GCP location measurements taken from the field survey and UAS imagery when viewed in stereo. These GCPs are shown in Figure 19 in Section 3.2.1.1.

Table 15. Granbury Regional Airport Location Variance between Field Survey and UAS Test 1-1 (X7)

| GCP | RMSE X (ft) | RMSE Y (ft) | RMSE Z (ft) | Maximum Horizontal Error (ft) | Maximum Vertical Error (ft) |
|---|---|---|---|---|---|
| **6006** | 0.04 | 0.05 | 0.24 | 0.10 | 0.29 |
| **6007** | 0.13 | 0.06 | 0.39 | 0.22 | 0.89 |
| **6008** | 0.11 | 0.06 | 0.37 | 0.21 | 0.46 |
| **6009** | 0.04 | 0.12 | 0.13 | 0.18 | 0.13 |
| **6010** | 0.08 | 0.11 | 0.28 | 0.22 | 0.52 |
| **6011** | 0.16 | 0.12 | 0.31 | 0.22 | 0.55 |
| **6012** | 0.04 | 0.09 | 0.12 | 0.19 | 0.17 |
| **6014** | 0.03 | 0.10 | 0.18 | 0.20 | -0.31 |
| **6015** | 0.12 | 0.14 | 0.21 | 0.23 | 0.28 |
| **AVERAGE:** | **0.08** | **0.09** | **0.25** | | |

As indicated by the green shading in Table 15, the average RMSEs and maximum individual error for each GCP fell within the accuracy tolerance stated in AC 150/5300-17 (FAA, 2017b). This analysis confirmed that this UAS data set was viable for obstacle data collection.

### 3.2.4 Stereo Analysis—UAS Imagery to Manned Imagery Comparison Results

Sixteen obstacles were chosen at GDJ from the manned aircraft aerial survey conducted in September 2020 and used as the basis of comparison in evaluating the accuracy of the UAS-collected obstacle data. These obstacles, whose locations are shown in Figure 23, were intentionally varied in both their geographic location and their type (e.g., trees and bushes, fencing, traffic lights, utility poles).

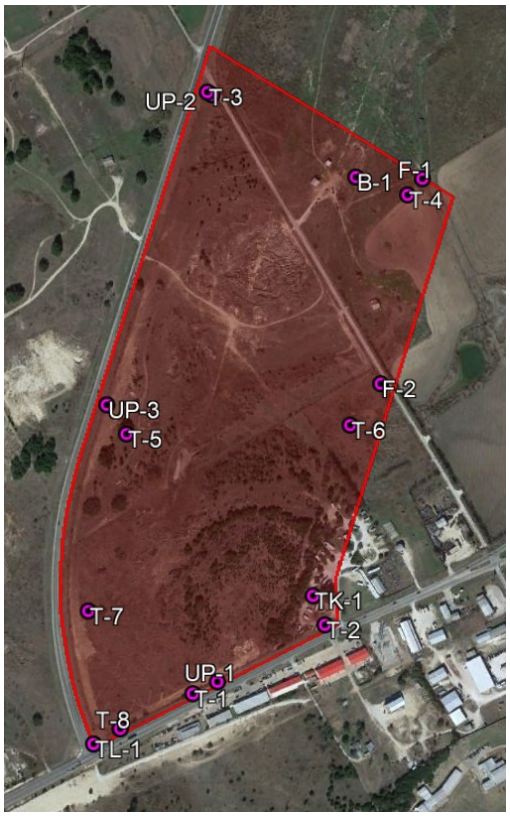


Figure 23. Granbury Regional Airport Obstacle Locations

Table 16 presents a comparison of the x, y, and z measurements for each of these obstacles as measured using both the UAS and manned aircraft imagery collected during Test 1-1. The cell highlighted in red falls outside the acceptable tolerance of 3.28 ft (1 meter) for well-defined points prescribed by AC 150/5300-17C (FAA, 2017b).

When compared to data collected with manned aircraft, all obstacle locations were within the most stringent (1A) AC 150/5300-18 accuracy requirements (20 ft horizontal, 3 ft vertical) for obstacles, except for one tree that had a delta of 3.15 ft vertically (FAA, 2014). However, this variance was deemed to be acceptable because trees are not considered to be well-defined points. In stereo analysis, tree canopies can have differences in the measured highest point due to environmental factors such as wind swaying the tops of trees, tree growth, or broken limbs. Figure 24 illustrates this concept with a photo collected through the telescope of a total station during obstacle measurement. In the figure, the blue line depicts the measured height of the tree canopy as defined by 6 in. imagery, and the red line depicts the tree canopy as measured by the 1-in. imagery.

Table 16. Obstacle Location Variance between Manned Imagery and UAS Test 1-1 (X7)

| Obstacle | Manned Imagery (ft) | | | UAS Imagery (ft) | | | Delta (ft) | | |
|---|---|---|---|---|---|---|---|---|---|
| | x | y | z | x | y | z | x | y | z |
| **Bush (B-1)** | 2177232.47 | 6844068.16 | 827.39 | 2177231.35 | 6844065.89 | 826.91 | 1.12 | 2.27 | 0.48 |
| **Fence (F-1)** | 2177631.82 | 6844064.42 | 810.41 | 2177631.02 | 6844064.36 | 809.74 | 0.79 | 0.06 | 0.67 |
| **Fence (F-2)** | 2177389.24 | 6842838.17 | 808.32 | 2177389.35 | 6842838.07 | 809.11 | -0.11 | 0.10 | -0.79 |
| **Tank (TK-1)** | 2176992.33 | 6841572.53 | 844.76 | 2176993.14 | 6841572.93 | 844.03 | -0.80 | -0.40 | 0.73 |
| **Traffic Light (TL-1)** | 2175687.62 | 6840686.22 | 876.45 | 2175687.52 | 6840686.55 | 877.60 | 0.10 | -0.33 | -1.15 |
| **Tree (T-1)** | 2176277.63 | 6840986.93 | 864.86 | 2176277.16 | 6840987.28 | 865.50 | 0.47 | -0.35 | -0.64 |
| **Tree (T-2)** | 2177064.09 | 6841398.88 | 865.35 | 2177061.44 | 6841400.87 | 864.57 | 2.65 | -1.99 | 0.79 |
| **Tree (T-3)** | 2176337.03 | 6844573.16 | 832.50 | 2176337.40 | 6844572.71 | 835.14 | -0.38 | 0.45 | -2.64 |
| **Tree (T-4)** | 2177543.24 | 6843966.52 | 819.07 | 2177544.54 | 6843966.32 | 819.18 | -1.30 | 0.20 | -0.11 |
| **Tree (T-5)** | 2175868.68 | 6842528.12 | 873.58 | 2175868.35 | 6842528.54 | 873.66 | 0.33 | -0.43 | -0.07 |
| **Tree (T-6)** | 2177207.24 | 6842589.58 | 811.68 | 2177206.30 | 6842589.29 | 812.72 | 0.93 | 0.30 | -1.04 |
| **Tree (T-7)** | 2175648.09 | 6841473.12 | 858.65 | 2175644.93 | 6841474.17 | 861.80 | 3.16 | -1.05 | -3.15 |
| **Tree (T-8)** | 2175845.58 | 6840776.25 | 881.90 | 2175846.14 | 6840773.35 | 882.52 | -0.56 | 2.89 | -0.62 |
| **Utility Pole (UP-1)** | 2176423.93 | 6841058.25 | 867.10 | 2176419.81 | 6841058.29 | 867.53 | 4.12 | -0.04 | -0.43 |
| **Utility Pole (UP-2)** | 2176365.81 | 6844557.57 | 846.52 | 2176365.66 | 6844557.81 | 846.17 | 0.16 | -0.24 | 0.35 |
| **Utility Pole (UP-3)** | 2175751.40 | 6842700.77 | 870.56 | 2175751.43 | 6842700.97 | 872.17 | -0.04 | -0.20 | -1.61 |

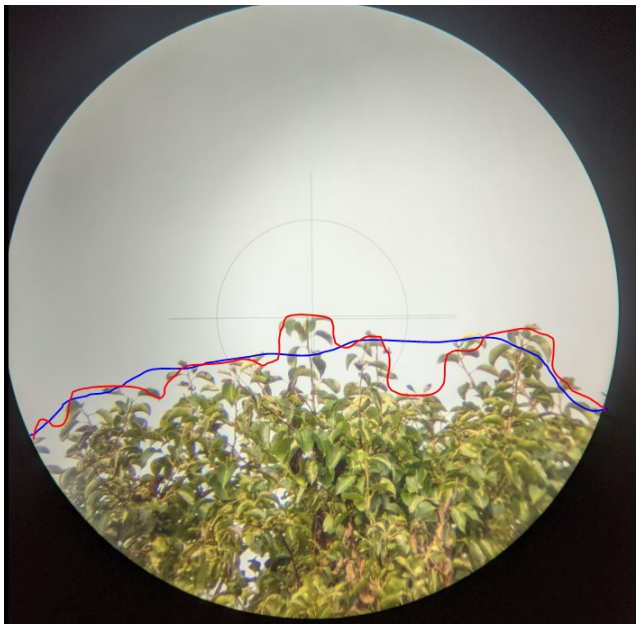

Figure 24. Tree Canopy Differences—6-in. GSD Manned Imagery (Blue line) and 1-in. GSD UAS Imagery (Red line)

### 3.2.5 Findings

Of the eight obstacle data sets collected and processed, four produced valid AT solutions, and one was found to be viable for obstacle data collection and measurement. This viable AT solution was collected with the M210 and X7 using 80%/60% forward and side overlap values and a 1-in. GSD, and processed using UASMaster. When compared to measurements taken from data collected using manned aircraft, the UAS data set had deltas within the minimum tolerance (3.28 ft) for well-defined points stated in AC 150/5300-17 and within the most stringent accuracy requirements (20 ft horizontal, 3 ft vertical) for obstacles stated in AC 150/5300-18 (FAA, 2017b; FAA, 2014).

The choice of processing software continued to play a significant role in the success of the AT solution processing. The M210/X7 data set that produced a viable AT solution when processed using UASMaster was unable to produce a viable AT solution when processed with Pix4D. This was due to the inability for pixel dimensions to be calibrated in Pix4D, which resulted in significant parallax and measurement error. UASMaster has the capability to account for differing x and y pixel dimensions, which greatly reduced the presence of parallax in the AT solution.

Flights using lower forward overlap settings of 70% were unable to produce AT solutions that were viable for accurate stereo analysis using the given GCP layout. The AT solutions produced from these flights showed considerably more parallax and geometric distortion than flights conducted with an 80% forward overlap. This resulted in high residuals when measuring GCP locations in stereo, indicating that the data sets were not suitable for obstacle data collection.

The X5S camera payload was incompatible with both processing software packages used during testing. This incompatibility resulted in the failure of the X5S to accurately report yaw, pitch, and roll values within the processing software, which prevented the calculation of each image's

exterior orientation. While these values are present in the metadata of the raw imagery, they are unable to be exported to an external format where they could be manually uploaded into the processing software. Without the ability to manually input these values, and the inability of the software to interpret them, no viable AT solution could be generated. Due to this finding, the X5S was excluded from further testing.

## 3.3 PERRY-FOLEY AIRPORT

FPY is a dual runway (18/36 and 12/30), non-towered airport in Perry, Florida, located in Class G airspace from the surface to 700 ft AGL. FPY was selected due to the availability of obstacle data collected in the study area using manned aircraft 3 months prior to UAS data collection.

The purpose of UAS obstacle data collection at FPY was to validate data collection parameters that generated successful data sets at WWD and GDJ in a third environment, while reintroducing the eBee X and WingtraOne platforms that could not operate at GDJ. An additional purpose was to further evaluate GCP layout requirements in areas of vegetation, as well as the visibility of alternative GCP construction methods.

Following the success of data collection and processing at FPY, select data sets were provided to the NGS for their review and validation. The NGS were brought into the research effort at this point due to the successful validation of technical and operational considerations developed during testing at WWD and GDJ. It was determined that an independent, unbiased evaluation of the data would ensure the validity of ensuing findings and recommendations.

Sections 3.3.1 through 3.3.6 describe the FPY study area, data collection parameters, procedures for obstacle data collection, results of data processing/analysis, and findings.

### 3.3.1 Data Collection

The study area at FPY was located on the south side of the airfield in the approach surface for Runway 36, as shown in the red-shaded area in Figure 25. A diverse range of obstacles were present in this area, including trees and man-made structures such as a building, fencing, a roadway, and airfield lights. Similar to WWD, the study area also included a substantial area of dense vegetation.

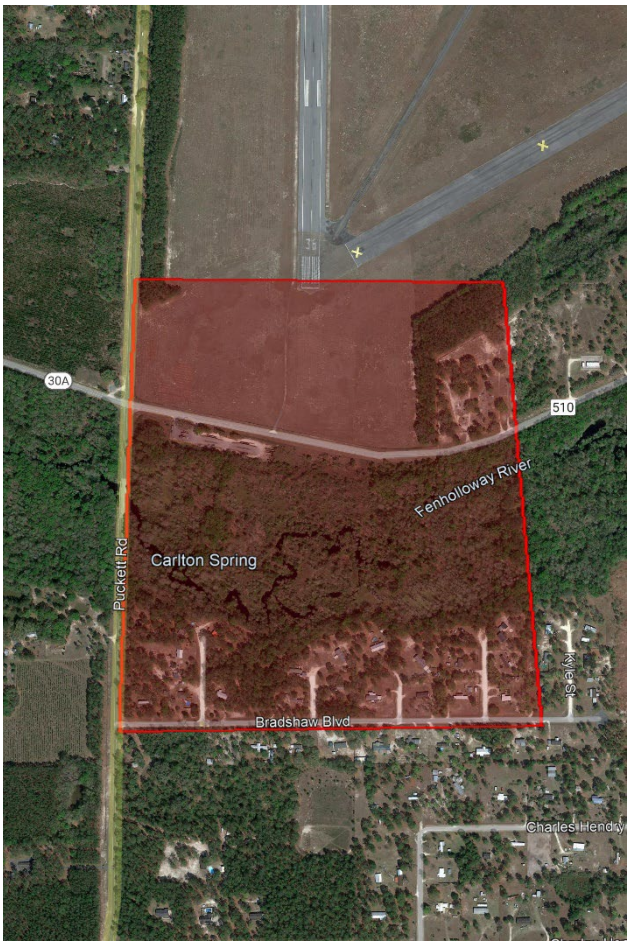


Figure 25. Perry-Foley Airport Study Limit

3.3.1.1 Onsite Preparation

Figure 26 depicts the approximate locations of the 24 GCPs that were established at FPY and used as part of the data post-processing workflow.

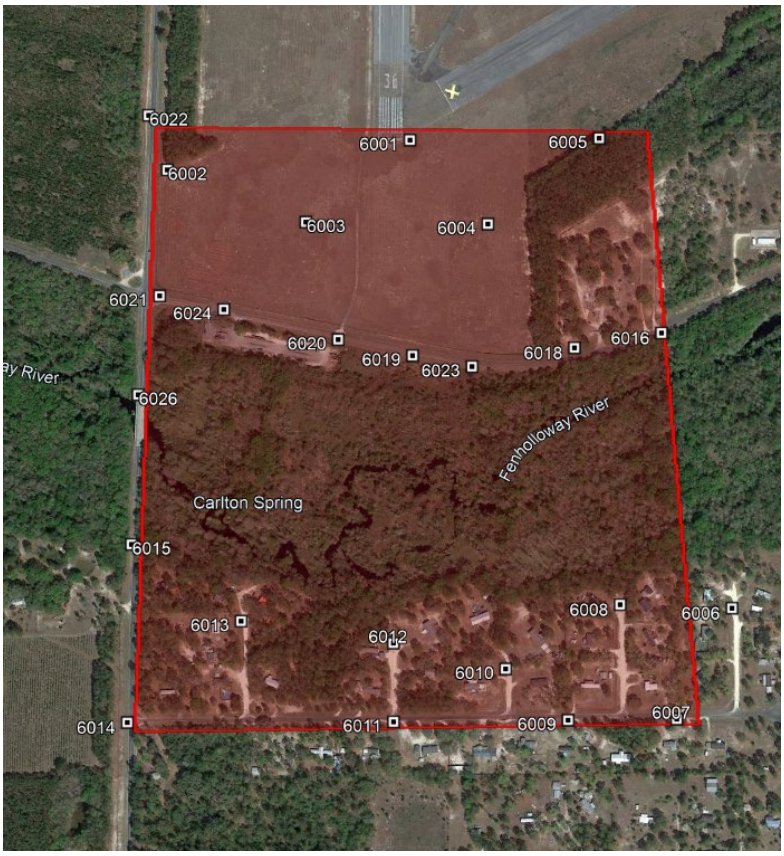


Figure 26. Perry-Foley Airport GCP Locations

UAS testing at WWD found that large areas without control had inconsistent tie point generation and, therefore, could not consistently support AT solutions that were viable for obstacle data collection when viewed in stereo. This finding was leveraged during the GCP layout design process at FPY by closely spacing GCPs surrounding the area of dense vegetation in the center of the study area. Many of the GCPs along the road in the center of the study area and in the neighborhood to the south are spaced considerably tighter than in previous test effort, and ranged from 300 ft to 500 ft apart.

The visibility of alternative GCP construction techniques was also evaluated at FPY. In addition to the standard chevron GCPs, redundant GCPs were placed at many locations using various alternative visual targets, such as 12-in. black-and-white circular tiles or white and black square tiles. These alternate GCPs were used solely to evaluate visibility and ease of identification within the imagery, and were not used when locating or measuring obstacles.

3.3.1.2 UAS Data Collection Parameters

The purpose of UAS data collection at FPY was to validate the parameters that were found to generate acceptable obstacle data sets at WWD and GDJ. These parameters included 80%/60% forward and side overlap values, and a GSD on 1 in. In addition to conducting data collection with the M210, the eBee X and WingtraOne (fixed-wing aircraft) were reintroduced after being unable

to collect data at GDJ. Due to 14 CFR 107.51 restrictions (Operating Limitations for Small Unmanned Aircraft, 2016), the WingtraOne could not be flown high enough to achieve a 1 in. GSD, and instead collected data with a 0.5-in. GSD as it did during a successful data collection effort at WWD. In total, three UAS data sets were collected. Table 17 summarizes the collection parameters for each UAS aerial survey conducted at FPY. Figure 27 depicts the UAS flight operations.

Table 17. Perry-Foley Airport UAS Aerial Survey Data Collection Parameters

| Date Collected | UAS | Sensor | Estimated GSD (in.) | Forward Overlap (%) | Side Overlap (%) | Altitude (ft AGL) | Sun Angle (degrees) | Flight Time (min) | Photo Count |
|---|---|---|---|---|---|---|---|---|---|
| 1/26/2021 | M210 | X7 | 1 | 80 | 60 | 340.5 | 42.2 | 40 | 499 |
| 1/26/2021 | eBee X | S.O.D.A. 3D | 1 | 80 | 60 | 368.1 | 28.4 | 28 | 703 |
| 1/26/2021 | WingtraOne | RXIR-II | 0.5 | 80 | 60 | 310.5 | 35.5 | 21 | 1050 |


Figure 27. Perry-Foley Airport UAS Operations Area

3.3.1.3 Manned Aircraft Data Collection

Approximately 3 months prior to UAS data collection, a manned aircraft survey was completed at FPY in accordance with guidance stated in AC 150/5300-17. Data were collected using an

UltraCam Eagle at a GSD of 6 in. and 60%/50% forward and side overlap values. Table 18 presents complete parameters for the manned aircraft aerial.

Table 18. Perry-Foley Airport Manned Aircraft Aerial Survey Parameters

| Date Collected | Sensor | Estimated GSD (in.) | Forward Overlap (%) | Side Overlap (%) | AGL (ft) | Flight Time (min) | Photo Count |
|---|---|---|---|---|---|---|---|
| 10/30/2020 | UltraCam Eagle | 6 | 60 | 50 | 9200 | ~5 | 11 |

### 3.3.2 Data Processing Results

Following data processing at GDJ, it was found that Pix4D did not produce valid AT solutions because it did not include the capability to customize pixel dimensions. Due to this limitation, each data set collected at FPY was processed using UASMaster. Table 19 presents the results of this processing effort. All three data sets were processed successfully, resulting in valid AT solutions with viable stereo pairs that were suitable for obstacle data collection during stereo analysis.

Table 19. Perry-Foley Airport Data Processing Results

| Test # | Processing Software | UAS | Sensor | Estimated GSD (in.) | Forward and Side Overlap % | Processing Results |
|---|---|---|---|---|---|---|
| **1** | UAS Master | M210 | Zenmuse X7 | 1 | 80/60 | Valid AT solution and viable stereo imagery. |
| **2** | UAS Master | eBee X | S.O.D.A. 3D | 1 | 80/60 | Valid AT solution and viable stereo imagery. |
| **3** | UAS Master | WingtraOne | Sony RX1R II | 0.5 | 80/60 | Valid AT solution and viable stereo imagery. |

### 3.3.3 Stereo Analysis—GCP Comparison Results

A stereo analysis effort was initiated to measure the surveyed GCP locations captured in each valid AT solution generated from UAS data collected at FPY. These locations were validated by comparing them to the field-surveyed GCP locations.

#### 3.3.3.1 Flight 1

Table 20 shows the RMSE between the GCP locations derived from the field survey and the M210 UAS imagery when measured in stereo. Cells shaded in red indicate measurements that do not meet the 3.28 ft (1 meter) accuracy standard stated in AC 150/5300-17 Section 8.1.1.2. Despite the inaccuracies of these individual points, the average RMSE for all GCPs is within the minimum tolerance (3.28 ft) stated in AC 150/5300-17, indicating that this data set was viable for obstacle data collection (FAA, 2017b).

Table 20. Ground Control Point Location Variance between Field Survey and UAS Test 1 (M210)

| GCP | RMSE X (ft) | RMSE Y (ft) | RMSE Z (ft) | Maximum Horizontal Error (ft) | Maximum Vertical Error (ft) |
|---|---|---|---|---|---|
| **6001** | 1.38 | 2.39 | 2.88 | 3.32 | 7.14 |
| **6002** | 0.44 | 1.91 | 0.37 | 2.13 | -0.82 |
| **6003** | 0.78 | 1.63 | 0.23 | 1.99 | 0.44 |
| **6004** | 2.05 | 1.59 | 0.20 | 2.75 | 0.41 |
| **6005** | 2.19 | 1.90 | 1.37 | 3.50 | 2.08 |
| **6006** | 2.70 | 0.55 | 1.01 | 2.81 | -1.06 |
| **6007** | 2.29 | 0.49 | 1.25 | 3.52 | 3.22 |
| **6008** | 1.86 | 0.83 | 0.31 | 2.36 | -0.60 |
| **6009** | 1.64 | 1.15 | 1.27 | 3.63 | 3.78 |
| **6010** | 1.64 | 0.66 | 0.38 | 2.00 | -0.73 |
| **6011** | 1.65 | 0.78 | 0.44 | 2.23 | 1.03 |
| **6012** | 1.82 | 0.51 | 0.11 | 2.03 | -0.18 |
| **6013** | 0.20 | 0.22 | 0.77 | 0.37 | -1.00 |
| **6014** | 0.13 | 0.41 | 0.67 | 0.52 | -0.54 |
| **6015** | 0.20 | 0.19 | 1.17 | 0.38 | -1.58 |
| **6016** | 3.13 | 0.12 | 1.15 | 3.27 | 1.35 |
| **6018** | 3.04 | 0.07 | 0.67 | 3.32 | -1.31 |
| **6019** | 1.80 | 0.53 | 0.40 | 2.06 | 0.56 |
| **6020** | 0.99 | 0.89 | 0.52 | 1.62 | 1.02 |
| **6021** | 0.46 | 0.99 | 0.53 | 1.24 | -0.74 |
| **6022** | 0.60 | 2.40 | 1.09 | 2.56 | 1.35 |
| **6023** | 2.71 | 0.56 | 0.34 | 3.04 | 0.71 |
| **6024** | 0.10 | 0.81 | 0.53 | 1.07 | -0.75 |
| **6026** | 0.52 | 0.90 | 0.42 | 1.06 | -0.65 |
| **AVERAGE:** | **1.41** | **0.88** | **0.70** | | |

The data in Table 20 show a significant decrease in accuracy when compared to previous data sets collected with the M210 and X7 at GDJ. The variances between the UAS data and field surveyed data were attributed to an unidentified issue with the X7 payload in which it failed to consistently remain in focus, and uncalibrated imagery on the northeast side of the test area. Figure 28 illustrates this uncalibrated imagery. In the figure, each overlapping green rectangle represents an image that was successfully calibrated. As outlined by the yellow rectangle (added later to illustrate failed calibration), many of the images in the easternmost flight lines failed to calibrate. This was a result of failed tie point extraction attributed to dense vegetation and lack of GCPs in this area to support processing.

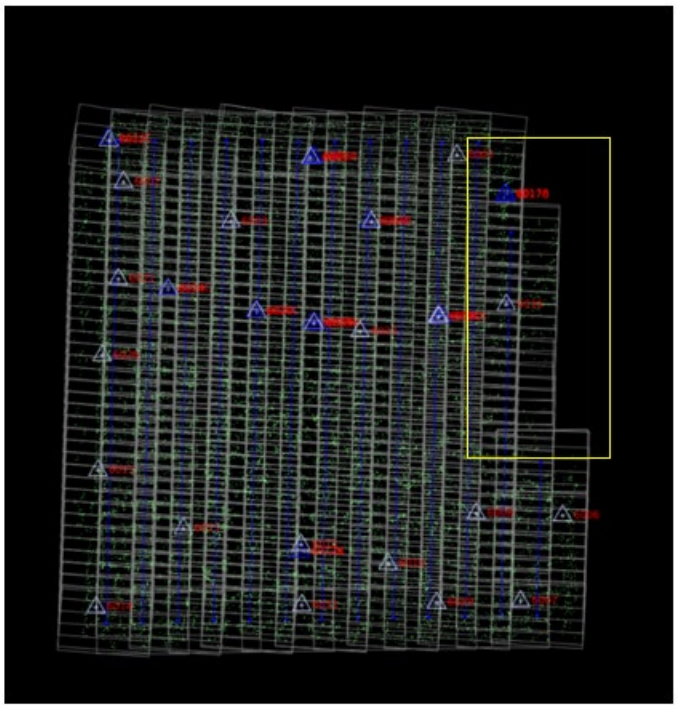

Figure 28. Failed Image Calibration (M210, X7)

3.3.3.2 Flight 2

Table 21 illustrates the RMSE between the GCP locations derived from the field survey and the eBee X UAS imagery when measured in stereo. As denoted by the green shading in all cells, this data set's overall average RMSE and all individual GCP locations were within the minimum tolerance (3.28 ft) stated in AC 150/5300-17, indicating that this data set was viable for obstacle data collection (FAA, 2017b).

Table 21. Ground Control Point Location Variance between Field Survey and UAS Test 2 (eBee X)

| GCP | RMSE X (ft) | RMSE Y (ft) | RMSE Z (ft) | Maximum Horizontal Error (ft) | Maximum Vertical Error (ft) |
|---|---|---|---|---|---|
| **6001** | 0.09 | 0.30 | 0.31 | 0.41 | 0.69 |
| **6002** | 0.33 | 0.20 | 0.57 | 0.82 | 1.28 |
| **6003** | 0.32 | 0.38 | 0.89 | 1.39 | 2.11 |
| **6004** | 0.23 | 0.27 | 0.72 | 0.57 | 1.33 |
| **6005** | 0.21 | 0.26 | 0.74 | 0.59 | 1.27 |
| **6006** | 0.21 | 0.17 | 0.43 | 0.42 | -0.90 |
| **6007** | 0.14 | 0.20 | 0.39 | 0.39 | 0.71 |
| **6008** | 0.17 | 0.45 | 0.69 | 1.22 | 1.78 |
| **6009** | 0.20 | 0.41 | 0.69 | 0.81 | 1.66 |
| **6010** | 0.22 | 0.07 | 0.32 | 0.35 | 0.71 |
| **6011** | 0.10 | 0.73 | 0.36 | 1.06 | 0.57 |
| **6012** | 0.28 | 0.52 | 0.52 | 1.49 | 1.50 |
| **6013** | 0.14 | 0.22 | 0.36 | 0.55 | 0.82 |
| **6014** | 0.12 | 0.36 | 0.27 | 0.54 | -0.42 |
| **6015** | 0.45 | 0.27 | 0.49 | 0.74 | -0.65 |
| **6016** | 0.19 | 0.16 | 0.28 | 0.55 | 0.73 |
| **6018** | 0.28 | 0.25 | 0.64 | 0.63 | 1.00 |
| **6019** | 0.08 | 0.15 | 0.49 | 0.31 | 0.82 |
| **6020** | 0.23 | 0.19 | 0.60 | 0.67 | 1.37 |
| **6021** | 0.44 | 0.28 | 0.95 | 1.00 | -1.83 |
| **6022** | 0.20 | 0.28 | 0.75 | 0.67 | 1.34 |
| **6023** | 0.38 | 0.21 | 0.67 | 0.66 | -1.49 |
| **6024** | 0.21 | 0.23 | 0.40 | 0.53 | 0.76 |
| **6026** | 0.27 | 0.47 | 0.69 | 0.74 | 1.51 |
| **AVERAGE:** | **0.23** | **0.29** | **0.55** | | |

3.3.3.3 Flight 3

Table 22 illustrates the RMSE between the GCP locations derived from the field survey and the WingtraOne imagery when measured in stereo. This data set's overall average RMSE and all individual GCP locations were within the minimum tolerance (3.28 ft) stated in AC 150/5300-17, indicating that this data set was viable for obstacle data collection (FAA, 2017b).

Table 22. Ground Control Point Location Variance between Field Survey and UAS Test 3 (WingtraOne)

| GCP | RMSE x (ft) | RMSE y (ft) | RMSE z (ft) | Maximum Horizontal Error (ft) | Maximum Vertical Error (ft) |
|---|---|---|---|---|---|
| **6001** | 0.10 | 0.05 | 0.32 | 0.17 | 0.40 |
| **6002** | 0.12 | 0.17 | 0.32 | 0.28 | 0.52 |
| **6003** | 0.09 | 0.12 | 0.32 | 0.20 | 0.62 |
| **6004** | 0.11 | 0.08 | 0.21 | 0.22 | 0.33 |
| **6005** | 0.07 | 0.08 | 0.25 | 0.18 | 0.47 |
| **6006** | 0.07 | 0.12 | 0.12 | 0.20 | -0.15 |
| **6007** | 0.19 | 0.17 | 0.28 | 0.36 | 0.38 |
| **6008** | 0.21 | 0.16 | 0.47 | 0.37 | 0.61 |
| **6009** | 0.15 | 0.32 | 0.25 | 0.48 | 0.38 |
| **6010** | 0.15 | 0.24 | 0.33 | 0.37 | 0.51 |
| **6011** | 0.19 | 0.24 | 0.37 | 0.54 | 0.47 |
| **6012** | 0.03 | 0.07 | 0.28 | 0.10 | 0.48 |
| **6013** | 0.10 | 0.07 | 0.40 | 0.13 | 0.45 |
| **6013** | 0.34 | 0.11 | 0.39 | 0.53 | 0.69 |
| **6014** | 0.10 | 0.26 | 0.11 | 0.32 | -0.20 |
| **6015** | 0.42 | 0.05 | 0.50 | 0.47 | -0.56 |
| **6016** | 0.20 | 0.16 | 0.33 | 0.46 | 0.53 |
| **6018** | 0.12 | 0.14 | 0.37 | 0.31 | 0.53 |
| **6019** | 0.09 | 0.08 | 0.24 | 0.23 | 0.46 |
| **6020** | 0.05 | 0.20 | 0.24 | 0.31 | 0.39 |
| **6021** | 0.11 | 0.09 | 0.14 | 0.18 | 0.27 |
| **6022** | 0.14 | 0.20 | 0.72 | 0.34 | 0.84 |
| **6023** | 0.14 | 0.15 | 0.30 | 0.34 | 0.39 |
| **6024** | 0.13 | 0.08 | 0.30 | 0.35 | 0.58 |
| **6026** | 0.23 | 0.06 | 0.22 | 0.27 | -0.29 |
| **AVERAGE:** | **0.15** | **0.14** | **0.31** | | |

### 3.3.4 Stereo Analysis—UAS Imagery to Manned Imagery Comparison Results

Sixteen obstacles were chosen at FPY from the manned aircraft aerial survey conducted in October 2020 and used as the basis of comparison in evaluating the accuracy of the UAS-collected obstacle data. These obstacles, whose locations are shown in Figure 29, were intentionally varied in both their geographic location and their type (e.g., trees, fencing, a building, utility poles).

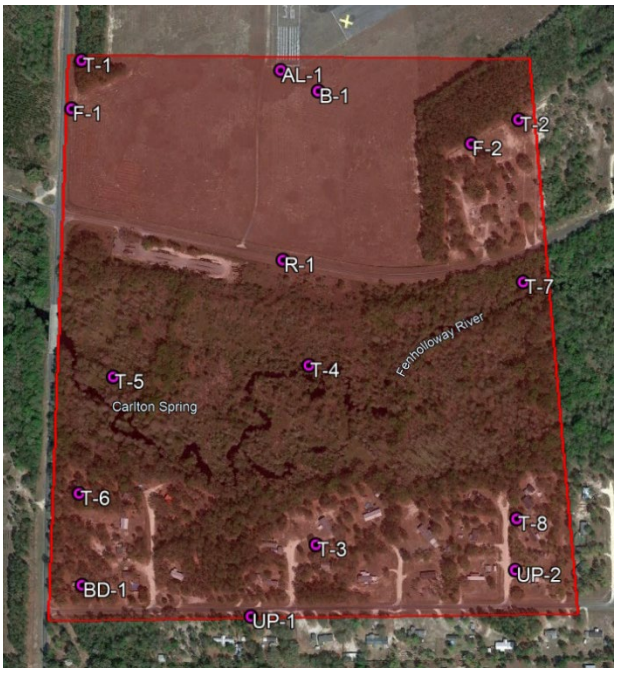


Figure 29. Perry-Foley Airport Obstacle Locations

3.3.4.1 Flight 1

Table 23 compares the x, y, and z locations for each of these obstacles derived from imagery collected using manned aircraft and the M210. This comparison shows that the locations of a significant number of obstacle locations did not meet the most stringent accuracy requirements (20 ft horizontal, 3 ft vertical) stated in AC-150/5300-18 when compared to data collected using manned aircraft (FAA, 2014). This failure to meet the accuracy standards was attributed to the dense vegetation present in the study area and lack of clarity in the imagery due to focus issues.

Table 23. Obstacle Location Variance between Manned Imagery and UAS Test 1 (M210)

| Obstacle | Manned Imagery (ft) | | | UAS Imagery (ft) | | | Delta (ft) | | |
|---|---|---|---|---|---|---|---|---|---|
| | x | y | z | x | y | z | x | y | z |
| **Airfield Light (AL-1)** | 2257858.27 | 387528.80 | 41.64 | 2257856.77 | 387530.79 | 40.66 | 1.50 | -1.99 | 0.98 |
| **Building (BD-1)** | 2256986.33 | 385224.08 | 51.08 | 2256986.56 | 385223.81 | 48.28 | -0.23 | 0.26 | 2.80 |
| **Bush (B-1)** | 2258027.31 | 387437.93 | 42.94 | 2258026.27 | 387437.15 | 41.50 | 1.04 | 0.78 | 1.43 |
| **Fence (F-1)** | 2256922.71 | 387350.77 | 45.97 | 2256922.97 | 387352.45 | 43.78 | -0.26 | -1.68 | 2.19 |
| **Fence (F-2)** | 2258715.05 | 387208.99 | 45.94 | 2258716.62 | 387212.74 | 45.41 | -1.57 | -3.75 | 0.52 |
| **Road (R-1)** | 2257875.48 | 386682.58 | 41.34 | 2257875.36 | 386682.70 | 40.23 | 0.12 | -0.13 | 1.11 |
| **Tree (T-1)** | 2256965.66 | 387566.78 | 48.99 | 2256965.87 | 387564.67 | 48.11 | -0.21 | 2.11 | 0.88 |
| **Tree (T-2)** | 2258926.27 | 387318.21 | 96.00 | 2258924.88 | 387320.21 | 82.56 | 1.39 | -2.00 | 13.44 |
| **Tree (T-3)** | 2258033.35 | 385413.60 | 91.80 | 2258033.90 | 385419.66 | 81.48 | -0.56 | -6.07 | 10.32 |
| **Tree (T-4)** | 2257995.04 | 386213.27 | 79.41 | 2257992.46 | 386217.36 | 70.32 | 2.58 | -4.09 | 9.08 |
| **Tree (T-5)** | 2257117.39 | 386154.75 | 85.98 | 2257117.75 | 386163.03 | 76.04 | -0.36 | -8.28 | 9.94 |
| **Tree (T-6)** | 2256969.46 | 385633.41 | 116.19 | 2256965.99 | 385633.48 | 97.72 | 3.47 | -0.06 | 18.46 |
| **Tree (T-7)** | 2258953.48 | 386593.78 | 94.15 | 2258960.23 | 386593.78 | 87.90 | -6.76 | 0.00 | 6.25 |
| **Tree (T-8)** | 2258932.41 | 385536.03 | 90.47 | 2258929.53 | 385541.52 | 72.81 | 2.88 | -5.50 | 17.66 |
| **Utility Pole (UP-1)** | 2257744.59 | 385090.73 | 71.85 | 2257742.66 | 385089.68 | 63.35 | 1.93 | 1.05 | 8.50 |
| **Utility Pole (UP-2)** | 2258927.54 | 385307.11 | 65.79 | 2258924.95 | 385307.32 | 56.23 | 2.59 | -0.21 | 9.56 |

3.3.4.2 Flight 2

Table 24 compares the x, y, and z measurements of obstacles derived from imagery collected using manned aircraft and the eBee X. As indicated by the red-shaded, the variance between a significant number of vertical obstacle locations in these data sets exceeded the accuracy requirements (20 ft horizontal, 3 ft vertical) stated in AC 150/5300-18 (FAA, 2014).

Table 24. Obstacle Location Variance between Manned Imagery and UAS Test 2 (eBee X)

| Obstacle | Manned Imagery (ft) | | | UAS Imagery (ft) | | | Delta (ft) | | |
|---|---|---|---|---|---|---|---|---|---|
| | x | y | z | x | y | z | x | y | z |
| **Airfield Light (AL-1)** | 2257858.27 | 387528.80 | 41.64 | 2257858.16 | 387528.11 | 42.15 | 0.10 | 0.69 | -0.51 |
| **Building (BD-1)** | 2256986.33 | 385224.08 | 51.08 | 2256986.17 | 385224.92 | 52.60 | 0.17 | -0.84 | -1.51 |
| **Bush (B-1)** | 2258027.31 | 387437.93 | 42.94 | 2258028.31 | 387438.02 | 43.41 | -1.00 | -0.09 | -0.47 |
| **Fence (F-1)** | 2256922.71 | 387350.77 | 45.97 | 2256922.59 | 387351.18 | 46.98 | 0.12 | -0.41 | -1.01 |
| **Fence (F-2)** | 2258715.05 | 387208.99 | 45.94 | 2258714.81 | 387209.66 | 47.07 | 0.23 | -0.66 | -1.13 |
| **Road (R-1)** | 2257875.48 | 386682.58 | 41.34 | 2257875.47 | 386682.24 | 41.68 | 0.01 | 0.33 | -0.34 |
| **Tree (T-1)** | 2256965.66 | 387566.78 | 48.99 | 2256965.14 | 387566.67 | 50.85 | 0.51 | 0.11 | -1.86 |
| **Tree (T-2)** | 2258926.27 | 387318.21 | 96.00 | 2258926.91 | 387318.29 | 100.64 | -0.64 | -0.08 | -4.64 |
| **Tree (T-3)** | 2258033.35 | 385413.60 | 91.80 | 2258031.56 | 385415.39 | 95.26 | 1.79 | -1.79 | -3.46 |
| **Tree (T-4)** | 2257995.04 | 386213.27 | 79.41 | 2257994.90 | 386212.35 | 83.10 | 0.15 | 0.92 | -3.69 |
| **Tree (T-5)** | 2257117.39 | 386154.75 | 85.98 | 2257117.14 | 386155.94 | 89.96 | 0.25 | -1.19 | -3.97 |
| **Tree (T-6)** | 2256969.46 | 385633.41 | 116.19 | 2256970.35 | 385637.26 | 122.97 | -0.90 | -3.84 | -6.79 |
| **Tree (T-7)** | 2258953.48 | 386593.78 | 94.15 | 2258954.20 | 386593.46 | 98.75 | -0.73 | 0.32 | -4.60 |
| **Tree (T-8)** | 2258932.41 | 385536.03 | 90.47 | 2258933.21 | 385535.22 | 94.91 | -0.80 | 0.81 | -4.44 |
| **Utility Pole (UP-1)** | 2257744.59 | 385090.73 | 71.85 | 2257743.80 | 385091.48 | 77.30 | 0.79 | -0.74 | -5.45 |
| **Utility Pole (UP-2)** | 2258927.54 | 385307.11 | 65.79 | 2258926.55 | 385307.94 | 63.11 | 0.99 | -0.83 | 2.68 |

An analysis of the eBee X imagery in UASMaster indicated that the inaccuracies observed in this data set were a result of significant lens distortion present in the S.O.D.A. 3D camera payload, and the failure of two flight lines on the eastern side of the test area to calibrate. This failed calibration, as illustrated in Figure 30, was attributed to failed tie point extraction caused by dense vegetation and insufficient GCPs in the area to support processing.

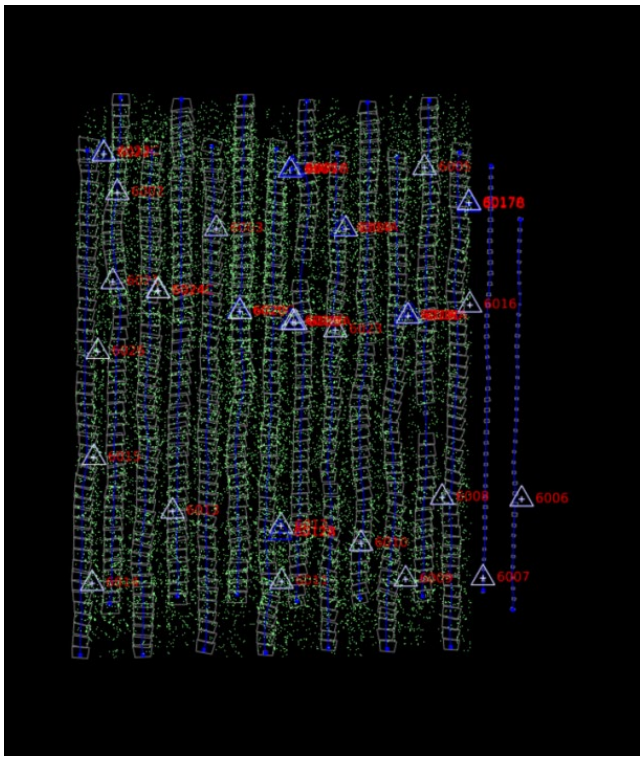


Figure 30. Failed Image Calibration (eBee X, S.O.D.A. 3D)

Despite the vertical discrepancies shown in Table 24, the horizontal locations between the manned and UAS data sets were remarkably similar, with only two obstacles with RMSEs greater than 2 ft (2.53 ft and 3.94 ft). The significant number of vertical discrepancies indicated that the comparison of UAS obstacle data to manned aircraft data might require augmentation via further ground truthing methods moving forward.

3.3.4.3 Flight 3

Table 25 compares the x, y, and z measurements of obstacles derived from imagery collected using manned aircraft and the WingtraOne. The WingtraOne produced the data set with the highest accuracies at FPY. As indicated by the red-shaded cells, three elevation values had a variance greater than the 3-ft vertical tolerance stated in the strictest accuracy requirements of AC 150/5300-18 (FAA, 2014). These discrepancies were attributed to failed image calibration and unsatisfactory tie point generation on the east side of the test area.

Table 25. Obstacle Location Variance between Manned Imagery and UAS Test 3 (WingtraOne)

| Obstacle | Manned Imagery (ft) | | | UAS Imagery (ft) | | | Delta (ft) | | |
|---|---|---|---|---|---|---|---|---|---|
| | x | y | z | x | y | z | x | y | z |
| **Airfield Light (AL-1)** | 2257858.27 | 387528.80 | 41.64 | 2257858.31 | 387528.37 | 41.65 | -0.04 | 0.43 | -0.01 |
| **Building (BD-1)** | 2256986.33 | 385224.08 | 51.08 | 2256986.45 | 385224.03 | 50.39 | -0.11 | 0.04 | 0.69 |
| **Bush (B-1)** | 2258027.31 | 387437.93 | 42.94 | 2258028.55 | 387437.90 | 43.18 | -1.24 | 0.03 | -0.25 |
| **Fence (F-1)** | 2256922.71 | 387350.77 | 45.97 | 2256922.60 | 387350.70 | 45.16 | 0.11 | 0.07 | 0.82 |
| **Fence (F-2)** | 2258715.05 | 387208.99 | 45.94 | 2258714.74 | 387209.66 | 46.08 | 0.30 | -0.67 | -0.14 |
| **Road (R-1)** | 2257875.48 | 386682.58 | 41.34 | 2257875.48 | 386682.58 | 40.87 | 0.00 | 0.00 | 0.46 |
| **Tree (T-1)** | 2256965.66 | 387566.78 | 48.99 | 2256965.47 | 387566.28 | 48.96 | 0.18 | 0.49 | 0.04 |
| **Tree (T-2)** | 2258926.27 | 387318.21 | 96.00 | 2258925.56 | 387318.29 | 98.63 | 0.72 | -0.08 | -2.64 |
| **Tree (T-3)** | 2258033.35 | 385413.60 | 91.80 | 2258032.78 | 385413.05 | 109.88 | 0.57 | 0.55 | -18.09 |
| **Tree (T-4)** | 2257995.04 | 386213.27 | 79.41 | 2257994.02 | 386213.73 | 78.30 | 1.03 | -0.46 | 1.10 |
| **Tree (T-5)** | 2257117.39 | 386154.75 | 85.98 | 2257117.31 | 386155.72 | 88.91 | 0.08 | -0.97 | -2.92 |
| **Tree (T-6)** | 2256969.46 | 385633.41 | 116.19 | 2256972.33 | 385635.77 | 114.99 | -2.88 | -2.36 | 1.19 |
| **Tree (T-7)** | 2258953.48 | 386593.78 | 94.15 | 2258953.50 | 386593.94 | 96.73 | -0.03 | -0.16 | -2.59 |
| **Tree (T-8)** | 2258932.41 | 385536.03 | 90.47 | 2258931.88 | 385535.52 | 100.74 | 0.53 | 0.51 | -10.27 |
| **Utility Pole (UP-1)** | 2257744.59 | 385090.73 | 71.85 | 2257744.37 | 385089.79 | 71.94 | 0.23 | 0.94 | -0.09 |
| **Utility Pole (UP-2)** | 2258927.54 | 385307.11 | 65.79 | 2258926.49 | 385307.76 | 62.51 | 1.05 | -0.66 | 3.27 |

Figure 31 depicts failed image calibration in the WingtraOne data set in the northeast of the study area. Despite this failure, the image calibration issues were significantly better than those experienced by the M210 and eBee X data sets shown in Figures 28 and 30, respectively. The increased success of the WingtraOne in comparison to the other platforms was attributed to the higher quality lens of the RX1R-II, which experienced significantly less lens distortion than the other camera payloads.

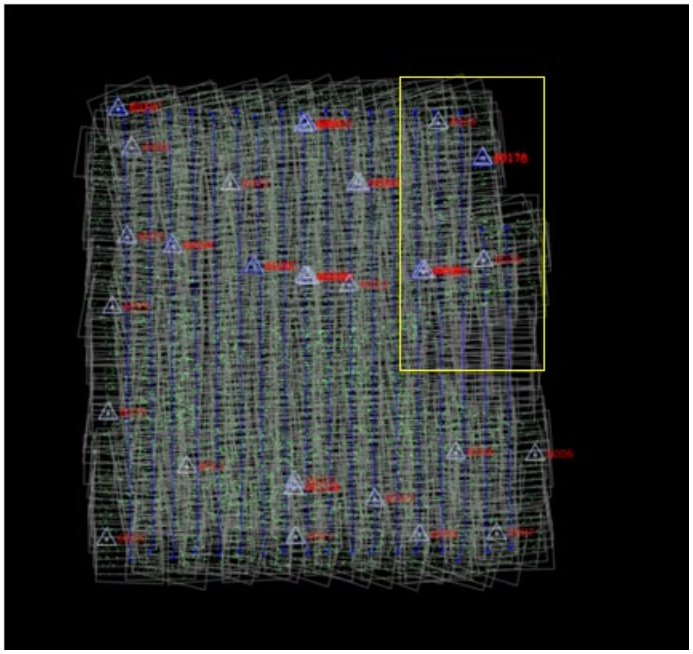

Figure 31. Failed Image Calibration (WingtraOne, RX1R-II)

As shown in Table 25, horizontal discrepancies between the WingtraOne data and manned aircraft were minimal, with only a single obstacle with a combined horizontal RMSE greater than 2 ft. This high level of horizontal consistency mixed with a significant number of vertical discrepancies closely matched the results from Flight 2, and served as an additional indication that future testing and evaluations would benefit from using further ground-truthing methods.

### 3.3.5 National Geodetic Survey Stereo Analysis—UAS Imagery to Manned Imagery Comparison Results

The data sets collected using the eBee X and WingtraOne (Flights 2 and 3) were provided to the NGS along with the data collected using manned aircraft. The NGS performed their own independent stereo analysis on each data set, in which they independently identified 29 obstacles rather than using the 16 previously used during internal stereo analysis. These obstacles were used to compare the measurements derived from the different data sources.

#### 3.3.5.1 Flight 2

Table 26 compares the NGS' x, y, and z measurements of obstacles derived from imagery collected using manned aircraft and the eBee X. As indicated by the red-shaded cells, only elevation values had a variance greater than the 3-ft vertical tolerance stated in the strictest accuracy requirements of AC 150/5300-18 (FAA, 2014). These data validated the results from the internal stereo analysis that showed horizontal locations between the UAS and manned aircraft falling within this tolerance while several of the vertical locations did not.

Table 26. National Geodetic Survey Obstacle Location Variance between Manned Imagery and UAS Test 2 (eBee X)

| Obstacle Type | Manned Imagery (ft) | | | UAS Imagery (ft) | | | Delta (ft) | | |
|---|---|---|---|---|---|---|---|---|---|
| | x | y | z | x | y | z | x | y | z |
| **Fence** | 2256923 | 387350.9 | 46 | 2256922 | 387350.6 | 45.3 | 1 | 0.3 | 0.7 |
| **Pole** | 2256836 | 386941 | 79.8 | 2256835 | 386939.6 | 79.7 | 0.7 | 1.4 | 0.1 |
| **Primary Road** | 2257839 | 386689.4 | 57 | 2257838 | 386689.6 | 55.4 | 1.3 | -0.2 | 1.6 |
| **Primary Road** | 2257707 | 386716.7 | 56 | 2257708 | 386715.2 | 55.6 | -1 | 1.5 | 0.4 |
| **Primary Road** | 2256874 | 387091.9 | 54 | 2256873 | 387091 | 53.6 | 1.4 | 0.9 | 0.4 |
| **Primary Road** | 2256885 | 387435.4 | 54 | 2256885 | 387434.7 | 53.5 | 0.2 | 0.7 | 0.5 |
| **Primary Road** | 2258049 | 386648.7 | 57 | 2258048 | 386648.7 | 56.8 | 0.4 | 0 | 0.2 |
| **Primary Road** | 2257643 | 386728.3 | 56 | 2257642 | 386728.3 | 56.3 | 0.7 | 0 | -0.3 |
| **Tree** | 2257011 | 386146.4 | 117.5 | 2257015 | 386154.5 | 114.3 | -3.6 | -8.1 | 3.2 |
| **Tree** | 2257540 | 385452.5 | 112.5 | 2257545 | 385452.6 | 113.9 | -5.7 | -0.1 | -1.4 |
| **Tree** | 2257483 | 386709.8 | 81 | 2257486 | 386712 | 83 | -3.4 | -2.2 | -2 |
| **Tree** | 2259133 | 385381.5 | 98 | 2259131 | 385380.7 | 100 | 2 | 0.8 | -2 |
| **Tree** | 2257706 | 385483.2 | 94.5 | 2257707 | 385483.2 | 97.8 | -0.2 | 0 | -3.3 |
| **Tree** | 2257539 | 385500 | 112.5 | 2257542 | 385499 | 118.5 | -2.8 | 1 | -6 |
| **Tree** | 2257696 | 385163.8 | 97.5 | 2257692 | 385166.5 | 98.8 | 4 | -2.7 | -1.3 |
| **Tree** | 2257833 | 385160.9 | 92.5 | 2257833 | 385162.7 | 96.7 | -0.3 | -1.8 | -4.2 |
| **Tree** | 2256925 | 386215.4 | 103.5 | 2256920 | 386211.2 | 106.7 | 5.8 | 4.2 | -3.2 |
| **Tree** | 2257803 | 385152.6 | 88.5 | 2257803 | 385152.6 | 90.3 | 0.3 | 0 | -1.8 |
| **Tree** | 2256876 | 385469.4 | 110.5 | 2256875 | 385472.2 | 110.2 | 1.1 | -2.8 | 0.3 |
| **Tree** | 2258219 | 385347.9 | 103.5 | 2258219 | 385345.3 | 107 | -0.1 | 2.6 | -3.5 |
| **Tree** | 2257624 | 385636.1 | 89.5 | 2257624 | 385638.7 | 91.3 | 0.3 | -2.6 | -1.8 |
| **Tree** | 2257047 | 385461.7 | 111.5 | 2257048 | 385460.1 | 111.8 | -0.8 | 1.6 | -0.3 |
| **Tree** | 2257649 | 385460.5 | 93.5 | 2257646 | 385456.4 | 100.5 | 2.2 | 4.1 | -7 |
| **Tree** | 2258161 | 385495.9 | 91.5 | 2258156 | 385496.5 | 102.8 | 4.9 | -0.6 | -11.3 |
| **Tree** | 2256855 | 385307.6 | 120.5 | 2256856 | 385307.2 | 125.5 | -0.2 | 0.4 | -5 |
| **Tree** | 2256970 | 385633.8 | 114.5 | 2256971 | 385635.4 | 121.2 | -1.8 | -1.6 | -6.7 |
| **Tree** | 2258036 | 385414.1 | 93.5 | 2258038 | 385408 | 89.8 | -2.57 | 6.1 | 3.7 |
| **Tree** | 2259216 | 385249.8 | 108 | 2259211 | 385255.3 | 112.6 | 5.7 | -5.5 | -4.6 |
| **Tree** | 2259281 | 385551.4 | 95 | 2259281 | 385556.3 | 100.6 | -0.1 | -4.9 | -5.6 |

### 3.3.5.2 Flight 3

Table 27 compares the NGS' x, y, and z measurements of obstacles derived from imagery collected using manned aircraft and the WingtraOne when viewed in stereo. This data set further validated results from internal analysis in which all horizontal obstacle positions derived from UAS data were within the strictest accuracy requirements (20 ft) stated in AC 150/5300-18 (FAA, 2014), but several vertical locations did not meet the requirement (3 ft).

Table 27. National Geodetic S Obstacle Location Variance between Manned Imagery and UAS Test 3 (WingtraOne)

| Obstacle | Manned Imagery (ft) | | | UAS Imagery (ft) | | | Delta (ft) | | |
|---|---|---|---|---|---|---|---|---|---|
| | x | y | z | x | y | z | x | y | z |
| **Fence** | 2256922.5 | 387351 | 46 | 2256922 | 387351 | 45.1 | 1 | 0.1 | 0.9 |
| **Pole** | 2256836.1 | 386941 | 79.8 | 2256836 | 386941 | 79.7 | -0.1 | 0 | 0.1 |
| **Primary Road** | 2257839 | 386689 | 57 | 2257840 | 386690 | 56 | -0.7 | -0.2 | 1 |
| **Primary Road** | 2257707 | 386717 | 56 | 2257707 | 386716 | 55.9 | 0 | 1 | 0.1 |
| **Primary Road** | 2256874.4 | 387092 | 54 | 2256874 | 387091 | 53.2 | 0.7 | 0.6 | 0.8 |
| **Primary Road** | 2256884.9 | 387435 | 54 | 2256885 | 387435 | 53.4 | 0.4 | 0.2 | 0.6 |
| **Primary Road** | 2258048.5 | 386649 | 57 | 2258048 | 386649 | 56.2 | 0.5 | 0 | 0.8 |
| **Primary Road** | 2257642.8 | 386728 | 56 | 2257642 | 386728 | 55 | 0.7 | 0.1 | 1 |
| **Tree** | 2257011.2 | 386146 | 118 | 2257011 | 386145 | 110 | 0.3 | 1.3 | 7.7 |
| **Tree** | 2257539.6 | 385453 | 113 | 2257542 | 385452 | 109 | -2.5 | 0.4 | 3.9 |
| **Tree** | 2257483 | 386710 | 81 | 2257486 | 386712 | 79.7 | -3 | -2.5 | 1.3 |
| **Tree** | 2259132.6 | 385382 | 98 | 2259131 | 385381 | 96.5 | 2.1 | 0.8 | 1.5 |
| **Tree** | 2257706.4 | 385483 | 94.5 | 2257707 | 385483 | 93 | -0.9 | -0.1 | 1.5 |
| **Tree** | 2257539.2 | 385500 | 113 | 2257540 | 385500 | 112 | -0.9 | 0.4 | 0.1 |
| **Tree** | 2257695.7 | 385164 | 97.5 | 2257694 | 385164 | 95.2 | 2.2 | -0.2 | 2.3 |
| **Tree** | 2257832.9 | 385161 | 92.5 | 2257834 | 385161 | 92.1 | -1.5 | 0.2 | 0.4 |
| **Tree** | 2256925.4 | 386215 | 104 | 2256925 | 386217 | 97.8 | 0.6 | -1.9 | 5.7 |
| **Tree** | 2257803 | 385153 | 88.5 | 2257803 | 385151 | 86.9 | -0.1 | 1.6 | 1.6 |
| **Tree** | 2256876 | 385469 | 111 | 2256876 | 385471 | 107 | -0.2 | -1.9 | 4 |
| **Tree** | 2258218.9 | 385348 | 104 | 2258219 | 385346 | 101 | 0 | 2.3 | 3 |
| **Tree** | 2257624.3 | 385636 | 89.5 | 2257625 | 385639 | 88.4 | -0.3 | -2.9 | 1.1 |
| **Tree** | 2257047.4 | 385462 | 112 | 2257047 | 385460 | 107 | 0.8 | 1.3 | 4.2 |
| **Tree** | 2257648.5 | 385461 | 93.5 | 2257649 | 385457 | 96.9 | -0.1 | 3.5 | -3.4 |
| **Tree** | 2258160.6 | 385496 | 91.5 | 2258157 | 385498 | 93.6 | 3.9 | -1.8 | -2.1 |
| **Tree** | 2256855.3 | 385308 | 121 | 2256854 | 385304 | 119 | 1.1 | 3.6 | 1.9 |
| **Tree** | 2256969.6 | 385634 | 115 | 2256971 | 385634 | 115 | -1.6 | 0.3 | -0.6 |
| **Tree** | 2258035.6 | 385414 | 93.5 | 2258027 | 385413 | 87.3 | 8.63 | 0.9 | 6.2 |
| **Tree** | 2259216.3 | 385250 | 108 | 2259209 | 385255 | 108 | 7.1 | -4.8 | -0.3 |
| **Tree** | 2259280.6 | 385551 | 95 | 2259279 | 385556 | 97.4 | 1.6 | -4.8 | -2.4 |

### 3.3.6 Findings

All UAS obstacle data sets collected at FPY produced valid AT solutions when processed with UASMaster and were found to be viable for obstacle data collection and measurement. This validated the efficacy of using 80%/60% forward and side overlap settings with a 1.0-in. GSD for the eBee X and M210, and a 0.5-in. GSD for the WingtraOne.

When comparing GCP location accuracy between data collected using manned aircraft and UASs, the data sets had deltas within the minimum tolerance for well-defined points (3.28 ft) stated in

AC 150/5300-17 (FAA, 2017b). When comparing obstacle locations, all obstacles were found to be within the horizontal accuracy requirement (20 ft) stated in AC 150/5300-18 (FAA, 2014); however, a significant number of obstacles in each data set, all of which were trees, failed to meet the vertical accuracy requirement (3 ft).

Following their independent analysis, the NGS found that the quality and accuracy of the UAS imagery collected at FPY was comparable to imagery collected by manned aircraft. They did, however, express concern regarding the number of images required to cover the survey area versus manned aircraft and its impact on the time required for verification and validation.

The GCP layout established at FPY was sufficient to develop AT solutions and complete the subsequent stereo analysis, however, the east side of the survey area did not have sufficient ground control due to extensive vegetation, as shown in Figure 26 in Section 3.3.1.1. This was the only area at FPY where GCPs were consistently spaced more than 500 ft apart, resulting in failed image calibration along two flight lines on the east side of the test area for all three data sets.

The alternative GCP construction methods used at FPY had no significant effect on measurement accuracy. Neither the alternative coloration nor alternative shapes were reported as being easier to pick out of the imagery by the photogrammetric technician when compared to the standard white chevrons. It was found that as long as the imagery was properly exposed, that these alternative GCPs did not make a substantial contribution to the collection and measurement process. The white chevrons were found to be the preferred target for operation efficiency and visual acuity.

## 3.4 CINCINNATI WEST AIRPORT

I67 is a single runway (1/19), non-towered airport in Harrison, Ohio, located in Class G airspace from the surface to 700 ft AGL. I67 was selected due to the presence of a diverse set of man-made and natural obstacles.

In addition to the continued validation of previous findings regarding overlap, GSD, processing software, and GCP layout, the goal of data collection at I67 was to address additional questions regarding obstacle data collection, including the effects of sun angle, additional RTK equipment, and alternative flight line layouts. Limited flights were also conducted with higher and lower overlaps than what was previously validated to see if they could develop acceptable data sets when paired with a more robust GCP layout.

During FPY data analysis it was hypothesized that the UAS data might be capable of measuring obstacles with greater accuracy than manned aircraft. To assess the true accuracy of the UAS obstacle data, a traditional field survey was conducted at I67 and used as the control data set when evaluating UASs and manned aircraft data accuracy.

Following internal analysis, select UAS data sets were again provided to the NGS for independent verification and validation. The NGS performed their own obstacle data collection using the UAS data and previously collected manned aircraft imagery in stereo and compared the results with the FAA-collected field survey data.

Sections 3.4.1 through 3.4.7 describe the I67 study area, data collection parameters, procedures for obstacle data collection, results of data processing/analysis, and findings.

### 3.4.1 Data Collection

The study area at I67, shown in the red-shaded area in Figure 32, covered the entire airfield. A diverse range of obstacles was present in this area, including natural obstacles such as trees and man-made structures including buildings, fencing, a roadway, and airfield lights.

Due to the volume of air traffic at I67 and the size of the testing site, the study area was divided into three areas. This allowed for the use of shorter flight plans, reducing the likelihood of a test being interrupted by manned air traffic. All three areas had both man-made and natural obstacles for analysis. To decrease the impact on airport operations, only Test Area C was flown for the low overlap and sun angle test flights. Test Area C was chosen because of its particularly diverse mix of man-made and vegetative obstacles. Multiple VOs were used in each area to ensure no nonparticipants were present in the UAS operations areas during data collection.

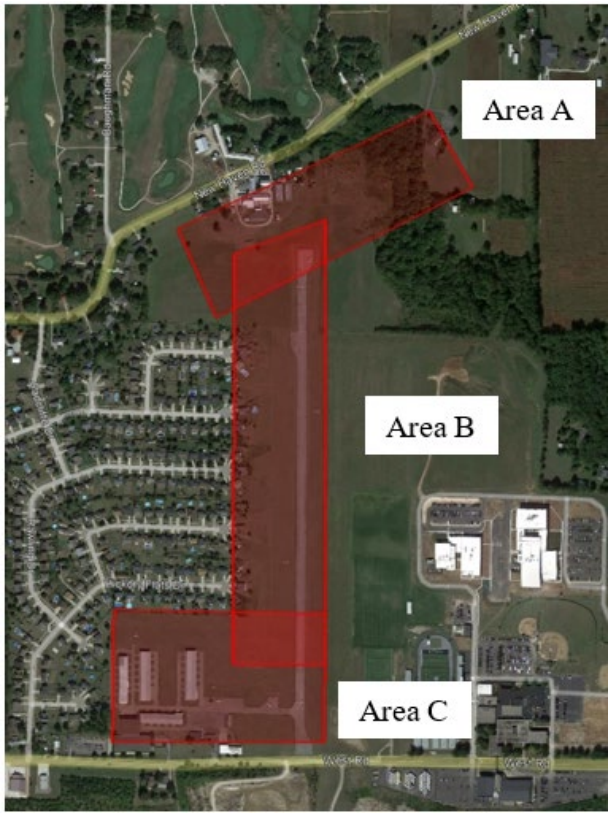


Figure 32. Cincinnati West Airport Study Area

#### 3.4.1.1 Onsite Preparation

Figure 33 depicts the study limits and the approximate location of the 37 GCPs that were used as part of the data post-processing workflow.

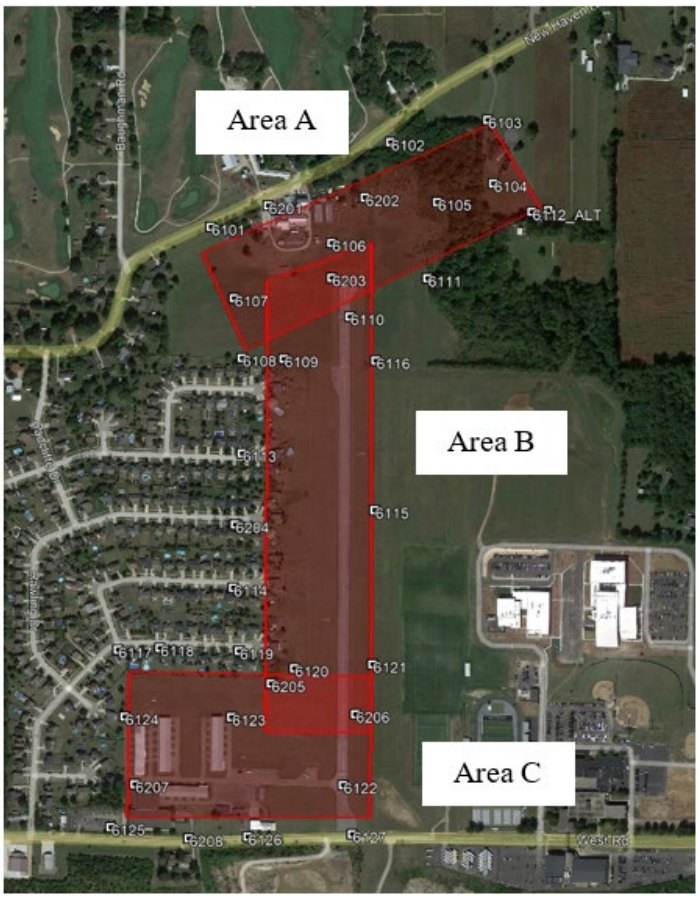


Figure 33. Cincinnati West Airport GCP Locations

While designing the GCP layout for I67, GCPs were placed surrounding the entire test area no more than 500 ft apart. This was based on the finding from FPY in which the only area that failed to produce adequate tie points was in an area where GCPs were more than 500 ft apart. Additional control was placed within Test Area A due to the presense of dense vegetation.

Testing at FPY found that alternative GCP construction methods provided no benefit with respect to data processing efficiency or accuracy when compared to the standard white chevrons. Based on this finding, only white chevrons and existing photo identifiable points (such as sidewalk corners) were used as GCPs at I67.

3.4.1.2 UAS Data Collection Parameters

The primary purpose of UAS data collection at I67 was to validate the parameters that had consistently generated acceptable obstacle data sets at WWD, GDJ, and FPY, including 80%/60% forward and side overlap values and GSD values of 1 in. and 0.5 in. In addition to validating these parameters, flights were conducted to assess the effects of additional factors, including sun angle, RTK and non-RTK UASs, and interlaced flight lines. In total, 28 UAS data sets were collected at I67.

In addition to the M210, eBee X, and WingtraOne, the Inspire 2 was used with the X7 to compare against data collected by the M210. By collecting data with the same camera payload, these tests allowed for an assessment of the Inspire 2's and M210's different GPS modules, and specifically RTK versus non-RTK.

The effect of interlaced flight lines was assessed at I67 using the eBee X. The eBee X is capable of performing missions with interlaced flight lines rather than the standard sequential flight lines, which can improve the efficiency of fixed-wing operations by traversing flight lines in an alternating sequence. This enables the platform to make smaller turns which reduces time spent flying outside of the study area. Figure 34 illustrates the differences between interlaced and sequential flight lines.

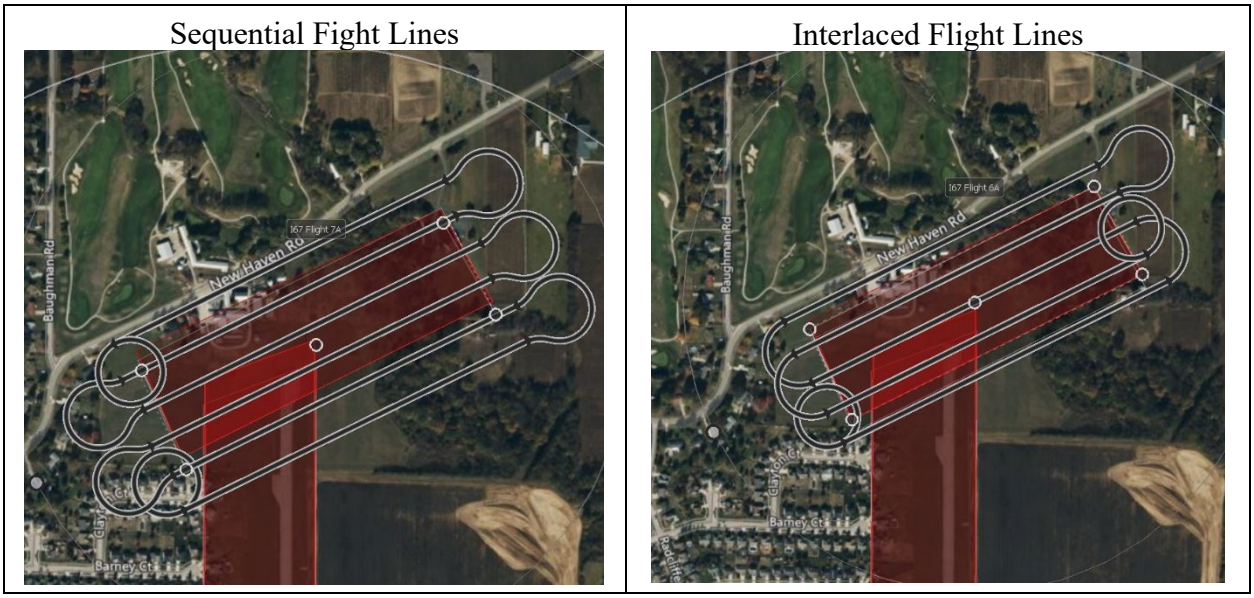


Figure 34. Comparison of eBee X Flight Plans with Sequential and Interlaced Flight Lines

Tests 9 and 10 were flown to evaluate the effect of sun angle (during different times of the day) on the quality of the UAS aerial survey data. Both flights were conducted with the M210 with identical data collection parameters. Test 9 was flown from 7:43 A.M. to 8:07 A.M. when the sun angle averaged 15°, and Test 10 was flown approximately 12 hours later from 7:37 P.M. to 7:52 P.M. when the sun angle averaged 13°. The results from these flights were intended to be compared to Test 1-C, which was an identical flight conducted at midday. All other tests were conducted with the sun angle ranging from 28.09° to 69.84°.

Higher and lower overlap settings were previously tested at WWD and GDJ, but they were done so with less than adequate GCP layouts. Since the GCP layout at I67 was so robust, additional tests of varying overlap settings were conducted to assess their effect on collection efficiency and data quality. In particular, a data set was collected with each UAS using 70%/70% forward and side overlap settings to evaluate their effect on the data quality. The 70% forward overlap allowed each UAS to fly faster than flights conducted with an 80% forward overlap, improving operational efficiency. Table 28 summarizes the collection parameters for each of the 28 UAS aerial surveys conducted at I67. Figure 35 presents the three UAS operations areas used at I67.

Table 28. Cincinnati West Airport UAS Data Collection Parameters

| Test # | Test Area | Date Collected | UAS | Sensor | Estimated GSD (in.) | Forward Overlap (%) | Side Overlap (%) | Altitude (ft AGL) | Sun Angle (degrees) | Flight Time (min) | Photo Count |
|---|---|---|---|---|---|---|---|---|---|---|---|
| **1-A** | A | 7/20/2021 | M210 | X7 | 1 | 80 | 80 | 340.5 | 32.4 | 23 | 282 |
| **1-B** | B | 7/19/2021 | M210 | X7 | 1 | 80 | 80 | 340.5 | 55.5 | 19 | 300 |
| **1-C** | C | 7/20/2021 | M210 | X7 | 1 | 80 | 80 | 340.5 | 70.4 | 19 | 260 |
| **2-A** | A | 7/20/2021 | M210 | X7 | 1 | 80 | 60 | 340.5 | 35.9 | 9 | 147 |
| **2-B** | B | 7/19/2021 | M210 | X7 | 1 | 80 | 60 | 340.5 | 60.3 | 9 | 149 |
| **2-C** | C | 7/20/2021 | M210 | X7 | 1 | 80 | 60 | 340.5 | 55.7 | 7 | 117 |
| **3-A** | A | 7/20/2021 | M210 | X7 | 1 | 80 | 60 | 340.5 | 37.8 | 9 | 146 |
| **3-B** | B | 7/19/2021 | M210 | X7 | 1 | 80 | 60 | 340.5 | 66.2 | 8 | 149 |
| **3-C** | C | 7/19/2021 | M210 | X7 | 1 | 80 | 60 | 340.5 | 28.3 | 8 | 118 |
| **4-A** | A | 7/20/2021 | Inspire 2 | X7 | 1 | 80 | 80 | 340.5 | 61 | 16 | 287 |
| **4-B** | B | 7/19/2021 | Inspire 2 | X7 | 1 | 80 | 80 | 340.5 | 68.9 | 15 | 302 |
| **4-C** | C | 7/19/2021 | Inspire 2 | X7 | 1 | 80 | 80 | 340.5 | 31.8 | 15 | 262 |
| **5-A** | A | 7/20/2021 | Inspire 2 | X7 | 1 | 80 | 60 | 340.5 | 67.7 | 9 | 149 |
| **5-B** | B | 7/20/2021 | Inspire 2 | X7 | 1 | 80 | 60 | 340.5 | 43.6 | 10 | 154 |
| **5-C** | C | 7/19/2021 | Inspire 2 | X7 | 1 | 80 | 60 | 340.5 | 38.5 | 12 | 119 |
| **6-A** | A | 7/19/2021 | eBee X | S.O.D.A. 3D | 1 | 80 | 60 | 368.1 | 57.7 | 6 | 151 |
| **6-B** | B | 7/19/2021 | eBee X | S.O.D.A. 3D | 1 | 80 | 60 | 368.1 | 61.7 | 11 | 272 |
| **6-C** | C | 7/20/2021 | eBee X | S.O.D.A. 3D | 1 | 80 | 60 | 368.1 | 65.4 | 24 | 184 |
| **7-A** | A | 7/19/2021 | eBee X | S.O.D.A. 3D | 1 | 80 | 60 | 368.1 | 56.5 | 9 | 182 |
| **7-B** | B | 7/19/2021 | eBee X | S.O.D.A. 3D | 1 | 80 | 60 | 368.1 | 59.6 | 15 | 255 |
| **7-C*** | C | 7/19/2021 | eBee X | S.O.D.A. 3D | 1 | 80 | 60 | 368.1 | *N/A | *N/A | *N/A |
| **8-A** | A | 7/19/2021 | WingtraOne | RXIR-II | 0.5 | 80 | 60 | 310.5 | 71.2 | 9 | 314 |
| **8-B** | B | 7/19/2021 | WingtraOne | RXIR-II | 0.5 | 80 | 60 | 310.5 | 70.8 | 9 | 447 |
| **8-C** | C | 7/19/2021 | WingtraOne | RXIR-II | 0.5 | 80 | 60 | 310.5 | 70.4 | 8 | 312 |
| **9** | C | 7/20/2021 | M210 | X7 | 1 | 80 | 80 | 340.5 | 15.6 | 15 | 259 |
| **10** | C | 7/20/2021 | M210 | X7 | 1 | 80 | 80 | 340.5 | 13 | 16 | 249 |
| **11** | A | 7/20/2021 | WingtraOne | RXIR-II | 0.5 | 70 | 70 | 310.5 | 65.5 | 10 | 251 |
| **12** | A | 7/19/2021 | eBee X | S.O.D.A. 3D | 1 | 70 | 70 | 368.1 | 54.2 | 17 | 172 |
| **13** | A | 7/20/2021 | M210 | X7 | 1 | 70 | 70 | 340.5 | 52.2 | 9 | 130 |

*Unable to fly due to the presence of nonparticipants.

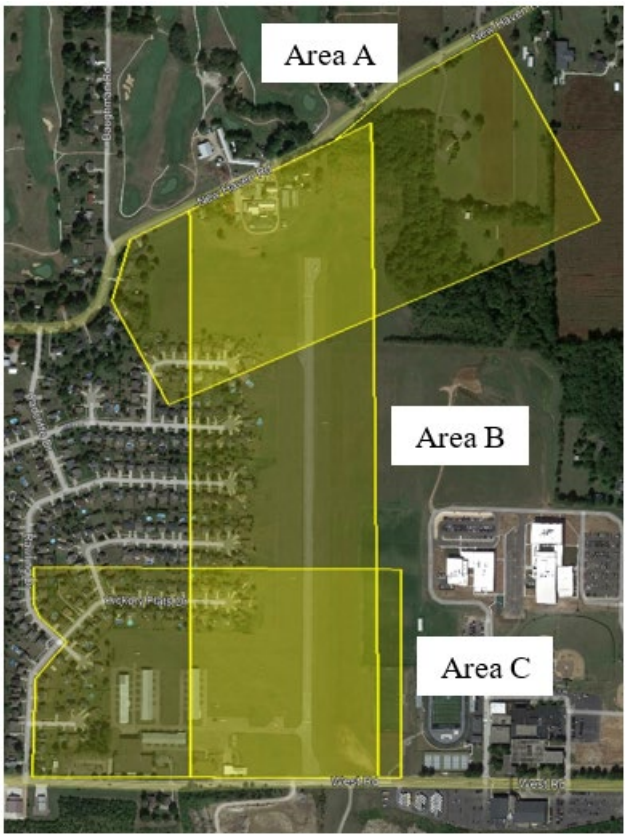


Figure 35. Cincinnati West Airport UAS Operations Areas

3.4.1.3 Manned Aircraft Data Collection

Approximately 3 years prior to UAS data collection, a manned aircraft survey was completed at I67 in accordance with guidance stated in AC 150/5300-17 (FAA, 2017b). Because of the age of the manned imagery and likely subsequent tree growth, it was only used for man-made obstacle comparisons. Data were collected using a Z/I Imaging DMC IIe 230 camera at with a GSD of 6 in. and 60%/50% forward and side overlap values. Table 29 presents the complete parameters for the manned aircraft aerial survey.

Table 29. Cincinnati West Airport Manned Aircraft Aerial Survey Parameters

| Date Collected | Sensor | Estimated GSD (in.) | Forward Overlap (%) | Side Overlap (%) | AGL (ft) | Flight Time (min) | Photo Count |
|---|---|---|---|---|---|---|---|
| 09/30/2018 | DMC IIe 230 | 6 | 60 | 50 | 8,067 | 2 | 6 |

3.4.1.4 Field Data Collection

When the NGS reviewed the UAS obstacle data collected at FPY and compared it to the manned aircraft data, vertical discrepancies were found between obstacles measured with manned and UAS imagery. During subsequent discussions with the NGS, it was hypothesized that these

discrepancies were an indication that the measurements taken from UAS imagery were more accurate than those derived from manned aircraft imagery.

To further assess the accuracy of the UAS, precise measurements of the obstacles at I67 were collected using conventional field survey techniques on the same day UAS imagery was taken. These field obstacle measurements served as an additional truth source when evaluating both manned aircraft and UAS obstacle data collected at I67.

### 3.4.2 Data Processing Results

Each data set collected at I67 was processed using UASMaster, the results of which are shown in Table 30. The table is color-coded to highlight the flights that produced no valid AT solution (red), a valid AT solution without viable stereo pairs (orange), and valid AT solutions that are viable for obstacle data collection stereo analysis (green). Of the 28 data sets collected, 19 produced valid AT solutions viable for stereo analysis, 5 created valid AT solutions that were not viable for stereo analysis, and 4 did not make it to stereo analysis after failing to create a valid AT solution.

During initial processing of Tests 2A, 2B, and 2C in UASMaster, tie point extraction and image orientation failed. This failure was attributed to inconsistencies with the M210. The cause of these inconsistencies is undetermined; however, they were isolated to the M210. These issues with tie point extraction and image orientation were not observed in flights with the WingtraOne or eBee X, nor with the Inspire 2 when collecting data with the same camera payload (X7) as the M210. This lack of tie points had an adverse effect on the computed exterior orientation and photo center of each image, resulting in severe distortion in the data set.

Figure 36 shows screenshots taken from UASMaster following initial processing of data from Tests 4A and 2A. The blue dotted lines in Figure 36 are the UAS flight lines and individual points where photos were taken during data collection. These flight lines and photo locations are based on the time and assumed camera position stored within the metadata and the image name. The data set from Test 4A shown in Figure 36(a) was successfully processed, and images are properly positioned and spaced to accurately depict the survey area. The initial processing results from Test 2A produced severe distortion as shown in Figure 36(b). Rather than overlapping in a regular pattern covering the entire survey area, the images in this data set were inaccurately located and stacked on top of one another. This was due to the improper orientation of the images and lack of tie point generation during initial processing.

Table 30. Cincinnati West Airport Data Processing Results

| Test # | Test Area | Processing Software | UAS | Sensor | Estimated GSD (in.) | Forward/ Side Overlap % | Processing Results |
|---|---|---|---|---|---|---|---|
| **1A** | A | UASMaster | M210 (RTK ON) | X7 | 1 | 80/80 | Valid AT solution. No viable stereo. Observed flat stereo imagery in some pairs and parallax. |
| **1B** | B | | | | | | |
| **1C** | C | | | | | | |
| **2A** | A | UASMaster | M210 (RTK ON) | X7 | 1 | 80/60 | No Valid AT solution. Did not go for stereo analysis. |
| **2B** | B | | | | | | |
| **2C** | C | | | | | | |
| **3A** | A | UASMaster | M210 (RTK OFF) | X7 | 1 | 80/60 | Valid AT solution, however, initial control measurements were very poor. No viable stereo. Flat imagery and parallax observed. |
| **3B** | B | | | | | | |
| **3C** | C | | | | | | No Valid AT solution. Did not go for stereo analysis. |
| **4A** | A | UASMaster | Inspire 2 | X7 | 1 | 80/80 | Valid AT solution and viable stereo imagery. However, observed flat stereo imagery. |
| **4B** | B | | | | | | |
| **4C** | C | | | | | | |
| **5A** | A | UASMaster | Inspire 2 | X7 | 1 | 80/60 | Valid AT solution and viable stereo imagery. However, observed flat stereo imagery. |
| **5B** | B | | | | | | |
| **5C** | C | | | | | | |
| **6A** | A | UASMaster | eBee X | S.O.D.A. 3D | 1 | 80/60 | Valid AT solution and viable stereo imagery. However, observed a fuzzy or mushy effect during stereo analysis. Target edges were difficult to discern even with modifying stereo software imagery adjustment options. Observed imagery color inconsistent and highly variable between images and a sloping in some image pairs. |
| **6B** | B | | | | | | |
| **6C** | C | | | | | | |
| **7A** | A | UASMaster | eBee X | S.O.D.A. 3D | 1 | 80/60 | Valid AT solution and viable stereo imagery. However, color inconsistency and fuzzy imagery appearance. |
| **7B** | B | | | | | | |
| **7C** | C | | | | | | Unable to fly due to the presence of nonparticipants. |
| **8A** | A | UASMaster | WingtraOne | RXIR-II | 0.5 | 80/60 | Valid AT solution and viable stereo imagery. However, it was observed that some images appeared “mushy.” For some stereo pairs, the imagery seemed skewed/stretched. |
| **8B** | B | | | | | | |
| **8C** | C | | | | | | |
| **9** | C | UASMaster | M210 (RTK ON) | X7 | 1 | 80/80 | Valid AT solution and viable stereo imagery. However, noted inconsistent tone and image quality. |
| **10** | C | UASMaster | M210 (RTK ON) | X7 | 1 | 80/80 | Valid AT and viable stereo imagery. However, observed inconsistent tone, exposure, and contrast. Some parallax was also present as well as haloed and fuzzy imagery. |

| Test # | Test Area | Processing Software | UAS | Sensor | Estimated GSD (in.) | Forward/ Side Overlap % | Processing Results |
|---|---|---|---|---|---|---|---|
| **11** | A | UASMaster | WingtraOne | RXIR-II | 0.5 | 70/70 | Valid AT and viable stereo imagery. However, imagery tone/color was inconsistent, with some images appearing blurry. Sloping also observed in this data set. |
| **12** | A | UASMaster | eBee X | S.O.D.A. 3D | 1 | 70/70 | Valid AT and viable stereo imagery. However, a lot of non-flat imagery: twisted/sloped in appearance. Imagery is blurry/fuzzy. |
| **13** | A | UASMaster | M210 (RTK ON) | X7 | 1 | 70/70 | Initial processing determined no valid AT. However, upon further review, valid AT was produced. |

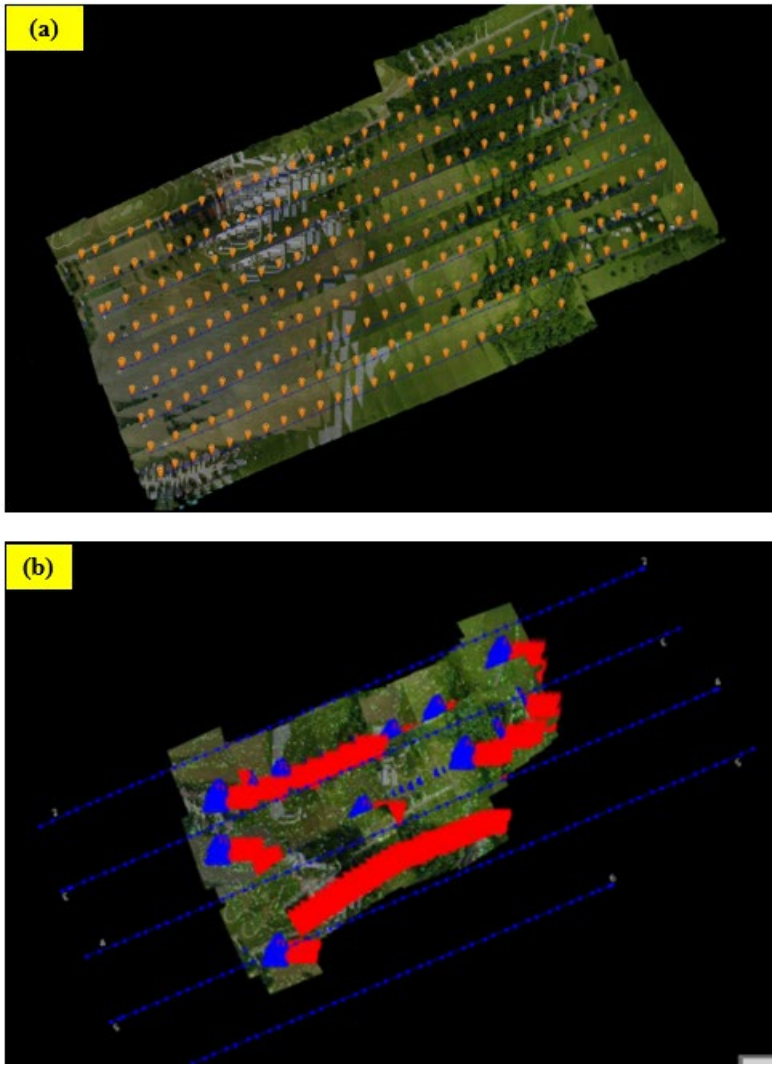


Figure 36. Comparison of Initial Processing Results in UASMaster: (a) Test 4A and (b) Test 2A

Similar issues were experienced while processing data from Test 3C, in which only half of the survey area extracted tie points. This lack of tie points had an adverse effect on the computed exterior orientation and photo center of each image, and caused the severe distortion shown in Figure 37.

Tests 1A, 1B, 1C, 3A, and 3B produced valid AT solutions with unviable stereo imagery. Consistent parallax was observed in each of these data sets that manifested as extremely flat imagery. Flat imagery results in topography surrounding points that are close to the ground (such as a light or a utility pole) to appear flat or tilted, preventing the stereo analyst from fully measuring the image in 3D space. Figure 38 depicts examples of this phenomenon. During stereo analysis the yellow circle seen on these images moved horizontally (x, y) and vertically (z). The vertical movement of this cursor, seen in 3D in the stereo environment, is absent or diminished when the imagery appears flat.

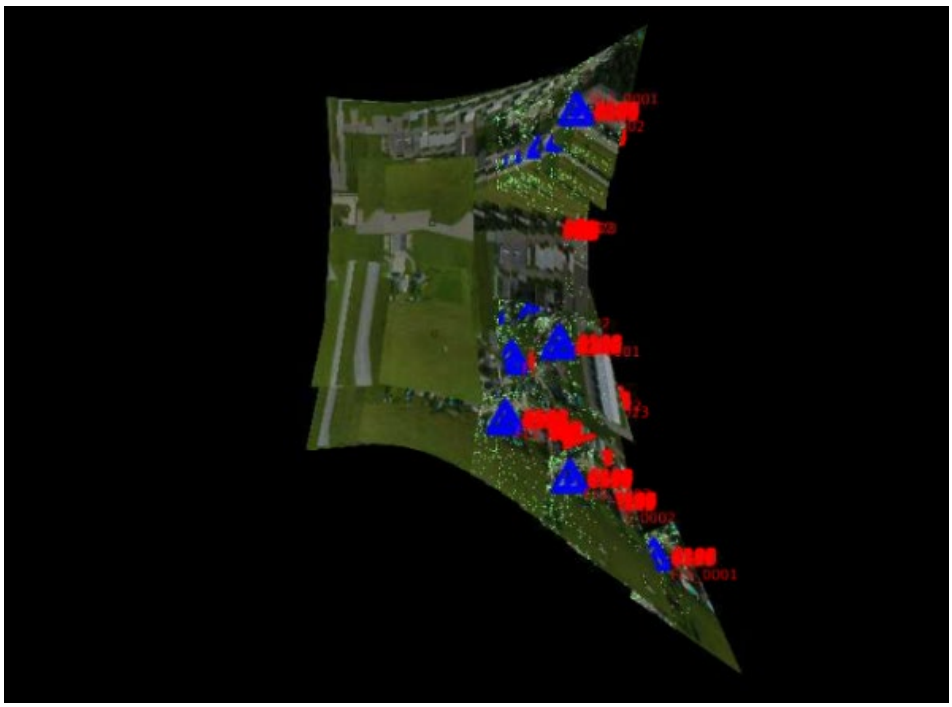

Figure 37. Distorted Orthomosaic Due to Lack of Tie Points in Test 3C


Figure 38. Flat Imagery Observed in Data from Test 4B

All data sets collected during Tests 4 and 5 produced AT solutions viable for stereo analysis despite the presence of flat imagery as depicted in Figure 38. This indicated that flat imagery occurred in degrees of severity and did not necessarily render a data set invalid.

### 3.4.3 Stereo Analysis—GCP Comparison Results

A stereo analysis effort was initiated to measure the surveyed GCP locations captured in each valid AT solution generated from UAS data collected at I67. These locations were validated by comparing them to the field-surveyed GCP locations captured while they were being established.

AC 150/5300-17 Section 8.1.1.2 states that the positions of well-defined points determined from stereo imagery must be within 3.28 ft (1 meter) relative to the NSRS for imagery to be accepted by the NGS (FAA, 2017b). While there is no specific standard for photo control GCP checks, the same minimum requirement was applied to determine the viability of each AT solution for obstacle data collection.

#### 3.4.3.1 Tests 1, 2, and 3: M210 Validation and RTK vs Non-RTK

Tests 1, 2, and 3 were conducted with the M210 to validate previously successful parameters, to evaluate the effect of using RTK versus not using RTK, and to evaluate the effect of higher forward and side overlap values of 80%/80%. None of these data sets produced viable stereo imagery suitable for stereo analysis, and, therefore, were not included in this analysis.

#### 3.4.3.2 Tests 4 and 5: Test of 80%/60% and 80%/80% Forward and Side Overlap Values (Inspire 2/X7)

Tables 31, 32, and 33 present the RMSEs between the GCP locations derived from field survey data and Inspire 2 UAS imagery collected in Tests 4A, 4B, and 4C when measured in stereo. Test 4 was flown with 80%/80% forward and side overlap settings to test the impact on flight times, control RMSEs, and measure obstacles when compared to Test 5 which used 80%/60% forward and side overlap settings. Test 4 was also intended as a comparison to Test 1 to observe the difference between the non-RTK GPS module in the Inspire 2 and the RTK GPS module in the M210, however the failure of the data set from Test 1 prevented this analysis.

During stereo analysis, flattening in the imagery and some minor parallax were observed, however, each data set's overall average RMSE and all but two individual GCP locations were within the accuracy tolerance (3.28 ft) stated in AC 150/5300-17 (FAA, 2017b). This indicated that these data sets were viable for obstacle data collection.

Table 31. Ground Control Point Location Variance between Field Survey and UAS Test 4A (Inspire 2)

| GCP | RMSE X (ft) | RMSE Y (ft) | RMSE Z (ft) | Maximum Horizontal Error (ft) | Maximum Vertical Error (ft) |
|---|---|---|---|---|---|
| **6101** | 0.27 | 1.63 | 1.21 | 1.76 | -0.83 |
| **6102** | 0.71 | 0.99 | 0.43 | 1.37 | 0.10 |
| **6103** | 1.04 | 0.83 | 1.03 | 2.15 | 2.56 |
| **6107** | 0.42 | 0.57 | 1.01 | 0.87 | 1.05 |
| **6108** | 0.97 | 0.21 | 1.86 | 1.08 | -1.12 |
| **6109** | 1.03 | 0.87 | 1.63 | 1.54 | -1.05 |
| **6110** | 0.55 | 0.93 | 0.69 | 1.20 | -0.45 |
| **6111** | 0.22 | 0.94 | 0.38 | 1.17 | -0.02 |
| **6112** | 0.27 | 1.10 | 0.53 | 1.23 | 0.41 |
| **6116** | 0.52 | 1.69 | 1.20 | 1.80 | -1.11 |
| **6201** | 0.34 | 1.57 | 0.80 | 1.81 | -0.33 |
| **6105** | 0.38 | 0.36 | 0.32 | 0.73 | 0.32 |
| **6106** | 0.17 | 0.28 | 0.25 | 0.62 | 0.22 |
| **6202** | 0.24 | 0.40 | 0.24 | 0.71 | 0.10 |
| **6203** | 0.11 | 0.30 | 0.33 | 0.51 | 0.09 |
| **6104** | 0.36 | 0.24 | 0.33 | 0.67 | 0.77 |
| **AVERAGE:** | **0.47** | **0.81** | **0.76** | | |

Table 32. Ground Control Point Location Variance between Field Survey and UAS Test 4B (Inspire 2)

| GCP | RMSE X (ft) | RMSE Y (ft) | RMSE Z (ft) | Maximum Horizontal Error (ft) | Maximum Vertical Error (ft) |
|---|---|---|---|---|---|
| **6108** | 2.07 | 0.81 | 0.40 | 2.32 | 0.57 |
| **6110** | 0.70 | 0.49 | 0.59 | 1.28 | 0.21 |
| **6113** | 1.81 | 1.38 | 0.53 | 2.34 | -0.14 |
| **6114** | 1.24 | 1.54 | 0.38 | 2.05 | -0.09 |
| **6115** | 1.42 | 0.95 | 0.56 | 1.86 | -0.19 |
| **6116** | 1.08 | 0.61 | 0.43 | 1.38 | -0.01 |
| **6119** | 0.61 | 1.10 | 0.40 | 1.40 | 0.77 |
| **6121** | 1.01 | 0.38 | 0.21 | 1.22 | 0.03 |
| **6123** | 0.41 | 0.13 | 1.00 | 0.48 | 2.04 |
| **6203** | 1.21 | 0.44 | 2.63 | 1.42 | 0.00 |
| **6204** | 1.60 | 1.67 | 0.44 | 2.36 | 0.00 |
| **6205** | 0.23 | 0.34 | 0.44 | 0.64 | 0.83 |
| **6206** | 1.00 | 0.17 | 0.39 | 1.13 | 1.07 |
| **6120** | 0.24 | 0.36 | 0.33 | 0.71 | 0.75 |
| **6109** | 0.89 | 0.97 | 0.38 | 1.82 | 1.03 |
| **AVERAGE:** | **1.03** | **0.76** | **0.61** | | |

Table 33. Ground Control Point Location Variance between Field Survey and UAS Test 4C (Inspire 2)

| GCP | RMSE X (ft) | RMSE Y (ft) | RMSE Z (ft) | Maximum Horizontal Error (ft) | Maximum Vertical Error (ft) |
|---|---|---|---|---|---|
| **6117** | 1.73 | 0.11 | 0.30 | 1.82 | 0.46 |
| **6118** | 0.79 | 0.20 | 0.52 | 0.91 | 0.81 |
| **6119** | 0.41 | 0.44 | 0.16 | 0.73 | 0.22 |
| **6120** | 0.90 | 0.72 | 0.26 | 1.39 | 0.48 |
| **6121** | 1.40 | 0.58 | 0.35 | 1.70 | 0.72 |
| **6122** | 0.75 | 0.96 | 0.46 | 1.53 | 0.12 |
| **6123** | 0.13 | 0.31 | 0.45 | 0.49 | -0.04 |
| **6124** | 1.50 | 0.80 | 1.74 | 2.48 | 5.54 |
| **6125** | 0.90 | 1.26 | 0.66 | 1.67 | 0.30 |
| **6126** | 0.15 | 2.13 | 1.06 | 2.39 | -0.42 |
| **6127** | 0.62 | 1.47 | 1.10 | 1.77 | 3.52 |
| **6205** | 0.53 | 0.32 | 0.34 | 0.74 | 0.11 |
| **6206** | 1.08 | 0.19 | 0.27 | 1.22 | 0.67 |
| **6207** | 1.03 | 1.06 | 0.86 | 1.63 | 2.48 |
| **6208** | 0.60 | 2.18 | 1.30 | 2.35 | -1.13 |
| **AVERAGE:** | **0.83** | **0.85** | **0.66** | | |

Tables 34, 35, and 36 present the RMSEs between the GCP locations derived from field survey data and Inspire 2 UAS imagery collected in Test 5 when measured in stereo. Similar to Test 4, parallax was observed in the form of flat imagery in this data set, indicating that overlap settings do not have an impact on the presence of this distortion. Test 4 did produce more accurate control measurements than Test 5, indicating that higher overlap resulted in greater accuracy. In all three data sets, the overall average RMSE falls within the tolerance (3.28 ft) stated in AC 150/5300-17 (FAA, 2017b), indicating that these data sets were viable for obstacle data collection.

Table 34. Ground Control Point Location Variance between Field Survey and UAS Test 5A (Inspire 2)

| GCP | RMSE X (ft) | RMSE Y (ft) | RMSE Z (ft) | Maximum Horizontal Error (ft) | Maximum Vertical Error (ft) |
|---|---|---|---|---|---|
| **6101** | 0.19 | 1.63 | 0.55 | 1.75 | 1.05 |
| **6102** | 0.70 | 1.43 | 1.94 | 1.89 | -1.53 |
| **6103** | 0.61 | 0.71 | 0.87 | 1.08 | 1.93 |
| **6104** | 0.28 | 0.10 | 1.56 | 0.47 | -1.16 |
| **6105** | 0.51 | 0.20 | 1.39 | 0.72 | -1.02 |
| **6106** | 0.34 | 0.47 | 0.68 | 0.68 | -0.42 |
| **6107** | 0.25 | 0.67 | 0.73 | 1.06 | -0.36 |
| **6108** | 0.81 | 0.21 | 1.04 | 1.00 | -0.11 |
| **6109** | 0.88 | 0.84 | 1.21 | 1.26 | -0.92 |
| **6110** | 0.36 | 0.83 | 0.91 | 0.93 | -0.59 |
| **6111** | 0.11 | 0.75 | 1.18 | 0.83 | -0.82 |
| **6112** | 0.58 | 0.97 | 0.43 | 1.22 | 0.72 |

| GCP | RMSE X (ft) | RMSE Y (ft) | RMSE Z (ft) | Maximum Horizontal Error (ft) | Maximum Vertical Error (ft) |
|---|---|---|---|---|---|
| **6116** | 0.34 | 1.64 | 1.24 | 1.79 | -1.07 |
| **6201** | 0.52 | 1.85 | 0.21 | 2.10 | 0.40 |
| **6202** | 0.41 | 0.59 | 0.52 | 0.85 | -0.30 |
| **6203** | 0.04 | 0.17 | 1.23 | 0.36 | -0.81 |
| **AVERAGE:** | **0.43** | **0.82** | **0.98** | | |

Table 35. Ground Control Point Location Variance between Field Survey and UAS Test 5B (Inspire 2)

| GCP | RMSE X (ft) | RMSE Y (ft) | RMSE Z (ft) | Maximum Horizontal Error (ft) | Maximum Vertical Error (ft) |
|---|---|---|---|---|---|
| **6107** | 4.41 | 2.82 | 6.50 | 8.43 | 10.31 |
| **6108** | 1.50 | 0.71 | 2.17 | 2.27 | 6.40 |
| **6109** | 1.38 | 0.94 | 1.35 | 4.94 | 4.58 |
| **6110** | 1.14 | 0.52 | 1.20 | 1.70 | 0.14 |
| **6113** | 1.47 | 1.26 | 0.39 | 1.98 | -0.15 |
| **6114** | 0.88 | 1.79 | 0.74 | 2.05 | -0.55 |
| **6115** | 1.86 | 1.30 | 2.19 | 2.35 | -2.02 |
| **6116** | 1.57 | 0.92 | 1.46 | 1.86 | -1.31 |
| **6119** | 0.08 | 1.53 | 0.50 | 1.58 | -0.28 |
| **6120** | 1.01 | 0.74 | 0.78 | 1.46 | -0.51 |
| **6121** | 1.77 | 0.62 | 2.11 | 2.05 | -1.95 |
| **6123** | 0.96 | 0.95 | 1.02 | 3.13 | 2.81 |
| **6204** | 1.31 | 1.67 | 0.47 | 2.21 | -0.26 |
| **6205** | 0.55 | 0.84 | 0.25 | 1.20 | 0.11 |
| **6206** | 1.79 | 1.17 | 1.70 | 3.44 | 3.57 |
| **AVERAGE:** | **1.45** | **1.18** | **1.52** | | |

Table 36. Ground Control Point Location Variance between Field Survey and UAS Test 5C (Inspire 2)

| GCP | RMSE X (ft) | RMSE Y (ft) | RMSE Z (ft) | Maximum Horizontal Error (ft) | Maximum Vertical Error (ft) |
|---|---|---|---|---|---|
| **6117** | 1.34 | 0.25 | 1.93 | 1.38 | -1.83 |
| **6118** | 0.50 | 0.30 | 1.81 | 0.63 | -1.68 |
| **6119** | 0.55 | 0.04 | 2.04 | 0.61 | -1.82 |
| **6120** | 1.18 | 0.27 | 1.59 | 1.25 | -1.26 |
| **6121** | 1.80 | 0.27 | 1.63 | 1.96 | 0.21 |
| **6122** | 0.82 | 1.46 | 2.51 | 1.80 | -2.12 |
| **6123** | 0.34 | 0.77 | 1.82 | 1.04 | -1.46 |
| **6124** | 1.27 | 0.95 | 1.21 | 1.75 | -0.18 |
| **6125** | 1.10 | 1.68 | 2.41 | 2.30 | -2.07 |
| **6126** | 0.05 | 2.70 | 3.13 | 2.80 | -2.92 |
| **6127** | 0.77 | 2.04 | 3.06 | 2.33 | -2.46 |
| **6205** | 0.77 | 0.12 | 1.62 | 0.88 | -1.37 |
| **6206** | 1.34 | 0.55 | 1.61 | 1.48 | -1.11 |
| **6207** | 0.95 | 1.65 | 1.75 | 2.11 | -1.15 |

| GCP | RMSE X (ft) | RMSE Y (ft) | RMSE Z (ft) | Maximum Horizontal Error (ft) | Maximum Vertical Error (ft) |
|---|---|---|---|---|---|
| **6208** | 0.41 | 2.71 | 2.98 | 2.77 | -2.82 |
| **AVERAGE:** | **0.88** | **1.05** | **2.07** | | |

3.4.3.3 Tests 6 and 7: Test of Interlaced and Sequential Flight Lines (eBee X/S.O.D.A. 3D)

Tests 6 and 7 were flown to evaluate the effect of interlaced flight lines on the quality of the aerial survey data collected. Both flights were conducted with the Sensefly eBee X using previously successful data collection parameters of a 1-in. GSD and 80%/60% forward and side overlap values.

Tables 37, 38, and 39 present the RMSEs between the GCP locations derived from field survey data and the eBee X UAS imagery collected in flight 6 when measured in stereo. This flight was conducted with interlaced flight lines, which shortened the flight time and improved operational efficiency. In all three data sets, the overall average RMSEs were slightly higher than what is typical for this sensor, but nevertheless fall within the tolerance (3.28 ft) stated in AC 150/5300-17 (FAA, 2017b), indicating that these data sets were viable for obstacle data collection.

Table 37. Ground Control Point Location Variance between Field Survey and UAS Test 6A (eBee X)

| GCP | RMSE X (ft) | RMSE Y (ft) | RMSE Z (ft) | Maximum Horizontal Error (ft) | Maximum Vertical Error (ft) |
|---|---|---|---|---|---|
| **6101** | 0.12 | 0.10 | 0.26 | 0.20 | 0.33 |
| **6102** | 0.05 | 0.11 | 0.39 | 0.15 | 0.63 |
| **6103** | 0.10 | 0.11 | 1.15 | 0.24 | 1.56 |
| **6104** | 0.08 | 0.18 | 0.30 | 0.27 | 0.25 |
| **6105** | 0.30 | 0.27 | 0.49 | 0.54 | 0.83 |
| **6106** | 0.13 | 0.26 | 0.34 | 0.51 | 0.55 |
| **6107** | 0.21 | 0.24 | 0.43 | 0.69 | 1.07 |
| **6108** | 0.12 | 0.08 | 0.94 | 0.20 | 0.95 |
| **6109** | 0.16 | 0.14 | 0.94 | 0.33 | 1.22 |
| **6110** | 0.08 | 0.05 | 0.36 | 0.20 | 0.65 |
| **6111** | 0.13 | 0.21 | 0.49 | 0.46 | 0.90 |
| **6112** | 0.07 | 0.06 | 0.23 | 0.15 | 0.33 |
| **6201** | 0.07 | 0.09 | 0.23 | 0.15 | 0.31 |
| **6202** | 0.19 | 0.21 | 0.58 | 0.44 | 0.89 |
| **6203** | 0.09 | 0.24 | 0.28 | 0.52 | 0.58 |
| **AVERAGE:** | **0.13** | **0.16** | **0.49** | | |

Table 38. Ground Control Point Location Variance between Field Survey and UAS Test 6B (eBee X)

| GCP | RMSE X (ft) | RMSE Y (ft) | RMSE Z (ft) | Maximum Horizontal Error (ft) | Maximum Vertical Error (ft) |
|---|---|---|---|---|---|
| **6106** | 0.12 | 0.14 | 0.37 | 0.32 | 0.64 |
| **6107** | 0.32 | 0.09 | 1.21 | 0.40 | 1.34 |
| **6108** | 0.33 | 0.32 | 0.99 | 0.53 | 1.72 |
| **6109** | 0.16 | 0.54 | 0.85 | 1.07 | 1.65 |
| **6110** | 0.12 | 0.16 | 0.27 | 0.26 | 0.00 |
| **6111** | 0.18 | 0.07 | 0.70 | 0.25 | 0.00 |
| **6113** | 0.17 | 2.80 | 1.34 | 2.98 | 1.91 |
| **6114** | 0.22 | 1.61 | 0.54 | 1.80 | 0.96 |
| **6115** | 0.14 | 0.76 | 0.37 | 0.90 | 0.55 |
| **6116** | 0.21 | 0.47 | 0.33 | 0.73 | 0.50 |
| **6119** | 0.65 | 1.46 | 0.63 | 1.93 | 1.07 |
| **6120** | 0.15 | 0.75 | 0.44 | 0.92 | 0.81 |
| **6121** | 0.39 | 0.64 | 0.49 | 1.16 | 0.89 |
| **6123** | 0.75 | 0.80 | 0.37 | 1.23 | 0.41 |
| **6201** | 0.19 | 0.19 | 1.45 | 0.29 | 1.71 |
| **6202** | 0.66 | 0.06 | 0.54 | 0.66 | 0.54 |
| **6203** | 0.11 | 0.17 | 0.36 | 0.36 | 0.84 |
| **6204** | 0.42 | 5.38 | 0.94 | 5.55 | 1.55 |
| **6205** | 0.34 | 0.83 | 0.39 | 1.00 | 0.61 |
| **6206** | 0.06 | 0.56 | 0.31 | 0.67 | 0.27 |
| **AVERAGE:** | **0.28** | **0.89** | **0.64** | | |

Table 39. Ground Control Point Location Variance between Field Survey and UAS Test 6C (eBee X)

| GCP | RMSE X (ft) | RMSE Y (ft) | RMSE Z (ft) | Maximum Horizontal Error (ft) | Maximum Vertical Error (ft) |
|---|---|---|---|---|---|
| **6114** | 0.25 | 2.03 | 2.66 | 2.04 | 2.66 |
| **6117** | 0.82 | 1.15 | 0.69 | 1.52 | 0.87 |
| **6118** | 0.43 | 1.40 | 0.94 | 1.52 | 1.58 |
| **6119** | 0.21 | 1.13 | 0.90 | 1.24 | 1.68 |
| **6120** | 0.59 | 0.62 | 0.80 | 1.35 | 1.43 |
| **6121** | 0.70 | 0.21 | 1.51 | 1.11 | 1.84 |
| **6122** | 0.18 | 0.07 | 0.30 | 0.46 | 0.21 |
| **6123** | 0.09 | 0.61 | 0.35 | 0.67 | 0.12 |
| **6124** | 0.53 | 0.79 | 0.28 | 1.16 | 0.58 |
| **6125** | 0.08 | 0.12 | 0.62 | 0.18 | 0.90 |
| **6126** | 0.10 | 0.30 | 0.44 | 0.36 | 0.35 |
| **6127** | 0.18 | 0.11 | 0.37 | 0.41 | 0.73 |
| **6205** | 0.35 | 0.63 | 0.31 | 0.90 | 0.53 |
| **6206** | 0.29 | 0.34 | 0.66 | 0.53 | 0.91 |
| **6207** | 0.15 | 0.37 | 0.23 | 0.50 | 0.37 |
| **6208** | 0.13 | 0.23 | 0.45 | 0.32 | 0.63 |
| **AVERAGE:** | **0.32** | **0.63** | **0.72** | | |

Tables 40 and 41present the RMSEs between the GCP locations derived from field survey data and eBee X UAS imagery collected in flight 7 when measured in stereo. Area C could not be flown due to the presence of nonparticipants. Flight 7 was conducted with traditional flight lines, and the RMSEs for the Y and Z values are slightly lower than flight 6 in both areas. RMSEs for the X values were nearly identical, differing by 0.01 ft in both areas. In both data sets collected during flight 7, the overall average RMSE falls within the tolerance (3.28 ft) stated in AC 150/5300-17 (FAA, 2017b), indicating that these data sets were viable for obstacle data collection.

Table 40. Ground Control Point Location Variance between Field Survey and UAS Test 7A (eBee X)

| GCP | RMSE X (ft) | RMSE Y (ft) | RMSE Z (ft) | Maximum Horizontal Error (ft) | Maximum Vertical Error (ft) |
|---|---|---|---|---|---|
| **6101** | 0.16 | 0.15 | 0.32 | 0.36 | 0.42 |
| **6102** | 0.07 | 0.29 | 0.52 | 0.60 | 0.82 |
| **6103** | 0.07 | 0.15 | 0.75 | 0.35 | 1.15 |
| **6104** | 0.05 | 0.20 | 0.29 | 0.25 | 0.46 |
| **6105** | 0.22 | 0.14 | 0.45 | 0.37 | 0.71 |
| **6106** | 0.22 | 0.17 | 0.46 | 0.48 | 0.74 |
| **6107** | 0.17 | 0.07 | 0.27 | 0.29 | 0.53 |
| **6108** | 0.07 | 0.07 | 0.62 | 0.15 | 0.77 |
| **6109** | 0.16 | 0.06 | 0.37 | 0.28 | 0.59 |
| **6110** | 0.12 | 0.11 | 0.38 | 0.26 | 0.73 |
| **6111** | 0.09 | 0.17 | 0.35 | 0.34 | 0.86 |
| **6112** | 0.28 | 0.07 | 0.07 | 0.42 | 0.02 |
| **6116** | 0.20 | 0.05 | 0.23 | 0.31 | 0.38 |
| **6201** | 0.13 | 0.13 | 0.51 | 0.27 | 0.75 |
| **6202** | 0.20 | 0.17 | 0.36 | 0.44 | 0.59 |
| **6203** | 0.10 | 0.15 | 0.29 | 0.28 | 0.40 |
| **AVERAGE:** | **0.14** | **0.13** | **0.39** | | |

Table 41. Ground Control Point Location Variance between Field Survey and UAS Test 7B (eBee X)

| GCP | RMSE X (ft) | RMSE Y (ft) | RMSE Z (ft) | Maximum Horizontal Error (ft) | Maximum Vertical Error (ft) |
|---|---|---|---|---|---|
| **6106** | 0.11 | 0.23 | 0.43 | 0.39 | 0.58 |
| **6107** | 0.50 | 0.15 | 0.47 | 0.58 | 0.99 |
| **6108** | 0.58 | 0.37 | 0.47 | 0.72 | 0.14 |
| **6109** | 0.20 | 0.53 | 0.19 | 0.66 | 0.23 |
| **6110** | 0.22 | 0.15 | 0.29 | 0.30 | 0.30 |
| **6111** | 0.26 | 0.15 | 0.34 | 0.40 | 0.20 |
| **6113** | 0.34 | 1.49 | 0.43 | 1.90 | 0.33 |
| **6114** | 0.04 | 1.77 | 0.16 | 1.88 | 0.23 |
| **6115** | 0.19 | 0.78 | 0.31 | 0.95 | 0.49 |
| **6116** | 0.14 | 0.53 | 0.36 | 0.77 | 0.42 |
| **6119** | 0.57 | 1.62 | 0.34 | 1.96 | 0.64 |
| **6120** | 0.15 | 0.84 | 0.43 | 1.16 | 0.69 |
| **6121** | 0.43 | 0.58 | 0.67 | 0.83 | 0.99 |
| **6123** | 0.81 | 0.81 | 0.58 | 1.32 | 1.23 |

| GCP | RMSE X (ft) | RMSE Y (ft) | RMSE Z (ft) | Maximum Horizontal Error (ft) | Maximum Vertical Error (ft) |
|---|---|---|---|---|---|
| **6203** | 0.12 | 0.17 | 0.46 | 0.44 | 0.85 |
| **6204** | 0.19 | 1.57 | 0.40 | 1.90 | 0.70 |
| **6205** | 0.29 | 0.81 | 0.46 | 1.15 | 0.73 |
| **6206** | 0.15 | 0.46 | 0.67 | 0.54 | 0.95 |
| **AVERAGE:** | **0.29** | **0.72** | **0.42** | | |

3.4.3.4 Test 8: WingtraOne Validation (WingtraOne/RX1R-II)

Tables 42, 43, and 44 present the RMSEs between the GCP locations derived from field survey data and WingtraOne UAS imagery collected in Test 8 when measured in stereo. Test 8 sought to validate previously successful data collection parameters of 0.5 in. GSD and 80%/60% forward and side overlap values. The WingtraOne data produced the lowest RMSEs, outperforming the other platforms. In all three data sets collected during flight 8, the overall average RMSE falls within the tolerance (3.28 ft) stated in AC 150/5300-17 (FAA, 2017b), indicating that these data sets were viable for obstacle data collection.

Table 42. Ground Control Point Location Variance between Field Survey and UAS Test 8A (WingtraOne)

| GCP | RMSE X (ft) | RMSE Y (ft) | RMSE Z (ft) | Maximum Horizontal Error (ft) | Maximum Vertical Error (ft) |
|---|---|---|---|---|---|
| **6101** | 0.08 | 0.05 | 0.18 | 0.13 | -0.05 |
| **6102** | 0.07 | 0.12 | 0.28 | 0.16 | -0.19 |
| **6103** | 0.04 | 0.06 | 0.23 | 0.11 | 0.34 |
| **6104** | 0.05 | 0.09 | 0.30 | 0.14 | 0.40 |
| **6105** | 0.08 | 0.09 | 0.32 | 0.27 | 0.67 |
| **6106** | 0.07 | 0.07 | 0.22 | 0.25 | 0.38 |
| **6107** | 0.09 | 0.05 | 0.61 | 0.16 | 0.70 |
| **6108** | 0.04 | 0.06 | 0.56 | 0.14 | 0.76 |
| **6109** | 0.09 | 0.09 | 0.17 | 0.15 | 0.24 |
| **6110** | 0.13 | 0.10 | 0.08 | 0.22 | 0.16 |
| **6111** | 0.11 | 0.15 | 0.11 | 0.27 | 0.09 |
| **6112** | 0.09 | 0.05 | 0.23 | 0.14 | 0.30 |
| **6116** | 0.07 | 0.06 | 0.67 | 0.09 | 0.00 |
| **6201** | 0.04 | 0.07 | 0.38 | 0.11 | 0.00 |
| **6202** | 0.12 | 0.07 | 0.12 | 0.20 | 0.23 |
| **6203** | 0.03 | 0.05 | 0.26 | 0.10 | 0.33 |
| **AVERAGE:** | **0.07** | **0.08** | **0.29** | | |

Table 43. Ground Control Point Location Variance between Field Survey and UAS Test 8B (WingtraOne)

| GCP | RMSE X (ft) | RMSE Y (ft) | RMSE Z (ft) | Maximum Horizontal Error (ft) | Maximum Vertical Error (ft) |
|---|---|---|---|---|---|
| **6106** | 0.02 | 0.02 | 0.24 | 0.05 | 0.29 |
| **6107** | 0.03 | 0.02 | 0.17 | 0.07 | 0.17 |
| **6108** | 0.04 | 0.07 | 0.05 | 0.13 | 0.05 |
| **6109** | 0.14 | 0.04 | 0.36 | 0.26 | 0.44 |
| **6110** | 0.13 | 0.03 | 0.08 | 0.18 | 0.14 |
| **6111** | 0.09 | 0.09 | 1.26 | 0.18 | -1.12 |
| **6113** | 0.05 | 0.03 | 0.09 | 0.12 | 0.09 |
| **6114** | 0.12 | 0.03 | 0.17 | 0.20 | -0.14 |
| **6115** | 0.04 | 0.10 | 0.17 | 0.18 | 0.01 |
| **6116** | 0.04 | 0.03 | 0.31 | 0.08 | -0.10 |
| **6119** | 0.03 | 0.05 | 0.19 | 0.08 | -0.11 |
| **6120** | 0.05 | 0.10 | 0.34 | 0.20 | 0.46 |
| **6121** | 0.08 | 0.03 | 0.10 | 0.17 | 0.21 |
| **6123** | 0.01 | 0.06 | 0.18 | 0.09 | -0.10 |
| **6203** | 0.05 | 0.07 | 0.22 | 0.15 | 0.40 |
| **6204** | 0.08 | 0.02 | 0.07 | 0.09 | 0.07 |
| **6205** | 0.04 | 0.10 | 0.13 | 0.13 | 0.28 |
| **6206** | 0.03 | 0.04 | 0.39 | 0.09 | 0.58 |
| **AVERAGE:** | **0.06** | **0.05** | **0.25** | | |

Table 44. Ground Control Point Location Variance between Field Survey and UAS Test 8C (WingtraOne)

| GCP | RMSE X (ft) | RMSE Y (ft) | RMSE Z (ft) | Maximum Horizontal Error (ft) | Maximum Vertical Error (ft) |
|---|---|---|---|---|---|
| **6117** | 0.05 | 0.07 | 0.14 | 0.10 | -0.06 |
| **6118** | 0.03 | 0.01 | 0.34 | 0.06 | -0.26 |
| **6119** | 0.05 | 0.02 | 0.32 | 0.07 | -0.17 |
| **6120** | 0.06 | 0.03 | 0.05 | 0.11 | 0.02 |
| **6121** | 0.08 | 0.07 | 0.62 | 0.14 | 0.65 |
| **6122** | 0.06 | 0.03 | 0.19 | 0.12 | 0.26 |
| **6123** | 0.05 | 0.04 | 0.11 | 0.09 | 0.17 |
| **6124** | 0.03 | 0.06 | 0.35 | 0.12 | 0.40 |
| **6125** | 0.02 | 0.06 | 0.22 | 0.09 | 0.31 |
| **6126** | 0.07 | 0.05 | 0.41 | 0.13 | -0.28 |
| **6127** | 0.07 | 0.04 | 0.21 | 0.16 | -0.29 |
| **6205** | 0.05 | 0.08 | 0.06 | 0.14 | 0.11 |
| **6206** | 0.04 | 0.04 | 0.50 | 0.08 | 0.52 |
| **6207** | 0.07 | 0.05 | 0.43 | 0.18 | 0.56 |
| **6208** | 0.12 | 0.05 | 0.31 | 0.18 | -0.14 |
| **AVERAGE:** | **0.06** | **0.05** | **0.28** | | |

3.4.3.5 Tests 9 and 10: Test of Sun Angle (M210/X7)

Tests 9 and 10 were conducted to evaluate the effect of sun angle on the quality of the aerial survey data collected. Table 45 presents the RMSEs between the GCP locations derived from field survey data and the M210 UAS imagery collected in flight 9 when measured in stereo.

Table 45. Ground Control Point Location Variance between Field Survey and UAS Test 9 (M210)

| GCP | RMSE X (ft) | RMSE Y (ft) | RMSE Z (ft) | Maximum Horizontal Error (ft) | Maximum Vertical Error (ft) |
|---|---|---|---|---|---|
| **6117** | 1.60 | 0.59 | 0.77 | 1.79 | 1.30 |
| **6118** | 0.80 | 0.56 | 0.29 | 1.12 | 0.34 |
| **6119** | 0.62 | 0.09 | 0.42 | 0.78 | 0.00 |
| **6120** | 1.35 | 0.47 | 0.27 | 1.70 | 0.24 |
| **6121** | 2.02 | 0.57 | 0.72 | 2.44 | 1.77 |
| **6122** | 0.87 | 0.95 | 0.82 | 1.38 | 0.00 |
| **6123** | 0.30 | 0.67 | 1.26 | 1.67 | 0.19 |
| **6124** | 1.60 | 1.18 | 1.42 | 2.69 | 3.93 |
| **6125** | 1.22 | 1.56 | 2.10 | 2.15 | 6.95 |
| **6126** | 0.27 | 2.43 | 1.89 | 2.54 | 0.00 |
| **6127** | 1.24 | 1.78 | 3.24 | 5.48 | 8.38 |
| **6205** | 0.80 | 0.15 | 0.79 | 1.06 | -0.44 |
| **6206** | 1.48 | 0.25 | 0.72 | 1.72 | 2.56 |
| **6207** | 1.32 | 1.96 | 3.48 | 5.54 | 10.15 |
| **6208** | 0.75 | 2.62 | 2.17 | 2.78 | 0.00 |
| **AVERAGE:** | **1.08** | **1.05** | **1.36** | | |

As indicated by the red-shaded cells in Table 45, during the control measurements in stereo, there were several measurements with high residuals. These high residuals were attributed to inconsistent imagery observed during AT processing and stereo analysis; this included issues with image texture and exposure and instances where the GCP chevrons would appear to have a haloed effect, which made them difficult to accurately measure. Figure 39 shows this inconsistent "halo" effect between two consecutive images of a GCP from Test 9. Despite these issues, the overall RMSEs still fell within the accuracy tolerance (3.28 ft) stated in AC 150/5300-17 (FAA, 2017b), indicating that this data set was viable for obstacle data collection.

| Flight Line 9, Image Pair 0018/0019 | Flight Line 9, Image Pair 0017/0018 |
|---|---|
|  |  |

Figure 39. Inconsistency between Images Taken with DJI M210 v2 RTK

Table 46 presents the RMSEs between the GCP locations derived from field survey data and the M210 UAS imagery collected in flight 10 when measured in stereo. The control measurements for Test 10 were slightly better than Test 9, but the improvement was not significant enough to make a definitive conclusion regarding which sun angle could be expected to produce consistently better results. The average RMSEs for all GCPs in this data set fell within the accuracy tolerance (3.28 ft) stated in AC 150/5300-17 (FAA, 2017b), indicating that this data set was viable for obstacle data collection.

Table 46. Ground Control Point Location Variance between Field Survey and UAS Test 10 (M210)

| GCP | RMSE X (ft) | RMSE Y (ft) | RMSE Z (ft) | Maximum Horizontal Error (ft) | Maximum Vertical Error (ft) |
|---|---|---|---|---|---|
| **6117** | 1.57 | 0.56 | 0.80 | 1.71 | 1.03 |
| **6118** | 0.67 | 0.54 | 0.52 | 0.97 | 0.74 |
| **6119** | 0.66 | 0.10 | 0.37 | 0.87 | 0.64 |
| **6120** | 1.50 | 0.41 | 0.21 | 1.75 | 0.33 |
| **6121** | 2.20 | 0.79 | 0.70 | 2.58 | 1.77 |
| **6122** | 1.00 | 1.11 | 1.74 | 2.07 | -0.47 |
| **6123** | 0.22 | 0.63 | 1.05 | 0.81 | -0.67 |
| **6124** | 1.64 | 1.17 | 1.28 | 2.62 | 3.51 |
| **6125** | 1.34 | 1.74 | 1.27 | 2.46 | 1.95 |
| **6126** | 0.36 | 2.44 | 2.46 | 2.61 | -1.80 |
| **6127** | 0.62 | 1.42 | 1.48 | 1.76 | 1.21 |
| **6205** | 0.95 | 0.14 | 0.54 | 1.10 | -0.11 |
| **6206** | 1.69 | 0.18 | 0.74 | 1.80 | -0.06 |
| **6207** | 1.40 | 1.60 | 1.08 | 2.28 | -0.80 |
| **6208** | 0.70 | 2.52 | 2.25 | 2.64 | -2.12 |
| **AVERAGE:** | **1.10** | **1.02** | **1.10** | | |

The inconsistency in image exposure and texture and the halo effect on some of the GCP chevrons were also present in this data set. The presence of these issues in both data sets indicates that the platform and payload are likely the cause, rather than the sun angle. The inconsistencies with exposure and texture are shown in Figure 40, which compares consecutive images from Test 10. The first image is blurred or "soft" around the car, treetop, and paint lines. In the next sequential image, this blurring effect is not present.


Figure 40. Example of Exposure and Texture Discrepancies from Flight 10

3.4.3.6 Tests 11, 12, and 13: Test of 70%/70% Forward and Side Overlap Values

Tests 11, 12, and 13 used 70%/70% forward and side overlap settings, allowing the aircraft to fly faster and improving operational efficiency. During testing at WWD, flights with forward overlap settings below 80% failed to produce valid AT solutions due to areas of dense vegetation. At I67, this was offset by implementing a denser GCP layout that provided extra support to vegetated areas. The low RMSEs of each test in this series demonstrated the effectiveness of the improved GCP layout surrounding the area of vegetation.

Table 47 presents the RMSEs between the GCP locations derived from field survey data and the WingtraOne UAS imagery collected in Test 11 when measured in stereo. As indicated by the green shading in all cells, the RMSEs fell within the accuracy tolerance (3.28 ft) stated in AC 150/5300-17 (FAA, 2017b), indicating that this data set was viable for obstacle data collection.

Table 47. Ground Control Point Location Variance between Field Survey and UAS Test 11 (WingtraOne)

| GCP | RMSE X (ft) | RMSE Y (ft) | RMSE Z (ft) | Maximum Horizontal Error (ft) | Maximum Vertical Error (ft) |
|---|---|---|---|---|---|
| **6101** | 0.04 | 0.02 | 0.03 | 0.06 | -0.03 |
| **6102** | 0.04 | 0.20 | 0.06 | 0.20 | 0.06 |
| **6103** | 0.06 | 0.06 | 0.28 | 0.11 | 0.39 |
| **6104** | 0.07 | 0.10 | 0.32 | 0.17 | 0.36 |
| **6105** | 0.08 | 0.06 | 0.35 | 0.15 | 0.44 |
| **6106** | 0.09 | 0.04 | 0.22 | 0.13 | 0.27 |
| **6107** | 0.11 | 0.04 | 0.41 | 0.16 | 0.50 |
| **6108** | 0.02 | 0.03 | 0.34 | 0.05 | 0.43 |
| **6109** | 0.07 | 0.06 | 0.05 | 0.11 | 0.07 |
| **6110** | 0.05 | 0.02 | 0.06 | 0.08 | 0.05 |
| **6111** | 0.04 | 0.16 | 0.13 | 0.28 | 0.02 |
| **6112** | 0.07 | 0.09 | 0.14 | 0.17 | 0.17 |
| **6201** | 0.02 | 0.04 | 0.22 | 0.06 | -0.14 |
| **6202** | 0.08 | 0.09 | 0.28 | 0.14 | 0.41 |
| **6203** | 0.05 | 0.04 | 0.20 | 0.10 | 0.26 |
| **AVERAGE:** | **0.06** | **0.07** | **0.21** | | |

Table 48 presents the RMSEs between the GCP locations derived from field survey data and the eBee X UAS imagery collected in flight 11 when measured in stereo. This data set produced greater accuracy than Test 6A, flown with a higher 80% forward overlap. All RMSE values fell well within the accuracy tolerance (3.28 ft) stated in AC 150/5300-17 (FAA, 2017b), indicating that this data set was viable for obstacle data collection.

Table 48. Ground Control Point Location Variance between Field Survey and UAS Test 12 (eBee X)

| GCP | RMSE X (ft) | RMSE Y (ft) | RMSE Z (ft) | Maximum Horizontal Error (ft) | Maximum Vertical Error (ft) |
|---|---|---|---|---|---|
| **6101** | 0.08 | 0.21 | 0.36 | 0.30 | 0.59 |
| **6102** | 0.06 | 0.20 | 0.50 | 0.42 | 0.63 |
| **6103** | 0.07 | 0.07 | 0.59 | 0.17 | 1.18 |
| **6104** | 0.11 | 0.23 | 0.30 | 0.34 | 0.62 |
| **6105** | 0.30 | 0.12 | 0.65 | 0.43 | 1.16 |
| **6106** | 0.15 | 0.10 | 0.36 | 0.25 | 0.24 |
| **6107** | 0.14 | 0.05 | 0.16 | 0.18 | 0.28 |
| **6108** | 0.08 | 0.22 | 0.51 | 0.27 | 0.68 |
| **6109** | 0.09 | 0.09 | 0.37 | 0.20 | 0.51 |
| **6110** | 0.09 | 0.10 | 0.21 | 0.25 | 0.32 |
| **6111** | 0.06 | 0.24 | 0.36 | 0.42 | 0.54 |
| **6112** | 0.11 | 0.09 | 0.33 | 0.28 | 0.21 |
| **6116** | 0.17 | 0.11 | 0.47 | 0.26 | 0.76 |
| **6201** | 0.08 | 0.09 | 0.40 | 0.21 | 0.68 |
| **6202** | 0.13 | 0.25 | 0.49 | 0.47 | 0.85 |
| **6203** | 0.17 | 0.14 | 0.38 | 0.43 | 0.29 |
| **AVERAGE:** | **0.12** | **0.15** | **0.40** | | |

Table 49 presents the RMSEs between the GCP locations derived from field survey data and the M210 UAS imagery collected in Test 13 when measured in stereo. This test was conducted with the M210, and was the last test conducted with 70%/70% forward and side overlap values. The RMSEs from this flight also fell well within the accuracy tolerance (3.28 ft) stated in AC 150/5300-17 (FAA, 2017b), indicating that this data set was viable for obstacle data collection.

Table 49. Ground Control Point Location Variance between Field Survey and UAS Test 13 (M210)

| GCP | RMSE X (ft) | RMSE Y (ft) | RMSE Z (ft) | Maximum Horizontal Error (ft) | Maximum Vertical Error (ft) |
|---|---|---|---|---|---|
| **6101** | 0.04 | 1.75 | 0.75 | 1.82 | 1.18 |
| **6102** | 0.83 | 1.83 | 0.41 | 2.16 | 0.23 |
| **6103** | 0.82 | 1.01 | 0.96 | 1.52 | 2.08 |
| **6104** | 0.08 | 0.12 | 0.79 | 0.19 | -0.06 |
| **6105** | 0.53 | 0.55 | 1.70 | 1.18 | -0.93 |
| **6106** | 0.37 | 0.27 | 1.00 | 0.54 | -0.72 |
| **6107** | 0.22 | 0.54 | 1.03 | 0.95 | 1.47 |
| **6108** | 0.87 | 0.97 | 1.47 | 1.70 | 3.21 |
| **6109** | 1.07 | 1.66 | 0.35 | 2.04 | 0.51 |
| **6110** | 0.64 | 1.54 | 0.51 | 1.73 | -0.15 |
| **6111** | 0.14 | 1.53 | 0.49 | 1.59 | -0.11 |
| **6112** | 0.05 | 1.30 | 0.34 | 1.33 | 0.57 |
| **6201** | 0.95 | 2.02 | 0.28 | 2.30 | 0.57 |
| **6202** | 0.55 | 0.70 | 0.99 | 0.97 | -0.54 |
| **6203** | 0.08 | 0.61 | 1.07 | 0.83 | -0.50 |
| **AVERAGE:** | **0.48** | **1.09** | **0.81** | | |

### 3.4.4 Stereo Analysis—Internal UAS Imagery to Field Survey Comparison Results

Thirty-seven total obstacles were selected at I67 from the field survey and used to evaluate the accuracy of the UAS-collected obstacle data. This included 8 obstacles in Test Area A, shown in Figure 41; 18 obstacles in Test Area B, shown in Figure 42; and 11 obstacles in Test Area C, shown in Figure 43. To ensure a comprehensive assessment, these obstacles were intentionally varied in both their geographic location and their type (e.g., trees and bushes, fencing, traffic lights, utility poles).

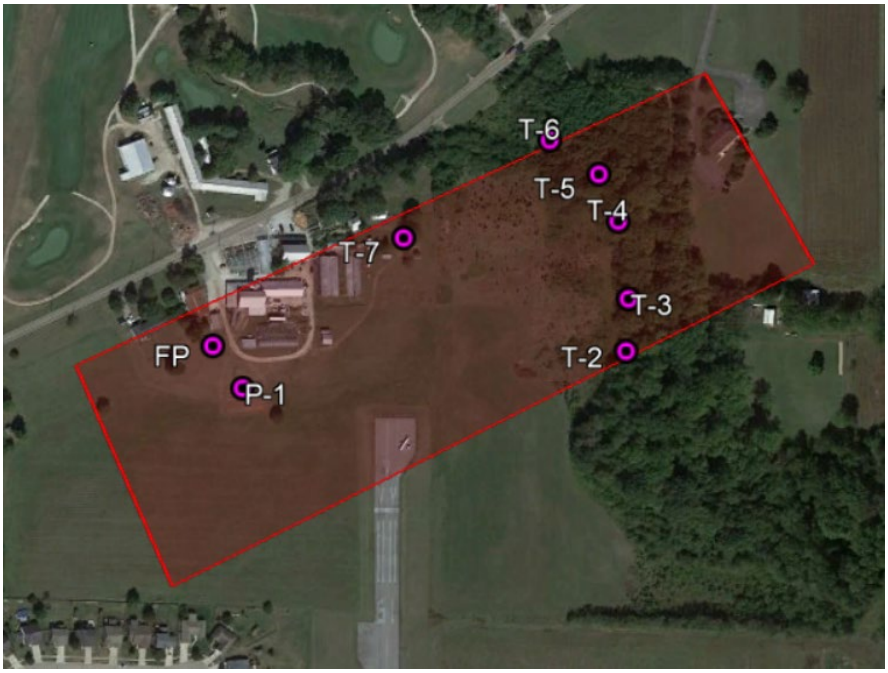


Figure 41. Cincinnati West Airport Obstacle Locations in Test Area A

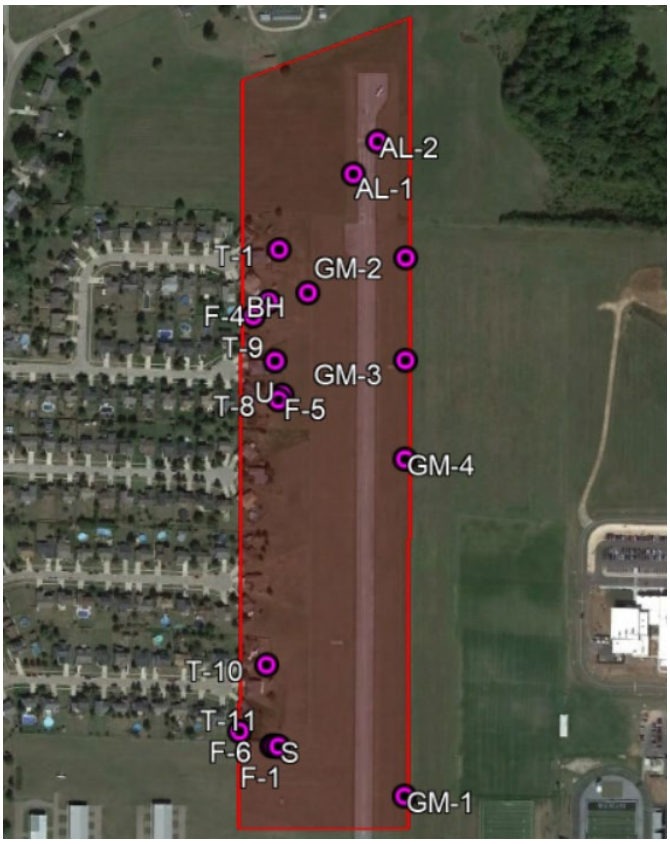


Figure 42. Cincinnati West Airport Obstacle Locations in Test Area B

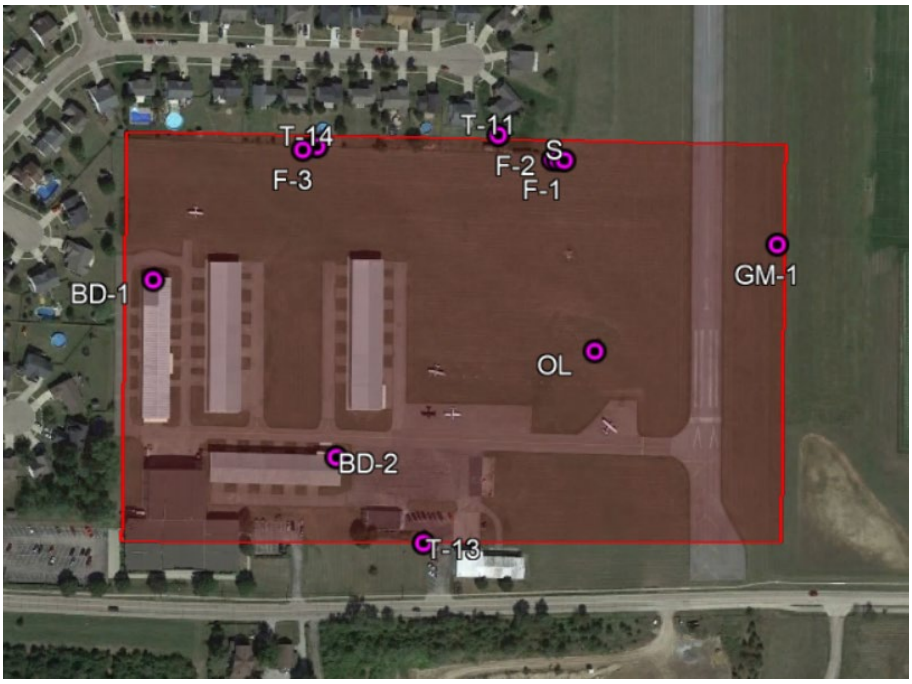


Figure 43. Cincinnati West Airport Obstacle Locations in Test Area C

A stereo analysis effort was conducted to identify and measure each obstacle collected in the field survey using the UAS data. The obstacle locations derived from the field survey were intentionally degraded before delivery to the stereo analyst to encourage an unbiased selection of each obstacle. All tables in this section are color-coded to indicate measurements that meet the most stringent obstacle accuracy requirements of AC 150/5300-18 (green), measurements that meet the accuracy requirements but are outliers (orange), and measurements that fall outside of accuracy requirements (red).

#### 3.4.4.1 Tests 4 and 5: Test of 80%/60% and 80%/80% Forward and Side Overlap Values

Tables 50, 51, and 52 present comparisons between obstacle locations derived from traditional field survey techniques and the UAS imagery collected during Test 4 when measured in stereo. These data sets were collected by the Inspire 2 and X7 using 80%/80% forward and side overlap values. During the stereo analysis process, parallax was observed in the form of flat imagery, however the results show all the measurements fall within the most stringent obstacle accuracy requirements of AC 150/5300-18B (FAA, 2014).

Tables 53, 54, and 55 present comparisons between obstacle locations derived from traditional field survey techniques and the UAS imagery collected during Test 5 when measured in stereo. These data sets were collected using the DJI Inspire 2 and X7 with 80%/60% forward and side overlap values.

The delta values from Test 5 are significantly increased compared to Test 4, which was flown with the same platform at a higher overlap. A significant number of obstacles in each test fell outside of the accuracy requirements (20 ft horizontal, 3 ft vertical) stated in AC 150/5300-18 (FAA, 2014). The results were particularly degraded in blocks A and B, which are vegetated areas. Whether this discrepancy is due to the decrease in overlap or inconsistency in the platform itself is unknown. There is no indication that external factors had a significant effect on the performance of the platform during flight.

Table 50. Obstacle Location Variance between Field Survey and UAS Test 4A (Inspire 2)

| Obstacle | Field Survey (ft) | | | UAS Imagery (ft) | | | Delta (ft) | | |
|---|---|---|---|---|---|---|---|---|---|
| | x | y | z | x | y | z | x | y | z |
| **Flagpole (FP)** | 1324223.78 | 468350.62 | 614.8 | 1324223.48 | 468350.07 | 616.24 | 0.31 | 0.55 | -1.43 |
| **Light On Pole (P-1)** | 1324293.79 | 468245.86 | 596.77 | 1324293.65 | 468245.78 | 597.79 | 0.14 | 0.08 | -1.02 |
| **Tree (T-2)** | 1325231.96 | 468312.17 | 631.87 | 1325231.73 | 468313.45 | 634.4 | 0.22 | -1.28 | -2.53 |
| **Tree (T-3)** | 1325241.12 | 468439.3 | 644.74 | 1325239.97 | 468440.2 | 646.68 | 1.14 | -0.9 | -1.94 |
| **Tree (T-4)** | 1325220.80 | 468628.74 | 637.97 | 1325221.02 | 468628.33 | 640.51 | -0.22 | 0.41 | -2.54 |
| **Tree (T-5)** | 1325176.38 | 468744.19 | 636.69 | 1325187.64 | 468747.26 | 639.65 | -11.26 | -3.08 | -2.96 |
| **Tree (T-6)** | 1325058.63 | 468830.05 | 621.36 | 1325059.6 | 468829.32 | 623.2 | -0.97 | 0.73 | -1.84 |
| **Tree (T-7)** | 1324695.98 | 468601.33 | 629.81 | 1324706.2 | 468599.6 | 631.24 | -10.22 | 1.73 | -1.43 |

Table 51. Obstacle Location Variance between Field Survey and UAS Test 4B (Inspire 2)

| Obstacle | Field Survey (ft) | | | UAS Imagery (ft) | | | Delta (ft) | | |
|---|---|---|---|---|---|---|---|---|---|
| | x | y | z | x | y | z | x | y | z |
| **Airfield Light (AL-1)** | 1324593.4 | 467832.36 | 582.72 | 1324593.19 | 467832.93 | 582.91 | 0.21 | -0.57 | -0.19 |
| **Airfield Light (AL-2)** | 1324676.26 | 467937.74 | 582.43 | 1324675.72 | 467938.13 | 582.48 | 0.53 | -0.39 | -0.04 |
| **Birdhouse (BH)** | 1324432.59 | 467444.24 | 585.41 | 1324432.79 | 467445.02 | 585.53 | -0.2 | -0.77 | -0.12 |
| **Fence (F-1)** | 1324275.23 | 465952.14 | 588.67 | 1324275.31 | 465952.69 | 588.63 | -0.08 | -0.54 | 0.03 |
| **Fence (F-4)** | 1324302.72 | 467418.27 | 587.44 | 1324303.61 | 467419.38 | 587.6 | -0.88 | -1.11 | -0.16 |
| **Fence (F-5)** | 1324338.25 | 467109 | 585.9 | 1324338.67 | 467110.23 | 586.36 | -0.42 | -1.23 | -0.46 |
| **Fence (F-6)** | 1324285.34 | 465951.63 | 589.24 | 1324285.14 | 465952.06 | 589.17 | 0.2 | -0.43 | 0.07 |
| **Gas Line Marker (GM-1)** | 1324710.76 | 465775.09 | 588.83 | 1324709.77 | 465775.35 | 588.14 | 0.99 | -0.26 | 0.69 |
| **Gas Line Marker (GM-2)** | 1324759.66 | 467551.1 | 587.24 | 1324758.36 | 467551.73 | 587.66 | 1.29 | -0.64 | -0.42 |
| **Gas Line Marker (GM-3)** | 1324750.44 | 467213.06 | 587.42 | 1324749.07 | 467214.01 | 587.9 | 1.37 | -0.95 | -0.48 |
| **Gas Line Marker (GM-4)** | 1324740.67 | 466887.22 | 588.45 | 1324739.26 | 466888.29 | 588.98 | 1.42 | -1.07 | -0.53 |
| **Patio Umbrella (U)** | 1324318.33 | 467221.95 | 594.99 | 1324318.82 | 467223.16 | 595.59 | -0.49 | -1.21 | -0.6 |
| **Sign (S)** | 1324297.74 | 465949.89 | 588.55 | 1324297.56 | 465950.33 | 588.36 | 0.18 | -0.44 | 0.19 |
| **Tree (T-1)** | 1324340.96 | 467589.01 | 599.92 | 1324341.08 | 467589.6 | 600.31 | -0.12 | -0.6 | -0.39 |
| **Tree (T-8)** | 1324326.37 | 467093.14 | 596.76 | 1324323.52 | 467095.25 | 597.15 | 2.86 | -2.11 | -0.39 |
| **Tree (T-9)** | 1324249.98 | 467371.83 | 591.97 | 1324250.81 | 467372.67 | 592.34 | -0.83 | -0.84 | -0.37 |
| **Tree (T-10)** | 1324264.82 | 466219.68 | 613.15 | 1324263.17 | 466219.38 | 612.62 | 1.65 | 0.3 | 0.54 |
| **Tree (T-11)** | 1324169.86 | 466002.46 | 606.51 | 1324170.13 | 466002.08 | 604.85 | -0.28 | 0.38 | 1.66 |

Table 52. Obstacle Location Variance between Field Survey and UAS Test 4C (Inspire 2)

| Obstacle | Field Survey (ft) | | | UAS Imagery (ft) | | | Delta (ft) | | |
|---|---|---|---|---|---|---|---|---|---|
| | x | y | z | x | y | z | x | y | z |
| **Fence (F-1)** | 1324275.23 | 465952.14 | 588.67 | 1324276.06 | 465951.88 | 588.57 | -0.84 | 0.26 | 0.09 |
| **Fence (F-2)** | 1324285.34 | 465951.63 | 589.24 | 1324285.92 | 465951.3 | 589.35 | -0.58 | 0.33 | -0.11 |
| **Fence (F-3)** | 1323786.01 | 465983.39 | 584.59 | 1323785.63 | 465983.52 | 584.6 | 0.38 | -0.13 | -0.01 |
| **Gas Line Marker (GM-1)** | 1324710.76 | 465775.09 | 588.83 | 1324711.91 | 465775.08 | 588.24 | -1.15 | 0.01 | 0.59 |
| **Hangar (BD-1)** | 1323486.62 | 465737.1 | 602.73 | 1323485.63 | 465737.51 | 601.66 | 0.99 | -0.41 | 1.07 |
| **Light On Building (BD-2)** | 1323836.59 | 465382.3 | 601.55 | 1323836.3 | 465383.61 | 601.98 | 0.29 | -1.32 | -0.43 |
| **Obstruction Light on Windsock (OL)** | 1324347.95 | 465576.2 | 602.62 | 1324348.44 | 465576.73 | 602.8 | -0.5 | -0.53 | -0.18 |
| **Sign (S)** | 1324297.74 | 465949.89 | 588.55 | 1324298.36 | 465949.53 | 588.68 | -0.62 | 0.37 | -0.13 |
| **Tree (T-11)** | 1324169.86 | 466002.46 | 606.51 | 1324170.19 | 466002.35 | 606.48 | -0.34 | 0.11 | 0.03 |
| **Tree (T-13)** | 1324003.25 | 465210.75 | 601.19 | 1324002.38 | 465213.84 | 601.89 | 0.88 | -3.09 | -0.7 |
| **Tree (T-14)** | 1323813.79 | 465989.33 | 607.29 | 1323817.02 | 465990.54 | 608.5 | -3.23 | -1.21 | -1.22 |

Table 53. Obstacle Location Variance between Field Survey and UAS Test 5A (Inspire 2)

| Obstacle | Field Survey (ft) | | | UAS Imagery (ft) | | | Delta (ft) | | |
|---|---|---|---|---|---|---|---|---|---|
| | x | y | z | x | y | z | x | y | z |
| **Flagpole (FP)** | 1324223.78 | 468350.62 | 614.80 | 1324223.70 | 468349.94 | 611.52 | 0.08 | 0.68 | 3.28 |
| **Light On Pole (P-1)** | 1324293.79 | 468245.86 | 596.77 | 1324293.80 | 468245.63 | 595.49 | -0.01 | 0.23 | 1.28 |
| **Tree (T-2)** | 1325231.96 | 468312.17 | 631.87 | 1325232.10 | 468313.21 | 627.02 | -0.14 | -1.04 | 4.85 |
| **Tree (T-3)** | 1325241.12 | 468439.30 | 644.74 | 1325238.43 | 468438.38 | 636.81 | 2.69 | 0.92 | 7.93 |
| **Tree (T-4)** | 1325220.80 | 468628.74 | 637.97 | 1325221.03 | 468627.47 | 633.08 | -0.23 | 1.27 | 4.89 |
| **Tree (T-5)** | 1325176.38 | 468744.19 | 636.69 | 1325186.71 | 468747.96 | 628.93 | -10.33 | -3.77 | 7.76 |
| **Tree (T-6)** | 1325058.63 | 468830.05 | 621.36 | 1325057.73 | 468829.88 | 617.56 | 0.90 | 0.16 | 3.79 |
| **Tree (T-7)** | 1324695.98 | 468601.33 | 629.81 | 1324705.99 | 468599.91 | 624.16 | -10.01 | 1.43 | 5.65 |

Table 54. Obstacle Location Variance between Field Survey and UAS Test 5B (Inspire 2)

| Obstacle | Field Survey (ft) | | | UAS Imagery (ft) | | | Delta (ft) | | |
|---|---|---|---|---|---|---|---|---|---|
| | x | y | z | x | y | z | x | y | z |
| **Airfield Light (AL-1)** | 1324593.4 | 467832.36 | 582.72 | 1324592.69 | 467833.13 | 583.34 | 0.71 | -0.77 | -0.62 |
| **Airfield Light (AL-2)** | 1324676.26 | 467937.74 | 582.43 | 1324675.13 | 467938.29 | 583.02 | 1.13 | -0.55 | -0.59 |
| **Birdhouse (BH)** | 1324432.59 | 467444.24 | 585.41 | 1324432.17 | 467445.06 | 585.59 | 0.41 | -0.81 | -0.18 |
| **Fence (F-1)** | 1324275.23 | 465952.14 | 588.67 | 1324274.55 | 465953.1 | 587.97 | 0.68 | -0.96 | 0.69 |
| **Fence (F-4)** | 1324302.72 | 467418.27 | 587.44 | 1324303.13 | 467419.32 | 586.93 | -0.4 | -1.05 | 0.52 |
| **Fence (F-5)** | 1324338.25 | 467109 | 585.9 | 1324338.3 | 467110.29 | 586.1 | -0.05 | -1.28 | -0.2 |
| **Fence (F-6)** | 1324285.34 | 465951.63 | 589.24 | 1324284.38 | 465952.51 | 588.23 | 0.96 | -0.88 | 1.01 |
| **Gas Line Marker (GM-1)** | 1324710.76 | 465775.09 | 588.83 | 1324708.64 | 465775.26 | 589.25 | 2.12 | -0.17 | -0.42 |
| **Gas Line Marker (GM-2)** | 1324759.66 | 467551.1 | 587.24 | 1324757.84 | 467552.1 | 587.52 | 1.82 | -1 | -0.29 |
| **Gas Line Marker (GM-3)** | 1324750.44 | 467213.06 | 587.42 | 1324748.57 | 467214.34 | 588.11 | 1.86 | -1.28 | -0.7 |
| **Gas Line Marker (GM-4)** | 1324740.67 | 466887.22 | 588.45 | 1324738.66 | 466888.56 | 589.25 | 2.01 | -1.34 | -0.8 |
| **Patio Umbrella (U)** | 1324318.33 | 467221.95 | 594.99 | 1324318.57 | 467223.12 | 593.32 | -0.24 | -1.17 | 1.67 |
| **Sign (S)** | 1324297.74 | 465949.89 | 588.55 | 1324296.88 | 465950.8 | 587.71 | 0.87 | -0.91 | 0.84 |
| **Tree (T-1)** | 1324340.96 | 467589.01 | 599.92 | 1324341.03 | 467589.28 | 596.91 | -0.07 | -0.27 | 3.01 |
| **Tree (T-8)** | 1324326.37 | 467093.14 | 596.76 | 1324324.12 | 467095.54 | 594.93 | 2.25 | -2.4 | 1.83 |
| **Tree (T-9)** | 1324249.98 | 467371.83 | 591.97 | 1324250.72 | 467372.55 | 590.48 | -0.74 | -0.72 | 1.49 |
| **Tree (T-10)** | 1324264.82 | 466219.68 | 613.15 | 1324264.44 | 466218.4 | 607.14 | 0.38 | 1.28 | 6.02 |
| **Tree (T-11)** | 1324169.86 | 466002.46 | 606.51 | 1324169.91 | 466003.6 | 601.73 | -0.05 | -1.14 | 4.78 |

Table 55. Obstacle Location Variance between Field Survey and UAS Test 5C (Inspire 2)

| Obstacle | Field Survey (ft) | | | UAS Imagery (ft) | | | Delta (ft) | | |
|---|---|---|---|---|---|---|---|---|---|
| | x | y | z | x | y | z | x | y | z |
| **Fence (F-1)** | 1324275.23 | 465952.14 | 588.67 | 1324276.32 | 465952.31 | 589.52 | -1.09 | -0.17 | -0.85 |
| **Fence (F-2)** | 1324285.34 | 465951.63 | 589.24 | 1324286.09 | 465951.76 | 590.39 | -0.75 | -0.13 | -1.15 |
| **Fence (F-3)** | 1323786.01 | 465983.39 | 584.59 | 1323785.74 | 465983.79 | 585.52 | 0.27 | -0.39 | -0.93 |
| **Gas Line Marker (GM-1)** | 1324710.76 | 465775.09 | 588.83 | 1324712.27 | 465775.32 | 590.13 | -1.51 | -0.23 | -1.3 |
| **Hangar (BD-1)** | 1323486.62 | 465737.1 | 602.73 | 1323485.57 | 465738 | 602.84 | 1.05 | -0.9 | -0.11 |
| **Light On Building (BD-2)** | 1323836.59 | 465382.3 | 601.55 | 1323836.45 | 465384.2 | 602.49 | 0.14 | -1.91 | -0.94 |
| **Obstruction Light on Windsock (OL)** | 1324347.95 | 465576.2 | 602.62 | 1324348.61 | 465577.26 | 603.34 | -0.66 | -1.06 | -0.72 |
| **Sign (S)** | 1324297.74 | 465949.89 | 588.55 | 1324298.59 | 465950.07 | 589.66 | -0.85 | -0.17 | -1.11 |
| **Tree (T-11)** | 1324169.86 | 466002.46 | 606.51 | 1324170.39 | 466002.65 | 606.34 | -0.53 | -0.19 | 0.17 |
| **Tree (T-13)** | 1324003.25 | 465210.75 | 601.19 | 1324002.52 | 465213.12 | 602.47 | 0.73 | -2.37 | -1.28 |
| **Tree (T-14)** | 1323813.79 | 465989.33 | 607.29 | 1323817.07 | 465990.53 | 608.96 | -3.29 | -1.21 | -1.67 |

3.4.4.2 Tests 6 and 7: Interlaced versus Sequential Flight Lines

Tests 6 and 7 were conducted to evaluate the effect of using interlaced flight lines versus standard sequential flight lines, as illustrated in Figure 34 in Section 3.4.1.2. Beyond the flight line pattern these flights were conducted with identical data collection parameters 80%/60% forward and side overlap and a GSD of 1 in.

Tables 56, 57, and 58 present comparisons between obstacle locations derived from traditional field survey techniques and the eBee X UAS imagery collected during Test 6 when measured in stereo. This flight used interlaced flight lines.

During Test 6A, nearly all vertical obstacle measurements fell outside of the accuracy requirements (3 ft) stated in AC 150/5300-18B; however, all measurements in Tests 6B and 6C met the requirements (FAA, 2014). One obstacle during Test 6B was not able to be measured (T11) because it was not visible in stereo imagery.

Wind gusts increased during Tests 6A and 6B, but it is unknown whether the slightly higher values over the vegetative areas in Test Area A were due to the increase in environmental factors, such as wind, or if the distortion previously seen in the sensor had a significant effect on the obstacle measurement.

Tables 59 and 60 present comparisons between obstacle locations derived from traditional field survey techniques and the eBee X UAS imagery collected during Test 7 when measured in stereo. This test used sequential flight lines, and the delta values are slightly better in these data sets versus Test 6. All measurements closely matched the field survey results, with the exception of a single tree. This was the only measurement that did not meet the strictest accuracy requirements (20 ft horizontal, 3 ft vertical) stated in AC 150/5300-18 (FAA, 2014). The increased accuracy of Test 7 data versus Test 6 was attributed directly to the use of sequential flight lines rather than the interlaced flight lines used in Test 6.

Table 56. Obstacle Location Variance between Field Survey and UAS Test 6A (eBee X)

| Obstacle | Field Survey (ft) | | | UAS Imagery (ft) | | | Delta (ft) | | |
|---|---|---|---|---|---|---|---|---|---|
| | x | y | z | x | y | z | x | y | z |
| **Flagpole (FP)** | 1324223.78 | 468350.62 | 614.80 | 1324223.49 | 468350.84 | 613.81 | 0.08 | 0.68 | 3.28 |
| **Light On Pole (P-1)** | 1324293.79 | 468245.86 | 596.77 | 1324293.64 | 468246.30 | 596.40 | -0.01 | 0.23 | 1.28 |
| **Tree (T-2)** | 1325231.96 | 468312.17 | 631.87 | 1325231.95 | 468311.93 | 631.40 | -0.14 | -1.04 | 4.85 |
| **Tree (T-3)** | 1325241.12 | 468439.30 | 644.74 | 1325238.61 | 468439.00 | 642.44 | 2.69 | 0.92 | 7.93 |
| **Tree (T-4)** | 1325220.80 | 468628.74 | 637.97 | 1325221.44 | 468626.30 | 635.57 | -0.23 | 1.27 | 4.89 |
| **Tree (T-5)** | 1325176.38 | 468744.19 | 636.69 | 1325197.06 | 468712.56 | 636.05 | -10.33 | -3.77 | 7.76 |
| **Tree (T-6)** | 1325058.63 | 468830.05 | 621.36 | 1325058.04 | 468830.24 | 620.11 | 0.90 | 0.16 | 3.79 |
| **Tree (T-7)** | 1324695.98 | 468601.33 | 629.81 | 1324706.20 | 468599.89 | 628.64 | -10.01 | 1.43 | 5.65 |

Table 57. Obstacle Location Variance between Field Survey and UAS Test 6B (eBee X)

| Obstacle | Field Survey (ft) | | | UAS Imagery (ft) | | | Delta (ft) | | |
|---|---|---|---|---|---|---|---|---|---|
| | x | y | z | x | y | z | x | y | z |
| **Airfield Light (AL-1)** | 1324593.4 | 467832.36 | 582.72 | 1324593.39 | 467832.66 | 582.53 | 0.01 | -0.3 | 0.18 |
| **Airfield Light (AL-2)** | 1324676.26 | 467937.74 | 582.43 | 1324676.29 | 467938.03 | 582.61 | -0.03 | -0.29 | -0.18 |
| **Birdhouse (BH)** | 1324432.59 | 467444.24 | 585.41 | 1324432.68 | 467444.67 | 584.83 | -0.1 | -0.42 | 0.58 |
| **Fence (F-1)** | 1324275.23 | 465952.14 | 588.67 | 1324275.13 | 465953.17 | 588.89 | -0.09 | 1.03 | 0.22 |
| **Fence (F-4)** | 1324302.72 | 467418.27 | 587.44 | 1324302.95 | 467419.1 | 586.67 | -0.22 | -0.83 | 0.77 |
| **Fence (F-5)** | 1324338.25 | 467109 | 585.9 | 1324338.28 | 467110.09 | 585.41 | -0.02 | -1.08 | 0.49 |
| **Fence (F-6)** | 1324285.34 | 465951.63 | 589.24 | 1324285.06 | 465952.59 | 589.13 | -0.28 | 0.96 | -0.11 |
| **Gas Line Marker (GM-1)** | 1324710.76 | 465775.09 | 588.83 | 1324710.94 | 465775.42 | 588.79 | -0.18 | -0.33 | 0.04 |
| **Gas Line Marker (GM-2)** | 1324759.66 | 467551.1 | 587.24 | 1324759.65 | 467551.56 | 587.12 | 0.01 | -0.46 | 0.11 |
| **Gas Line Marker (GM-3)** | 1324750.44 | 467213.06 | 587.42 | 1324750.49 | 467213.87 | 587.2 | -0.05 | -0.81 | 0.22 |
| **Gas Line Marker (GM-4)** | 1324740.67 | 466887.22 | 588.45 | 1324740.77 | 466888.14 | 588.3 | -0.09 | -0.92 | 0.15 |
| **Patio Umbrella (U)** | 1324318.33 | 467221.95 | 594.99 | 1324318.42 | 467222.98 | 594.86 | -0.09 | -1.03 | 0.13 |
| **Sign (S)** | 1324297.74 | 465949.89 | 588.55 | 1324297.48 | 465950.88 | 588.71 | -0.26 | 0.99 | 0.16 |
| **Tree (T-1)** | 1324340.96 | 467589.01 | 599.92 | 1324341.04 | 467588.73 | 599.48 | -0.08 | 0.28 | 0.45 |
| **Tree (T-8)** | 1324326.37 | 467093.14 | 596.76 | 1324324.15 | 467095.19 | 597 | 2.22 | -2.04 | -0.24 |
| **Tree (T-9)** | 1324249.98 | 467371.83 | 591.97 | 1324250.01 | 467372.36 | 591.43 | -0.04 | -0.53 | 0.54 |
| **Tree (T-10)** | 1324264.82 | 466219.68 | 613.15 | 1324264.61 | 466218.78 | 614.13 | -0.2 | -0.9 | 0.98 |
| **Tree (T-11)** | 1324169.86 | 466002.459 | 606.51 | N/A | N/A | N/A | N/A | N/A | N/A |

Table 58. Obstacle Location Variance between Field Survey and UAS Test 6C (eBee X)

| Obstacle | Field Survey (ft) | | | UAS Imagery (ft) | | | Delta (ft) | | |
|---|---|---|---|---|---|---|---|---|---|
| | x | y | z | x | y | z | x | y | z |
| **Fence (F-1)** | 1324275.23 | 465952.14 | 588.67 | 1324275.98 | 465952.89 | 587.74 | -0.76 | -0.75 | 0.92 |
| **Fence (F-2)** | 1324285.34 | 465951.63 | 589.24 | 1324285.68 | 465952.36 | 588.86 | -0.34 | -0.73 | 0.38 |
| **Fence (F-3)** | 1323786.01 | 465983.39 | 584.59 | 1323786.01 | 465984.63 | 583.59 | -0.01 | -1.24 | 1 |
| **Gas Line Marker (GM-1)** | 1324710.76 | 465775.09 | 588.83 | 1324711.06 | 465775.18 | 587.67 | -0.31 | -0.09 | 1.17 |
| **Hangar (BD-1)** | 1323486.62 | 465737.1 | 602.73 | 1323486.22 | 465737.72 | 602.53 | 0.4 | -0.62 | 0.2 |
| **Light On Building (BD-2)** | 1323836.59 | 465382.3 | 601.55 | 1323836.56 | 465382.55 | 601.5 | 0.02 | -0.25 | 0.05 |
| **Obstruction Light on Windsock (OL)** | 1324347.95 | 465576.2 | 602.62 | 1324348.35 | 465576.45 | 602.37 | -0.4 | -0.25 | 0.25 |
| **Sign (S)** | 1324297.74 | 465949.89 | 588.55 | 1324298.08 | 465950.65 | 587.99 | -0.33 | -0.76 | 0.56 |
| **Tree (T-11)** | 1324169.86 | 466002.46 | 606.51 | 1324170.01 | 466002.9 | 605.36 | -0.15 | -0.44 | 1.15 |
| **Tree (T-13)** | 1324003.25 | 465210.75 | 601.19 | 1324002.64 | 465212.41 | 601.09 | 0.61 | -1.67 | 0.1 |
| **Tree (T-14)** | 1323813.79 | 465989.33 | 607.29 | 1323817.36 | 465990.16 | 607.81 | -3.58 | -0.84 | -0.52 |

Table 59. Obstacle Location Variance between Field Survey and UAS Test 7A (eBee X)

| Obstacle | Field Survey (ft) | | | UAS Imagery (ft) | | | Delta (ft) | | |
|---|---|---|---|---|---|---|---|---|---|
| | x | y | z | x | y | z | x | y | z |
| **Flagpole (FP)** | 1324223.78 | 468350.62 | 614.80 | 1324223.53 | 468350.91 | 614.82 | 0.25 | -0.29 | -0.02 |
| **Light On Pole (P-1)** | 1324293.79 | 468245.86 | 596.77 | 1324293.85 | 468246.34 | 596.71 | -0.06 | -0.48 | 0.05 |
| **Tree (T-2)** | 1325231.96 | 468312.17 | 631.87 | 1325232.01 | 468312.47 | 631.83 | -0.05 | -0.29 | 0.04 |
| **Tree (T-3)** | 1325241.12 | 468439.30 | 644.74 | 1325239.63 | 468438.23 | 645.75 | 1.48 | 1.07 | -1.01 |
| **Tree (T-4)** | 1325220.80 | 468628.74 | 637.97 | 1325221.42 | 468627.62 | 641.61 | -0.62 | 1.12 | -3.64 |
| **Tree (T-5)** | 1325176.38 | 468744.19 | 636.69 | 1325186.71 | 468747.67 | 636.58 | -10.34 | -3.48 | 0.11 |
| **Tree (T-6)** | 1325058.63 | 468830.05 | 621.36 | 1325058.12 | 468830.26 | 621.68 | 0.51 | -0.22 | -0.33 |
| **Tree (T-7)** | 1324695.98 | 468601.33 | 629.81 | 1324705.29 | 468599.79 | 629.63 | -9.31 | 1.55 | 0.18 |

Table 60. Obstacle Location Variance between Field Survey and UAS Test 7B (eBee X)

| Obstacle | Field Survey (ft) | | | UAS Imagery (ft) | | | Delta (ft) | | |
|---|---|---|---|---|---|---|---|---|---|
| | x | y | z | x | y | z | x | y | z |
| **Airfield Light (AL-1)** | 1324593.4 | 467832.36 | 582.72 | 1324593.45 | 467832.63 | 582.56 | -0.05 | -0.27 | 0.16 |
| **Airfield Light (AL-2)** | 1324676.26 | 467937.74 | 582.43 | 1324676.19 | 467937.94 | 582.38 | 0.07 | -0.2 | 0.06 |
| **Birdhouse (BH)** | 1324432.59 | 467444.24 | 585.41 | 1324432.55 | 467444.98 | 585.6 | 0.03 | -0.73 | -0.19 |
| **Fence (F-1)** | 1324275.23 | 465952.14 | 588.67 | 1324275.14 | 465953.08 | 588.54 | 0.09 | -0.94 | 0.13 |
| **Fence (F-4)** | 1324302.72 | 467418.27 | 587.44 | 1324303.06 | 467419.22 | 587.22 | -0.34 | -0.95 | 0.22 |
| **Fence (F-5)** | 1324338.25 | 467109 | 585.9 | 1324338.49 | 467110.08 | 586.16 | -0.24 | -1.08 | -0.26 |
| **Fence (F-6)** | 1324285.34 | 465951.63 | 589.24 | 1324285.11 | 465952.46 | 588.83 | 0.23 | -0.83 | 0.41 |
| **Gas Line Marker (GM-1)** | 1324710.76 | 465775.09 | 588.83 | 1324710.98 | 465775.41 | 588.03 | -0.22 | -0.32 | 0.8 |
| **Gas Line Marker (GM-2)** | 1324759.66 | 467551.1 | 587.24 | 1324759.61 | 467551.56 | 587.3 | 0.05 | -0.47 | -0.06 |
| **Gas Line Marker (GM-3)** | 1324750.44 | 467213.06 | 587.42 | 1324750.47 | 467213.79 | 587.55 | -0.03 | -0.73 | -0.13 |
| **Gas Line Marker (GM-4)** | 1324740.67 | 466887.22 | 588.45 | 1324740.73 | 466888.14 | 588.57 | -0.05 | -0.92 | -0.12 |
| **Patio Umbrella (U)** | 1324318.33 | 467221.95 | 594.99 | 1324318.57 | 467223.1 | 595.44 | -0.24 | -1.15 | -0.45 |
| **Sign (S)** | 1324297.74 | 465949.89 | 588.55 | 1324297.43 | 465950.67 | 588.15 | 0.31 | -0.78 | 0.4 |
| **Tree (T-1)** | 1324340.96 | 467589.01 | 599.92 | 1324340.84 | 467589.49 | 600.31 | 0.12 | -0.48 | -0.39 |
| **Tree (T-8)** | 1324326.37 | 467093.14 | 596.76 | 1324323.46 | 467095.12 | 596.88 | 2.92 | -1.97 | -0.11 |
| **Tree (T-9)** | 1324249.98 | 467371.83 | 591.97 | 1324250.26 | 467372.58 | 592.5 | -0.28 | -0.75 | -0.53 |
| **Tree (T-10)** | 1324264.82 | 466219.68 | 613.15 | 1324263.56 | 466219.34 | 613.66 | 1.26 | 0.35 | -0.51 |
| **Tree (T-11)** | 1324169.86 | 466002.46 | 606.51 | 1324169.74 | 466002.38 | 605.11 | 0.12 | 0.08 | 1.4 |

#### 3.4.4.3 Test 8: WingtraOne Validation

Tables 61, 62, and 63 present comparisons between obstacle locations derived from traditional field survey techniques and the UAS imagery collected during Test 8 when measured in stereo. These data sets were collected using the WingtraOne with 80%/60% forward and side overlap settings. This flight successfully replicated and validated the successful results achieved at FPY, and each obstacle measurement met the accuracy requirements (20 ft horizontal, 3 ft vertical) stated in AC 150/5300-18 (FAA, 2014). The only anomalies observed in the deltas were on treetops. Two obstacles in Test Area B, a tree (T-9) and a fence (F-4), were not visible in the stereo imagery and could not be measured.

Table 61. Obstacle Location Variance between Field Survey and UAS Test 8A (WingtraOne)

| Obstacle | Field Survey (ft) | | | UAS Imagery (ft) | | | Delta (ft) | | |
|---|---|---|---|---|---|---|---|---|---|
| | x | y | z | x | y | z | x | y | z |
| **Flagpole (FP)** | 1324223.78 | 468350.62 | 614.80 | 1324223.51 | 468350.82 | 614.74 | 0.27 | -0.20 | 0.06 |
| **Light On Pole (P-1)** | 1324293.79 | 468245.86 | 596.77 | 1324293.75 | 468246.30 | 596.49 | 0.03 | -0.44 | 0.28 |
| **Tree (T-2)** | 1325231.96 | 468312.17 | 631.87 | 1325232.28 | 468312.88 | 630.47 | -0.32 | -0.71 | 1.41 |
| **Tree (T-3)** | 1325241.12 | 468439.30 | 644.74 | 1325238.52 | 468437.66 | 641.59 | 2.59 | 1.63 | 3.14 |
| **Tree (T-4)** | 1325220.80 | 468628.74 | 637.97 | 1325220.68 | 468627.29 | 638.22 | 0.12 | 1.45 | -0.25 |
| **Tree (T-5)** | 1325176.38 | 468744.19 | 636.69 | 1325186.95 | 468747.31 | 639.03 | -10.57 | -3.12 | -2.34 |
| **Tree (T-6)** | 1325058.63 | 468830.05 | 621.36 | 1325057.87 | 468830.13 | 621.26 | 0.76 | -0.08 | 0.09 |
| **Tree (T-7)** | 1324695.98 | 468601.33 | 629.81 | 1324705.73 | 468599.85 | 629.20 | -9.76 | 1.49 | 0.61 |

Table 62. Obstacle Location Variance between Field Survey and UAS Test 8B (WingtraOne)

| Obstacle | Field Survey (ft) | | | UAS Imagery (ft) | | | Delta (ft) | | |
|---|---|---|---|---|---|---|---|---|---|
| | x | y | z | x | y | z | x | y | z |
| **Airfield Light (AL-1)** | 1324593.4 | 467832.36 | 582.72 | 1324593.33 | 467832.37 | 582.68 | 0.06 | -0.01 | 0.04 |
| **Airfield Light (AL-2)** | 1324676.26 | 467937.74 | 582.43 | 1324676.23 | 467937.72 | 582.41 | 0.03 | 0.02 | 0.02 |
| **Birdhouse (BH)** | 1324432.59 | 467444.24 | 585.41 | 1324432.56 | 467444.05 | 585.19 | 0.02 | 0.19 | 0.21 |
| **Fence (F-1)** | 1324275.23 | 465952.14 | 588.67 | 1324275.43 | 465952.22 | 588.46 | -0.2 | -0.08 | 0.21 |
| **Fence (F-4)** | 1324302.7 | 467418.27 | 587.44 | N/A | N/A | N/A | N/A | N/A | N/A |
| **Fence (F-5)** | 1324338.25 | 467109 | 585.9 | 1324338.13 | 467109.04 | 585.68 | 0.13 | -0.03 | 0.22 |
| **Fence (F-6)** | 1324285.34 | 465951.63 | 589.24 | 1324285.31 | 465951.62 | 589.03 | 0.03 | 0.01 | 0.2 |
| **Gas Line Marker (GM-1)** | 1324710.76 | 465775.09 | 588.83 | 1324710.76 | 465775.07 | 588.68 | 0 | 0.02 | 0.16 |
| **Gas Line Marker (GM-2)** | 1324759.66 | 467551.1 | 587.24 | 1324759.59 | 467551.08 | 587.56 | 0.07 | 0.02 | -0.32 |
| **Gas Line Marker (GM-3)** | 1324750.44 | 467213.06 | 587.42 | 1324750.41 | 467213.04 | 587.67 | 0.02 | 0.02 | -0.25 |
| **Gas Line Marker (GM-4)** | 1324740.67 | 466887.22 | 588.45 | 1324740.6 | 466887.19 | 588.61 | 0.07 | 0.03 | -0.16 |
| **Patio Umbrella (U)** | 1324318.33 | 467221.95 | 594.99 | 1324318.21 | 467222.05 | 595.1 | 0.11 | -0.11 | -0.11 |
| **Sign (S)** | 1324297.74 | 465949.89 | 588.55 | 1324297.61 | 465949.82 | 588.3 | 0.14 | 0.07 | 0.25 |
| **Tree (T-1)** | 1324340.96 | 467589.01 | 599.92 | 1324340.46 | 467588.92 | 599.96 | 0.5 | 0.09 | -0.04 |
| **Tree (T-8)** | 1324326.37 | 467093.14 | 596.76 | 1324323.48 | 467095.25 | 597.12 | 2.89 | -2.11 | -0.36 |
| **Tree (T-9)** | 1324249.98 | 467371.83 | 591.97 | N/A | N/A | N/A | N/A | N/A | N/A |
| **Tree (T-10)** | 1324264.82 | 466219.68 | 613.15 | 1324263.57 | 466219.04 | 613.07 | 1.25 | 0.65 | 0.08 |
| **Tree (T-11)** | 1324169.86 | 466002.46 | 606.51 | 1324169.58 | 466002.35 | 606.69 | 0.27 | 0.11 | -0.18 |

Table 63. Obstacle Location Variance between Field Survey and UAS Test 8C (WingtraOne)

| Obstacle | Field Survey (ft) | | | UAS Imagery (ft) | | | Delta (ft) | | |
|---|---|---|---|---|---|---|---|---|---|
| | x | y | z | x | y | z | x | y | z |
| **Fence (F-1)** | 1324275.23 | 465952.14 | 588.67 | 1324275.98 | 465952.89 | 587.74 | -0.75 | -0.76 | 0.92 |
| **Fence (F-2)** | 1324285.34 | 465951.63 | 589.24 | 1324285.68 | 465952.36 | 588.86 | -0.73 | -0.34 | 0.38 |
| **Fence (F-3)** | 1323786.01 | 465983.39 | 584.59 | 1323786.01 | 465984.63 | 583.59 | -1.24 | -0.01 | 1 |
| **Gas Line Marker (GM-1)** | 1324710.76 | 465775.09 | 588.83 | 1324711.06 | 465775.18 | 587.67 | -0.09 | -0.31 | 1.17 |
| **Hangar (BD-1)** | 1323486.62 | 465737.1 | 602.73 | 1323486.22 | 465737.72 | 602.53 | -0.62 | 0.4 | 0.2 |
| **Light On Building (BD-2)** | 1323836.59 | 465382.3 | 601.55 | 1323836.56 | 465382.55 | 601.5 | -0.25 | 0.02 | 0.05 |
| **Obstruction Light on Windsock (OL)** | 1324347.95 | 465576.2 | 602.62 | 1324348.35 | 465576.45 | 602.37 | -0.25 | -0.4 | 0.25 |
| **Sign (S)** | 1324297.74 | 465949.89 | 588.55 | 1324298.08 | 465950.65 | 587.99 | -0.76 | -0.33 | 0.56 |
| **Tree (T-11)** | 1324169.86 | 466002.46 | 606.51 | 1324170.01 | 466002.9 | 605.36 | -0.44 | -0.15 | 1.15 |
| **Tree (T-13)** | 1324003.25 | 465210.75 | 601.19 | 1324002.64 | 465212.41 | 601.09 | -1.67 | 0.61 | 0.1 |
| **Tree (T-14)** | 1323813.79 | 465989.33 | 607.29 | 1323817.36 | 465990.16 | 607.81 | -0.84 | -3.58 | -0.52 |

#### 3.4.4.4 Tests 9 and 10: Sun Angle

Tests 9 and 10 were conducted to evaluate the effect of sun angle on the quality of the survey data collected. Both tests used the M210 with 80%/80% forward and side overlap values. Test 9 was flown from 7:43 A.M. to 8:07 A.M., and Test 10 was flown approximately 12 hours later from 7:37 P.M. to 7:52 P.M. Unfortunately, a high amount of haze in the air due to wildfires out west minimized the effect of shadows, which are a key consideration regarding the effect of low sun angles of aerial imagery.

Table 64 compares obstacle locations derived from traditional field survey techniques and the UAS imagery collected during Test 9 when measured in stereo.

The low sun angle had no apparent impact on the accuracy of the obstacle measurements taken from the UAS imagery. However, during stereo analysis it was found that the data set was inconsistent in color, exposure, and texture. The imagery was at times fuzzy, very soft and flat in places making obstacles difficult to measure. Despite these issues, each obstacle measurement derived from Test 9 met the accuracy standard (20 ft horizontal, 3 ft vertical) stated in AC 150/5300-18 (FAA, 2014).

Table 65 compares obstacle locations derived from traditional field survey techniques and the UAS imagery collected during Test 10 when measured in stereo. Each obstacle measurement from data collected during Test 10 met the accuracy standard (20 ft horizontal, 3 ft vertical) stated in AC 150/5300-18 (FAA, 2014).

Test 10 produced similar results to Test 9, and the low sun angle had no apparent impact on the obstacle measurements taken from imagery collected during Test 10. The imagery suffered from the same issues as Test 9, including inconsistencies in color, exposure, and texture; and low contrast and haziness.

Table 64. Obstacle Location Variance between Field Survey and UAS Test 9 (M210)

| Obstacle | Field Survey (ft) | | | UAS Imagery (ft) | | | Delta (ft) | | |
|---|---|---|---|---|---|---|---|---|---|
| | x | y | z | x | y | z | x | y | z |
| **Fence (F-1)** | 1324275.23 | 465952.14 | 588.67 | 1324276.34 | 465952.21 | 589.2 | -1.11 | -0.06 | -0.53 |
| **Fence (F-2)** | 1324285.34 | 465951.63 | 589.24 | 1324286.26 | 465951.59 | 589.81 | -0.92 | 0.04 | -0.57 |
| **Fence (F-3)** | 1323786.01 | 465983.39 | 584.59 | 1323785.76 | 465984.06 | 584.92 | 0.25 | -0.66 | -0.33 |
| **Gas Line Marker (GM-1)** | 1324710.76 | 465775.09 | 588.83 | 1324712.45 | 465775.1 | 588.37 | -1.69 | -0.01 | 0.47 |
| **Hangar (BD-1)** | 1323486.62 | 465737.1 | 602.73 | 1323485.49 | 465737.96 | 602.42 | 1.13 | -0.86 | 0.31 |
| **Light On Building (BD-2)** | 1323836.59 | 465382.3 | 601.55 | 1323836.19 | 465383.95 | 603.31 | 0.4 | -1.65 | -1.76 |
| **Obstruction Light on Windsock (OL)** | 1324347.95 | 465576.2 | 602.62 | 1324348.91 | 465577.27 | 603.67 | -0.97 | -1.07 | -1.05 |
| **Sign (S)** | 1324297.74 | 465949.89 | 588.55 | 1324298.68 | 465949.78 | 589.13 | -0.94 | 0.11 | -0.58 |
| **Tree (T-11)** | 1324169.86 | 466002.46 | 606.51 | 1324170.53 | 466002.54 | 607.32 | -0.68 | -0.08 | -0.81 |
| **Tree (T-13)** | 1324003.25 | 465210.75 | 601.19 | 1324002.3 | 465212.94 | 602.9 | 0.95 | -2.19 | -1.71 |
| **Tree (T-14)** | 1323813.79 | 465989.33 | 607.29 | 1323816.97 | 465991.08 | 609.37 | -3.18 | -1.75 | -2.08 |

Table 65. Obstacle Variance between Field Survey and Test 10 (M210)

| Obstacle | Field Survey (ft) | | | UAS Imagery (ft) | | | Delta (ft) | | |
|---|---|---|---|---|---|---|---|---|---|
| | x | y | z | x | y | z | x | y | z |
| **Fence (F-1)** | 1324710.76 | 465775.09 | 588.83 | 1324712.63 | 465774.97 | 589.68 | -1.87 | 0.12 | -0.85 |
| **Fence (F-2)** | 1324297.74 | 465949.89 | 588.55 | 1324298.83 | 465949.85 | 588.98 | -1.09 | 0.05 | -0.43 |
| **Fence (F-3)** | 1324285.34 | 465951.63 | 589.24 | 1324286.37 | 465951.67 | 589.63 | -1.04 | -0.04 | -0.39 |
| **Gas Line Marker (GM-1)** | 1324275.23 | 465952.14 | 588.67 | 1324276.37 | 465952.33 | 589.1 | -1.15 | -0.18 | -0.44 |
| **Hangar (BD-1)** | 1324347.95 | 465576.2 | 602.62 | 1324348.75 | 465576.75 | 604.5 | -0.8 | -0.55 | -1.88 |
| **Light On Building (BD-2)** | 1324169.86 | 466002.46 | 606.51 | 1324170.07 | 466002.62 | 606.21 | -0.21 | -0.16 | 0.3 |
| **Obstruction Light on Windsock (OL)** | 1323486.62 | 465737.1 | 602.73 | 1323485.35 | 465738.24 | 603.07 | 1.27 | -1.14 | -0.34 |
| **Sign (S)** | 1323813.79 | 465989.33 | 607.29 | 1323817.07 | 465990.86 | 609.39 | -3.28 | -1.53 | -2.1 |
| **Tree (T-11)** | 1323786.01 | 465983.39 | 584.59 | 1323785.71 | 465984.08 | 584.4 | 0.3 | -0.68 | 0.19 |
| **Tree (T-13)** | 1323836.59 | 465382.3 | 601.55 | 1323836.08 | 465384.01 | 603.49 | 0.51 | -1.71 | -1.94 |
| **Tree (T-14)** | 1324003.25 | 465210.75 | 601.19 | 1324002.73 | 465212.68 | 603.56 | 0.52 | -1.94 | -2.37 |

3.4.4.5 Tests 11, 12, and 13: Test of 70%/70% Forward and Side Overlap Values

Tests 11, 12, and 13 evaluated 70%/70% forward and side overlap values, which allowed for reduced flight times when compared to previously validated 80%/60% forward and side overlap settings. The lower overlap settings did not negatively affect the obstacle measurements taken from these data sets and, in fact, all three tests produced higher accuracies than earlier tests conducted with higher overlap settings. All three data sets met the accuracy standard (20 ft horizontal, 3 ft vertical) stated in AC 150/5300-18 (FAA, 2014).

Table 66 compares obstacle locations derived from traditional field survey techniques and the WingtraOne UAS imagery collected during Test 10 when measured in stereo.

Table 67 compares obstacle locations derived from traditional field survey techniques and the eBee X UAS imagery collected during Test 12 when measured in stereo.

Table 68 compares obstacle locations derived from traditional field survey techniques and the M210 UAS imagery collected during Test 13 when measured in stereo.

Test 13 was the third of the matching overlap tests conducted using 70%/70% forward and side overlap values. The lower overlap had minimal effect on the accuracy of obstacle data collection, and the average residuals are similar to the results of Test 9 and Test 10, which were conducted with 80%/60% forward and side overlap values.

Table 66. Obstacle Variance between Field Survey and Test 11 (WingtraOne)

| Obstacle | Field Survey (ft) | | | UAS Imagery (ft) | | | Delta (ft) | | |
|---|---|---|---|---|---|---|---|---|---|
| | x | y | z | x | y | z | x | y | z |
| **Flagpole (FP)** | 1324223.78 | 468350.62 | 614.80 | 1324223.54 | 468350.87 | 614.76 | 0.24 | -0.24 | 0.05 |
| **Light On Pole (P-1)** | 1324293.79 | 468245.86 | 596.77 | 1324293.81 | 468246.28 | 596.55 | -0.02 | -0.42 | 0.22 |
| **Tree (T-2)** | 1325231.96 | 468312.17 | 631.87 | 1325232.11 | 468312.44 | 632.08 | -0.15 | -0.26 | -0.20 |
| **Tree (T-3)** | 1325241.12 | 468439.30 | 644.74 | 1325239.70 | 468437.73 | 644.94 | 1.41 | 1.57 | -0.20 |
| **Tree (T-4)** | 1325220.80 | 468628.74 | 637.97 | 1325221.16 | 468627.73 | 637.68 | -0.36 | 1.01 | 0.29 |
| **Tree (T-5)** | 1325176.38 | 468744.19 | 636.69 | 1325186.70 | 468747.20 | 637.35 | -10.32 | -3.02 | -0.65 |
| **Tree (T-6)** | 1325058.63 | 468830.05 | 621.36 | 1325057.70 | 468830.07 | 620.28 | 0.93 | -0.02 | 1.07 |
| **Tree (T-7)** | 1324695.98 | 468601.33 | 629.81 | 1324705.72 | 468599.92 | 629.64 | -9.74 | 1.42 | 0.17 |

Table 67. Obstacle Variance between Field Survey and Test 12 (eBee X)

| Obstacle | Field Survey (ft) | | | UAS Imagery (ft) | | | Delta (ft) | | |
|---|---|---|---|---|---|---|---|---|---|
| | x | y | z | x | y | z | x | y | z |
| **Flagpole (FP)** | 1324223.78 | 468350.62 | 614.80 | 1324223.41 | 468350.86 | 614.25 | 0.37 | -0.24 | 0.55 |
| **Light On Pole (P-1)** | 1324293.79 | 468245.86 | 596.77 | 1324293.85 | 468246.38 | 596.45 | -0.06 | -0.52 | 0.32 |
| **Tree (T-2)** | 1325231.96 | 468312.17 | 631.87 | 1325232.19 | 468312.61 | 630.34 | -0.23 | -0.44 | 1.53 |
| **Tree (T-3)** | 1325241.12 | 468439.30 | 644.74 | 1325239.03 | 468438.22 | 641.92 | 2.08 | 1.07 | 2.82 |
| **Tree (T-4)** | 1325220.80 | 468628.74 | 637.97 | 1325220.81 | 468626.85 | 639.81 | -0.01 | 1.89 | -1.84 |
| **Tree (T-5)** | 1325176.38 | 468744.19 | 636.69 | 1325185.22 | 468751.30 | 635.01 | -8.84 | -7.11 | 1.68 |
| **Tree (T-6)** | 1325058.63 | 468830.05 | 621.36 | 1325057.73 | 468830.25 | 620.35 | 0.90 | -0.20 | 1.00 |
| **Tree (T-7)** | 1324695.98 | 468601.33 | 629.81 | 1324706.18 | 468600.49 | 628.25 | -10.20 | 0.85 | 1.56 |

Table 68. Obstacle Variance between Field Survey and Test 13 (M210)

| Obstacle | Field Survey (ft) | | | UAS Imagery (ft) | | | Delta (ft) | | |
|---|---|---|---|---|---|---|---|---|---|
| | x | y | z | x | y | z | x | y | z |
| **Flagpole (FP)** | 1324223.78 | 468350.62 | 614.80 | 1324223.71 | 468350.03 | 615.71 | -0.08 | -0.59 | 0.90 |
| **Light On Pole (P-1)** | 1324293.79 | 468245.86 | 596.77 | 1324293.88 | 468245.96 | 597.71 | 0.09 | 0.10 | 0.94 |
| **Tree (T-2)** | 1325231.96 | 468312.17 | 631.87 | 1325232.12 | 468313.94 | 634.49 | 0.16 | 1.77 | 2.62 |
| **Tree (T-3)** | 1325241.12 | 468439.30 | 644.74 | 1325240.18 | 468440.40 | 647.95 | -0.94 | 1.10 | 3.21 |
| **Tree (T-4)** | 1325220.80 | 468628.74 | 637.97 | 1325221.20 | 468628.60 | 640.04 | 0.40 | -0.14 | 2.07 |
| **Tree (T-5)** | 1325176.38 | 468744.19 | 636.69 | 1325187.99 | 468747.24 | 638.90 | 11.61 | 3.05 | 2.20 |
| **Tree (T-6)** | 1325058.63 | 468830.05 | 621.36 | 1325058.42 | 468829.97 | 622.96 | -0.20 | -0.08 | 1.61 |
| **Tree (T-7)** | 1324695.98 | 468601.33 | 629.81 | 1324706.23 | 468599.57 | 630.70 | 10.25 | -1.76 | 0.89 |

### 3.4.5 National Geodetic Survey Stereo Analysis—Manned Imagery to Field Survey Comparison Results

To assess the relative accuracy of the UAS obstacle data, FAA researchers provided the field-surveyed obstacle locations to the NGS. The NGS then viewed the manned aircraft imagery in stereo and collected obstacle locations for comparison. Due to the age of the manned imagery (~3 years) only man-made obstacles were evaluated to eliminate the variable of vegetation growth. In addition, not all the man-made features surveyed in 2021 were present at the time of the 2018 manned imagery collection. Table 69 compares obstacle locations the NGS derived from the manned aircraft imagery when measured in stereo and the field survey.

Of the 36 man-made obstacles used for comparison, the manned aircraft imagery was unable to locate or reliably measure 10 obstacles, indicated by the yellow-shaded cells. These were primarily narrow obstacles, such as lightning rods or antennas, that manned imagery has trouble locating due to its 6-in. GSD. As indicated by the green-shaded cells, all horizontal measurements met the accuracy requirements (20 ft) stated in AC 150/5300-18 (FAA, 2014). Three vertical measurements did not meet the vertical accuracy requirement of 3 ft, as indicated by the red-shaded cells.

Table 69. National Geodetic Survey Obstacle Location Variance between Manned Imagery and Field Survey

| Obstacle Type | Field Survey (ft) | | | Manned Imagery (ft) | | | Delta (ft) | | |
|---|---|---|---|---|---|---|---|---|---|
| | x | y | z | x | y | z | x | y | z |
| **Antenna Mast on Building** | 1323951.36 | 465233.05 | 598.61 | N/A | N/A | N/A | N/A | N/A | N/A |
| **Antenna On Building** | 1323951.26 | 465233.16 | 600.62 | N/A | N/A | N/A | N/A | N/A | N/A |
| **Antenna On Building** | 1323946.11 | 465266.04 | 606.861 | 1323946.47 | 465266.22 | 598.801 | -0.359 | -0.182 | 8.06 |
| **APBN On Building** | 1324085.86 | 465186.6 | 605.248 | 1324086.26 | 465185.85 | 604.263 | -0.406 | 0.751 | 0.985 |
| **Building** | 1323889.94 | 465469.65 | 598.894 | 1323890.87 | 465469.75 | 598.316 | -0.927 | -0.106 | 0.578 |
| **Building** | 1323919.15 | 465468.84 | 596.419 | 1323920.42 | 465469.11 | 594.562 | -1.263 | -0.275 | 1.857 |
| **Building** | 1323374.06 | 465419.84 | 612.644 | N/A | N/A | N/A | N/A | N/A | N/A |
| **Building** | 1323834.64 | 465321.34 | 594.592 | 1323835.05 | 465321.32 | 593.712 | -0.404 | 0.027 | 0.88 |
| **Building** | 1323950.86 | 465230.45 | 590.879 | 1323951.29 | 465230.66 | 590.594 | -0.426 | -0.21 | 0.285 |
| **Chain Link Fence** | 1324275.23 | 465952.14 | 588.665 | 1324275.44 | 465952.32 | 586.588 | -0.212 | -0.182 | 2.077 |
| **Chain Link Fence Post** | 1324285.34 | 465951.63 | 589.238 | 1324286.24 | 465951.43 | 586.614 | -0.897 | 0.199 | 2.624 |
| **Chain Link Fence Top** | 1323786.01 | 465983.39 | 584.589 | 1323786.47 | 465983.45 | 581.591 | -0.467 | -0.055 | 2.998 |
| **Chain Link Fence Top Rail** | 1324272.06 | 465952.39 | 588.524 | 1324272.79 | 465952.38 | 586.915 | -0.727 | 0.01 | 1.609 |
| **Gas Line Marker** | 1324710.76 | 465775.09 | 588.834 | N/A | N/A | N/A | N/A | N/A | N/A |
| **Hangar Roof** | 1323898.98 | 465761.56 | 598.917 | 1323899.97 | 465761.29 | 598.733 | -0.99 | 0.267 | 0.184 |
| **Hangar Roof** | 1323621.71 | 465763.6 | 597.829 | 1323622.62 | 465763.07 | 597.738 | -0.907 | 0.534 | 0.091 |
| **Hangar Roof** | 1323486.62 | 465737.1 | 602.73 | 1323487.6 | 465736.38 | 602.256 | -0.975 | 0.721 | 0.474 |
| **Instrument On AWOS** | 1324299.86 | 465755.82 | 615.709 | N/A | N/A | N/A | N/A | N/A | N/A |
| **Instrument On AWOS** | 1324299.83 | 465753.14 | 615.589 | N/A | N/A | N/A | N/A | N/A | N/A |
| **Light On Building** | 1323832.2 | 465321.28 | 600.308 | 1323832.58 | 465321.56 | 598.894 | -0.38 | -0.287 | 1.414 |
| **Light On Building** | 1323836.59 | 465382.3 | 601.551 | 1323836.69 | 465381.75 | 601.73 | -0.1 | 0.547 | -0.179 |
| **Lightning Rod On AWOS** | 1324300.55 | 465755.75 | 618.274 | N/A | N/A | N/A | N/A | N/A | N/A |
| **Metal Sign** | 1324297.74 | 465949.89 | 588.55 | 1324298.31 | 465950.14 | 586.176 | -0.565 | -0.242 | 2.374 |
| **Obstruction Light On AWOS** | 1324299.84 | 465756.01 | 613.219 | 1324300.34 | 465754.46 | 611.562 | -0.504 | 1.545 | 1.657 |
| **Obstruction Light On AWOS** | 1324299.1 | 465756.03 | 613.213 | N/A | N/A | N/A | N/A | N/A | N/A |
| **Obstruction Light on Windsock** | 1324347.95 | 465576.2 | 602.623 | 1324348.87 | 465576.87 | 599.49 | -0.923 | -0.668 | 3.133 |
| **Pole** | 1324066.35 | 465097.16 | 611.987 | 1324067.81 | 465095.8 | 611.179 | -1.457 | 1.362 | 0.808 |
| **Pole** | 1323955.61 | 465097 | 611.332 | 1323956.36 | 465096.04 | 608.988 | -0.75 | 0.962 | 2.344 |

| Obstacle Type | Field Survey (ft) | | | Manned Imagery (ft) | | | Delta (ft) | | |
|---|---|---|---|---|---|---|---|---|---|
| | x | y | z | x | y | z | x | y | z |
| **Pole** | 1323729.24 | 465097.16 | 621.675 | 1323730.24 | 465096.04 | 618.133 | -1.003 | 1.118 | 3.542 |
| **Post On Building** | 1324190.03 | 465149.69 | 601.806 | 1324191.26 | 465148.62 | 601.128 | -1.228 | 1.071 | 0.678 |
| **Roof Peak** | 1324214.44 | 466119.77 | 598.887 | 1324215.65 | 466120.11 | 598.246 | -1.203 | -0.337 | 0.641 |
| **Signpost** | 1324688.91 | 465961.86 | 588.32 | 1324689.75 | 465961.64 | 587.339 | -0.84 | 0.215 | 0.981 |
| **Signpost** | 1324396.51 | 466144.59 | 587.447 | 1324397.51 | 466144.42 | 586.951 | -0.998 | 0.172 | 0.496 |
| **Vent** | 1324138.09 | 465293.93 | 592.289 | N/A | N/A | N/A | N/A | N/A | N/A |
| **Vent On Building** | 1324183.55 | 466052.92 | 602.774 | 1324184.18 | 466052.77 | 602.189 | -0.627 | 0.144 | 0.585 |
| **Wood Fence** | 1324279.26 | 466209.37 | 585.625 | N/A | N/A | N/A | N/A | N/A | N/A |

AWOS = Automated weather observing system

### 3.4.6 National Geodetic Survey Stereo Analysis—UAS Imagery to Field Survey Comparison Results

Table 70 compares the x, y, and z measurements of obstacles from the FAA field survey and the NGS' analysis of eBee X imagery when viewed in stereo. While 11 of the 65 obstacles identified in the field survey could not be located or accurately measured during stereo analysis of the UAS imagery, every other obstacle measured was within the most stringent (1A) accuracy requirement (20 ft horizontal, 3 ft vertical) stated in AC 150/5300-18 (FAA, 2014), when compared to the field survey.

Of the 11 obstacles that could not be located, 5 were man-made obstacles and 6 were trees. These five man-made obstacles were among the same obstacles that could not be located using the manned aircraft imagery. The other five obstacles that could not be located in the manned imagery were visible in the UAS data and measured with accuracy meeting current requirements. This analysis found that the eBee X data set collected at I67 outperformed the manned aircraft data set in terms of both accuracy and completeness.

Table 71 compares the x, y, and z measurements of obstacles from the FAA field survey and the NGS' analysis of WingtraOne imagery when viewed in stereo. The results from this evaluation closely match those from the eBee X data, with all measured obstacles found to be well within the strictest accuracy requirements (20 ft horizontal, 3 ft vertical) stated in AC 150/5300-18 (FAA, 2014). Ten obstacles could not be located or effectively measured in the UAS data, but the obstacles that were located were found to be exceedingly accurate, with the vast majority within 1 ft of the field survey data.

Mirroring the results of the eBee data set, the NGS analysis showed that five man-made obstacles could not be located in the Wingtra data. Each of these five obstacles also could not be located in the manned aircraft imagery. The other five obstacles that couldn't be located in the manned data were measured in the Wingtra data set and measured with accuracy meeting the current requirements. This analysis found the WingtraOne data set collected at I67 outperformed the manned aircraft obstacle data in terms of both accuracy and completeness.

Table 70. National Geodetic Survey Obstacle Location Variance between Field Survey and UAS Test 7 (eBee X)

| Obstacle Type | Field Survey (ft) | | | UAS Imagery (ft) | | | Delta (ft) | | |
|---|---|---|---|---|---|---|---|---|---|
| | x | y | z | x | y | z | x | y | z |
| **Antenna Mast on Building** | 1323951.36 | 465233.05 | 598.61 | 1323951.28 | 465233.23 | 599.283 | 0.081 | -0.173 | -0.673 |
| **Antenna on Building** | 1323951.26 | 465233.16 | 600.62 | N/A | N/A | N/A | N/A | N/A | N/A |
| **Antenna on Building** | 1323946.11 | 465266.04 | 606.861 | 1323946.19 | 465266.29 | 606.469 | -0.079 | -0.254 | 0.392 |
| **APBN on Building** | 1324085.86 | 465186.6 | 605.248 | 1324085.85 | 465186.72 | 604.846 | 0.007 | -0.12 | 0.402 |
| **Building** | 1323889.94 | 465469.65 | 598.894 | 1323890.03 | 465470.03 | 599.077 | -0.086 | -0.381 | -0.183 |
| **Building** | 1323919.15 | 465468.84 | 596.419 | 1323919.24 | 465469.18 | 596.791 | -0.088 | -0.341 | -0.372 |
| **Building** | 1323374.06 | 465419.84 | 612.644 | N/A | N/A | N/A | N/A | N/A | N/A |
| **Building** | 1323834.64 | 465321.34 | 594.592 | 1323834.61 | 465321.59 | 594.116 | 0.033 | -0.246 | 0.476 |
| **Building** | 1323950.86 | 465230.45 | 590.879 | 1323950.91 | 465230.14 | 590.657 | -0.047 | 0.303 | 0.222 |
| **Chain Link Fence Post** | 1324285.34 | 465951.63 | 589.238 | 1324285.66 | 465952.34 | 588.946 | -0.317 | -0.707 | 0.292 |
| **Chain Link Fence Post** | 1324275.23 | 465952.14 | 588.665 | 1324274.93 | 465952.86 | 588.671 | 0.292 | -0.716 | -0.006 |
| **Chain Link Fence Top** | 1323786.01 | 465983.39 | 584.589 | 1323786.44 | 465984.34 | 582.907 | -0.437 | -0.948 | 1.682 |
| **Chain Link Fence Top Rail** | 1324272.06 | 465952.39 | 588.524 | 1324272.16 | 465953.17 | 588.037 | -0.092 | -0.778 | 0.487 |
| **Gas Line Marker** | 1324710.76 | 465775.09 | 588.834 | 1324710.88 | 465775.19 | 587.794 | -0.122 | -0.103 | 1.04 |
| **Hangar Roof** | 1323898.98 | 465761.56 | 598.917 | 1323898.94 | 465762.14 | 599.254 | 0.039 | -0.587 | -0.337 |
| **Hangar Roof** | 1323621.71 | 465763.6 | 597.829 | 1323621.08 | 465764.36 | 597.493 | 0.629 | -0.755 | 0.336 |
| **Hangar Roof** | 1323486.62 | 465737.1 | 602.73 | 1323485.95 | 465737.48 | 602.211 | 0.667 | -0.381 | 0.519 |
| **Instrument on AWOS** | 1324299.86 | 465755.82 | 615.709 | N/A | N/A | N/A | N/A | N/A | N/A |
| **Instrument on AWOS** | 1324299.83 | 465753.14 | 615.589 | 1324299.99 | 465753.55 | 615.048 | -0.167 | -0.407 | 0.541 |
| **Light on Building** | 1323832.2 | 465321.28 | 600.308 | 1323832.22 | 465321.35 | 599.96 | -0.022 | -0.075 | 0.348 |
| **Light on Building** | 1323836.59 | 465382.3 | 601.551 | 1323836.45 | 465382.9 | 601.531 | 0.137 | -0.605 | 0.02 |
| **Lightning Rod on AWOS** | 1324300.55 | 465755.75 | 618.274 | N/A | N/A | N/A | N/A | N/A | N/A |
| **Metal Sign** | 1324297.74 | 465949.89 | 588.55 | 1324298.02 | 465950.62 | 588.235 | -0.275 | -0.728 | 0.315 |
| **Obstruction Light on AWOS** | 1324299.84 | 465756.01 | 613.219 | 1324299.13 | 465756.42 | 612.903 | 0.708 | -0.411 | 0.316 |
| **Obstruction Light on AWOS** | 1324299.1 | 465756.03 | 613.213 | N/A | N/A | N/A | N/A | N/A | N/A |
| **Obstruction Light on Windsock** | 1324347.95 | 465576.2 | 602.623 | 1324348.36 | 465576.52 | 602.524 | -0.411 | -0.324 | 0.099 |
| **Pole** | 1324066.35 | 465097.16 | 611.987 | 1324066.4 | 465097.2 | 612.123 | -0.047 | -0.043 | -0.136 |

| Obstacle Type | Field Survey (ft) | | | UAS Imagery (ft) | | | Delta (ft) | | |
|---|---|---|---|---|---|---|---|---|---|
| | x | y | z | x | y | z | x | y | z |
| **Pole** | 1323955.61 | 465097 | 611.332 | 1323955.42 | 465097.06 | 611.481 | 0.187 | -0.059 | -0.149 |
| **Pole** | 1323729.24 | 465097.16 | 621.675 | 1323728.97 | 465097.3 | 621.295 | 0.265 | -0.14 | 0.38 |
| **Post on Building** | 1324190.03 | 465149.69 | 601.806 | 1324190.34 | 465149.76 | 601.734 | -0.314 | -0.07 | 0.072 |
| **Roof Peak** | 1324214.44 | 466119.77 | 598.887 | 1324214.86 | 466120.72 | 598.082 | -0.419 | -0.951 | 0.805 |
| **Signpost** | 1324688.91 | 465961.86 | 588.32 | 1324689.37 | 465962.15 | 587.299 | -0.461 | -0.298 | 1.021 |
| **Signpost** | 1324396.51 | 466144.59 | 587.447 | 1324397.15 | 466145.44 | 586.515 | -0.639 | -0.851 | 0.932 |
| **Tree** | 1324264.82 | 466219.68 | 613.154 | 1324264.69 | 466219.07 | 611.686 | 0.122 | 0.612 | 1.468 |
| **Tree** | 1324265.44 | 466218.05 | 613.479 | 1324265.06 | 466218.74 | 612.695 | 0.376 | -0.698 | 0.784 |
| **Tree** | 1324271.2 | 466098.89 | 602.904 | 1324271.26 | 466099.57 | 601.414 | -0.054 | -0.677 | 1.49 |
| **Tree** | 1324269.3 | 466097.56 | 601.982 | N/A | N/A | N/A | N/A | N/A | N/A |
| **Tree** | 1324169.86 | 466002.46 | 606.509 | N/A | N/A | N/A | N/A | N/A | N/A |
| **Tree** | 1324232.63 | 466051.01 | 598.067 | 1324232.78 | 466051.91 | 597.87 | -0.145 | -0.898 | 0.197 |
| **Tree** | 1324233.54 | 466050.9 | 597.632 | 1324233.83 | 466050.34 | 597.067 | -0.292 | 0.56 | 0.565 |
| **Tree** | 1324232.96 | 466047.83 | 597.092 | 1324233.46 | 466048.54 | 597.12 | -0.497 | -0.711 | -0.028 |
| **Tree** | 1323871.3 | 465223.88 | 614.123 | 1323871.44 | 465224.05 | 612.634 | -0.141 | -0.172 | 1.489 |
| **Tree** | 1323896.11 | 465224.58 | 611.822 | 1323895.82 | 465223.92 | 611.881 | 0.284 | 0.668 | -0.059 |
| **Tree** | 1323898.36 | 465223.41 | 610.812 | 1323898.57 | 465223.71 | 609.658 | -0.204 | -0.305 | 1.154 |
| **Tree** | 1324003.25 | 465210.75 | 601.192 | 1324003.33 | 465211.48 | 601.027 | -0.082 | -0.733 | 0.165 |
| **Tree** | 1324002.29 | 465212.35 | 600.399 | 1324002.61 | 465212.48 | 601.123 | -0.314 | -0.134 | -0.724 |
| **Tree** | 1324002.8 | 465212.3 | 601.122 | 1324002.64 | 465212.02 | 601.302 | 0.159 | 0.282 | -0.18 |
| **Tree** | 1324111.21 | 465121.96 | 609.62 | 1324110.7 | 465120.91 | 609.051 | 0.501 | 1.054 | 0.569 |
| **Tree** | 1324107.7 | 465120.79 | 609.605 | 1324107.68 | 465121.02 | 609.309 | 0.027 | -0.234 | 0.296 |
| **Tree** | 1324159.03 | 465118.63 | 611.625 | 1324158.69 | 465118.98 | 612.107 | 0.335 | -0.345 | -0.482 |
| **Tree Tips** | 1323392.74 | 465798 | 612.687 | 1323392.22 | 465797.79 | 612.549 | 0.519 | 0.213 | 0.138 |
| **Tree Tips** | 1323397.78 | 465790.42 | 615.016 | 1323396.93 | 465791.01 | 614.782 | 0.855 | -0.585 | 0.234 |
| **Tree Tips** | 1323399.84 | 465785.39 | 614.005 | 1323399.21 | 465785.72 | 613.769 | 0.63 | -0.33 | 0.236 |
| **Tree Tips** | 1323338.26 | 465979.43 | 610.384 | 1323337.62 | 465980.38 | 609.72 | 0.64 | -0.955 | 0.664 |
| **Tree Tips** | 1323336.4 | 465984.75 | 612.336 | 1323335.83 | 465985.72 | 611.184 | 0.567 | -0.972 | 1.152 |
| **Tree Tips** | 1323677.57 | 466060.51 | 611.824 | N/A | N/A | N/A | N/A | N/A | N/A |
| **Tree Tips** | 1323730.21 | 466064.7 | 614.196 | 1323730.73 | 466065.27 | 613.066 | -0.522 | -0.575 | 1.13 |
| **Tree Tips** | 1323747.26 | 466050.99 | 609.725 | N/A | N/A | N/A | N/A | N/A | N/A |
| **Tree Tips** | 1323767.74 | 466051.92 | 613.81 | N/A | N/A | N/A | N/A | N/A | N/A |
| **Tree Tips** | 1323813.79 | 465989.33 | 607.288 | 1323814.01 | 465990.14 | 606.271 | -0.22 | -0.815 | 1.017 |
| **Tree Tips** | 1323814.2 | 465984.54 | 606.545 | 1323814.02 | 465985.82 | 606.051 | 0.184 | -1.273 | 0.494 |
| **Tree Tips** | 1323822.69 | 465982.11 | 606.102 | N/A | N/A | N/A | N/A | N/A | N/A |

| Obstacle Type | Field Survey (ft) | | | UAS Imagery (ft) | | | Delta (ft) | | |
|---|---|---|---|---|---|---|---|---|---|
| | x | y | z | x | y | z | x | y | z |
| **Vent** | 1324138.09 | 465293.93 | 592.289 | 1324138.18 | 465294.14 | 592.821 | -0.097 | -0.216 | -0.532 |
| **Vent on Building** | 1324183.55 | 466052.92 | 602.774 | 1324183.6 | 466054.02 | 601.329 | -0.055 | -1.105 | 1.445 |
| **Wood Fence** | 1324279.26 | 466209.37 | 585.625 | 1324280.1 | 466209.79 | 585.27 | -0.839 | -0.413 | 0.355 |

APBN = Airport beacon
AWOS = Automated weather observing system

Table 71. National Geodetic Survey Obstacle Location Variance between Field Survey and UAS Test 8 (WingtraOne)

| Obstacle Type | Field Survey (ft) | | | UAS Imagery (ft) | | | Delta (ft) | | |
|---|---|---|---|---|---|---|---|---|---|
| | x | y | z | x | y | z | x | y | z |
| **Antenna Mast on Building** | 1323951.36 | 465233.05 | 598.61 | 1323951.3 | 465233.13 | 598.964 | 0.058 | -0.072 | -0.354 |
| **Antenna on Building** | 1323951.26 | 465233.16 | 600.62 | N/A | N/A | N/A | N/A | N/A | N/A |
| **Antenna on Building** | 1323946.11 | 465266.04 | 606.861 | 1323946 | 465266.05 | 606.911 | 0.107 | -0.01 | -0.05 |
| **Airport Beacon on Building** | 1324085.86 | 465186.6 | 605.248 | 1324084.97 | 465186.54 | 605.527 | 0.888 | 0.061 | -0.279 |
| **Building** | 1323889.94 | 465469.65 | 598.894 | 1323889.81 | 465469.69 | 598.987 | 0.135 | -0.042 | -0.093 |
| **Building** | 1323919.15 | 465468.84 | 596.419 | 1323919.17 | 465468.86 | 596.35 | -0.019 | -0.024 | 0.069 |
| **Building** | 1323374.06 | 465419.84 | 612.644 | N/A | N/A | N/A | N/A | N/A | N/A |
| **Building** | 1323834.64 | 465321.34 | 594.592 | 1323834.37 | 465321.32 | 594.677 | 0.275 | 0.027 | -0.085 |
| **Building** | 1323950.86 | 465230.45 | 590.879 | 1323950.61 | 465229.95 | 590.901 | 0.253 | 0.5 | -0.022 |
| **Chain Link Fence Post** | 1324285.34 | 465951.63 | 589.238 | 1324285.38 | 465951.6 | 589.435 | -0.046 | 0.034 | -0.197 |
| **Chain Link Fence Post** | 1324275.23 | 465952.14 | 588.665 | 1324275.13 | 465952.24 | 588.62 | 0.094 | -0.1 | 0.045 |
| **Chain Link Fence Top** | 1323786.01 | 465983.39 | 584.589 | 1323786.02 | 465983.37 | 584.415 | -0.011 | 0.026 | 0.174 |
| **Chain Link Fence Top Rail** | 1324272.06 | 465952.39 | 588.524 | 1324271.23 | 465952.44 | 588.599 | 0.839 | -0.053 | -0.075 |
| **Gas Line Marker** | 1324710.76 | 465775.09 | 588.834 | 1324710.75 | 465775.01 | 588.41 | 0.014 | 0.08 | 0.424 |
| **Hangar Roof** | 1323898.98 | 465761.56 | 598.917 | 1323899.02 | 465761.55 | 598.966 | -0.044 | 0.002 | -0.049 |
| **Hangar Roof** | 1323621.71 | 465763.6 | 597.829 | 1323621.8 | 465763.62 | 597.696 | -0.091 | -0.019 | 0.133 |
| **Hangar Roof** | 1323486.62 | 465737.1 | 602.73 | 1323486.57 | 465737.01 | 602.251 | 0.056 | 0.09 | 0.479 |

| Obstacle Type | Field Survey (ft) | | | UAS Imagery (ft) | | | Delta (ft) | | |
|---|---|---|---|---|---|---|---|---|---|
| | x | y | z | x | y | z | x | y | z |
| **Instrument on AWOS** | 1324299.86 | 465755.82 | 615.709 | 1324299.75 | 465754.46 | 615.03 | 0.103 | 1.356 | 0.679 |
| **Instrument on AWOS** | 1324299.83 | 465753.14 | 615.589 | 1324299.82 | 465753.14 | 615.002 | 0.002 | 0.001 | 0.587 |
| **Light on Building** | 1323832.2 | 465321.28 | 600.308 | 1323831.93 | 465320.98 | 600.231 | 0.264 | 0.297 | 0.077 |
| **Light on Building** | 1323836.59 | 465382.3 | 601.551 | 1323835.94 | 465382.14 | 601.459 | 0.645 | 0.162 | 0.092 |
| **Lightning Rod on AWOS** | 1324300.55 | 465755.75 | 618.274 | N/A | N/A | N/A | N/A | N/A | N/A |
| **Metal Sign** | 1324297.74 | 465949.89 | 588.55 | 1324297.69 | 465949.83 | 588.407 | 0.051 | 0.064 | 0.143 |
| **Obstruction Light on AWOS** | 1324299.84 | 465756.01 | 613.219 | N/A | N/A | N/A | N/A | N/A | N/A |
| **Obstruction Light on AWOS** | 1324299.1 | 465756.03 | 613.213 | N/A | N/A | N/A | N/A | N/A | N/A |
| **Obstruction Light on Windsock** | 1324347.95 | 465576.2 | 602.623 | 1324347.92 | 465576.11 | 602.328 | 0.032 | 0.09 | 0.295 |
| **Pole** | 1324066.35 | 465097.16 | 611.987 | 1324066.18 | 465096.97 | 612.493 | 0.176 | 0.186 | -0.506 |
| **Pole** | 1323955.61 | 465097 | 611.332 | 1323955.43 | 465096.87 | 611.726 | 0.177 | 0.135 | -0.394 |
| **Pole** | 1323729.24 | 465097.16 | 621.675 | 1323729.09 | 465097.27 | 621.971 | 0.151 | -0.11 | -0.296 |
| **Post on Building** | 1324190.03 | 465149.69 | 601.806 | 1324190.26 | 465149.61 | 602.034 | -0.228 | 0.075 | -0.228 |
| **Roof Peak** | 1324214.44 | 466119.77 | 598.887 | 1324214.39 | 466119.6 | 599.294 | 0.053 | 0.169 | -0.407 |
| **Signpost** | 1324688.91 | 465961.86 | 588.32 | 1324689.01 | 465961.9 | 588.152 | -0.105 | -0.04 | 0.168 |
| **Signpost** | 1324396.51 | 466144.59 | 587.447 | 1324396.55 | 466144.58 | 587.79 | -0.032 | 0.015 | -0.343 |
| **Tree** | 1324264.82 | 466219.68 | 613.154 | 1324264.6 | 466219.67 | 613.827 | 0.212 | 0.016 | -0.673 |
| **Tree** | 1324265.44 | 466218.05 | 613.479 | 1324265.34 | 466218.11 | 614.09 | 0.098 | -0.059 | -0.611 |
| **Tree** | 1324271.2 | 466098.89 | 602.904 | 1324270.89 | 466099.58 | 602.966 | 0.313 | -0.694 | -0.062 |
| **Tree** | 1324269.3 | 466097.56 | 601.982 | 1324269.4 | 466096.85 | 602.073 | -0.096 | 0.708 | -0.091 |
| **Tree** | 1324169.86 | 466002.46 | 606.509 | 1324169.73 | 466002.33 | 606.369 | 0.13 | 0.126 | 0.14 |
| **Tree** | 1324232.63 | 466051.01 | 598.067 | 1324232.04 | 466051.31 | 598.351 | 0.591 | -0.302 | -0.284 |
| **Tree** | 1324233.54 | 466050.9 | 597.632 | 1324233.53 | 466050.8 | 597.909 | 0.014 | 0.096 | -0.277 |
| **Tree** | 1324232.96 | 466047.83 | 597.092 | 1324232.82 | 466047.79 | 597.457 | 0.14 | 0.04 | -0.365 |
| **Tree** | 1323871.3 | 465223.88 | 614.123 | 1323871.3 | 465223.99 | 613.738 | -0.002 | -0.109 | 0.385 |

| Obstacle Type | Field Survey (ft) | | | UAS Imagery (ft) | | | Delta (ft) | | |
|---|---|---|---|---|---|---|---|---|---|
| | x | y | z | x | y | z | x | y | z |
| **Tree** | 1323896.11 | 465224.58 | 611.822 | 1323896.23 | 465224.44 | 610.637 | -0.119 | 0.14 | 1.185 |
| **Tree** | 1323898.36 | 465223.41 | 610.812 | 1323898.61 | 465223.66 | 611.053 | -0.242 | -0.253 | -0.241 |
| **Tree** | 1324003.25 | 465210.75 | 601.192 | 1324003.19 | 465210.7 | 601.208 | 0.059 | 0.045 | -0.016 |
| **Tree** | 1324002.29 | 465212.35 | 600.399 | 1324002.28 | 465212.36 | 600.446 | 0.013 | -0.009 | -0.047 |
| **Tree** | 1324002.8 | 465212.3 | 601.122 | 1324002.8 | 465212.24 | 600.904 | -0.003 | 0.069 | 0.218 |
| **Tree** | 1324111.21 | 465121.96 | 609.62 | N/A | N/A | N/A | N/A | N/A | N/A |
| **Tree** | 1324107.7 | 465120.79 | 609.605 | N/A | N/A | N/A | N/A | N/A | N/A |
| **Tree** | 1324159.03 | 465118.63 | 611.625 | N/A | N/A | N/A | N/A | N/A | N/A |
| **Tree Tips** | 1323392.74 | 465798 | 612.687 | 1323392.09 | 465798.57 | 611.698 | 0.647 | -0.568 | 0.989 |
| **Tree Tips** | 1323397.78 | 465790.42 | 615.016 | 1323396.49 | 465790.32 | 615.438 | 1.29 | 0.104 | -0.422 |
| **Tree Tips** | 1323399.84 | 465785.39 | 614.005 | N/A | N/A | N/A | N/A | N/A | N/A |
| **Tree Tips** | 1323338.26 | 465979.43 | 610.384 | 1323338.5 | 465979.49 | 610.294 | -0.242 | -0.058 | 0.09 |
| **Tree Tips** | 1323336.4 | 465984.75 | 612.336 | 1323335.8 | 465985.02 | 611.781 | 0.602 | -0.277 | 0.555 |
| **Tree Tips** | 1323677.57 | 466060.51 | 611.824 | 1323677.25 | 466060.38 | 611.541 | 0.318 | 0.129 | 0.283 |
| **Tree Tips** | 1323730.21 | 466064.7 | 614.196 | 1323730.63 | 466063.79 | 614.13 | -0.414 | 0.907 | 0.066 |
| **Tree Tips** | 1323747.26 | 466050.99 | 609.725 | N/A | N/A | N/A | N/A | N/A | N/A |
| **Tree Tips** | 1323767.74 | 466051.92 | 613.81 | 1323767.74 | 466051.81 | 613.73 | -0.002 | 0.107 | 0.08 |
| **Tree Tips** | 1323813.79 | 465989.33 | 607.288 | 1323813.78 | 465989.29 | 607.593 | 0.001 | 0.038 | -0.305 |
| **Tree Tips** | 1323814.2 | 465984.54 | 606.545 | 1323814.25 | 465984.7 | 606.51 | -0.047 | -0.159 | 0.035 |
| **Tree Tips** | 1323822.69 | 465982.11 | 606.102 | 1323822.88 | 465982.25 | 605.974 | -0.184 | -0.134 | 0.128 |
| **Vent** | 1324138.09 | 465293.93 | 592.289 | 1324137.97 | 465293.81 | 592.455 | 0.118 | 0.119 | -0.166 |
| **Vent on Building** | 1324183.55 | 466052.92 | 602.774 | 1324183.29 | 466053.02 | 602.914 | 0.257 | -0.099 | -0.14 |
| **Wood Fence** | 1324279.26 | 466209.37 | 585.625 | 1324279.32 | 466208.77 | 586.11 | -0.059 | 0.603 | -0.485 |

### 3.4.7 Findings

Of the 28 data sets collected at I67, 24 produced valid AT solutions when processed with UASMaster, 19 of which were viable for obstacle data collection in stereo. All nine data sets that failed to either produce a valid AT solution or viable stereo imagery were collected with the M210 UAS.

NGS analysis of select WingtraOne and eBee X data (collected with 80%/60% forward and side overlap settings and GSDs of ≤1 in.) found that these data sets outperformed the manned aircraft data in terms of accuracy and completeness. Each obstacle located in these UAS data sets met the accuracy requirements in AC 150/5300-18. In addition, when compared to the manned aircraft data, the UAS data reduced the number of man-made obstacles that were unable to be located by 50% (from 10 obstacles to 5).

The M210 UAS continued to produce inconsistent results when compared to the other platforms used, including the Inspire 2, which also used the X7 payload. The M210 data sets that failed to produce valid AT solutions did so due to improper image orientation, which led to inconsistent tie point extraction. It is unknown why the M210 did not collect proper image orientation during Tests 1 and 2, but the other UAS platforms did not experience this issue. The data sets that produced a valid AT solution but were not viable for stereo analysis failed due to extreme parallax distortion which caused an inability to measure control. In the solutions that did generate valid AT and viable stereo, the imagery experienced inconsistent exposure and texture and had extreme flattening and a "halo" effect in some areas.

Closely spacing the GCPs no more than 500 ft apart significantly increased the accuracy and consistency of UAS data sets. The increased density of this GCP layout versus those employed in previous test efforts allowed for the use of a lower forward overlap setting of 70% in conjunction with a 70% side overlap with no negative effect on the generation of valid AT solutions or the accuracy of measurements in stereo.

Testing of 80%/80% forward and side overlap settings with the Inspire 2 produced significantly more accurate data sets than similar flights with 80%/60% forward and side overlap settings; however, the higher overlap increased the combined total flight time to capture areas A, B, and C by 50%.

Testing regarding the effect of sun angle was inconclusive. The data sets collected at low sun angles in the morning and evening produced similar results; however, the data set collected during midday with the same parameters failed to produce viable stereo imagery due to the aforementioned issues with the M210. This prevented a comparison between high and low sun angle between tests with otherwise identical parameters.

Tests conducted with the eBee X using sequential flight lines significantly outperformed the test that used interlaced flight lines. Interlaced flight lines specifically struggled over the vegetated areas, and obstacle measurements did not meet AC 150/5300-18 standards for vertical accuracy (FAA, 2014) when compared to the field survey measurements. The failure of interlaced flight lines to produce accurate data was attributed to temporal distortion created by the time difference between the data captured on adjacent flight lines. This concern can also be applied to long

traditional flight lines that result in a significant capture time difference between adjacent flight lines.

Due to the failure of the M210 to produce valid AT solutions that were viable for stereo analysis during Tests 1 and 2, a comparison of data set accuracy with and without the use of RTK was unable to be completed.

## 3.5 SUFFOLK EXECUTIVE AIRPORT

SFQ is a dual runway (4/22 and 7/25), non-towered airport in Suffolk, Virginia, located in Class G airspace from the surface to 700 ft AGL. SFQ was selected by the NGS due to its diverse man-made and natural obstacles, proximity to their office, and their existing relationship with the airport, which allowed them to conduct their own independent field survey.

The purpose of testing at SFQ was to allow the NGS to independently validate the accuracy of the UAS-collected obstacle data. In previous tests FAA researchers commissioned or personally collected the manned aircraft or field survey data used to evaluate the accuracy of the UAS obstacle data. During this test effort, the NGS selected the airport and test area and performed their own independent field survey to identify and measure the obstacles used to evaluate the accuracy of the UAS data. In addition, FAA researchers used the NGS obstacle data to evaluate the accuracy of a manned aircraft survey conducted shortly after UAS data collection.

Sections 3.5.1 through 3.5.6 describe the SFQ study area, data collection parameters, procedures for obstacle data collection, results of data processing/analysis, and findings.

### 3.5.1 Data Collection

The study area at SFQ was located on the southwest side of the airfield in and in between the approach surfaces for Runways 4 and 7, as shown in the red-shaded area in Figure 44. A diverse range of obstacles were present in this area, including natural obstacles such as trees and man-made structures such as buildings, fencing, and antennas.


Figure 44. Suffolk Executive Airport Study Limit

3.5.1.1 Onsite Preparation

Figure 45 depicts the study limits and approximate locations of the 27 GCPs that were usedas part of the data post-processing workflow.

During the GCP layout design process for SFQ, the greatest concern was establishing sufficient control for the vegetated area in the southern portion of the study area. Unlike previous tests, the study area was not positioned in such a way as as to allow GCPs to surround the area of dense vegetation. To accommodate this, the study limits and the control field were extended to the south to aid in the development of successful AT solutions of trees in the vegetated area.

During previous testing it was found that different methods of GCP contruction had no effect on the accuracy of GCP or obstacle measurements. Due to this finding, all GCPs at SFQ were constructed with the standard white chevron marker.

Since several public roadways were located within the study area, traffic control measures were taken during UAS operations to restrict traffic within the study area. This ensured that the UAS did not fly over any persons or vehicles.


Figure 45. Suffolk Executive Airport GCP Locations

3.5.1.2 UAS Data Collection Parameters

This test effort served as the final validation test during this research program and sought to provide the NGS with a single data set from each UAS used, including the M210, eBee X, and WingtraOne. Data collection parameters were selected that developed successful obstacle measurements in previous test efforts, including 80%/60% forward and side overlap settings, and a GSD value of 1 in. Due to 14 CFR 107.51 (Operating Limitations for Small Unmanned Aircraft, 2016), the WingtraOne could not be flown higher to achieve a 1 in. GSD, and instead collected imagery at 0.5 in. In total, three UAS data sets were collected. Table 72 summarizes the data collection parameters for each UAS data set collected at SFQ. Figure 46 depicts the UAS flight operations area.

Table 72. Suffolk Executive Airport UAS Aerial Survey Data Collection Parameters

| Date Collected | UAS | Sensor | Estimated GSD (in.) | Forward Overlap (%) | Side Overlap (%) | AGL (ft) | Sun Angle (degrees) | Flight Time (min) | Photo Count |
|---|---|---|---|---|---|---|---|---|---|
| 8/18/2021 | M210 | X7 | 1 | 80 | 60 | 340.5 | 65.8 | 25 | 473 |
| 8/18/2021 | eBee X | S.O.D.A. 3D | 1 | 80 | 60 | 368.1 | 50.5 | 28 | 673 |
| 8/18/2021 | WingtraOne | RXIR-II | 0.5 | 80 | 60 | 310.5 | 58.65 | 29 | 1115 |


Figure 46. Suffolk Executive Airport UAS Operations Area

3.5.1.3 Manned Aircraft Data Collection

Approximately a week after UAS data collection, a manned aircraft survey was completed at SFQ in accordance with guidance stated in AC 150/5300-17 (FAA, 2017b). Data were collected using an UltraCam Falcon Prime with a GSD of 6 in. and 60%/50% forward and side overlap values. Table 73 presents complete parameters for the manned aircraft aerial survey at SFQ.

Table 73. Suffolk Executive Airport Manned Aircraft Aerial Survey Parameters

| Date Collected | Sensor | Estimated GSD (in.) | Forward Overlap (%) | Side Overlap (%) | AGL (ft) | Flight Time (min) | Photo Count |
|---|---|---|---|---|---|---|---|
| 08/26/2021 | UltraCam Falcon Prime | 6 | 60 | 0 | 8500.0 | ~5 | 5 |

3.5.2 Data Processing Results

Each data set collected at SFQ was processed using UASMaster. Table 74 presents the results of this processing effort. As indicated by the green-shaded cells, two data sets were processed successfully, resulting in viable AT solutions that went to stereo analysis for control measurement and obstacle comparison.

Table 74. Suffolk Executive Airport Data Processing Results

| Test Number | Processing Software | Airframe | Sensor | Estimated GSD (in.) | Forward and Side Overlap % | Processing Results |
|---|---|---|---|---|---|---|
| **1** | UASMaster | M210 | X7 | 1 | 80/60 | No valid AT solution due to inaccurate image orientations. Did not go for stereo analysis. |
| **2** | UASMaster | eBee X | S.O.D.A. 3D | 1 | 80/60 | Valid AT solution and viable stereo imagery. |
| **3** | UASMaster | WingtraOne | RX1R II | 0.5 | 80/60 | Valid AT solution and viable stereo imagery. |

The data set collected during Test 1 failed to produce a valid AT solution when processed with UASMaster. During data collection the M210 and X7 failed to collect accurate image orientation information (omega, phi, kappa). While the imagery passed the field QC checks, the incorrect metadata were not noticed until the data were processed in the office, preventing a repeat of the test. This continued the trend observed throughout this research program of DJI hardware experiencing inconsistencies during data collection.

Recorded winds at ground level during data collection at SFQ were 10 mph with gusts of 15 mph. This resulted in instability with the fixed-wing UAS when operating at altitude, because the flight lines are positioned perpendicular to the wind direction to allow for a consistent cruise speed. This resulted in WingtraOne and eBee X deviating from the planned flight lines. While the data sets were ultimately successful, they required a higher level of effort during initial processing to achieve a valid AT solution and viable stereo.

### 3.5.3 Stereo Analysis—GCP Comparison Results

A stereo analysis effort was initiated to measure and validate the surveyed control data captured in the two valid AT solutions collected at SFQ. Table 75 presents the RMSEs between the GCP locations derived from surveyed control data and the eBee X imagery collected in flight 2 when measured in stereo. AC 150/5300-17 Section 8.1.1.2 states that the positions of well-defined points determined from the stereo imagery must be within 3.28 ft (1 meter) relative to the NSRS for imagery to be accepted by the NGS (FAA, 2017b). While there is no specific standard for photo-control GCP checks, the same minimum requirement was applied, and Table 75 shows that the average RMSE is within the minimum tolerances stated. This analysis confirms that this UAS data set is viable for obstacle data collection.

Table 75. Ground Control Point Location Variance between Field Survey and UAS Test 2-1 (eBee X)

| GCP | RMSE X (ft) | RMSE Y (ft) | RMSE Z (ft) | Maximum Horizontal Error (ft) | Maximum Vertical Error (ft) |
|---|---|---|---|---|---|
| **6101** | 0.25 | 0.14 | 0.38 | 0.46 | 0.60 |
| **6102** | 0.07 | 0.16 | 0.49 | 0.26 | 0.68 |
| **6103** | 0.12 | 0.23 | 0.35 | 0.52 | 0.58 |
| **6104** | 0.20 | 0.10 | 0.44 | 0.40 | 1.17 |
| **6105** | 0.20 | 0.27 | 0.50 | 0.56 | 0.82 |
| **6106** | 0.14 | 0.24 | 0.27 | 0.55 | 0.67 |
| **6107** | 0.11 | 0.16 | 0.20 | 0.35 | 0.30 |
| **6108** | 0.28 | 0.15 | 0.24 | 0.52 | 0.16 |
| **6109** | 0.32 | 0.14 | 0.26 | 0.58 | 0.45 |
| **6110** | 0.20 | 0.20 | 0.11 | 0.45 | 0.22 |
| **6111** | 0.24 | 0.09 | 0.27 | 0.39 | 0.48 |
| **6112** | 0.08 | 0.17 | 0.22 | 0.36 | 0.35 |
| **6113** | 0.19 | 0.17 | 0.33 | 0.43 | 0.56 |
| **6114** | 0.04 | 0.25 | 0.13 | 0.33 | 0.22 |
| **6115** | 0.04 | 0.14 | 0.19 | 0.22 | 0.08 |
| **6116** | 0.19 | 0.19 | 0.23 | 0.61 | 0.53 |
| **6117** | 0.09 | 0.19 | 0.17 | 0.39 | 0.40 |
| **6118** | 0.19 | 0.11 | 0.18 | 0.31 | 0.12 |
| **6119** | 0.12 | 0.12 | 0.62 | 0.37 | 0.80 |
| **6120** | 0.09 | 0.09 | 0.94 | 0.21 | 1.42 |
| **6121** | 0.11 | 0.35 | 0.15 | 0.62 | 0.24 |
| **6122** | 0.12 | 0.06 | 0.32 | 0.27 | 0.44 |
| **6201** | 0.14 | 0.13 | 0.18 | 0.41 | 0.33 |
| **6202** | 0.10 | 0.10 | 0.38 | 0.23 | 0.50 |
| **6203** | 0.19 | 0.14 | 0.29 | 0.67 | 0.84 |
| **6204** | 0.08 | 0.05 | 0.12 | 0.15 | 0.10 |
| **6205** | 0.14 | 0.11 | 0.27 | 0.31 | 0.67 |
| **AVERAGE:** | **0.16** | **0.16** | **0.32** | | |

Table 76 presents the RMSEs between the GCP locations derived from surveyed control data and the WingtraOne UAS imagery collected in flight 3 when measured in stereo. As indicated by the green shading, all measurements met the 3.28 ft (1 meter) accuracy requirement for well-defined points stated in AC 150/5300-17 (FAA, 2017b), confirming that this UAS data set is viable for obstacle data collection.

Despite all control measurements falling within the minimum applied accuracy tolerance, there were still three consecutive images in the vegetated area which failed to calibrate. This demonstrates that accurate GCP measurements alone are an insufficient test of overall data set quality.

Table 76. Ground Control Point Location Variance between Field Survey and UAS Test 3-1 (WingtraOne)

| GCP | RMSE X (ft) | RMSE Y (ft) | RMSE Z (ft) | Maximum Horizontal Error (ft) | Maximum Vertical Error (ft) |
|---|---|---|---|---|---|
| **6101** | 0.09 | 0.03 | 0.15 | 0.15 | 0.35 |
| **6102** | 0.06 | 0.17 | 0.15 | 0.36 | 0.38 |
| **6103** | 0.11 | 0.19 | 0.41 | 0.28 | 0.56 |
| **6104** | 0.11 | 0.09 | 0.40 | 0.18 | 0.47 |
| **6105** | 0.08 | 0.13 | 0.73 | 0.30 | 0.86 |
| **6106** | 0.08 | 0.05 | 0.66 | 0.16 | 0.85 |
| **6107** | 0.08 | 0.05 | 0.17 | 0.17 | 0.24 |
| **6108** | 0.16 | 0.05 | 0.33 | 0.24 | 0.47 |
| **6109** | 0.13 | 0.13 | 0.09 | 0.27 | 0.17 |
| **6110** | 0.13 | 0.11 | 0.47 | 0.26 | 0.58 |
| **6111** | 0.21 | 0.10 | 0.23 | 0.41 | 0.41 |
| **6112** | 0.20 | 0.20 | 0.51 | 0.88 | 1.80 |
| **6113** | 0.14 | 0.10 | 0.27 | 0.35 | 0.58 |
| **6114** | 0.03 | 0.15 | 0.17 | 0.27 | 0.26 |
| **6115** | 0.02 | 0.07 | 0.21 | 0.13 | 0.00 |
| **6116** | 0.04 | 0.11 | 0.13 | 0.18 | 0.04 |
| **6117** | 0.03 | 0.08 | 0.14 | 0.16 | 0.22 |
| **6118** | 0.17 | 0.11 | 0.10 | 0.31 | 0.30 |
| **6119** | 0.04 | 0.07 | 0.46 | 0.14 | 0.60 |
| **6120** | 0.07 | 0.07 | 0.21 | 0.16 | 0.00 |
| **6121** | 0.05 | 0.14 | 0.28 | 0.26 | 0.06 |
| **6122** | 0.03 | 0.06 | 0.57 | 0.13 | 0.00 |
| **6201** | 0.15 | 0.43 | 0.44 | 1.55 | 0.48 |
| **6202** | 0.04 | 0.03 | 0.20 | 0.10 | 0.30 |
| **6203** | 0.09 | 0.05 | 0.08 | 0.13 | 0.15 |
| **6204** | 0.03 | 0.03 | 0.14 | 0.07 | 0.00 |
| **6205** | 0.13 | 0.10 | 0.38 | 0.26 | 0.52 |
| **AVERAGE:** | **0.09** | **0.11** | **0.30** | | |

### 3.5.4 Stereo Analysis—UAS Imagery to NGS Field Survey Comparison Results

During their field obstacle data collection, the NGS identified 34 obstacles in the test area at SFQ that were used to assess the accuracy of UAS-collected data. Figure 47 shows the locations of these obstacles. The NGS did not disclose the locations of these obstacles prior to UAS data collection. Following data collection, the NGS provided a general vicinity map of the obstacles they requested be measured, along with annotated ground photographs of the features. This limited knowledge of the true position of obstacles ensured a fair test of the capability of UAS imagery to allow for the accurate collection of obstacle locations.


Figure 47. Suffolk Executive Airport Obstacle Locations

Once this information was received from the NGS, a stereo analysis effort was initiated to identify and measure each obstacle collected in the field survey using the UAS imagery. These measurements were provided to the NGS, who performed the comparison. The information in Tables 77 and 78 was provided by the NGS following their comparison. These tables are color-coded to indicate measurements that meet the most stringent obstacle requirements of AC 150/5300-18 (green), measurements that meet the requirements but are outliers (orange), and measurements that fall outside of the requirements (red).

Table 77 compares obstacle locations derived from NGS field survey and the eBee X UAS imagery collected during flight 2 when measured in stereo. This flight and each obstacle measurement achieved the most stringent accuracy requirement (20 ft horizontal, 3 ft vertical) stated in AC 150/5300-18 (FAA, 2014). Obstacles T-8, T-9, and T-10 were outliers, which met the accuracy

standard but showed a considerable horizontal discrepancy. Because the majority of obstacles measured in this data set fell within 1 ft horizontally of the field survey results, it is believed these larger discrepancies were a result of the research team's stereo analyst selecting different branches on the trees for measurement than were used during the field survey.

Table 78 compares obstacle locations derived from NGS field survey and the WingtraOne UAS imagery collected during flight 3 when measured in stereo. The results of this flight show issues with the same three obstacles that were outliers in the eBee X data set. The measurements for these obstacles in the WingtraOne data set closely match those in the eBee X data lending further credence to the hypothesis that the discrepancies were a result of the stereo analyst selecting a different branches on the same trees for measurement. As a result, two obstacles in this data set did not meet the accuracy standards stated in AC 150/5300-18 (FAA, 2014).

Table 77. Variance between NGS Field Survey and UAS Test 2-1 (eBee X)

| Obstacle | Field Survey (ft) | | | UAS Imagery (ft) | | | Delta (ft) | | |
|---|---|---|---|---|---|---|---|---|---|
| | x | y | z | x | y | z | x | y | z |
| **Antenna (A-1)** | 12038514.15 | 3412321.81 | 163.24 | 12038513.81 | 3412321.9 | 163.31 | 0.33 | -0.08 | -0.07 |
| **Antenna on Hangar (A-2)** | 12038696.55 | 3412848.89 | 96.47 | 12038696.95 | 3412849.58 | 94.77 | -0.4 | -0.69 | 1.69 |
| **Antenna on Hangar (A-3)** | 12038835.86 | 3412011.18 | 90.65 | 12038836.07 | 3412011.23 | 90.15 | -0.21 | -0.05 | 0.5 |
| **Beacon (APBN)** | 12038819.76 | 3412499.53 | 122.41 | 12038821.89 | 3412498.8 | 121.76 | -2.13 | 0.73 | 0.65 |
| **Hangar (BD-1)** | 12037414.12 | 3412405.33 | 96.35 | 12037414.01 | 3412405.46 | 96.26 | 0.11 | -0.14 | 0.09 |
| **Hangar (BD-2)** | 12038035.51 | 3412185.25 | 83.41 | 12038035.53 | 3412185.26 | 83.31 | -0.02 | -0.02 | 0.1 |
| **Hangar (BD-3)** | 12038085.34 | 3412446.09 | 82.11 | 12038085.4 | 3412446.39 | 81.97 | -0.06 | -0.29 | 0.14 |
| **Hangar (BD-4)** | 12038156.18 | 3412231.43 | 82.14 | 12038156.13 | 3412231.1 | 81.99 | 0.06 | 0.33 | 0.15 |
| **Hangar (BD-5)** | 12038277.62 | 3412270.94 | 81.82 | 12038277.57 | 3412271 | 81.55 | 0.05 | -0.06 | 0.27 |
| **Hangar (BD-6)** | 12038318.28 | 3412522.45 | 82.76 | 12038318.13 | 3412522.48 | 82.32 | 0.15 | -0.03 | 0.44 |
| **Hangar (BD-7)** | 12038494.4 | 3412370.71 | 83.85 | 12038494.38 | 3412370.73 | 83.48 | 0.01 | -0.02 | 0.37 |
| **Hangar (BD-8)** | 12038559.28 | 3412601.26 | 82.45 | 12038559.22 | 3412601.33 | 81.67 | 0.06 | -0.07 | 0.78 |
| **Hangar (BD-9)** | 12038631.31 | 3412380.78 | 82.5 | 12038631.42 | 3412380.84 | 82.2 | -0.11 | -0.06 | 0.31 |
| **Light Pole (LP-1)** | 12038757.01 | 3412356.87 | 102.62 | 12038757.02 | 3412357 | 102.1 | -0.02 | -0.13 | 0.52 |
| **Light Pole (LP-2)** | 12038826.03 | 3412274.64 | 103.02 | 12038826.18 | 3412274.64 | 102.46 | -0.15 | 0 | 0.56 |
| **Marker Ball (MB-1)** | 12037630.82 | 3412029.15 | 88.29 | 12037630.8 | 3412029.54 | 88.19 | 0.02 | -0.4 | 0.1 |
| **Marker Ball (MB-2)** | 12037705.68 | 3411893.26 | 96.26 | 12037705.49 | 3411893.22 | 95.8 | 0.19 | 0.04 | 0.47 |
| **Marker Ball (MB-3)** | 12037932.48 | 3412042.33 | 96.17 | 12037932.4 | 3412042.36 | 95.67 | 0.08 | -0.03 | 0.5 |
| **Pole (P-1)** | 12037434.72 | 3411716.13 | 100.48 | 12037434.78 | 3411715.84 | 100.22 | -0.06 | 0.29 | 0.26 |
| **Pole (P-2)** | 12037477.48 | 3412100.22 | 101.72 | 12037477.48 | 3412100.35 | 101.47 | 0 | -0.13 | 0.25 |
| **Pole (P-3)** | 12037796.24 | 3411952.79 | 100.68 | 12037796.17 | 3411952.78 | 100.89 | 0.07 | 0.01 | -0.2 |
| **Pole (P-4)** | 12038245.36 | 3412247.3 | 96.15 | 12038245.26 | 3412247.49 | 96.11 | 0.1 | -0.19 | 0.04 |
| **Pole (P-5)** | 12038339.82 | 3412273.57 | 99.2 | 12038339.84 | 3412273.64 | 98.88 | -0.02 | -0.08 | 0.32 |
| **Tree (T-1)** | 12037101.2 | 3411811.54 | 144.99 | 12037099.57 | 3411811.05 | 145.2 | 1.62 | 0.49 | -0.21 |
| **Tree (T-2)** | 12037251.98 | 3411398.29 | 147.39 | 12037252.34 | 3411399.48 | 148.1 | -0.37 | -1.19 | -0.71 |
| **Tree (T-3)** | 12037514.6 | 3411046.33 | 140.81 | 12037514.78 | 3411048.04 | 142.28 | -0.18 | -1.71 | -1.47 |
| **Tree (T-4)** | 12037516.52 | 3411584.29 | 158.96 | 12037518.27 | 3411583.47 | 158.66 | -1.75 | 0.82 | 0.3 |
| **Tree (T-5)** | 12037574.98 | 3411532.09 | 154.3 | 12037576.59 | 3411531.95 | 153.94 | -1.61 | 0.13 | 0.36 |
| **Tree (T-6)** | 12037584.64 | 3411479.78 | 167.16 | 12037583.99 | 3411479.08 | 167.26 | 0.64 | 0.7 | -0.11 |
| **Tree (T-7)** | 12037612.06 | 3411130.94 | 145.6 | 12037611.85 | 3411131.63 | 145.88 | 0.2 | -0.69 | -0.28 |

| Obstacle | Field Survey (ft) | | | UAS Imagery (ft) | | | Delta (ft) | | |
|---|---|---|---|---|---|---|---|---|---|
| | x | y | z | x | y | z | x | y | z |
| **Tree (T-8)** | 12038319.42 | 3410833.62 | 123.67 | 12038314.65 | 3410841.69 | 124.85 | 4.77 | -8.06 | -1.18 |
| **Tree (T-9)** | 12038333.4 | 3410870.91 | 126.52 | 12038332.36 | 3410862.09 | 123.88 | 1.04 | 8.82 | 2.64 |
| **Tree (T-10)** | 12038403.7 | 3411019.15 | 127.55 | 12038401.07 | 3411032.93 | 124.56 | 2.63 | -13.78 | 2.99 |
| **Vent on Hangar (BD-10)** | 12038712.77 | 3412057.94 | 88.52 | 12038713.01 | 3412057.78 | 88.13 | -0.24 | 0.17 | 0.39 |

Table 78. Variance between NGS Field Survey and UAS Test 3-1 (WingtraOne)

| Obstacle | Field Survey (ft) | | | UAS Imagery (ft) | | | Delta (ft) | | |
|---|---|---|---|---|---|---|---|---|---|
| | x | y | z | x | y | z | x | y | z |
| **Antenna (A-1)** | 12038514.15 | 3412321.81 | 163.24 | 12038513.89 | 3412321.86 | 163.82 | 0.26 | -0.05 | -0.58 |
| **Antenna on Hangar (A-2)** | 12038696.55 | 3412848.89 | 96.47 | 12038696.74 | 3412848.98 | 96.9 | -0.19 | -0.09 | -0.43 |
| **Antenna on Hangar (A-3)** | 12038835.86 | 3412011.18 | 90.65 | 12038835.87 | 3412011.26 | 90.67 | -0.01 | -0.08 | -0.02 |
| **Beacon (APBN)** | 12038819.76 | 3412499.53 | 122.41 | 12038821.86 | 3412498.53 | 122.33 | -2.11 | 1 | 0.09 |
| **Hangar (BD-1)** | 12037414.12 | 3412405.33 | 96.35 | 12037413.92 | 3412405.39 | 96.38 | 0.2 | -0.06 | -0.03 |
| **Hangar (BD-2)** | 12038035.51 | 3412185.25 | 83.41 | 12038035.51 | 3412185.26 | 83.42 | 0 | -0.02 | -0.01 |
| **Hangar (BD-3)** | 12038085.34 | 3412446.09 | 82.11 | 12038085.45 | 3412446.31 | 82.37 | -0.11 | -0.22 | -0.26 |
| **Hangar (BD-4)** | 12038156.18 | 3412231.43 | 82.14 | 12038156.21 | 3412230.98 | 82.17 | -0.02 | 0.45 | -0.03 |
| **Hangar (BD-5)** | 12038277.62 | 3412270.94 | 81.82 | 12038277.61 | 3412270.9 | 81.81 | 0.01 | 0.04 | 0.01 |
| **Hangar (BD-6)** | 12038318.28 | 3412522.45 | 82.76 | 12038318.22 | 3412522.39 | 83.07 | 0.06 | 0.06 | -0.31 |
| **Hangar (BD-7)** | 12038494.4 | 3412370.71 | 83.85 | 12038494.47 | 3412370.7 | 83.95 | -0.07 | 0.01 | -0.1 |
| **Hangar (BD-8)** | 12038559.28 | 3412601.26 | 82.45 | 12038559.27 | 3412601.25 | 82.79 | 0 | 0.01 | -0.34 |
| **Hangar (BD-9)** | 12038631.31 | 3412380.78 | 82.5 | 12038631.46 | 3412380.82 | 82.51 | -0.15 | -0.04 | -0.01 |
| **Light Pole (LP-1)** | 12038757.01 | 3412356.87 | 102.62 | 12038757.11 | 3412356.97 | 102.53 | -0.11 | -0.09 | 0.09 |
| **Light Pole (LP-2)** | 12038826.03 | 3412274.64 | 103.02 | 12038826.2 | 3412274.57 | 103.02 | -0.17 | 0.08 | 0 |
| **Marker Ball (MB-1)** | 12037630.82 | 3412029.15 | 88.29 | 12037630.94 | 3412029.45 | 87.68 | -0.13 | -0.31 | 0.6 |
| **Marker Ball (MB-2)** | 12037705.68 | 3411893.26 | 96.26 | 12037705.02 | 3411893.62 | 96.12 | 0.65 | -0.37 | 0.14 |
| **Marker Ball (MB-3)** | 12037932.48 | 3412042.33 | 96.17 | 12037932.36 | 3412042.35 | 95.4 | 0.12 | -0.02 | 0.77 |
| **Pole (P-1)** | 12037434.72 | 3411716.13 | 100.48 | 12037434.69 | 3411715.8 | 100.14 | 0.03 | 0.34 | 0.34 |
| **Pole (P-2)** | 12037477.48 | 3412100.22 | 101.72 | 12037477.32 | 3412100.33 | 101.79 | 0.16 | -0.11 | -0.07 |
| **Pole (P-3)** | 12037796.24 | 3411952.79 | 100.68 | 12037796.17 | 3411952.77 | 100.86 | 0.07 | 0.02 | -0.18 |
| **Pole (P-4)** | 12038245.36 | 3412247.3 | 96.15 | 12038245.31 | 3412247.42 | 96.44 | 0.05 | -0.12 | -0.29 |
| **Pole (P-5)** | 12038339.82 | 3412273.57 | 99.2 | 12038339.87 | 3412273.56 | 99.33 | -0.05 | 0 | -0.13 |
| **Tree (T-1)** | 12037101.2 | 3411811.54 | 144.99 | 12037099.16 | 3411810.87 | 144.93 | 2.04 | 0.67 | 0.06 |
| **Tree (T-2)** | 12037251.98 | 3411398.29 | 147.39 | 12037248.95 | 3411401.29 | 146.95 | 3.03 | -3.01 | 0.44 |
| **Tree (T-3)** | 12037514.6 | 3411046.33 | 140.81 | 12037514.58 | 3411048.44 | 142.42 | 0.01 | -2.11 | -1.61 |
| **Tree (T-4)** | 12037516.52 | 3411584.29 | 158.96 | 12037518.01 | 3411584.05 | 160.22 | -1.49 | 0.24 | -1.26 |

| Obstacle | Field Survey (ft) | | | UAS Imagery (ft) | | | Delta (ft) | | |
|---|---|---|---|---|---|---|---|---|---|
| | x | y | z | x | y | z | x | y | z |
| **Tree (T-5)** | 12037574.98 | 3411532.09 | 154.3 | 12037579.92 | 3411543.44 | 154.23 | -4.93 | -11.35 | 0.07 |
| **Tree (T-6)** | 12037584.64 | 3411479.78 | 167.16 | 12037585.62 | 3411479.96 | 167.49 | -0.98 | -0.18 | -0.33 |
| **Tree (T-7)** | 12037612.06 | 3411130.94 | 145.6 | 12037611.93 | 3411132.17 | 146.58 | 0.13 | -1.24 | -0.99 |
| **Tree (T-8)** | 12038319.42 | 3410833.62 | 123.67 | 12038313.58 | 3410839.47 | 124.76 | 5.84 | -5.84 | -1.09 |
| **Tree (T-9)** | 12038333.4 | 3410870.91 | 126.52 | 12038332.02 | 3410862.84 | 123.27 | 1.38 | 8.07 | 3.25 |
| **Tree (T-10)** | 12038403.7 | 3411019.15 | 127.55 | 12038402.81 | 3411033.6 | 123.3 | 0.89 | -14.45 | 4.25 |
| **Vent on Hangar (BD-10)** | 12038712.77 | 3412057.94 | 88.52 | 12038712.95 | 3412057.77 | 88.51 | -0.18 | 0.17 | 0.02 |

### 3.5.5 Stereo Analysis—Manned Imagery to NGS Field Survey Comparison Results

Stereo analysis was performed using manned aircraft imagery collected at SFQ to locate the obstacles identified by the NGS. Table 79 compares obstacle locations derived from NGS field survey and the manned aircraft imagery when measured in stereo. The manned aircraft performed similarly to the UAS platforms but could not match the accuracy and completeness of the UAS data sets. Two obstacle measurements fell outside of the most stringent vertical accuracy requirement (3 ft) stated in AC 150/5300-18 (FAA, 2014), and two obstacles were unable to be located in the manned aircraft imagery.

The manned imagery collected at SFQ struggled with the same three trees as the eBee X and WingtraOne, indicating that the increased error seen in the UAS tests was not due to an inherent limitation of UASs. In particular, the manned imagery struggled with the three antenna obstacles. Two antennas were unable to be seen in the imagery, while the third was located, but it did not meet the current accuracy standards. This inability to accurately locate the antennas was due to the 6 in. GSD of the manned imagery, which inherently would struggle to measure narrow obstacles such as antennas. Both UAS platforms were able to accurately measure all three antennas due to their significantly smaller GSD values (0.5 in. and 1 in.).

Table 80 compares the delta values for obstacle measurements derived from the WingtraOne imagery versus field survey (presented in Table 78) with the deltas from obstacle measurements derived from the manned aircraft imagery versus the field survey (presented in Table 79). The delta values demonstrate that the manned imagery struggled with finer features, such as antennas, while the the Wingtra and manned imagery performed equally well with larger features, such as hangers. For features such as poles, in the event the delta was over 0.5 ft, the Wingtra was closer to the surveyed elevations. The delta values for trees were inconsistent, with both manned and Wingtra imagery showing variation in horizontal and vertical values.

Table 79. Variance between NGS Field Survey and Manned Aircraft Imagery

| Obstacle | Field Survey (ft) | | | Manned Imagery (ft) | | | Delta (ft) | | |
|---|---|---|---|---|---|---|---|---|---|
| | x | y | z | x | y | z | x | y | z |
| **Antenna (A-1)** | 12038514.15 | 3412321.81 | 163.24 | 12038518.67 | 3412324.86 | 155.87 | -4.52 | -3.05 | 7.37 |
| **Antenna on Hangar (A-2)** | 12038696.55 | 3412848.89 | 96.47 | N/A | N/A | N/A | N/A | N/A | N/A |
| **Antenna on Hangar (A-3)** | 12038835.86 | 3412011.18 | 90.65 | N/A | N/A | N/A | N/A | N/A | N/A |
| **Beacon (APBN)** | 12038819.76 | 3412499.53 | 122.41 | 12038821.36 | 3412499.92 | 122.16 | -1.60 | -0.39 | 0.25 |
| **Hangar (BD-1)** | 12037414.12 | 3412405.33 | 96.35 | 12037413.84 | 3412404.64 | 96.45 | 0.28 | 0.69 | -0.10 |
| **Hangar (BD-2)** | 12038035.51 | 3412185.25 | 83.41 | 12038035.22 | 3412185.92 | 83.64 | 0.29 | -0.67 | -0.23 |
| **Hangar (BD-3)** | 12038085.34 | 3412446.09 | 82.11 | 12038085.88 | 3412445.95 | 82.28 | -0.54 | 0.14 | -0.17 |
| **Hangar (BD-4)** | 12038156.18 | 3412231.43 | 82.14 | 12038155.98 | 3412231.72 | 82.19 | 0.20 | -0.29 | -0.05 |
| **Hangar (BD-5)** | 12038277.62 | 3412270.94 | 81.82 | 12038277.29 | 3412271.48 | 81.71 | 0.33 | -0.54 | 0.11 |
| **Hangar (BD-6)** | 12038318.28 | 3412522.45 | 82.76 | 12038318.52 | 3412521.67 | 82.89 | -0.24 | 0.78 | -0.13 |
| **Hangar (BD-7)** | 12038494.40 | 3412370.71 | 83.85 | 12038494.56 | 3412371.37 | 84.13 | -0.16 | -0.66 | -0.28 |
| **Hangar (BD-8)** | 12038559.28 | 3412601.26 | 82.45 | 12038559.70 | 3412600.50 | 82.81 | -0.42 | 0.76 | -0.36 |
| **Hangar (BD-9)** | 12038631.31 | 3412380.78 | 82.50 | 12038630.96 | 3412381.29 | 83.03 | 0.35 | -0.51 | -0.53 |
| **Light Pole (LP-1)** | 12038757.01 | 3412356.87 | 102.62 | 12038757.15 | 3412356.94 | 102.41 | -0.14 | -0.07 | 0.21 |
| **Light Pole (LP-2)** | 12038826.03 | 3412274.64 | 103.02 | 12038826.13 | 3412274.58 | 102.36 | -0.10 | 0.06 | 0.66 |
| **Marker Ball (MB-1)** | 12037630.82 | 3412029.15 | 88.29 | 12037630.86 | 3412029.13 | 87.39 | -0.04 | 0.02 | 0.90 |
| **Marker Ball (MB-2)** | 12037705.68 | 3411893.26 | 96.26 | 12037705.63 | 3411893.14 | 96.01 | 0.05 | 0.12 | 0.25 |
| **Marker Ball (MB-3)** | 12037932.48 | 3412042.33 | 96.17 | 12037932.49 | 3412042.18 | 95.34 | -0.01 | 0.15 | 0.83 |
| **Pole (P-1)** | 12037434.72 | 3411716.13 | 100.48 | 12037434.92 | 3411715.40 | 101.50 | -0.20 | 0.73 | -1.02 |
| **Pole (P-2)** | 12037477.48 | 3412100.22 | 101.72 | 12037476.81 | 3412099.48 | 102.83 | 0.67 | 0.74 | -1.11 |
| **Pole (P-3)** | 12037796.24 | 3411952.79 | 100.68 | 12037796.07 | 3411952.51 | 101.13 | 0.17 | 0.28 | -0.45 |
| **Pole (P-4)** | 12038245.36 | 3412247.30 | 96.15 | 12038245.10 | 3412247.19 | 96.40 | 0.26 | 0.11 | -0.25 |
| **Pole (P-5)** | 12038339.82 | 3412273.57 | 99.20 | 12038338.45 | 3412274.31 | 98.56 | 1.37 | -0.74 | 0.64 |
| **Tree (T-1)** | 12037101.20 | 3411811.54 | 144.99 | 12037093.63 | 3411808.09 | 145.70 | 7.57 | 3.45 | -0.71 |
| **Tree (T-2)** | 12037251.98 | 3411398.29 | 147.39 | 12037241.65 | 3411402.95 | 146.18 | 10.33 | -4.66 | 1.21 |
| **Tree (T-3)** | 12037514.60 | 3411046.33 | 140.81 | 12037513.70 | 3411048.35 | 141.37 | 0.90 | -2.02 | -0.56 |
| **Tree (T-4)** | 12037516.52 | 3411584.29 | 158.96 | 12037523.13 | 3411583.26 | 157.44 | -6.61 | 1.03 | 1.52 |
| **Tree (T-5)** | 12037574.98 | 3411532.09 | 154.30 | 12037573.26 | 3411542.17 | 154.08 | 1.72 | -10.08 | 0.22 |
| **Tree (T-6)** | 12037584.64 | 3411479.78 | 167.16 | 12037584.45 | 3411478.74 | 168.24 | 0.19 | 1.04 | -1.08 |
| **Tree (T-7)** | 12037612.06 | 3411130.94 | 145.60 | 12037612.67 | 3411131.77 | 147.06 | -0.61 | -0.83 | -1.46 |
| **Tree (T-8)** | 12038319.42 | 3410833.62 | 123.67 | 12038314.53 | 3410841.52 | 126.81 | 4.89 | -7.90 | -3.14 |
| **Tree (T-9)** | 12038333.40 | 3410870.91 | 126.52 | 12038332.26 | 3410862.47 | 125.33 | 1.14 | 8.44 | 1.19 |
| **Tree (T-10)** | 12038403.70 | 3411019.15 | 127.55 | 12038400.06 | 3411038.48 | 124.85 | 3.64 | -19.33 | 2.70 |

| Obstacle | Field Survey (ft) | | | Manned Imagery (ft) | | | Delta (ft) | | |
|---|---|---|---|---|---|---|---|---|---|
| | x | y | z | x | y | z | x | y | z |
| **Vent On Hanger (BD-10)** | 12038712.77 | 3412057.94 | 88.52 | 12038713.04 | 3412057.43 | 87.56 | -0.27 | 0.51 | 0.96 |

Table 80.Variance between Delta Values from UAS Test 3-1 and Manned Aircraft Imagery When Compared to the NGS Ground Survey

| Obstacle | WingtraOne vs Field Survey (ft) | | | Manned Aircraft vs Field Survey (ft) | | | Delta (ft) | | |
|---|---|---|---|---|---|---|---|---|---|
| | x | y | z | x | y | z | x | y | z |
| **Antenna (A-1)** | 0.26 | -0.05 | -0.58 | -4.52 | -3.05 | 7.37 | 4.78 | 3.00 | 7.95 |
| **Antenna on Hangar (A-2)** | -0.19 | -0.09 | -0.43 | N/A | N/A | N/A | N/A | N/A | N/A |
| **Antenna on Hangar (A-3)** | -0.01 | -0.08 | -0.02 | N/A | N/A | N/A | N/A | N/A | N/A |
| **Beacon (APBN)** | -2.11 | 1.00 | 0.09 | -1.60 | -0.39 | 0.25 | 0.51 | 1.39 | 0.16 |
| **Hangar (BD-1)** | 0.2 | -0.06 | -0.03 | 0.28 | 0.69 | -0.10 | 0.08 | 0.75 | 0.07 |
| **Hangar (BD-2)** | 0.00 | -0.02 | -0.01 | 0.29 | -0.67 | -0.23 | 0.29 | 0.65 | 0.22 |
| **Hangar (BD-3)** | -0.11 | -0.22 | -0.26 | -0.54 | 0.14 | -0.17 | 0.43 | 0.36 | 0.09 |
| **Hangar (BD-4)** | -0.02 | 0.45 | -0.03 | 0.20 | -0.29 | -0.05 | 0.22 | 0.74 | 0.02 |
| **Hangar (BD-5)** | 0.01 | 0.04 | 0.01 | 0.33 | -0.54 | 0.11 | 0.32 | 0.58 | 0.10 |
| **Hangar (BD-6)** | 0.06 | 0.06 | -0.31 | -0.24 | 0.78 | -0.13 | 0.30 | 0.72 | 0.18 |
| **Hangar (BD-7)** | -0.07 | 0.01 | -0.10 | -0.16 | -0.66 | -0.28 | 0.09 | 0.67 | 0.18 |
| **Hangar (BD-8)** | 0.00 | 0.01 | -0.34 | -0.42 | 0.76 | -0.36 | 0.42 | 0.75 | 0.02 |
| **Hangar (BD-9)** | -0.15 | -0.04 | -0.01 | 0.35 | -0.51 | -0.53 | 0.50 | 0.47 | 0.52 |
| **Light Pole (LP-1)** | -0.11 | -0.09 | 0.09 | -0.14 | -0.07 | 0.21 | 0.03 | 0.02 | 0.12 |
| **Light Pole (LP-2)** | -0.17 | 0.08 | 0.00 | -0.10 | 0.06 | 0.66 | 0.07 | 0.02 | 0.66 |
| **Marker Ball (MB-1)** | -0.13 | -0.31 | 0.60 | -0.04 | 0.02 | 0.90 | 0.09 | 0.33 | 0.30 |
| **Marker Ball (MB-2)** | 0.65 | -0.37 | 0.14 | 0.05 | 0.12 | 0.25 | 0.60 | 0.49 | 0.11 |
| **Marker Ball (MB-3)** | 0.12 | -0.02 | 0.77 | -0.01 | 0.15 | 0.83 | 0.13 | 0.17 | 0.06 |
| **Pole (P-1)** | 0.03 | 0.34 | 0.34 | -0.20 | 0.73 | -1.02 | 0.23 | 0.39 | 1.36 |
| **Pole (P-2)** | 0.16 | -0.11 | -0.07 | 0.67 | 0.74 | -1.11 | 0.51 | 0.85 | 1.04 |
| **Pole (P-3)** | 0.07 | 0.02 | -0.18 | 0.17 | 0.28 | -0.45 | 0.10 | 0.26 | 0.27 |
| **Pole (P-4)** | 0.05 | -0.12 | -0.29 | 0.26 | 0.11 | -0.25 | 0.21 | 0.23 | 0.04 |
| **Pole (P-5)** | -0.05 | 0.00 | -0.13 | 1.37 | -0.74 | 0.64 | 1.42 | 0.74 | 0.77 |
| **Tree (T-1)** | 2.04 | 0.67 | 0.06 | 7.57 | 3.45 | -0.71 | 5.53 | 2.78 | 0.77 |
| **Tree (T-2)** | 3.03 | -3.01 | 0.44 | 10.33 | -4.66 | 1.21 | 7.30 | 1.65 | 0.77 |

| Obstacle | WingtraOne vs Field Survey (ft) | | | Manned Aircraft vs Field Survey (ft) | | | Delta (ft) | | |
|---|---|---|---|---|---|---|---|---|---|
| | x | y | z | x | y | z | x | y | z |
| **Tree (T-3)** | 0.01 | -2.11 | -1.61 | 0.90 | -2.02 | -0.56 | 0.89 | 0.09 | 1.05 |
| **Tree (T-4)** | -1.49 | 0.24 | -1.26 | -6.61 | 1.03 | 1.52 | 5.12 | 0.79 | 2.78 |
| **Tree (T-5)** | -4.93 | -11.35 | 0.07 | 1.72 | -10.08 | 0.22 | 6.65 | 1.27 | 0.15 |
| **Tree (T-6)** | -0.98 | -0.18 | -0.33 | 0.19 | 1.04 | -1.08 | 1.17 | 1.22 | 0.75 |
| **Tree (T-7)** | 0.13 | -1.24 | -0.99 | -0.61 | -0.83 | -1.46 | 0.74 | 0.41 | 0.47 |
| **Tree (T-8)** | 5.84 | -5.84 | -1.09 | 4.89 | -7.90 | -3.14 | 0.95 | 2.06 | 2.05 |
| **Tree (T-9)** | 1.38 | 8.07 | 3.25 | 1.14 | 8.44 | 1.19 | 0.24 | 0.37 | 2.06 |
| **Tree (T-10)** | 0.89 | -14.45 | 4.25 | 3.64 | -19.33 | 2.70 | 2.75 | 4.88 | 1.55 |
| **Vent on Hangar (BD-10)** | -0.18 | 0.17 | 0.02 | -0.27 | 0.51 | 0.96 | 0.09 | 0.34 | 0.94 |

### 3.5.6 Findings

The NGS found that the UAS imagery captured by the eBee X and WingtraOne at SFQ met their requirements with regard to image quality and data accuracy. Both data sets provided obstacle locations that were more accurate than the manned aircraft data when compared to the field survey.

The significantly higher resolution of the UAS imagery resulted in more complete obstacle data sets than those produced with the manned imagery. Two obstacles that were unable to be seen in the manned imagery were able to be accurately located by the UAS imagery.

The M210 and X7 continued to demonstrate inconsistency, failing to generate a valid AT solution and viable stereo despite collecting data using previously successful parameters. This failure was due to a software malfunction in which the image capture did not collect the correct image orientations.

Winds of 10 to 15 mph during data collection caused the fixed-wing UASs to deviate from their planned flight paths, requiring a higher level of effort during initial processing to achieve a valid AT solution and viable stereo.

Additional GCPs and flight lines were added surrounding the dense vegetation located in the southwest corner of the test area. These enhancements helped to ensure valid AT solutions and viable stereo from the WingtraOne and eBee X imagery by minimizing the number of uncalibrated images in the data sets.

## 4. SUMMARY

Sections 4.1 through 4.4 summarize the findings of this research program, including the overall assessment of UAS obstacle data accuracy, the benefits and limitations of UAS, technical and operational considerations, and recommended use cases for using UAS to perform airport obstacle data collection.

### 4.1 UAS OBSTACLE DATA ACCURACY FINDINGS

The FAA research team found that aerial imagery collected with UASs was capable of generating obstacle data that meet the FAA accuracy standards contained in AC 150/5300-17 and AC 150/5300-18 when using 3D stereo analysis techniques.

It was found that there is no “one size fits all” solution for collecting UAS aerial imagery that will generate a valid AT solution and accurate obstacle data. The accuracy of obstacle data is dependent on a variety of factors, including technology performance specifications such as camera sensor and lens quality, data collection parameters such as GSD and overlap settings, data processing considerations including the choice of AT solution software, environmental conditions during data collection, and site attributes such as the presence of large areas of dense vegetation or terrain. None of these individual considerations can be isolated, and many can be used to compensate for a challenging environment or for areas in which other considerations are lacking.

## 4.2 BENEFITS AND LIMITATIONS

### 4.2.1 Benefits

UASs provide several benefits when compared to surveys conducted using manned aircraft or traditional field techniques:

- For smaller scale surveys, mobilizing and collecting imagery with a UAS can provide a significant cost savings versus manned aircraft. This can allow surveys to be conducted more frequently. For example, regular inexpensive collection of the inner approach surfaces using UASs could allow an airport to monitor tree growth and proactively plan for clearing and topping projects.
- The resolution of UAS imagery is considerably higher than that collected using manned aircraft, allowing for the imaging and measurement of small and narrow obstacles manned aircraft cannot detect. For example, UAS aerial imagery collected under 400 ft AGL is significantly higher resolution (≤1 in. GSD) than imagery collected with manned aircraft, which is typically collected at several thousand feet with a ~5- to 6-in. GSD. During testing at I67 and SFQ, the increased resolution resulted in UAS imagery producing more complete obstacle data sets than manned aircraft imagery. This occurred because the increased resolution allowed UAS imagery to locate narrow obstacles the manned aircraft cannot detect (due to lower resolutions of 5 to 6-in. GSD).
- Aerial surveys (such as those conducted via UAS) can observe the entire survey area, allowing for a more thorough assessment of obstacles over a given area; whereas field surveys can only observe and measure a single layer of obstacles.

### 4.2.2 Limitations

There are currently several regulatory and technical limitations that could limit the use of UASs for conducting airport obstacle data collection surveys:

- While UASs can provide efficiencies for smaller scale surveys, several factors limit the scalability of the technology for larger surveys. The 400 ft AGL ceiling imposed by 14 CFR 107.51, *Operating Limitations for Small Unmanned Aircraft*, results in the land area captured in each photo taken by UASs being significantly smaller than those taken using manned aircraft (Operating Limitations of Small Unmanned Aircraft, 2016). As a result, UASs must take more photos to cover an equivalent land area versus manned aircraft. The NGS has estimated that the ratio of UASs to manned aircraft imagery required to cover an equivalent area could be as high as 350:1. This increase in the number of photos for a given survey area would significantly increase the time required to process and analyze these data sets prior to delivery to the NGS. This might render the use of UAS imagery collected at low altitudes impractical for large survey applications, such as those required when completing a complete airport survey compliant with AC 150/5300-18.

  In addition to increasing the time to process data, the 400 ft AGL ceiling and the limited land area captured in each photo also results in UAS aerial surveys taking significantly longer to complete than manned aircraft surveys for a given area (Operating Limitations of Small Unmanned Aircraft, 2016).

14 CFR 107.31, *Visual Line of Sight Aircraft Operation*, requires that the remote pilot in command (RPIC) or visual observer must maintain visual contact with the UAS in such a way that they can determine the aircraft's location, attitude, altitude, and heading; and observe the surrounding airspace for other hazards. Due to the relatively small size of most commercial UASs, this regulation places a considerable restriction on the amount of ground a UAS can cover in a single flight without relocating the RPIC or visual observer. (Visual Line of Sight Aircraft Operation, 2016)

- **Weather:** UASs are more susceptible to the effects of weather, particularly wind, than manned aircraft or field surveys. While operating limitations vary by manufacturer, UASs generally cannot operate in winds exceeding 20–25 mph, and the quality of the imagery can be negatively affected by winds approaching 15 mph.

  14 CFR 107.51 establishes the minimum visibility and cloud clearances required when operating a UAS. This regulation states that UASs may only be operated when the minimum flight visibility observed from the location of the GCS is at least 3 statute miles. During operation the UAS must remain at least 500 feet below and 2,000 feet horizontal from any clouds. If these conditions cannot be met, UAS operations may only be conducted if the operator has an airspace authorization modifying these requirements (Operating Limitations for Small Unmanned Aircraft, 2016).

- **Operational Limitations:** UAS aerial surveys at airports require considerably more pre-planning/coordination with air traffic than manned aircraft aerial surveys and field surveys. To operate in controlled airspace at airports, UAS operators must apply for and receive an approved Part 107 airspace authorization for the location and dates of the aerial survey. In many cases these airspace authorizations also require the RPIC to notify local air traffic and receive concurrence immediately prior to takeoff.

  14 CFR 107.37, *Operation near Aircraft; Right of Way Rules*, requires UASs to yield the right of way to all aircraft. When operating in the approach of a busy airport, this could lead to significant delays. For particularly busy airports, conducting a UAS aerial survey in the vicinity of a runway or approach surface could require the runway to be closed. This could offset the economic efficiencies presented by UAS surveys. (Operation Near Aircraft; Right-of-Way Rules, 2016).

  14 CFR 107.39, *Operation over Human Beings*, prohibits UAS operations over people or moving vehicles that are not directly participating in the aircraft's operation. Because airports typically have a multitude of people and vehicles operating in and around the property, this can present a challenge to ensure the UAS does not fly over any nonparticipants (Operation over Human Beings, 2016).

- **Regulatory Limitations:** During the execution of this research effort, FAA researchers performed a comprehensive review of all applicable regulatory standards guiding the collection and submission of airport aerial survey data. During this review, a number of provisions of AC 150/5300-17 were identified that would preclude UASs from being used,

as well as an instance where new guidance should be added to ensure adequate and thorough coverage when conducting obstacle data collection with UASs.

## 4.3 TECHNICAL AND OPERATIONAL CONSIDERATIONS

Sections 4.3.1 through 4.3.9 provide technical and operational considerations for using UASs to conduct airport obstacle data collection.

### 4.3.1 UAS Platform Selection Considerations

#### 4.3.1.1 UAS Type

- Different UAS airframe types (e.g., fixed-wing, multirotor, and hybrid) provide contrasting capabilities and limitations regarding conducting aerial surveys and operating in the airport environment.

- Fixed-wing and hybrid UASs are best suited for larger survey areas that can accommodate their turning radius and takeoff/landing space requirements. Fixed-wing UASs can typically fly faster and longer than multirotors but have a larger turning radius and are more susceptible to being affected by winds during flight. In addition, fixed-wing UASs also require a larger area for takeoff and landing. Hybrid VTOL UASs perform as fixed-wings, but their VTOL capability allows them to operate in areas with less open space than a typical fixed-wing requires to safely take off and land.

- Multirotor UASs are best suited for smaller survey areas or dense areas where maneuverability is a higher priority than collection speed. Multirotor UASs have the greatest maneuverability, enhancing safety by allowing for quick avoidance of obstacles or aircraft in the flight path. In addition, multirotor UASs require a smaller flight operations area versus fixed-wing or hybrid UASs for a given survey area because they are capable of VTOL and have no turning radius.

#### 4.3.1.2 Airborne GNSS RTK and PPK

Data collection should be completed using a UAS that has RTK or PPK capabilities. RTK and PPK increase the accuracy of onboard UAS GNSS and improve the quality of AT solutions and obstacle measurements. RTK and PPK increase the accuracy of image center coordinates captured during the imagery collection process, which improves the AT software's ability to calculate an exterior orientation.

### 4.3.2 Camera Payload Characteristics

#### 4.3.2.1 Sensor/IMU Metadata

The UAS platform or camera payload must collect camera orientation metadata (yaw, pitch, roll) to develop a valid AT solution.

#### 4.3.2.2 Camera Lens

- A camera lens with minimal distortion should be selected to ensure control measurement accuracy. Cameras with significant lens distortion along the edges minimize the area in the center of the image that is suitable for control measurement. Any control captured along the edges of these images (where lens distortion exists) will result in high residuals and increased parallax. The impact of distortion is dependent on site, GCP layout, and AT software. The more control that falls within the measurable area, the higher the likelihood that the AT solution will be viable. As a result, sensors with higher lens distortion may require additional ground control to support challenging areas. The effect of lens distortion is compounded if there is dense vegetation on site, causing successful auto-correlated tie points to be generated in much lower numbers. In this case, more GCPs are needed to support the solution. In contrast, when operating in open areas GCPs will be more likely to be visible in numerous images and in more locations in each of the images. This lessens the impact of lens distortion.

- The UAS should also capture imagery with the widest lens available to maximize efficiency and capture the largest image footprint possible. This will decrease the flight time required to capture data ands well as to reduce the number of images that need to be processed.

#### 4.3.2.3 Camera Shutter, Aperture, and ISO

- The camera used for data collection should have a global shutter. Camera payloads with global shutters introduce less distortion than those with rolling shutters. This is due to the nature of global shutters, in which the entire image is captured in a single precise moment, whereas rolling shutters capture the image one line of pixels at a time over a specified timeframe. The camera shutter speed should be sufficient to prevent motion blur in the imagery. The time difference between when the first and last lines of pixels in an image are captured creates what is known as temporal distortion in the image. The magnitude of temporal distortion is positively correlated to the speed at which the camera is moving. If using a camera with a rolling shutter, it is recommended to use AT software that is capable of correcting for the introduced artifacts. It is also recommended to ensure that the system has adequate memory writing speed to support the rate of data collection.

- The camera should have a variable aperture capability. The aperture during data collection should be carefully selected to balance the demands of the depth of field and shutter speed.

- The research team has no indication that ISO values (which describe a camera's sensitivity to light) lower than 800 have an impact on the accuracy of obstacle measurements. Depending on the noise characteristics of the platform in question, higher ISO values may be able to be used without degrading accuracy.

- The camera should use an intelligent auto exposure mode with the ability to set manual boundaries. The use of manual-only exposure risks inconsistent imagery as the lighting conditions can change during data collection. Due to the varied nature of the data capture

area, it is recommended to use the widest exposure metering mode available on the platform. The use of spot metering is not recommended as it can introduce a dramatic shift in exposure values from frame to frame in the data capture.

### 4.3.3 Geodetic Control

- AC 150/5300-16 and AC 150/5300-18 must be adhered to in order to ensure a high level of confidence in collecting geodetic control data and are required by NGS for safety-critical data, including obstacle data, entering Airports Geographic Information Systems (FAA, 2019; FAA 2014).
- The required number and positions of GCPs to support accurate UAS obstacle data collection are directly affected by characteristics of the site. In unobstructed sites or areas of moderate vegetation, GCPs should have a maximum spacing of 1,000 ft. In areas of dense vegetation, GCPs should be spaced closer together at a maximum spacing of 500 ft.
- The amount of ground control required is inversely related to the overlap parameters used during data collection. If a dense GCP layout is used with spacing less than 500 ft between points, lower overlap values may be used to successfully generate a valid AT solution. When a less dense GCP layout is used with spacing up to 1,000 ft between points, higher overlap values will be required to generate an AT solution of equivalent quality.
- The control layout should ensure that each feature intended to be measured in the stereo imagery is surrounded by the GCPs.
- To the greatest extent possible, the GCP layout should surround areas of dense vegetation to aid in the development of valid AT solutions.
- GCPs should be tied to the NSRS. RTK GNSS surveying in open areas is sufficient for producing photo control points at the 30 cm horizontal and 10 cm vertical accuracy requirements of AC 150/5300-17 (FAA, 2017b). If a project demands higher accuracies or if the GCP does not have a clear sky view, conventional total station surveying or differential leveling surveying techniques should be used to meet the established standard.
- RTK observations at each GCP should be performed twice with separate RTK initializations to help eliminate the possibility of an incorrect or bad initialization. In addition, a random sample of the GCPs should be revisited for additional independent observations as a quality control procedure.

### 4.3.4 UAS Data Collection Parameters

Sections 4.3.4.1 through 4.3.4.4 provide findings and considerations regarding UAS data collection parameters, including general considerations, overlap values, altitude/GSD, and UAS flight lines.

#### 4.3.4.1 Overlap

- The forward and side overlap values necessary to achieve a valid AT solution are dependent on the site characteristics (e.g., density of vegetation) and the GCP layout. Generally, overlap values are inversely related to GCP layout density, while a positive correlation exists between overlap and the time required for data collection.

- 80%/60% forward and side overlap values were found sufficient for most sites to produce a viable AT solution.
- 70%/70% forward and side overlap values were found to be the minimum for producing valid AT solutions at sites where a dense GCP layout is in use.
- 80%/80% forward and side overlap settings were found to be the maximum values in which a significant quality increase could be seen prior to diminishing returns offset by longer flight times.

#### 4.3.4.2 Altitude/GSD

- UAS imagery should be collected at the maximum altitude authorized. Flying at higher altitudes decreases the time required for data collection and decreases the presence of distortion in the imagery. This increases the likelihood of collecting imagery that will support a valid AT solution and decreases GCP requirements.
- Flying at lower altitudes increases the level of detail in the imagery at the expense of increased distortion and data collection time. However, this could be beneficial in certain instances for the collection of obstacles with smaller vertical cross-sections.

#### 4.3.4.3 Flight Lines

- UAS flight plans should use sequential flight lines rather than interlaced flight lines. During testing, it was found that interlaced flight lines produce data sets that are significantly less accurate than those produced using sequential flight lines. This was due to the time difference that occurred between photos of adjacent flight lines.
- When performing data collection using a fixed-wing UAS platform, flight lines should be positioned perpendicular to the wind direction to allow for a consistent cruise speed.
- The overall study area should be buffered by 2 to 3 flight lines at the sides of the area and 3 to 5 images at the start and end of each flight line to ensure adequate image calibration along the edges of the survey area.
- 2 to 3 flight lines should be added past the edges of dense vegetation to allow for the presence of GCPs or well-defined points surrounding these areas.

### 4.3.5 Imagery Collection Parameters

- Imagery should be captured in a nadir orientation (90° downward).
- Camera focus must be set at a control elevation and maintained throughout data collection.
- All imagery must have a GNSS position for an AT solution to be completed.
- UAS RTK/PPK capabilities should be used when possible.
- Each GCP should be visible from at least two flight lines to aid in the successful development of AT solutions.

### 4.3.6 Field Quality Control

Following UAS data collection, the raw imagery should be manually inspected for the following:

- The correct number of images were collected based on the predefined data collection parameters.
- All imagery was collected in the proper orientation and aspect ratio as expected.
- All imagery was collected with appropriate camera settings.
- All imagery is in focus.
- All imagery is properly exposed.
- All GCPs are clearly visible in the imagery as intended.
- The imagery covers the entire study area (with additional buffers, as necessary).

#### 4.3.7 Data Processing Software

- The choice of AT software was found to have a significant effect on the quality of AT solutions processed and their viability for obstacle data collection during stereo analysis. AT software choice is dependent upon the unique challenges of the site, the platform/sensor being flown, and the GCP layout. While simpler software offering fewer tools for customization during data processing did produce valid AT solutions that were viable for obstacle data collection, there were circumstances where AT software that allowed for customization of processing parameters was required to offset limitations with the sensor.

- If a site does not have large areas of dense vegetation and a high-quality sensor is used, simpler AT software might be sufficient to generate a valid AT solution. If there is a particularly challenging site (e.g., high-relief, dense-vegetation), with a weaker platform/sensor, AT software with more customizable processing options might need to be used to compensate for lens distortion, uneven flight lines, and weak GCP layout. AT software allowing the customization of parameters and manual processing techniques enables the user to compensate for gaps in the automated processing steps.

#### 4.3.8 Quality Control

- Entities using UAS for obstacle data collection should conduct their own testing and QC checks to ensure their specific combination of UAS hardware, camera payload, processing software, and data collection parameters is able to achieve the required level of accuracy for a given project.

#### 4.3.9 Data Storage

Due to the large size of UAS obstacle data sets, it is recommended that entities collecting and processing these data sets have adequate data storage capacity.

### 4.4 UAS OBSTACLE DATA COLLECTION USE CASE EXAMPLES

Sections 4.4.1 through 4.4.5 provide examples of UAS obstacle data collection surveys (use cases). It should be noted that these examples are not an exhaustive list, and other potential use cases might exist.

### 4.4.1 FAA Engineering Brief #91, Vegetation Management Projects

Engineering Brief (EB) #91 sets requirements for the management of vegetation in and around airports, including the collection, submission, and management of data describing vegetation. This EB provides a supplemental means for complying with the standards of AC 150/5300-18 (FAA, 2013).

When airport operators conduct surveys in support of EB #91 obstruction removal projects, they traditionally rely on field surveys or aerial surveys conducted with manned aircraft. In smaller projects, such as a single runway approach, collecting manned aerial imagery is often cost-prohibitive, and, in these cases, full AC 150/5300-18 surveys can provide a low return on investment for the airport operator. In these cases, UASs could provide a cost-efficient means to measure all the obstructions penetrating an approach surface. In addition, regular inexpensive collection of the inner approach surfaces using UASs would allow the airport to monitor tree growth and proactively plan for clearing and topping projects.

In 2018, Allentown Queen City Municipal Airport (XLL) performed significant tree clearing in the approach of Runway 15. Figure 48 depicts this approach area. In this figure, the red line outlines the 20:1 surface that the airport was attempting to clear, and the magenta points and green baselines identify the penetrating trees identified through field survey techniques. In support of this project, XLL commissioned a UAS survey of the area, which identified additional trees penetrating the surface that were not identified using field surveying. The trees identified by UASs are marked with yellow points in Figure 48. Figure 49 shows a comparison of before and after tree clearing performed using these data at XLL.

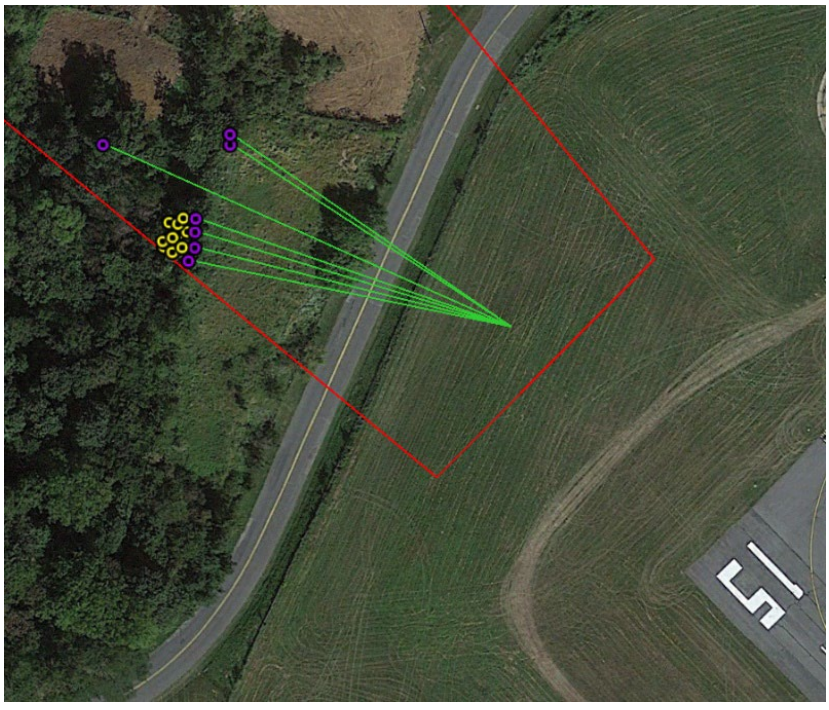


Figure 48. Allentown Queen City Municipal Airport Runway 15 EB-91 Tree Clearing Study Area

| Area Before Tree Clearing | Area After Tree Clearing |
|---|---|
| 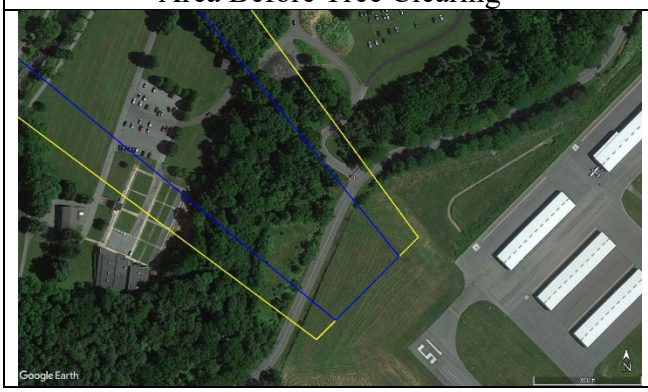 |  |

Figure 49. Before and After Vegetation Management at XLL

4.4.2 Preliminary Obstacle Data Collection Prior to AC 150/5300-18 Survey

Surveys conducted in compliance with AC 150/5300-18 costs can exceed $60,000 per survey, and when an airport undertakes construction projects that alter its current OISs, multiple surveys might be required to verify that obstacles penetrating its new OISs have been removed. In these circumstances, UASs can provide a more cost-effective method for performing an initial survey to identify obstacles that will penetrate the new OISs, and if there are any easements or property that must be acquired. Once the required actions to mitigate these penetrating obstacles are complete, a traditional AC 150/5300-18 survey can be completed to officially confirm the airport's compliance (Lamoureux, 2022).

UASs were used in this manner to conduct a preliminary planning survey at Millinocket Municipal Airport (MLT) for a runway extension project. The UAS survey data collected at MLT were used to create a 3D model of the airport to determine the obstructions that needed to be cleared prior to the project completion. Conducting the UAS obstruction analysis saved time and money by reducing the need for multiple expensive surveys. MLT benefited from a streamlined process for developing approach and departure plans while ensuring compliance with safety regulations (Lamoureux, 2022).

4.4.3 Verification of Obstacle Authoritative Source Database Entries

The Obstacle Authoritative Source (OAS) database has many legacy entries that might have been surveyed with a lower level of accuracy or might not reflect current obstacles. The use of UASs to position these obstacles with a higher accuracy would decrease their impact on flight procedures even if the obstacle is unable to be mitigated. Often, controlling obstacles at an airport defines the visibility minimums for an approach procedure, and airports go through great lengths to remove these obstacles. A targeted UAS obstacle survey could be an inexpensive means to verify accuracies and update controlling obstacles within the OAS database.

4.4.4 FAA Order 5010.4 Inspection Supplement

FAA Order 5010.4, *Airport Data and Information Management*, provides requirements and guidance for complying with the Airport Data and Information Management program. This

includes providing guidance regarding conducting inspections to collect information describing the physical infrastructure, characteristics, and operational environment of airports. With regard to obstacle data collection, inspections conducted in accordance with FAA Order 5010.4 assist with identifying unmarked obstructions, updating controlling obstructions (the obstruction that requires the steepest glide slope to clear, and identifying objects in safety areas. Since these inspections are typically conducted from the ground, they can fail to identify the true controlling obstruction if it is obscured behind another obstacle. Using UASs would ensure that all obstructions are identified and included in the Airport Data Management program (FAA, 2015).

### 4.4.5 Visual Glide Slope Indicator Surveys

EB #95, *Additional Siting and Survey Considerations for Precision Approach Path Indicator (PAPI) and Other Visual Glide Slope Indicators (VGSI)*, provides guidance regarding performing surveys for the establishment or inspection of VGSIs. Due to their placement adjacent to runways, the lights from PAPIs or other VGSIs can be seen outside of runway OCSs. To ensure the safety of approaching aircraft, EB #95 establishes a light signal clearance surface (LSCS), which must be kept free of light signal obstructions. A diagram depicting the typical difference between an OCS and LSCS from EB #95 is shown in Figure 50 (FAA 2017a).

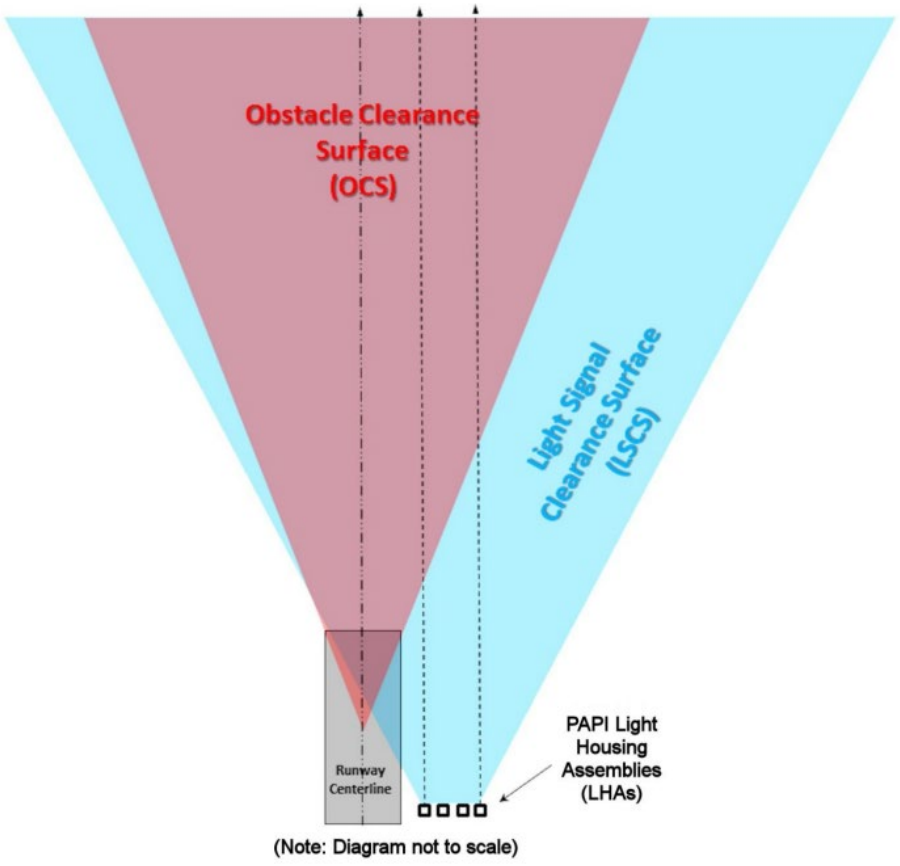


Figure 50. Precision Approach Path Indicator OCS and LSCS (FAA, 2017a)

The standards specified in EB #95 require airports to survey the LSCS when establishing or replacing a PAPI/VGSI. Typically, these surveys are completed using traditional field techniques. Figure 51 shows the results of a ground-based LSCS survey. As mentioned previously, field obstacle data surveys inherently struggle to identify obstacles that are not within immediate line of sight. Using UASs to conduct these surveys could allow for identifying all obstacles to the LSCS in one step (FAA, 2017a).

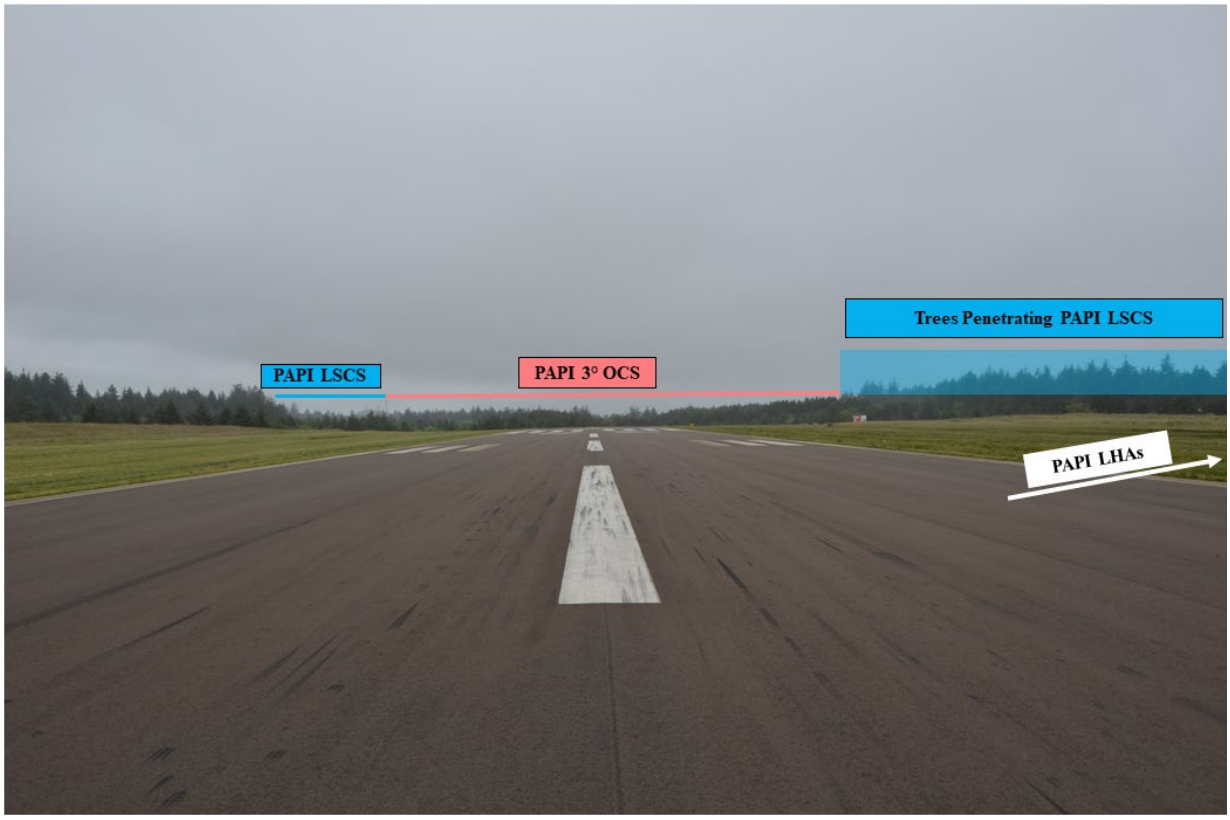


Figure 51. Results from Ground-Based LSCS Survey (not to scale)

## 5. CONCLUSIONS

The Federal Aviation Administration (FAA) Airport Technology Research and Development Branch conducted a research effort in collaboration with the National Oceanic and Atmospheric Administration's National Geodetic Survey (NGS) to evaluate the use of small unmanned aircraft systems (UASs) for conducting airport obstacle data collection. The objectives of this research effort were to evaluate the accuracy of UAS obstacle data, assess the benefits and limitations of this technology, develop technical and operational considerations for using UASs, and to identify practical use cases for the implementation of UASs for conducting obstacle data collection at airports.

UAS obstacle data collection was conducted at five airports using a variety of UAS platforms, camera payloads, and data collection parameters. These data sets were processed using two types of aerial triangulation (AT) software and analyzed using three-dimensional (3D) stereoscopic analysis techniques. The UAS data sets were evaluated based on their image quality, completeness,

and accuracy relative to current FAA standards. The accuracies of UAS-derived obstacle measurements were evaluated by comparing them with data sets collected using field survey techniques and aerial surveys using manned aircraft.

The results of both FAA and NGS review of the data found that UAS aerial imagery, in conjunction with 3D stereo analysis, is capable of collecting obstacle measurement data that meet current FAA Advisory Circular 150/5300-17 and 150/5300-18 accuracy standards. Furthermore, when compared to manned aircraft data, UAS imagery is significantly higher resolution, which can provide superior accuracy in measuring obstacle heights and can identify obstacles with smaller vertical cross-sections.

The accuracy of obstacle data is dependent on a variety of factors, including camera sensor and lens quality, data collection parameters such as ground sample distance and overlap settings, choice of processing software, and site attributes such as dense vegetation or terrain. None of these individual considerations can be isolated, and many can be used to compensate for a challenging environment or for areas in which other considerations are lacking. Due to this, it is recommended that entities using UASs for obstacle data collection conduct their own testing and quality control checks to ensure their specific combination of UAS hardware, camera payload, and processing software is able to achieve the required level of accuracy for a given project.

Due to technical and operational limitations, UASs are currently most practical for conducting small-scale surveys. Suggested UAS obstacle data collection applications include, but are not limited to, FAA Engineering Brief #91, *Management of Vegetation in the Airport Environment*; augmenting FAA Order 5010.4 surveys, updating entries in the Obstacle Authoritative Source, and surveying Precision Approach Path Indicator and Visual Glide Slope Indicators Obstacle Clearance Surface and Light Signal Clearance Surfaces.

## 6. REFERENCES


Da-Jiang Innovations (DJI). (2018a). *Zenmuse X5S User Manual v1.4*. https://dl.djicdn.com/downloads/zenmuse_x5s/20180420/Zenmuse+X5S+user+manual_v1.4_EN.pdf

DJI. (2018b). *Zenmuse X7 User Manual v1.4*. https://dl.djicdn.com/downloads/zenmuse+x7/20180718/Zenmuse+X7+User+Manual+EN+v1.4.pdf

DJI. (2019). *Inspire 2 Series User Manual v2.4*. https://dl.djicdn.com/downloads/inspire_2/20220614/INSPIRE_2_SERIES_User_Manual_EN_220614.pdf

DJI. (2020). *Matrice 200 Series V2 User Manual v2.0.* https://dl.djicdn.com/downloads/m200_v2/20200630/M200_Series_V2_User_Manual_en3.pdf

Definitions, 14 CFR § 107.3 (2016). https://www.ecfr.gov/current/title-14/chapter-I/subchapter-F/part-107/subpart-A/section-107.3

Federal Aviation administration (FAA). (2013). *Management of Vegetation in the Airport Environment* (Engineering Brief No. 91). https://www.faa.gov/airports/engineering/_briefs/media/eb-91.pdf

FAA. (2014, February 24). *General guidance and specifications for submission of aeronautical surveys to NGS: Field data collection and Geographic Information System (GIS) standards (Consolidated to include change 1)* (Advisory Circular (AC) 150/5300-18B). https://www.faa.gov/documentLibrary/media/Advisory_Circular/150-5300-18B-chg1-consolidated.pdf

FAA. (2015). *Airport data and information management* (Order 5010.4A). https://www.faa.gov/documentLibrary/media/Order/order-5010-4a-airport-data.pdf

FAA. (2017a). *Additional siting and survey considerations for Precision Approach Path Indictor (PAPI) and other Visual Glide Slope Indicators (VGSI)* (Engineering Brief No. 95). https://www.faa.gov/sites/faa.gov/files/airports/engineering/engineering_briefs/eb-95-papi-vgsi.pdf

FAA. (2017b, September 29)., *Standards for using remote sensing technologies in airport surveys (Consolidated to include change 1)* (AC 150/5300-17C). https://www.faa.gov/documentLibrary/media/Advisory_Circular/150-5300-17C-Chg1.pdf

FAA. (2019, July 8)., *General guidance and specifications for aeronautical surveys: Establishment of geodetic control and submission to the National Geodetic Survey* (AC 150/5300-16B). https://www.faa.gov/airports/resources/advisory_circulars/index.cfm/go/document.current/documentNumber/150_5300-16

FAA. (2020). *Flight procedures and airspace* (Order 8260.19I). https://www.faa.gov/documentLibrary/media/Order/Order_8260.19I.pdf

Lamoureux, Schuyler. (2022). *Obstruction Analysis: Utilizing Drones to Save Airports Time & Money.* https://hoyletanner.com/obstruction-analysis-utilizing-drones-to-save-airports-time-money/?nowprocket=1

National Resources Canada (NRCAN). (2016). *Concepts of Aerial Photography*. https://www.nrcan.gc.ca/maps-tools-publications/satellite-imagery-air-photos/air-photos/national-air-photo-library/about-aerial-photography/concepts-aerial-photography/9687

Obstructions, 14 CFR § 139.331 (2004). https://www.ecfr.gov/current/title-14/chapter-I/subchapter-G/part-139/subpart-D/section-139.331

Operating Limitations for Small Unmanned Aircraft, 14 CFR § 107.51 (2016). https://www.ecfr.gov/current/title-14/chapter-I/subchapter-F/part-107/subpart-B/section-107.51

Operation near Aircraft; Right-of-Way Rules, 14 CFR § 107.37 (2016). https://www.ecfr.gov/current/title-14/chapter-I/subchapter-F/part-107/subpart-B/section-107.37

Operation over Human Beings, 14 CFR § 139.39 (2016). https://www.ecfr.gov/current/title-14/chapter-I/subchapter-F/part-107/subpart-B/section-107.39

SenseFly (2019). *eBee X Drone User Manual Revision 1.7*. https://geomatika-smolcak.hr/wp-content/uploads/2018/10/ebee-x-drone-user-manual.pdf

SenseFly. (2020). *S.O.D.A. 3D Camera User Manual Revision 1.9*. https://www.flyingeye.fr/wp-content/uploads/2021/09/senseFly-S.O.D.A.-3D-Camera-User-Manual.pdf

Small Unmanned Aircraft Systems, 14 CFR § 107 (2016). https://www.ecfr.gov/current/title-14/chapter-I/subchapter-F/part-107

Sony. (2015). *Digital Still Camera Instruction Manual*. https://www.sony.com/electronics/support/res/manuals/4579/45798651M.pdf

Standards for Determining Obstructions to Air Navigation or Navigational Aids or Facilities, 14 CFR § 77 Subpart C (2010). https://www.ecfr.gov/current/title-14/chapter-I/subchapter-E/part-77/subpart-C

Visual Line of Sight Aircraft Operation, 14 CFR § 107 (2016). https://www.ecfr.gov/current/title-14/chapter-I/subchapter-F/part-107/subpart-B/section-107.31

Wingtra (2022). *WingtraOne Technical Specifications*. https://wingtra.com/wp-content/uploads/Wingtra-Technical-Specifications.pdf

# APPENDIX A—UAS PLATFORM SPECIFICATIONS

## A.1 INTRODUCTION

This appendix provides the specifications for the small unmanned aircraft system (UAS) platforms used during this research effort. Table A-1 shows the specifications for the Da-Jiang Innovations (DJI) Matrice 210 RTK v.2 (DJI M210); Table A-2 shows the specifications for the DJI Inspire 2; Table A-3 shows the specifications for the SenseFly eBee X RTK/PPK; and Table A-4 shows the specifications for the Wingtra WingtraOne PPK platform.

Table A-1. Specifications for the DJI M210 (DJI, 2020)

| **DJI M210 RTK v2** | |
|---|---|
| Type | Multirotor aircraft (4) |
| Wingspan | 25.3-in. motor-to-motor cross measurement |
| Weight | 10.83 lb without payload |
| Maximum flight time | 25 minutes |
| Average speed of flight during image capture | 15 mph |
| Operating temperature range | -4 °F–122 °F |
| Transmitter range | 5 miles (unobstructed) |
| Communication with transmitter | Radio (2.4000–2.4835 GHz; 5.725– 5.850 GHz) |
| Maximum sustained wind speed limit for safe flight | Up to 27 mph |
| Lost link procedure (if > 3 seconds) | Autonomous return-to-home at predetermined AGL with manual override available once link has been reestablished. |
| Low-battery procedure | Autonomous return-to-home if no action taken by the pilot after 10 seconds. If battery critically low, the UAS will initiate autonomous landing. |
| Operational area procedure | Onboard, preprogrammed flight area prohibits flying outside of predetermined geofence. |
| Obstacle avoidance | Forward, Down, Above, DJI AirSense (ADS-B Receiver) |
| Ingress protection rating | IP43 |

Table A-2. Specifications for the DJI Inspire 2 (DJI, 2019)

| **DJI Inspire 2** | |
|---|---|
| Type | Rotary aircraft (4) |
| Wingspan | 23.8-in. motor-to-motor cross measurement |
| MTOW | ±9.37 lb |
| Maximum flight time | ±27 minutes |
| Average speed of flight during image capture | 15 mph |
| Operating temperature range | -4 °F–104 °F |
| Transmitter range | 4.3 miles (unobstructed) |
| Communication with transmitter | Radio (2.4000–2.4835 GHz; 5.725–5.850 GHz) |
| Maximum sustained wind speed limit for safe flight | Up to 22 mph |
| Lost link procedure (if > 3 seconds) | Autonomous return-to-home at predetermined AGL with manual override available once link has been reestablished. |
| Low-battery procedure | Autonomous return-to-home if no action taken by the pilot after 10 seconds. If battery critically low, the UAS will initiate autonomous landing. |
| Operational area procedure | Onboard, preprogramed flight area prohibits flying outside of predetermined GeoFence. |
| Obstacle avoidance | Forward, Down, Above |

Table A-3. Specifications for the Sensefly eBee X (SenseFly, 2019)

| SenseFly eBee X RTK/PPK | |
|---|---|
| Type | Fixed-wing |
| Wingspan | 45.7 in. |
| Weight | 3.1 lb |
| Maximum flight time | 90 minutes |
| Average speed of flight during image capture | 25–50 mph (wind speed & direction dependent) |
| Operating temperature range | 5 °F–95 °F |
| Transmitter range | 5 miles |
| Communication with transmitter | Radio (2.4 GHs) |
| Maximum sustained wind speed limit for safe flight | Up to 29 mph |
| Lost link procedure (if > 30 seconds) | Autonomous return-to-home point, circular loiter until battery drain, then automatically land at predetermined landing spot if communication is not reestablished. |
| Low-battery procedure | Autonomous return-to-home at predetermined AGL, then autonomous landing following predetermined parameters. |
| Operational area procedure | Onboard, preprogrammed, radial flight area prohibits flying outside of predetermined GeoFence. If drone reaches the GeoFence, automatic return to home is triggered. |
| Obstacle avoidance | Down, ADS-B Receiver |

Table A-4. Specifications for the Wingtra WingtraOne (Wingtra, 2022)

| **Wingtra WingtraOne PPK** | |
|---|---|
| Type | Fixed-wing |
| Wingspan | 4.1 ft |
| Weight | 9.9 lb |
| Maximum flight time | 55 minutes |
| Average speed of flight during image capture | 35.8 mph (wind speed & direction dependent) |
| Operating temperature range | -4 °F–122 °F |
| Transmitter range | 5 miles |
| Communication with transmitter | 2.404 – 2.479 GHz |
| Maximum sustained wind speed limit for safe flight | Up to 28 mph in cruise, up to 18 mph for landing |
| Lost link procedure (if > 30 seconds) | Autonomous return-to-home point, then automatically land at predetermined landing spot if communication is not reestablished. |
| Low-battery procedure | Warning when battery at <45%, return to home initiated at 38% battery. If the battery reaches <2%, the UAS will initiate autonomous landing. |
| Operational area procedure | Onboard, preprogrammed, radial flight area prohibits flying outside of predetermined GeoFence. If drone reaches the GeoFence, automatic return to home is triggered. |
| Obstacle avoidance | Set transition height 65 ft above obstacles. Terrain following feature recommended. Assisted mode available with tablet and remote control. |

## A.2 REFERENCES


Da-Jiang Innovations (DJI) (2019). *Inspire 2 Series User Manual v2.4*. https://dl.djicdn.com/downloads/inspire_2/20220614/INSPIRE_2_SERIES_User_Manual_EN_220614.pdf

DJI. (2020). *Matrice 200 Series V2 User Manual v2.0.* https://dl.djicdn.com/downloads/m200_v2/20200630/M200_Series_V2_User_Manual_en3.pdf

SenseFly (2019). *eBee X Drone User Manual Revision 1.7*. https://geomatika-smolcak.hr/wp-content/uploads/2018/10/ebee-x-drone-user-manual.pdf

Wingtra (2022). *WingtraOne Technical Specifications*. https://wingtra.com/wp-content/uploads/Wingtra-Technical-Specifications.pdf

# APPENDIX B—CAMERA PAYLOAD SPECIFICATIONS

## B.1 INTRODUCTION

This appendix provides the camera payload specifications for the small unmanned aircraft system (UAS) platforms used during this research effort. Table B-1 shows the specifications for the Da-Jiang Innovations (DJI) Zenmuse X7; Table B-2 shows the specifications for the DJI Zenmuse X5S; Table B-3 shows the specifications for the SenseFly S.O.D.A. 3D; and Table B-4 shows the specifications for the Sony RX1R-II.

Table B-1. Specifications for the DJI Zenmuse X7 (DJI, 2018a)

| **DJI Zenmuse X7** | |
|---|---|
| Airframe Compatibility | Inspire 2, M210 |
| Gimbal Control<br>(3D Stabilized)<br>(Detachable Mount*) | Pitch: -125° to +40°<br>Pan: ±300°<br>Roll: +90° to -50° |
| Still Image Resolution | 24.0 MP (6016 x 4008) |
| Aspect Ratio | 3:2 |
| Sensor Type | CMOS - Super 35 |
| Sensor Size | APS-C (23.5 mm × 15.7 mm) |
| Focal Length | 16 mm (35 mm equivalent: 24 mm) |
| Still Image Format | JPEG, RAW, RAW + JPEG |
| Shutter Mode | Electronic Rolling |
| GSD @ 400 ft AGL | 1.18 in. |

GSD = Ground sample distance

Table B-2. Specifications for the DJI Zenmuse X5S (DJI, 2018b)

| **DJI Zenmuse X5S** | |
|---|---|
| Airframe Compatibility | Inspire 2, M210 |
| Gimbal Control<br>(3D Stabilized)<br>(Detachable Mount*) | Pitch: -125° to +40°<br>Pan: ±300°<br>Roll: +90° to -50° |
| Still Image Resolution | 20.8 MP (5280 x 3956) |
| Aspect Ratio | 4:3 |
| Sensor Type | CMOS |
| Sensor Size | 4/3 (17 mm × 13 mm) |
| Focal Length | 15 mm (35 mm equivalent: 30 mm) |
| Still Image Format | JPEG, RAW, RAW + JPEG |
| Shutter Mode | Electronic Rolling |
| GSD @ 400 ft AGL | 1.05 in. |

GSD = Ground sample distance

Table B-3. Specifications for the SenseFly S.O.D.A. 3D (SenseFly, 2020)

| SenseFly S.O.D.A. 3D | |
|---|---|
| Airframe Compatibility | eBee X |
| Gimbal Control (2D Stabilized) | Roll: 45°Left to 45°Right |
| Still Image Resolution | 20 MP (5472 x 3648) |
| Aspect Ratio | 3:2 |
| Sensor Type | CMOS |
| Sensor Size | 1 in. (13.2 mm x 8.8 mm) |
| Focal Length | 10.6 mm (35 mm equivalent: 29 mm) |
| Still Image Format | JPG, JPG+DNG |
| Shutter Mode | Mechanical Global |
| GSD @ 400 ft AGL | 1.08 in. |

GSD = Ground sample distance

Table B-4. Specifications for the Sony RX1R-II (Sony, 2015)

| Sony RX1R-II | |
|---|---|
| Airframe Compatibility | WingtraOne |
| Gimbal Control | None |
| Still Image Resolution | 42.4 MP (7952 x 5304) |
| Aspect Ratio | 3:2 |
| Sensor Type | Exmor R™ CMOS |
| Sensor Size | Full Frame (35.9 mm x 24 mm) |
| Lens Focal Length | 35 mm |
| Still Image Format | JPG, DNG, JPG+DNG |
| Shutter Mode | Mechanical Global |
| GSD @ 400 ft AGL | 0.64 in. |

GSD = Ground sample distance

## B.2 REFERENCES


Da-Jiang Innovations (DJI). (2018a). *Zenmuse X7 User Manual v1.4*. https://dl.djicdn.com/downloads/zenmuse+x7/20180718/Zenmuse+X7+User+Manual+EN+v1.4.pdf

DJI. (2018b). *Zenmuse X5S User Manual v1.4*. https://dl.djicdn.com/downloads/zenmuse_x5s/20180420/Zenmuse+X5S+user+manual_v1.4_EN.pdf

SenseFly. (2020). *S.O.D.A. 3D Camera User Manual Revision 1.9*. https://www.flyingeye.fr/wp-content/uploads/2021/09/senseFly-S.O.D.A.-3D-Camera-User-Manual.pdf

Sony. (2015). *Digital Still Camera Instruction Manual*. https://www.sony.com/electronics/support/res/manuals/4579/45798651M.pdf